Bioactive potentials of novel Enceleamycins A–C and *N* hydroxypyrazinone acid from *Amycolatopsis* sp.

By

Khan Abujunaid Habib

AcSIR Registration No. 10BB18A26033

A thesis submitted to the

Academy of Scientific & innovative Research

for the award of the degree of

DOCTOR OF PHILOSOPHY

in

SCIENCE

Under the supervision of

Dr. Syed G. Dastager

Council of Scientific and Industrial Research
National Chemical Laboratory

AcSYR

Academy of Scientific and Innovative Research

AcSIR Headquarters, CSIR-HRDC Campus

Sector 19, Kamla Nehru Nagar,

Ghaziabad, U.P. -201 002, India

Dec, 2023

Certificate

This is to certify that the work incorporated in this Ph.D. thesis entitled, "*Bioactive potentials of novel Enceleamycins A–C and N-hydroxypyrazinone acid from Amycolatopsis sp.*", submitted by *Mr. Khan Abujunaid Habib* to the Academy of Scientific and Innovative Research (AcSIR) in fulfillment of the requirements for the award of the Degree of *Doctor of Philosophy in Science,* embodies original research work carried-out by the student. We, further certify that this work has not been submitted to any other University or Institution in part or full for the award of any degree or diploma. Research material(s) obtained from other source(s) and used in this research work has/have been duly acknowledged in the thesis. Image(s), illustration(s), figure(s), table(s) etc., used in the thesis from other source(s), have also been duly cited and acknowledged.
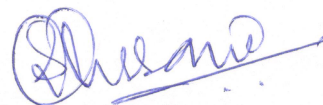

(Signature of Student)
Name with date

Abujunaid Khan
14th Dec, 2023

(Signature of Supervisor)
Name with date

Dr. Syed G. Dastager
14th Dec, 2023

STATEMENTS OF ACADEMIC INTEGRITY

I, <u>Mr. Khan Abujunaid Habib</u>, a Ph.D. student of the Academy of Scientific and Innovative Research (AcSIR) with Registration No. <u>10BB18A26033</u> hereby undertake that, the thesis entitled "<u>Bioactive potentials of novel Enceleamycins A–C and *N*-hydroxypyrazinone acid from *Amycolatopsis* sp.</u>" has been prepared by me and that the document reports original work carried out by me and is free of any plagiarism in compliance with the UGC Regulations on *"Promotion of Academic Integrity and Prevention of Plagiarism in Higher Educational Institutions (2018)"* and the CSIR Guidelines for *"Ethics in Research and in Governance (2020)"*.
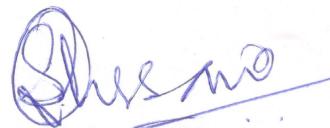
Signature of the Student
Name : Abujunaid Khan
Date   : 14th Dec, 2023
Place : Pune

It is hereby certified that the work done by the student, under my/our supervision, is plagiarism-free in accordance with the UGC Regulations on *"Promotion of Academic Integrity and Prevention of Plagiarism in Higher Educational Institutions (2018)"* and the CSIR Guidelines for *"Ethics in Research and in Governance (2020)"*.

Signature of the Supervisor
Name : Dr. Syed G. Dastager
Date   : 14th Dec, 2023
Place : Pune

Acknowledgement

I would like to express my sincere gratitude for all those who contributed and supported me during my Ph.D. journey. I am grateful to the God for blessing and providing me power, energy, and patience to overcome all obstacles and achieve my goal.

I would like to express my deepest gratitude and appreciation to my supervisor, Dr. Syed G. Dastager, for giving me the opportunity to work in this prestigious institute. I am grateful for his unwavering support, guidance, and mentorship throughout the course of this thesis. His expertise, dedication, and insightful feedback have been invaluable in shaping the direction and quality of this work. He has been supportive and has given me the freedom to pursue various projects without objection.

I would like to express my sincere thanks to Dr. Amol Kulkarni, Dr. Narendra Kadoo, and Dr. Mahesh Dharne for being the part of Doctoral Advisory Committee (DAC). Their constructive suggestions and timely evaluation help to shape my thesis. I would also like to express my special thanks to Dr. Mahesh Dharne for his constant support and encouragement throughout my Ph.D. journey.

My heart warming thanks to my lab mates, Dr. Gajanan, Dr. Hari, Dr. Rahul, Dr. Meghana, Dr Govinda, Dr. Kushal, Dr. Raja, Dr. Roopa, Dr. Vinodh, Digheshwar, Jini, Karthika, Manan, Vidyashree, Dr. Vasudev, Dr. Vibha, Pranav, Aashish, Rachel, Sayali, Dr. Vinita, Dr. Ekramul, Dr. Pranhita, Rinka, Priyanka, Vinod, Sambhaji, Anil, Amrapali, Vaishnavi, Subham, Sejal, and Deepak for always being there for me in good and bad times, and for their support and help. Dr. Amit Kumar Sahu gets special thanks for his valuable inputs during my initial work and his help in fermentation and purification. I would like to thanks Dr. Bharat, Dr. Vasudev and Rachel for their support and constructive discussion which help in design of experiments. I like to appreciate Vinay and Rakesh for their help in genome sequencing and Pradeep for docking analysis. Thanks to Priyanka and Pradeep for their help in different aspects of my work. I am fortunate to have good friends Pranav, Rakesh and Vinay that are continuously supporting, inspiring, and cheering me in all situations.

I am truly thankful to the NCIM staff members Mrs. Sandhya Sudge, Mrs. Shivani Chaudhari, Mrs. Shalaka Gaikaiwari, Mrs. Ratnamala Vasave, Mrs. Meeta Patil, Mr.

Abujunaid Khan
Dec, 2023

****

THIS THESIS IS DEDICATED TO

MY BELOVED PARENTS

THANK YOU FOR BEING A SOURCE OF INSPIRATION

****

Table of contents

Chapter 2: Screening and identification of bioactive compound producing actinobacteria

Chapter 4: Bioactivity of Enceleamycin A-C and *N*-hydroxypyrazinone acid

---

List of figures

Chapter 4: Bioactivity of Enceleamycin A-C and *N*-hydroxypyrazinone acid

Section 4A: Antibacterial study of Enceleamycins A-C and *N*-hydroxypyrazinone acid

Section 4A: Antibacterial study of Enceleamycins A-C and *N*-hydroxypyrazinone acid

Section 4B: Anticancer study of Enceleamycins A-C and *N*-hydroxypyrazinone acid

Abbreviations

°C	Degree Celsius
μg	Microgram
μL	Microliter
ACDSF	Anticancer Drug screening facility
ACTREC	Advanced Centre for Treatment, Research and Education in Cancer
AMR	Antimicrobial resistance
ATCC	American Type Culture Collection
BBB	Blood brain barrier
C-18	Octadecylsilane
CD	Circular dichroism
CD_3CN	Deuterated acetonitrile
$CDCl_3$	Deuterated chloroform
CFU	Colony Forming Units
CLSI	Clinical and Laboratory Standards Institute
cm	Centimetre
COSY	Correlation Spectroscopy
CTAB	Cetyltrimethylammonium bromide
Da	Dalton
DCM	Dichloromethane
DEPT	Distortion less Enhancement by Polarization Transfer
DMEM	Dulbecco's modified eagle's medium
DMSO	Dimethyl Sulfoxide
DMSO-d6	Deuterated DMSO
DNA	Deoxyribonucleic acid
EDTA	Ethylene diamine tetra-acetic acid
FBS	Fetal bovine serum
FE-SEM	Field Emission Scanning Electron Microscope
FIC	Fractional inhibitory concentration
FTIR	Fourier transform infrared
H_2DCFDA	2′,7′-Dichlorodihydrofluorescein diacetate
HCl	Hydrogen Chloride
HMBC	Heteronuclear Multiple-Bond Coherence

HPLC	High Performance Liquid Chromatography
HR-ESIMS	High-resolution electrospray ionisation mass spectrometry
HRMS	High-resolution mass-spectrometry
HSQC	Heteronuclear Single Quantum Coherence
ISP	International Streptomyces Project
Kcal/mol	kilocalorie per mole
MCC	Microbial Culture Collection
MEGA	Molecular evolutionary genetics analysis
Mg	Milligram
MIC	Minimum Inhibitory Concentration
mm	Millimetre
MRSA	Methicillin-resistant Staphylococcus aureus
MSSA	Methicillin-sensitive Staphylococcus aureus
MTT	3-(4,5-Dimethylthiazol-2-yl)-2,5-diphenyl tetrazolium bromide
NaCl	Sodium Chloride
NaOH	Sodium Hydroxide
NCBI	National Center for Biotechnology Information
NCCS	National Center for Cell Science
NCIM	National Collection of Industrial Microorganisms
NMR	Nuclear Magnetic Resonance
NOESY	Nuclear Overhauser Enhancement Spectroscopy
NRPSs	Non-ribosomal peptide synthetases
OD	Optical density
OSMAC	One strain many compounds
PCR	Polymerase chain reaction
PEG	Polyethylene glycol
PKSs	Polyketide synthases
RAST	Rapid Annotation and Subsystem Technology
Rg	Radius of gyration
RMSD	Root Mean Square Deviation
RMSF	Root mean square fluctuation
ROS	Reactive oxygen species
rRNA	Ribosomal ribonucleic acid
SEM	Scanning Electron Microscope

SI	Selectivity index
sp.	Species
SRB	Sulforhodamine B
TBE	Tris/Borate/EDTA
TE	Tris-EDTA
TLC	Thin Layer Chromatography
TNBC	Triple-negative breast cancer
UHPLC	Ultra High Performance Liquid Chromatography
VWD	Variable wavelength detector
WGS	Whole Genome Sequencing
XRD	X-ray diffraction

Chapter 1

Amycolatopsis: A repository of novel bioactive compounds

General introduction

1. Antimicrobial resistance

Antimicrobials are drugs used to treat infections caused by microorganisms without harming the host. Based on the growth inhibition of respective microbes, these antimicrobials are further classified as antibiotics, antifungal, antiviral, and antiparasitic for treating bacterial, fungal, viral, and parasitic infections. Antimicrobial resistance (AMR) is the in-efficiency of the antimicrobials to kill them, making infections difficult to treat (Tang et al. 2023). AMR has resulted in the in-effectiveness of antimicrobials, making the disease persist for a longer duration in the patient, which raises the possibility of spreading the infection to other people. AMR has now developed into a significant global concern of 21st century due to increase of AMR at an alarming rate and shortage of novel antimicrobials to tackle this problem (Prestinaci et al. 2015). One of the primary reasons for the current AMR issue is irresponsible and excessive use of antibiotics in various sectors like agriculture, clinical, animal healthcare and the food (Llor and Bjerrum 2014). AMR is now considered the "Silent Pandemic", which requires prompt attention and should be controlled more effectively (Founou et al. 2021).

Antibiotic resistance is the most challenging elements of antimicrobial resistance (AMR). As shown in Figure 1, there is a high rate of resistance development to various antibiotics used for bacterial infection treatment (Hutchings et al. 2019). In 2019, an estimated 4.95 million deaths were linked to bacterial AMR, of which 1.27 million deaths were attributed to bacterial AMR directly (Murray et al. 2022). If preventative steps are not taken to manage AMR, the number is expected to rise to almost ten million deaths yearly by 2050 (de Kraker et al. 2016). The critical hospital infections and high mortality risk are caused by pathogens associated with ESKAPEE group which includes *Enterococcus faecium*, *Staphylococcus aureus*, *Klebsiella pneumoniae*, *Acinetobacter baumannii*, *Pseudomonas aeruginosa*, *Enterobacter* spp. and *Escherichia coli* (Ruekit et al. 2022). Based on the urgency for newer antibiotics, these pathogens are categorized into critical and high priority. The critical priority pathogens include the Carbapenem resistant *P. aeruginosa*, *A. baumannii*, *Enterobacter* spp*., K. pneumoniae* and extended spectrum β-lactamase (ESBL). High priority pathogen group includes the vancomycin and methicillin resistant *S. aureus* (VRSA and MRSA) and vancomycin resistant *E. faecium* (VRE) (Mulani et al. 2019; Santajit and Indrawattana, 2016).
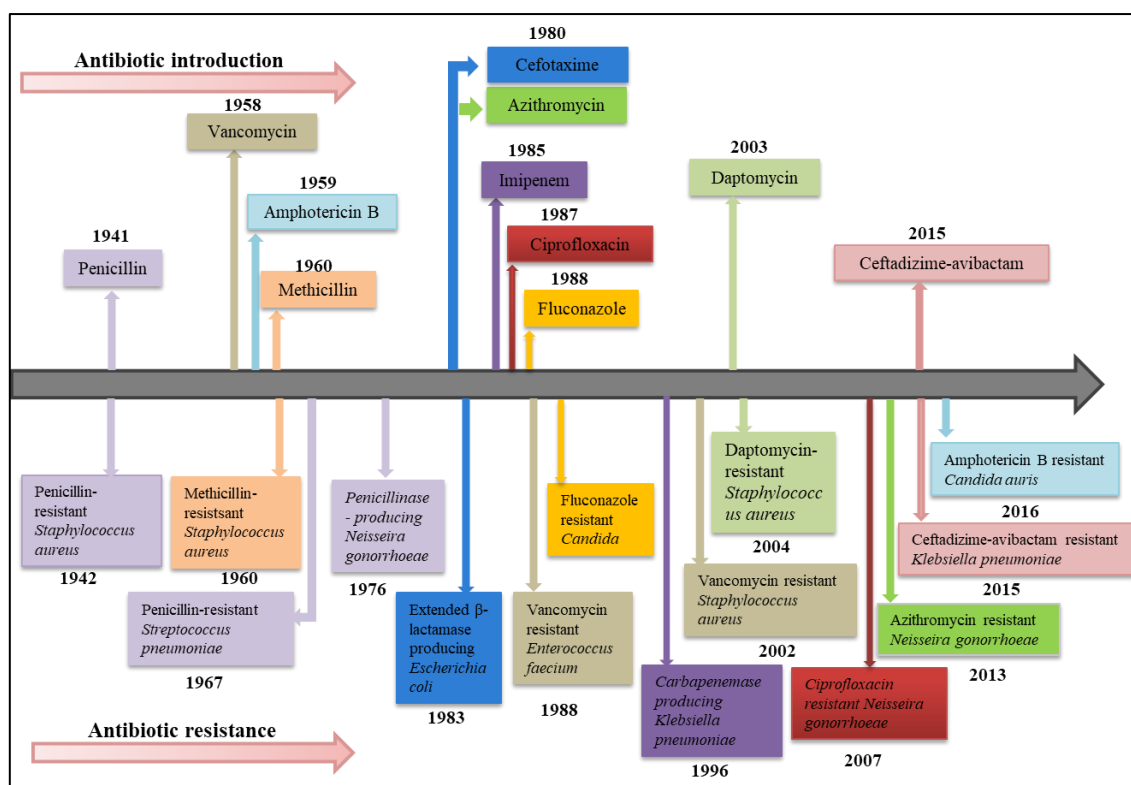
Figure 1. The timeline of antibiotic introduction and resistance (adapted from Hutchings et al. 2019).

1.1 Mechanism of antimicrobial resistance

The bacterial resistance to the available antibiotics may be natural or acquired. The natural resistance can be intrinsic in which the genes are always expressed in the organism or induced in which the gene is present in the organism however expressed only after the antibiotic exposure (Zhang and Cheng, 2022). An example of intrinsic resistance is the presence of lipopolysaccharide in gram-negative bacteria, which reduces the outer membrane permeability (Cox and Wright, 2013). The induced resistance is by a multidrug efflux pump, which elutes the drug outside the cell. The acquired resistance towards antibiotics is developed majorly due to the mutations in genes associated with target of the antibiotics or through the acquisition of resistance coding foreign genetic material by horizontal gene transfer (Coculescu, 2009). The mechanism of resistance is majorly classified into four types: (A) limiting the drug uptake, (B) active drug efflux, (C) modification of drug target, (D) inactivation of drug

(A) Limiting the drug uptake

Bacteria can reduce the cell membrane permeability, making it challenging for antibiotics to pass through and reach target site. The lipopolysaccharides layer in Gram-negative bacteria provides a structural barrier to various prominent antimicrobial agents (Blair et al. 2014). The other important factor in reducing drug uptake is lowering the number of porins or the mutations, which change the porin channel selectively (Kumar and Schweizer 2005). The example of resistance development in the *Enterobacteriaceae* family is by the reduction in the number of porins for carbapenems or by the mutation in the porin channel, which selectivity inhibits the uptake of cephalosporins and imipenem (Cornaglia et al. 1996; Chow and Shales, 1991). The sticky and thick consistent biofilm formation by the bacterial community containing polysaccharides and proteins makes it difficult for the antibiotic to reach the bacterial population and eliminate their growth. In addition, the proximity of bacteria in the biofilm matrix helps in horizontal gene transfer, making it easier to transfer the antimicrobial resistance conferring genes (Van Acker et al. 2014).

(B) Active drug efflux

Bacteria can extrude the antibiotics through efflux pumps from inside the cell, thereby reducing the concentration of antibiotics before they exert their effect. There are five major efflux pumps family classified based on the energy source, structural conformations and the range of substrate they extrude: small multidrug resistance (SMR), ATP-binding cassette (ABC), resistance nodulation cell-division (RND), major facilitator superfamily (MFS), and multidrug and toxic compound extrusion (MATE), (Piddock 2006). The ABC transporter family in Gram-positive bacteria results in macrolide resistance by efflux pumps MsrA and MsrC. MsrA was initially found in *S. epidermidis* as a plasmid-borne, whereas the MsrC was described in *E. faecalis* as a chromosomally encoded protein (Poole, 2005). The Tet efflux pump is an example of tetracycline resistance belonging to the MFS family, which removes tetracycline by using the proton as an energy source. The Tet efflux pumps are more common in Gram-negative bacteria, except Tet K and Tet L, which predominate in Gram-positive bacteria (Roberts, 2005). Examples of efflux pumps that extrude macrolides like erythromycin are encoded by *mef* genes found in Gram-positive organisms, including *Streptococcus pneumonia* and *Streptococcus pyogenes* (Ross et al. 1990). RND family efflux pumps are generally present in Gram-negative bacteria and act as a proton

antiporter, which excludes various antibiotics like tetracycline, fluoroquinolones, some β-lactams, novobiocin, fusidic acid and chloramphenicol (Munita and Arias 2016).

(C) Modification of a drug target

Bacteria can modify the target site of the antibiotics, making it difficult to interact with the target and resulting in the in-effectiveness of the drug. One example of such resistance occurs by modifying the ribosomal subunit, thereby leading to resistance to aminoglycosides and oxazolidinones, which interferes with drug-binding ability of ribosome (Roberts, 2004).

The resistance mechanism to the β-lactam antibiotic used by the Gram-positive bacteria is by the alteration in number or structure of penicillin-binding proteins (PBPs) involved in peptidoglycan construction in cell wall. The structural changes like PBP2a by acquiring *the mecA* gene in *S. aureus* inhibit the drug binding ability (Reygaert, 2009). The resistance towards the nucleic acid target drugs like fluoroquinolones is by the modifications in topoisomerase IV encoded by gene *grlA* in Gram-positive bacteria or DNA gyrase encoded by gene *gyrA* in Gram-negative bacteria (Redgrave et al. 2014).
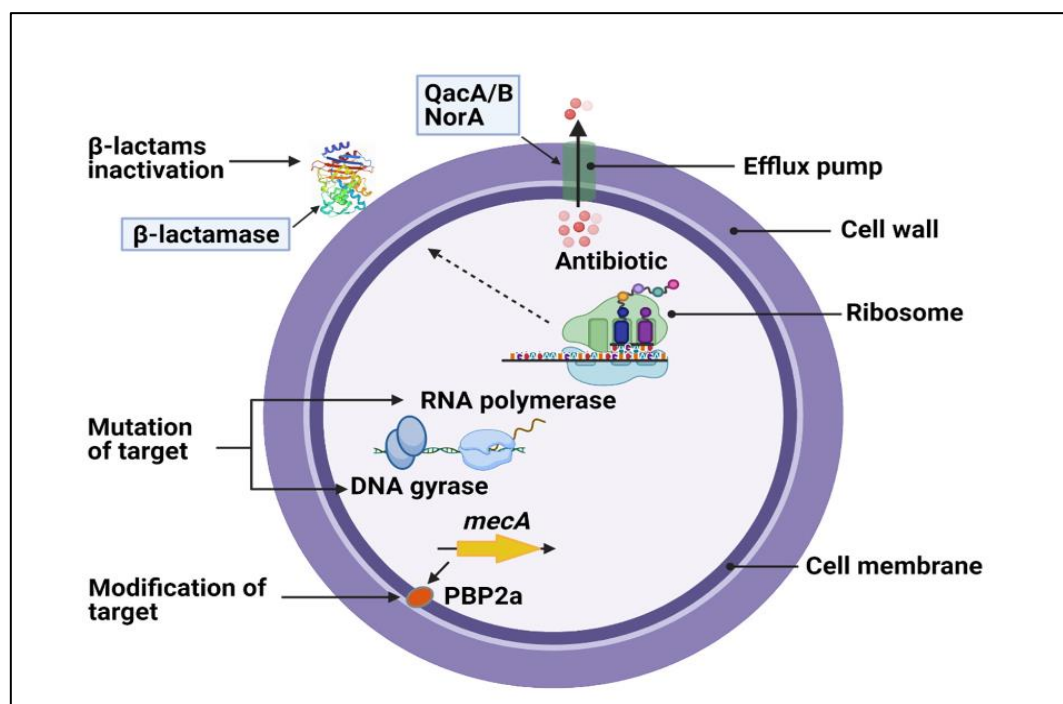
Figure 2. Antibiotic resistance mechanism in *Staphylococcus aureus* (Lade and Kim, 2021)

(D) Inactivation of a drug

The bacteria achieve the inactivation of drugs through the actual degradation of the drug or by the enzymatic modification of the drug. The β-lactamase is the major drug hydrolyzing enzyme which inactivates the β-lactam drugs. It hydrolyzes the amide bond of the β-lactam ring, resulting in the ring opening and loss of activity. The β-lactamase production is the dominant resistance mechanism of Gram-negative bacteria against penicillin and cephalosporins. The β-lactamase enzymes can be found on chromosomes or acquired by plasmid. The first chromosomally encoded β-lactamase was characterized in *E. coli* by the *ampC* gene and is resistant against penicillin's and a few cephalosporins from the first generation (Reygaert, 2018, Blair et al. 2015). Recently, there has been an emergence of β-lactamases in *Enterobacteriaceae* with activity against carbapenems known as Carbapenem-Resistant *Enterobacteriaceae* (CRE) enzymes and *Klebsiella pneumoniae* carbapenemases (KPCs) (Pfeifer et al. 2010). The drug inactivation by chemical group transfer is generally by the acetylation, adenylation or phosphorylation of drugs. The acetylation of aminoglycosides, fluoroquinolones, and chloramphenicol is the most diversely used mechanism, whereas the adenylation and phosphorylation are also used against aminoglycosides (Ramirez and Tolmasky, 2010; Robicsek et al. 2006).

1.2 Sources to tackle antimicrobial resistance

To ensure the microbial infections treatment and to tackle increasing antimicrobial resistance, there is a need for a new class of antibiotics. There has been tremendous decline in discovery of novel classes of antibiotics due to the regulatory, financial and lack of scientific innovations (Zorzet, 2014). Since the early antibiotic era, natural products have been the source of antimicrobial drug discovery (Taylor, 2013). Natural products are comprised of antimicrobial compounds isolated from plants, animals and microorganisms. Modification and total chemical synthesis of natural products have also been successfully incorporated in drug discovery. Since the synthesis and modification are primarily based on the natural products or the class of antibiotics already in use, the chance of resistance towards these molecules is considerably high. Bacteriophages can also be utilized as an alternative to the antibiotics in treating bacterial diseases; however, phage therapy has certain limitations due to its narrow host spectrum and the lysogenic phenomenon (Lin et al. 2022).

Several recent studies have suggested nanoparticles as an attractive therapeutic option for bacterial infections due to their valuable antimicrobial activities (Duval et al. 2019).

Nanoparticles can interfere with critical molecular pathways of pathogenic bacteria by penetrating the cell membrane. However, there needs to be more investigation into the mechanism, clearance, optimum dose for therapeutic activity and toxicity of nanoparticles. Translating into the clinic requires an in-depth knowledge of the pharmacokinetics and pharmacodynamics of nanoparticles (Lee et al. 2019). Since the emergence of resistance to any antibiotic is unavoidable, combination therapy with standard antibiotics is a further approach to minimize the development of drug resistance (Worthington et al. 2013). The synergistic interactions have also become a promising strategy for improving the efficacy of drugs by extending the therapeutic spectrum of drugs whose potential use may be constrained by toxicity concerns. As a result, synergistic activity might exhibit comparable effectiveness at lower, non-toxic levels. Additionally, using combinatorial therapy may prevent the emergence of resistance brought on by monotherapy (Sun et al. 2016).
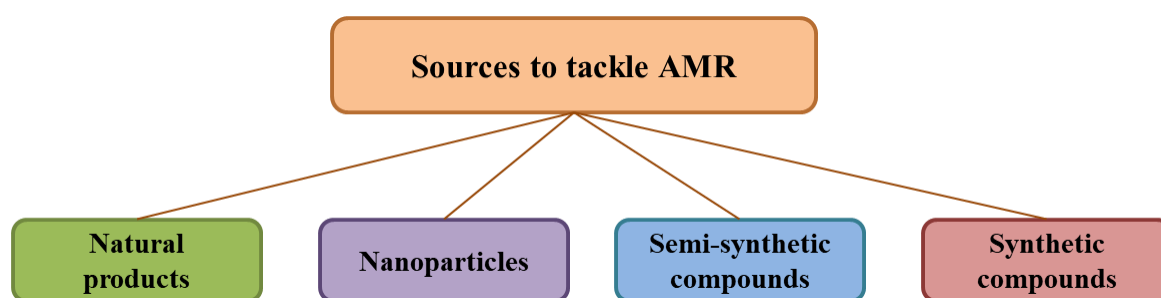
Figure 3. Different sources to tackle antimicrobial resistance

Even with the new alternative for antimicrobial therapy, natural products remain the major source of approved drugs and are essential in providing chemical diversity (Monciardini et al. 2014). Implementing novel approaches and techniques, such as culturing advances, improved analytical tools, genetic engineering strategies, and genome mining, has revitalized interest in natural products for tackling antimicrobial resistance (Atanasov et al. 2021).

2. Natural products

Natural products (NPs) are secondary metabolites considered non-essential for life and are derived from living organisms, including microorganisms, plants and animals. NPs have historically played a vital role in drug discovery in various therapeutic areas, especially for infectious diseases and cancer (Harvey et al. 2015). The relevance for infectious disease and cancer is explained by the evolutionary optimized structural diversity of NPs to serve specific biological functions, like regulating cell-to-cell communication and endogenous defence

mechanisms (Atanasov et al. 2021). Academic researchers and pharmaceutical companies have used natural products as the primary sources for novel bioactive compounds discovery. More than 50% of the drug leads under development are either from natural products, their semi-synthetic derivatives, or inspired by natural scaffolds (Veeresham 2012).

Plant natural products have long been known to exhibit bioactivities and yielded many essential drugs for human use. The plant natural products have resulted in the discovery of antimalarial quinine or opiate morphine in the early nineteenth century, and more recently, anticancer paclitaxel and antimalarial artemisinin have been discovered (Wright 2019). The plants are also a source of many antibacterial compounds like eugenol, propolin D, rhodomyrtosone B, sanguinarine and thymol (Álvarez-Martínez et al. 2021).

Animal natural products have been explored in recent years, and various novel bioactive molecules have been reported, especially from marine invertebrates. The isolation of two unusual arabinose-containing nucleosides, spongothymidine and spongouridine from the sponge *Cryptotethya crypta* led to synthesis of an antiviral drug, vidarabine (ara-A) and related anticancer drug cytarabine (ara-C). The anticancer ara-C was used to treat acute myeloid leukaemia, non-Hodgkin's lymphoma, and acute lymphocytic leukaemia (Anjum et al. 2016). In 2004, the FDA approved the toxic peptide ω-conotoxin MVIIA (Ziconitide), as an analgesic derived from venom of a predatory snail *Conus magus* (Jiménez, 2018). Antimicrobial peptides like cecropin, defensin, moricin, drosomycin, apidaecin, drosocin, gloverin, attacin, and lebocin have been reported from insects like worms, cockroaches and pests (Yi et al. 2014).

Various novel bioactive molecules have been reported from plants and animals; however, there are also many challenges in researching plant and animal natural products. The major concerns are the availability of plants and animals, authentication of the species and scale-up of the isolated bioactive compounds. The different species and geographical locations make it difficult to consistently obtain the desired molecule (Katiyar et al. 2012). Microbial natural products are good alternatives since they are easy to grow, characterize and scale up the potent bioactive compound. Since more than 90% of microbial sources are underexplored, natural products from microbes still need to be explored. Microbial secondary metabolites with diverse chemical entities can play an immense role in discovering novel antimicrobial and anticancer agents.

2.1 Microbial secondary metabolites

Microbial secondary metabolites are the bioactive compounds that microorganisms like bacteria and fungi produce. These bioactive compounds have versatile structures with numerous pharmaceutical applications like antibacterial, antifungal, anticancer and anti-inflammatory (Abdel-Razek et al. 2020). The microbial secondary metabolites in drug-discovery came into reality after penicillin's discovery from the fungus *Penicillium notatum* in 1928. The discovery of penicillin from a microbial source has motivated scientists to explore the microbial source. It has led to the golden period of antibiotics, where around 20 classes of antibiotics were discovered from 1940 to 1962 (Coates et al. 2011). The important class of antimicrobials produced are the β-lactam antibiotics, like penicillin and cephalosporins from fungi (Keller, 2019) and the aminoglycosides, macrolides, tetracyclines, glycopeptides, chloramphenicol, polyenes, and ansamycins from filamentous actinobacteria (Selim et al. 2021).

2.2 Biosynthesis of microbial secondary metabolites

The initiation of secondary metabolite biosynthesis depends on various biotic and abiotic factors. The expression of secondary metabolites biosynthesis is influenced by stages of the organism's development, nutrient availability and stress (Chandran et al. 2020; Ruiz et al. 2010). The chemically diverse secondary metabolites are mostly derived from primary metabolic pathways' intermediate and end products (Keller, 2019). The four primary building-block of secondary metabolism are shikimic acid, acetyl CoA, methylerythritol 4-phosphate and mevalonic acid. The primary metabolite acetyl CoA leads to the biosynthesis of fatty acids and polyketides, whereas shikimic acid produces aromatic amino acids and phenylpropanoids. The isopentenyl diphosphate (IPP) and dimethylallyl diphosphate (DMAPP) formed from mevalonic acid and methylerythritol 4-phosphate, takes part in the biosynthesis of terpenoids and steroids (Lin et al. 2023; Zhao et al. 2013).

Large multifunctional enzymes, such as polyketide synthases, non-ribosomal peptide synthetases, and ribosomally synthesized post-translationally modified peptides have a crucial function in biosynthesis of microbial secondary metabolites.

2.2.1 Polyketide synthases (PKSs)

Polycyclic aromatic secondary metabolites, also known as polyketides, are bio-synthesized by PKSs (Das and Khosla, 2009). PKSs are categorized into

a. Type I PKSs comprise various functional domains and are present in both fungi and bacteria,

b. Type II PKSs are comprised of discrete catalytic domains and mostly present in bacteria,

c. Type III PKSs are comprised of basic chalcone synthase type enzymes mainly present in bacteria and plants.

PKSs generally use acetyl and malonyl-CoA as a substrate and, by condensation processes, convert them into longer carbon chains (Nivina et al. 2019). The minimal biosynthetic domains for one PKS module include the acyltransferase for selecting building blocks, an acyl carrier protein (ACP) for covalently holding and transferring extending polyketide chain and ketosynthase (KS) for catalyzing the formation of the carbon-carbon bond. The polyketide chain produced is additionally modified with tailoring enzymes, like cyclases and oxidoreductases, to form a final polyketide compound with structural diversity (Shen, 2003). PKSs are responsible for the production of numerous secondary metabolites that are currently used like antibiotics (erythromycin), cancer chemotherapy (doxorubicin), cholesterol-lowering agents (lovastatin), and antiparasitic drugs (avermectin) (Cortes et al. 1990; Nivina et al. 2019).

2.2.2 Non-ribosomal peptides synthetases (NRPSs)

The non-ribosomal peptides (NRPs) are bio-synthesized by the non-ribosomal peptide synthetases using building block of amino acid and, in some cases, substrates such as amino-benzoic acid (Süssmuth and Mainz, 2017). The NRPSs module consist of an adenylation domain for selecting and transfering amino acids, peptidyl carrier protein domain for tethering and growing peptide chain by covalent thioester bond, and a condensation domain possessing catalytic activity for peptide bond formation between a new bound amino acid and an expanding chain of peptide. The other optional domains can also be present for oxidation, epimerization and methylation (Wang et al. 2014). NRPSs produce many medically relevant secondary metabolites, including cyclosporine, β-lactam antibiotics (Gaudelli et al. 2015) and daptomycin (Robbel and Marahiel, 2010). In addition, a combination of NRPS and PKS enzymes produces hybrid secondary metabolites by incorporating acyl and amino-acid building blocks (Miyanaga et al. 2018). Clinically important secondary metabolites that are

produced by a combination of NRPS and PKS function include the antitumor drug bleomycin (Mizuno et al. 2013) and the immunosuppressant rapamycin (Vézina et al. 1975).

2.2.3 Ribosomally synthesized post-translationally modified peptides (RiPPs)

Another crucial biosynthetic pathway for microbial secondary metabolites is RiPPs. The initial step of RiPPs biosynthesis is through ribosomal machinery using amino acids; however, in the later stages, a number of post translational modifications leads to chemically distinct secondary metabolites. A modification includes disulfide bridging of two cysteine residues and methylation by S-adenosyl methionine (Arnison et al. 2013). There are various structural classes of RiPPs, like thiopeptides, lasso-peptides, and lanthipeptides (Montalbán-López et al. 2021). The well-known RiPPS produced are nisin from *Lactococcus lactis* and thiostrepton from *Streptomyces azureus* (de Arauz et al. 1993; Mocek et al. 1993).
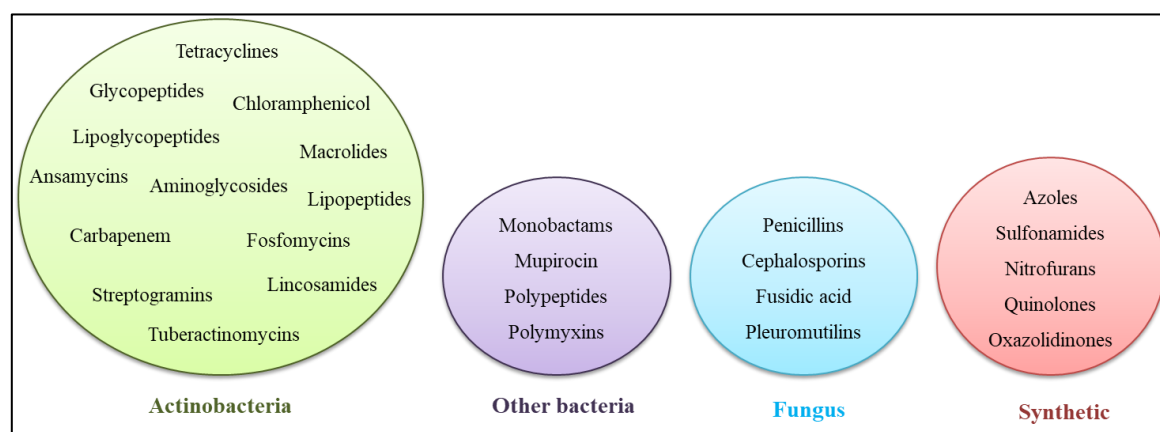
Figure 4. Clinically significant class of antibiotics from microbial and synthetic sources (Hutchings et al. 2019)

The different biosynthetic pathways and modifying tailoring enzymes have produced around 23,000 microbial secondary metabolites, of which over 10,000, i.e. 44%, are produced exclusively by actinobacteria. Fungal species produce 8,600, i.e., 38% of secondary metabolites; the remaining 4,400, i.e., 19%, are produced by non-filamentous eubacteria (Abdel-Razek et al. 2020). The actinobacteria group always inspires the search for novel molecules due to its large reservoir of diverse chemo-structural secondary metabolites.

2.3 Actinobacteria

Actinobacteria are Gram-positive, aerobic, and spore-producing filamentous bacteria having a considerable high levels of guanine plus cytosine (G+C) content in the genome (Ventura et al. 2007). They are ubiquitously distributed in natural ecosystems with a population density of 10^6 to 10^9 cells in a gram of soil. The growth of actinobacteria is initially by tip extension followed by branching of the hyphae, which has given name "*Actinomycetes*" derived from the Greek "atkis" (a ray) and "mykes" (fungus). It is considered as a transition between bacteria and fungi (Goodfellow and Williams, 1983). Although Actinobacteria forms a mycelium network like fungi, they are more closely assocciated to bacteria based on their cell morphology. The actinobacteria features closely related to bacteria are chromosome organized in prokaryotic nucleoid, cell wall with peptidoglycan composition and susceptibility to antibacterial compounds (Barka et al. 2016, Das et al. 2008).

Actinomycetales is an order of Actinobacteria, possessing substrate hyphae and forms aerial mycelia. Under favourable conditions, actinobacteria's aerial hypha produces sporophores with significantly distict structures. The spores are resistant to desiccation and can endure for prolonged period of time in the soil in a viable form (Jiang et al. 2016). This stage of the life cycle gives resistance to unfavorable environmental factors in soil including limited water and nutrient availability. Production of bioactive secondary metabolites like antibiotic, antifungal, anticancer, insecticidal, and antiviral compounds are linked to the initiation of sporulation (Barka et al. 2016, Berdy 2005).
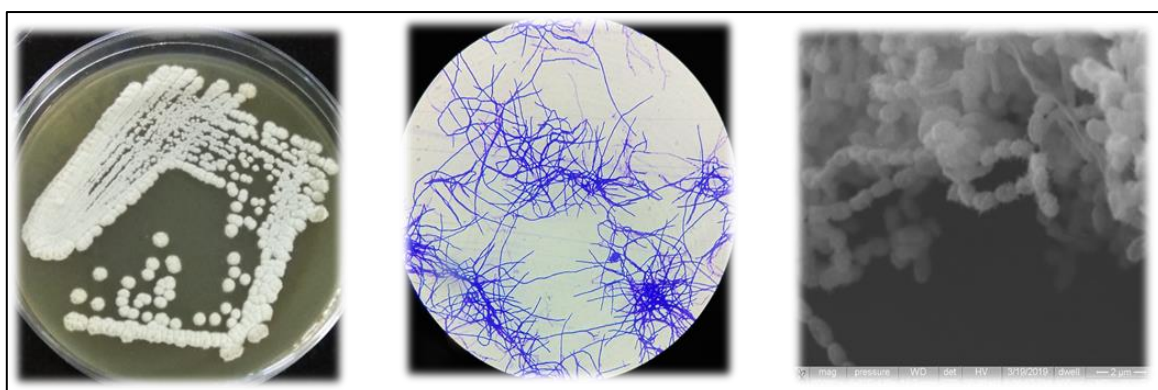
Figure 5. Morphology and microscopy of actinobacteria (a. Growth morphology, b. Gram-staining of mycelia, c. SEM image of spores (adapted from present work)
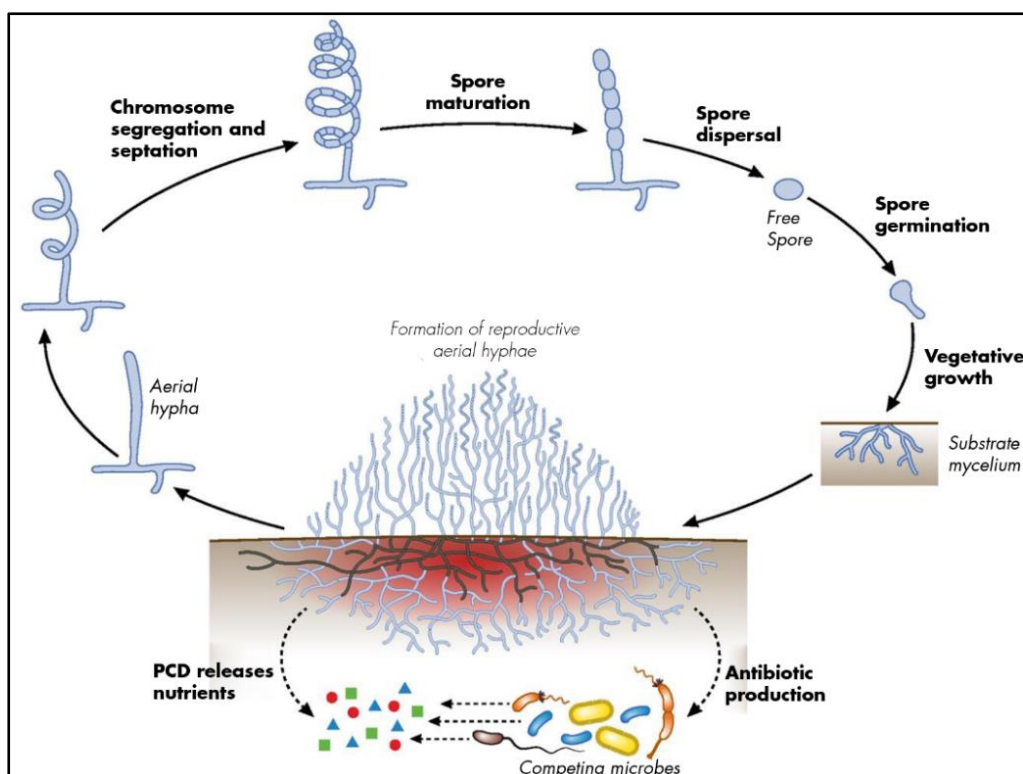
Figure 6. Developmental life cycle of sporulating actinobacteria (Meij *et al.* 2017)

The lifecycle of actinobacteria starts with the germination of a spore by forming germ tubes. The germ tubes develop into hyphae by branching and tip extension, leading to the establishment of a hyphal network and forming the vegetative mycelium. In case of stress, such as nutrient depletion, the part of mycelium is sacrificed by autolytic degradation via programmed cell death (PCD). The nutrients are released in surroundings through PCD and will be used for aerial hyphae and spores formation. The antibiotic production coincides with the onset of cell differentiation, which protects against competing microorganisms attracted by the nutrients released during PCD (Meij *et al.* 2017).

Actinobacteria are particularly interesting since they are phenotypically highly diverse and produce various bioactive compounds (Bredholt et al. 2008). They have the potential to tackle the emerging multidrug-resistant pathogens since approximately two thirds of all reported antibiotics are produced by these actinobacteria. The *Actinobacteria* phylum has six classes, sixteen orders, 39 families and 130 genera (Ventura et al. 2007). The most pharmaceutically significant genera are *Streptomyces* (873 species), *Micromonospora* (120 species), *Amycolatopsis* (96 species), *Actinoplanes* (52 species) and *Saccharopolyspora* (40 species). The *Streptomyces* genus has produced numerous compounds that had a profound impact due to their use in biotechnology, medicine and agriculture. The discovery of

avermectins from *S. avermitilis* (El-Saber Batiha et al. 2020) and streptomycin from *S. griseus* (Woodruff et al. 2014) has led to the Nobel Prize. In addition, the other essential anticancer compound glycopeptide bleomycin, was a product of *Streptomyces verticillus* (Blum et al. 1973) and the first lipopeptide antibiotic, daptomycin, was isolated from *Streptomyces roseosporus* (Tedesco and Rybak, 2004). Of the 10,000 bioactive compounds produced by filamentous actinobacteria, 7600 (75%) are derived from the single genus of *Streptomyces* and 2500 (25%) are from rare actinobacteria like *Actinomadura, Micromonospora, Saccharopolyspora* and *Amycolatopsis* (Berdy, 2005). Actinobacteria produces various secondary metabolites because of the functioning of multiple biosynthetic gene clusters like polyketide synthase and non-ribosomal peptide synthetase (Lee et al. 2014; Salomon et al. 2004). In a typical actinobacteria, about 5% of the genome (23–30 gene clusters) is involved in biosynthesis of secondary metabolism (Ikeda et al. 2003).
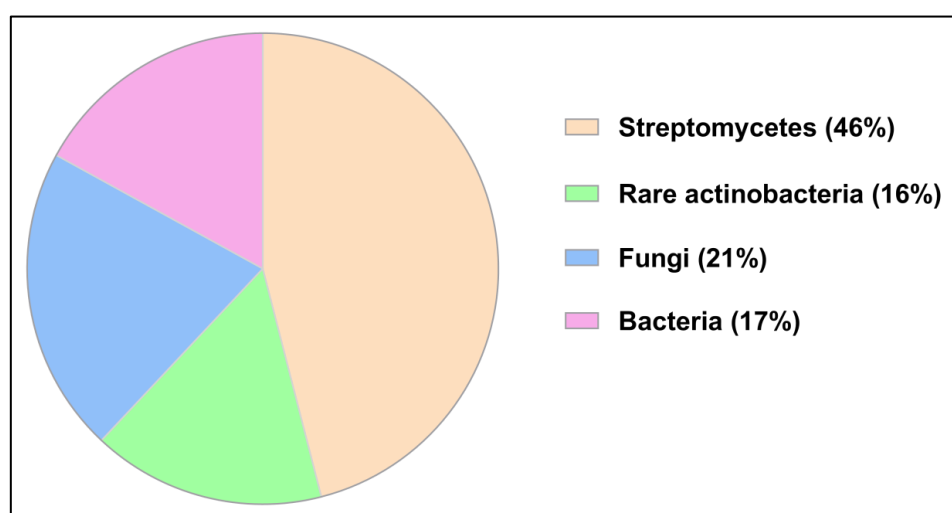
Figure 7. Microbial source of antibiotics (adapted from Ding et al. 2019)

2.4 Rare Actinobacteria

In recent years, it has been very crucial to discover new antibiotics because of the rising incidence of bacterial resistance. The continuous research and rediscovery of known compounds from *Streptomyces* species has shifted the focus of screening programs from *Streptomyces* to the non-*Streptomyces* group, also known as rare actinobacteria (Parra et al. 2023). The noteworthy capability of rare actinobacteria to produce antibiotics has drawn a lot of attention. Numerous effective antibiotics are produced by rare actinobacteria which include gentamicin by *Micromonospora purpurera,* teicoplanin by *Actinoplanes*

teichomyceticus, erythromycin by *Saccharopolyspora erythraea*, and rifamycins by *Amycolatopsis mediterranei* (Table 1). In the past 20 years, the percentage of antibiotics bio-synthesized by rare actinobacteria has risen to 25–30% of all known antibiotics (Tiwari et al. 2012). As a result, rare actinombacteria have emerged as a possible source for isolation of novel molecules with higher antimicrobial activity. Compared to *Streptomyces,* rare actinomycetes have a smaller population and a slower growth rate. They also possess distinctive physiological properties and require unusual growth conditions. Isolating rare actinobacteria from soil or other sources is more challenging than *Streptomyces* (Ding et al. 2019). Because of this, studies on the secondary metabolites of rare actinobacteria are less common compared to *Streptomyces*, making rare actinobacteria an important source for the discovery of novel antibiotics.

Table 1. Clinically used antibiotics produced by rare actinobacteria

Producing organism	Antibiotics	Class	References
Actinoplanes teichomyceticus	Teicoplanin	Glycopeptide	Parenti et al. 1978
Dactylosporangium aurantiacum	Fidaxomicin	Macrolide	Parenti et al. 1975
Micromonospora purpurera	Gentamicin	Aminoglycoside	Weinstein et al. 1963
Amycolatopsis rifamycinica	Rifamycin	Ansamycin	Sensi et al. 1959
Amycolatopsis orientalis	Vancomycin	Glycopeptide	McCormick et al. 1955
Saccharopolyspora erythraea	Erythromycin	Macrolide	McGuire et al. 1952

2.5 *Amycolatopsis* genus

Amycolatopsis, considered a rare actinobacteria, belongs to the Pseudonocardiaceae family and *Actinomycetia* class. The *Amycolatopsis* genus was first mis-identified as *Streptomyces*, later named as *Nocardia*, and in 1986 it was recognized finally as *Amycolatopsis* (Lechevalier et al. 1986). *Amycolatopsis* is nocardioform *Actinomycetes* without mycolic acids in cell wall and possessing type IV cell wall composition. The species of *Amycolatopsis* genus are aerobic to facultative anaerobic. It can form branching substrate hyphae with square or rod-shaped fragment elements (Sangal et al. 2018). So far, 96 species of *Amycolatopsis* have been identified (https://lpsn.dsmz.de/genus/amycolatopsis) from a variety of environments, including soils, freshwater, plants, clinical and ocean sediments. The genus *Amycolatopsis* is

well-known for the multiple commercial antibiotics production, including the medicinally important antibiotics rifamycin and vancomycin (Sangal et al. 2018). Vancomycin was isolated in 1950 from *Amycolatopsis orientalis* (previously classified as *S. orientalis*) and was approved in 1958 for Gram-positive bacterial infections treatment by US Food and Drug Administration (Levine, 2006). In 1957, the rifamycins were isolated from *Amycolatopsis mediterranei* (earlier recognized as *Streptomyces mediterranei* and later *Nocardia mediterranei).* Rifamycin B was the only compound from the five-compound complex isolated in pure form and moderately active against bacterial infections (Song et al. 2021; Sensi, 1983). Later, rifamycin SV was semi-synthesized from rifamycin B and was significantly active against *M. tuberculosis.* Rifamycin SV was the first antimicrobial that targeted RNA polymerase (Sensi, 1983).

Table 2. Secondary metabolites from species of *Amycolatopsis* genus

Species	Novel compounds	Bioactivity	References
Amycolatopsis sp. MST-135876	Suertides A–C	Antibacterial	Lacey et al. 2022
Amycolatopsis sp. DEM30355	Tatiomicin	Antibacterial	Kepplinger et al. 2022
Amycolatopsis hippodromi	Amycolasporins A−C	Antibacterial	Jin et al. 2020
Amycolatopsis sp. 26–4	Thioamycolamides A–E	Bioactivity not reported	Pan et al. 2020
Amycolatopsis sp. IRD-009	Pradimicin-IRD	Antibacterial	Bauermeister et al. 2019
Amycolatopsis sp. K16-0194	Dipyrimicin A and B	Antifungal Antibacterial	Izuta et al. 2018
Amycolatopsis sp. ML1-hF4	Valgamicin C, A,T and V	Bioactivity not reported	Hashizume et al. 2018
Amycolatopsis sp. HCa4	Rifamorpholines A–E (Bioactive Rifamorpholines B and D)	Antibacterial	Xiao et al. 2017
Amycolatopsis	Amycolamycin A- B	Bioactivity not	Ma et al. 2017

sp. HCa4		reported	
Amycolatopsis alba DSM 44262.	Two new sesquiterpenes and one new ansamycin	Bioactivity not reported	Li et al. 2017
Amycolatopsis sp. M39	Macrotermycin A–D (Macrotermycin A active)	Antibacterial Antifungal	Beemelmanns et al. 2017
Amycolatopsis sp. ICBB 8242	Apoptolidin A	Bioactivity not reported	Sheng et al. 2015
Amycolatopsis sp. LZ149	Siderochelin A and D-F	Bioactivity not reported	Chun-Hua et al. 2015
Amycolatopsis sp. HCa1	Actinotetraose L	Bioactivity not reported	Guo et al. 2015
A. alba var. nov. DVR D4	pyridinium	Antibacterial	Dasari et al. 2012
Amycolatopsis sp. HCa1	Amycomycin A-B	Bioactivity not reported	Guo et al. 2012
Amycolatopsis sp. HCa1	Methyltetrangomycin	Bioactivity not reported	Guo et al. 2011
A. fastidiosa MA7332	Thiazomycins and thiazolyl peptides	Antibacterial	Zhang et al. 2009
Amycolatopsis sp. ML1-hF4	Pargamicin-A	Antibacterial	Igarashi et al. 2008
Amycolatopsis strain 17128	Mutactimycin E	Antibacterial	Hopp et al. 2008
Amycolatopsis fastidiosa	Thiazomycin	Antibacterial	Jayasuriya et al. 2007
Amycolatopsis sp. SANK 60206	A-102395	Inhibitor for bacterial translocase I	Murakami et al. 2007
Amycolatopsis sp. ML630-mF1	Kigamicins	Antibacterial antitumor	Kunimoto et al. 2003

Amycolatopsis sp. ST 101170	Vancoresmycin	Antibacterial	Hopmann et al. 2002
Amycolatopsis sp. NNO 21702	Trigloside	Bioactivity not reported	Breinholt et al. 1998
Amycolatopsis sp. MJ347-81 F4	MJ347-81F4 A-B	Antibacterial	Sasaki et al. 1998
Amycolatopsis sp. MK299-95F4	Epoxyquinomicins A-D	Weak antibacterial	Matsumoto et al. 1997
Amycolatopsis sp. X16735	XR651	Interleukin -1 inhibitor	Bahl et al. 1997
Amycolatopsis sp. MK299-95F4	Epoxyguinomicins A-B	Moderate antibacterial	Tsuchida et al. 1996
Amycolatopsis sp. MJ950-89F4	Ochracenomicins A-C	Antibacterial	Igarashi et al. 1995
Amycolatopsis sp. MJ126-NF4	Azicemicins A-B	Moderate antibacterial	Tsuchida et al. 1995
Amycolatopsis sp. MI481-42F4	Amythiamicins A-D	Antibacterial	Shimanaka et al. 1994
Amycolatopsis sp. Y-86,21022	Balhimycin	Antibacterial	Nadkarni et al. 1994
Amycolatopsis mediterranei	Homorifamycin W	Bioactivity not reported	Wang et al. 1994
Amycolatopsis sp.	Amidenin	Plant growth-regulator	Kanbe et al. 1993
A. orientalis No. Q427-8	Quartromicin	Anti-viral	Tsunakawa et al. 1992
A. mediterranei MI710-51F6	Dethymicin	Immuno-suppressant	Ueno et al. 1992
Amycolatopsis	MM 55268 and MM	Antibacterial	Box et al. 1991

sp. NCIB 40089	55266		
A. orientalis NCIB 12608	MM 47761 and MM 47921	Antibacterial	Box et al. 1990
Amycolatopsis orientalis	LY264826	Antibacterial	Rolston et al. 1990
A. orientalis ATCC 53550	UK-69,753	Antibacterial	Jefson et al. 1989
Amycolatopsis sp. MG398 hF9	Octacosamicins A-B	Antifungal	Dobashi et al. 1988
Amycolatopsis sp.	Chloroorienticins	Antibacterial	Tsuji et al. 1988
A. orientalis M43-05865	M43 Antibiotics	Antibacterial	Nagarajan et al. 1988

More recently, other bioactive molecules like suertides A–C (Lacey et al. 2022), amycolasporins (Jin et al. 2020), pradimicin (Almeida et al. 2019), pargamicins B–D (Hashizume et al., 2017), macrotermycins A–D (Beemelmanns et al., 2017), and rifamorpholines A–E (Xiao et al., 2017) have been purified from various species of *Amycolatopsis*. Overall, around 159 novel compounds have been isolated in last three decades from species of *Amycolatopsis* inhabiting soil, plants, lichen, insects, and marine system (Table 2). The species from *Amycolatopsis* genus with 12 antibiotics are *A. orientalis*, followed by *A. mediterranei* with 5 antibiotics, and *A. sulphurea* with 3 antibiotics. These compounds are polyketides, macrolides, polyphenols, glycopeptides, cyclic peptides, sesquiterpenes, and glycoside derivatives. Forty-five compounds from the genus of *Amycolatopsis* displayed bioactivities like antimicrobial, anticancer, enzyme inhibition and antioxidant (Song et al. 2021).

The sequencing and characterisation of bacterial genomes have increased exponentially in recent years with the advancements in next-generation sequencing (NGS). According to the publicly available genome sequences, the *Amycolatopsis* has relatively large genomes in the form of circular chromosome, ranging from approximately 5.62 Mb (*A. granulosa*) to 10.94 Mb (*A. anabasis*), with a median genome size of 9.08 Mb. The median DNA GC content of genus *Amycolatopsis* is 70.1%, ranging from 67.8% (*A. palatopharingis*) to 72.7% (*A. arida*) (Kisil et al. 2021; Adamek et al. 2018).
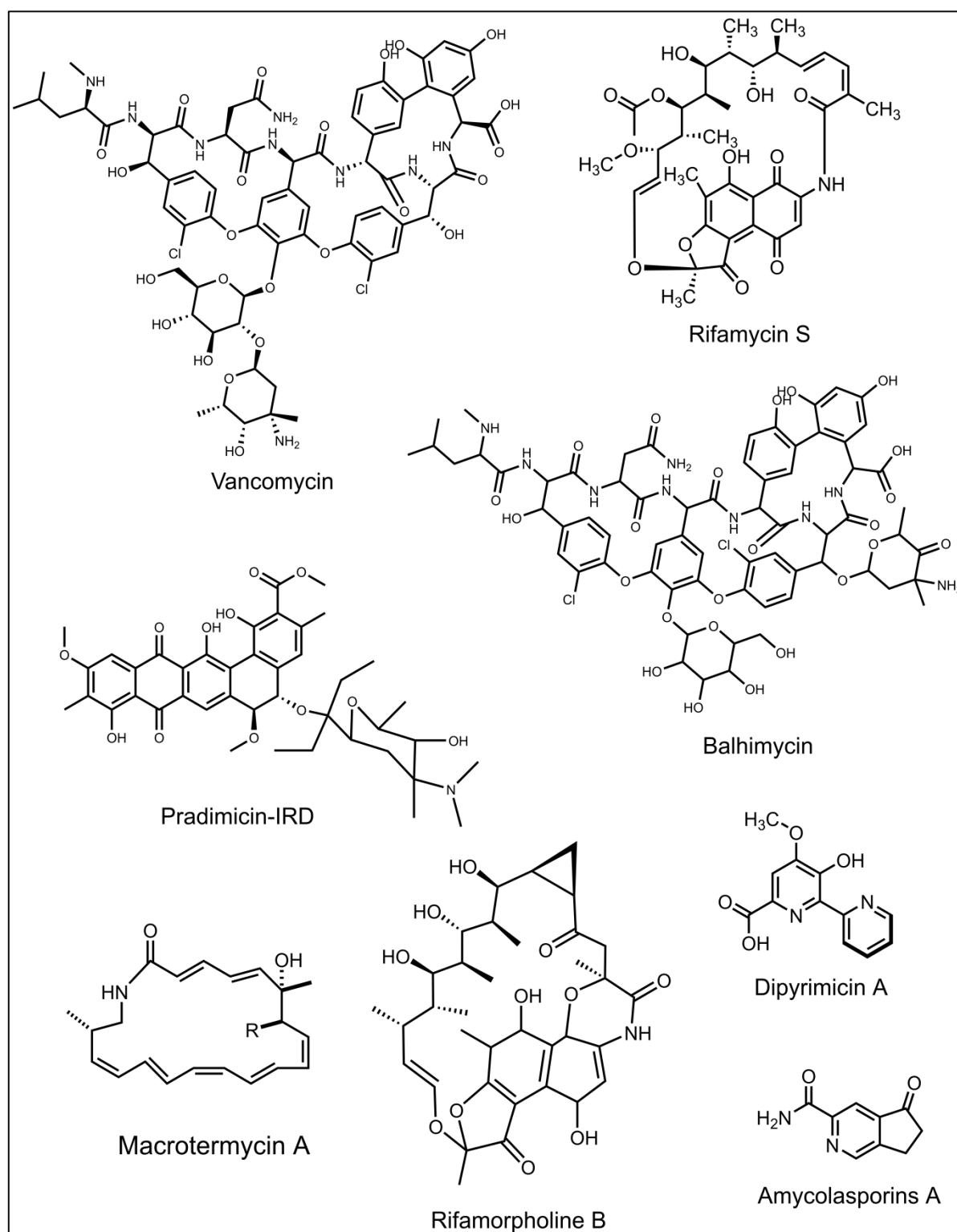
Figure 8. Structural diversity of bioactive secondary metabolites from species of *Amycolatopsis* genus (adapted from Kisil et al. 2018)

Based on the analysis of these genomes, the numbers of cryptic biosynthetic gene clusters (BGCs) present in *Amycolatopsis* strains are far higher than previously thought. The MIBiG (Minimum Information about a Biosynthetic Gene cluster) repository has a compilation of eleven BGCs from *Amycolatopsis* (Medema et al. 2015). Additionally, a more thorough assessment of microbial biosynthetic potential is made possible by the increased quantity of novel genome sequences that are accessible in public databases (Colston et al., 2014). These strains can produce several other secondary metabolites and can be exploited for various biotechnological applications (Sanchez-Hidalgo et al. 2018).

Conclusion

Antimicrobial resistance has become a global concern and demands the immediate development of novel antibiotics. There are different sources to tackle the antimicrobial resistance like natural products, nanoparticles, bacteriophage therapy, synthetic and derivatized molecules. With the limitations of other therapies, natural products still remains the major source of antimicrobial compounds. Of all NPs, the actinobacteria group have been explored with the highest number of antibiotics. With the rediscovery of known molecules from the most common *Streptomyces* genus, the rare actinobacteria has gained tremendous interest in isolating novel molecules. The review of *the Amycolatopsis* genus has shown its potential to produce novel molecules with various biological activities. The molecule with structural variations produced from the species of *Amycolatopsis* genus includes polyketides, glycopeptides, macrolides, cyclic peptides, sesquiterpenes, and glycoside derivatives. The isolation of new bioactive compounds from species of *Amycolatopsis* genus and study of their mode of action can help discover new drugs in the healthcare sector.

Organization of thesis

The current thesis is organized into five chapters. **The first chapter** includes introduction of antimicrobial resistance (AMR), its global impact on human health, and strategies to tackle this problem. The bioactive potentials of actinobacteria are discussed with more emphasis on rare actinobacteria, *Amycolatopsis* and its bioactive compounds. Further, naphthoquinones, its biosynthetic pathway and biological activities have been reported. At the end, the scope and objectives of research are discussed. **The second chapter** involves the screening and identification of the bioactive compounds producing actinobacteria. Further, the potential antimicrobial actinobacteria was subjected to genome sequencing, and biosynthetic gene cluster was analyzed for the bioactive compounds.

The third chapter covers the fermentation and bioactivity-guided purification of the compounds from *Amycolatopsis* sp. using chromatographic techniques. The structural elucidations of purified compounds were determined by NMR spectroscopy, HR-MS and single-crystal XRD. **The fourth chapter** deals with the antibacterial activity, MIC determination and probable mode of action of Enceleamycin A. Further, the anticancer study and the mode of action of Enceleamycin A were evaluated. The *in silico* physicochemical and pharmacokinetics of these compounds were also examined. **The fifth chapter** summarises the overall thesis findings and covers the work's future direction.

Statement of the problem

Antimicrobial resistance has become a global threat as the rapid growth of antibiotic resistant bacteria endangers the efficacy of present antibiotics. Novel antibiotics are required to combat the high level of antimicrobial resistance. There is also a need for novel anticancer drugs due to the increase in the number of cancer deaths and resistance towards the known cancer drugs. The species of *Amycolatopsis* genus are considered as the repository of novel compounds and its exploration under different growth conditions can help in the isolation of novel bioactive compounds.

Objectives

1. Screening and identification of bioactive compound producing actinobacteria
2. Production, purification and structural elucidation of the isolated purified compounds
3. Bioactivity study of Enceleamycins A-C and *N*-hydroxypyrazinone acid

References

Abdel-Razek AS, El-Naggar ME, Allam A, Morsy OM, Othman SI (2020) Microbial Natural Products in Drug Discovery. *Processes* 8:470.

Kepplinger B, Mardiana L, Cowell J, Morton-Laing S, Dashti Y, Wills C, Marrs ECL, Perry JD, Gray J, Goodfellow M, Errington J, Probert MR, Clegg W, Bogaerts J, Herrebout W, Allenby NEE, Hall MJ (2022) Discovery, isolation, heterologous expression and mode-of-action studies of the antibiotic polyketide tatiomicin from Amycolatopsis sp. DEM30355. Sci Rep 12:15579.

Hopp DC, Rabenstein J, Rhea J, Smith C, Romari K, Clarke M, Francis L, Irigoyen M, Milanowski D, Luche M, Carr GJ, Mocek U (2008) Mutactimycin E, a new anthracycline antibiotic with gram-positive activity. J Antibiot 61:675-679.

Adamek M, Alanjary M, Sales-Ortells H, Goodfellow M, Bull AT, Winkler A, Wibberg D, Kalinowski J, Ziemert N (2018) Comparative genomics reveals phylogenetic distribution patterns of secondary metabolites in *Amycolatopsis* species. *BMC Genomics* 19:426.

Almeida LC, Bauermeister A, Rezende-Teixeira P, Santos EAD, Machado-Neto JA, Costa-Lotufo LV(2019) Pradimicin-IRD exhibits antineoplastic effects by inducing DNA damage in colon cancer cells. *Biochem Pharmacol* 168:38-47.

Álvarez-Martínez FJ, Barrajón-Catalán E, Herranz-López M, Micol V (2021) Antibacterial plant compounds, extracts and essential oils: An updated review on their effects and putative mechanisms of action. *Phytomedicine* 90:153626.

Anjum K, Abbas SQ, Shah SA, Akhter N, Batool S, Hassan SS (2016) Marine Sponges as a Drug Treasure. *Biomol Ther (Seoul)* 24:347-362.

Arnison PG, Bibb MJ, Bierbaum G, Bowers AA, Bugni TS, Bulaj G, Camarero JA, Campopiano DJ, Challis GL, Clardy J, Cotter PD (2013) Ribosomally synthesized and post-translationally modified peptide natural products: overview and recommendations for a universal nomenclature. *Nat Prod Rep* 30:108-160.

Atanasov AG, Zotchev SB, Dirsch VM, International Natural Product Sciences Taskforce, Supuran CT (2021) Natural products in drug discovery: advances and opportunities. *Nat Rev Drug Discov* 20:200–216.

Bahl S, Martin S, Rawlins P, Sadeghi R, Smith PM, Steel J, Shanu-Wilson P, Wood KA, Wrigley SK (1997) XR651, a novel naphthacene-5,12-dione. *J Antibiot* 50:169-171.

Barka EA, Vatsa P, Sanchez L, Gaveau-vaillant N, Jacquard C, Klenk HP, Clément C, Ouhdouch Y, van Wezel GP (2016) Taxonomy, physiology, and natural products of actinobacteria. *Microbiol Mol Biol Rev* 80:1–43.

Bauermeister A, Calil FA, das C L Pinto F, Medeiros TCT, Almeida LC, Silva LJ, de Melo IS, Zucchi TD, Costa-Lotufo LV, Moraes LAB (2019) Pradimicin-IRD from *Amycolatopsis* sp. IRD-009 and its antimicrobial and cytotoxic activities. *Nat Prod Res* 33:1713-1720.

Beemelmanns C, Ramadhar TR, Kim KH, Klassen JL, Cao S, Wyche TP, Hou Y, Poulsen M, Bugni TS, Currie CR, Clardy J (2017) Macrotermycins A-D, Glycosylated Macrolactams from a Termite-Associated *Amycolatopsis* sp. M39. *Org Lett* 19:1000-1003.

Berdy J (2005) Bioactive microbial metabolites. *J. Antibiot* 58:1.

Blair JM, Richmond GE, Piddock LJ (2014) Multidrug efflux pumps in Gram-negative bacteria and their role in antibiotic resistance. *Future Microbiol* 9:1165–1177.

Blair JM, Webber MA, Baylay AJ, Ogbolu DO, Piddock LJ (2015) Molecular mechanisms of antibiotic resistance. *Nat Rev Microbiol* 13:42–51.

Blum RH, Carter SK, Agre K (1973) A clinical review of bleomycin—a new antineoplastic agent. *Cancer* 31:903-914.

Box SJ, Coates NJ, Davis CJ, Gilpin ML, Houge-Frydrych CS, Milner PH (1991) MM 55266 and MM 55268, glycopeptide antibiotics produced by a new strain of *Amycolatopsis*. Isolation, purification and structure determination. *J Antibiot* 44:807-813.

Box SJ, Elson AL, Gilpin ML, Winstanley DJ (1990) MM 47761 and MM 49721, glycopeptide antibiotics produced by a new strain of *Amycolatopsis orientalis*. Isolation, purification and structure determination. *J Antibiot* 43:931-937.

Bredholt H, Fjærvik E, Johnsen G, Zotchev SB (2008) Actinomycetes from sediments in the Trondheim fjord, Norway: diversity and biological activity. *Marine drugs* 6:1.

Breinholt, J. (1998). Trigloside: a new tigloylated tetrasaccharide from *Amycolatopsis* sp. *Acta Chem Scand* 52:1239-1242.

Chandran H, Meena M, Barupal T, Sharma K (2020) Plant tissue culture as a perpetual source for production of industrially important bioactive compounds. *Biotechnol Rep (Amst)* 26:e00450.

Chow JW, Shlaes DM (1991) Imipenem resistance associated with the loss of a 40 kDa outer membrane protein in Enterobacter aerogenes. *J Antimicrob Chemoth* 28:499–504.

Coates AR, Halls G, Hu Y (2011) Novel classes of antibiotics or more of the same? *Br J Pharmacol* 163:184-94.

Coculescu BI (2009) Antimicrobial resistance induced by genetic changes. *J Med Life* 2:114–123.

Colston SM, Fullmer MS, Beka L, Lamy B, Gogarten JP, Graf J (2014) Bioinformatic genome comparisons for taxonomic and phylogenetic assignments using *Aeromonas* as a test case. *mBio* 5:e02136.

Cornaglia G, Mazzariol A, Fontana R, Satta G (1996) Diffusion of carbapenems through the outer membrane of enterobacteriaceae and correlation of their activities with their periplasmic concentrations. *Microb Drug Resist* 2:273–276.

Cortes J, Haydock SF, Roberts GA, Bevitt DJ, Leadlay PF (1990) An unusually large multifunctional polypeptide in the erythromycin-producing polyketide synthase of *Saccharopolyspora erythraea*. *Nature* 348:176.

Cox G, Wright GD (2013) Intrinsic antibiotic resistance: mechanisms, origins, challenges and solutions. *Int J Med Microbiol* 303:287–292.

Das A, Khosla C (2009) Biosynthesis of aromatic polyketides in bacteria. *Acc Chem Res* 42:631-639.

Das S, Lyla PS, Ajmal Khan S (2008) Characterization and identification of marine actinomycetes-existing systems, complexities and future directions. *Natl Acad Sci Lett* 31:149-160.

Dasari VR, Muthyala MK, Nikku MY, Donthireddy SR (2012) Novel Pyridinium compound from marine actinomycete, *Amycolatopsis* alba var. nov. DVR D4 showing antimicrobial and cytotoxic activities in vitro. *Microbiol Res* 167:346-351.

de Arauz LJ, Jozala AF, Mazzola PG, Penna TC (2009) Nisin biotechnological production and application: a review *Trends Food Sci Technol* 20:146-54.

de Kraker ME, Stewardson AJ, Harbarth S (2016) Will 10 Million People Die a Year due to Antimicrobial Resistance by 2050? *PLoS Med* 13:e1002184.

Ding T, Yang LJ, Zhang WD, Shen YH (2019) The secondary metabolites of rare actinomycetes: chemistry and bioactivity. *RSC adv* 9:21964-21988.

Duval RE, Gouyau J, Lamouroux E (2019) Limitations of Recent Studies Dealing with the Antibacterial Properties of Silver Nanoparticles: Fact and Opinion. *Nanomaterials (Basel)* 9:1775.

El-Saber Batiha G, Alqahtani A, Ilesanmi OB, Saati AA, El-Mleeh A, Hetta HF (2020) Avermectin derivatives, pharmacokinetics, therapeutic and toxic dosages, mechanism of action, and their biological effects. *Pharmaceuticals* 13:196.

Founou RC, Blocker AJ, Noubom M, Tsayem C, Choukem SP, Dongen MV, Founou LL (2021) The COVID-19 pandemic: a threat to antimicrobial resistance containment. *Future Sci OA* 7:FSO736.

Gaudelli NM, Long DH, Townsend CA (2015) β-Lactam formation by a non-ribosomal peptide synthetase during antibiotic biosynthesis. *Nature* 520:383.

Goodfellow M, Williams ST (1983) Ecology of actinomycetes. *Annu Rev Microbiol 37:* 189-216.

Guo ZK, Liu SB, Jiao RH, Wang T, Tan RX, Ge HM (2012) Angucyclines from an insect-derived actinobacterium *Amycolatopsis* sp. HCa1 and their cytotoxic activity. *Bioorg Med Chem Lett* 22:7490-7493.

Guo ZK, Wang T, Guo Y, Song YC, Tan RX, Ge HM (2011) Cytotoxic angucyclines from Amycolatopsis sp. HCa1, a rare actinobacteria derived from *Oxya chinensis. Planta Med.* 77:2057-2060.

Guo ZK, Yan W, Tan RX, Ge HM (2015) Actinotetraose L, a new tetrasaccharide derivative isolated from the mycelia of *Amycolatopsis* sp. HCa1. *J Asian Nat Prod Res* 17:1109-1113.

Harvey AL, Edrada-Ebel R, Quinn RJ (2015) The re-emergence of natural products for drug discovery in the genomics era. *Nat Rev Drug Discov* 14:111-129.

Hashizume H, Iijima K, Yamashita K, Kimura T, Wada SI, Sawa R, Igarashi M (2018) Valgamicin C, a novel cyclic depsipeptide containing the unusual amino acid cleonine, and related valgamicins A, T and V produced by *Amycolatopsis* sp. ML1-hF4. *J Antibiot* 71:129-134.

Hashizume H, Sawa R, Yamashita K, Nishimura Y, Igarashi M (2017) Structure and antibacterial activities of new cyclic peptide antibiotics, pargamicins B, C and D, from *Amycolatopsis* sp. ML1-hF4. *J Antibiot* 70:699-704.

Helmy YA, Taha-Abdelaziz K, Hawwas HAE-H, Ghosh S, AlKafaas SS, Moawad MMM, Saied EM, Kassem II, Mawad AMM (2023) Antimicrobial Resistance and Recent Alternatives to Antibiotics for the Control of Bacterial Pathogens with an Emphasis on Foodborne Pathogens. *Antibiotics* 12:274.

Hopmann C, Kurz M, Brönstrup M, Wink J, LeBeller D (2002). Isolation and structure elucidation of vancoresmycin—a new antibiotic from *Amycolatopsis* sp. ST 101170. *Tetrahedron Lett* 43:435-438.

Hutchings MI, Truman AW, Wilkinson B (2019) Antibiotics: past, present and future. *Curr Opin Microbiol* 51:72-80.

Igarashi M, Sasao C, Yoshida A, Naganawa H, Hamada M, Takeuchi T (1995) Ochracenomicins A, B and C, new benz[a]anthraquinone antibiotics from *Amycolatopsis* sp. *J Antibiot* 48:335-7.

Igarashi M, Sawa R, Kinoshita N, Hashizume H, Nakagawa N, Homma Y, Nishimura Y, Akamatsu Y (2008) Pargamicin A, a novel cyclic peptide antibiotic from *Amycolatopsis* sp. *J Antibiot* 61:387-393.

Ikeda H, Ishikawa J, Hanamoto A, Shinose M, Kikuchi H, Shiba T, Ōmura S (2003) Complete genome sequence and comparative analysis of the industrial microorganism Streptomyces avermitilis. *Nat. Biotechnol* 21:526.

Izuta S, Kosaka S, Kawai M, Miyano R, Matsuo H, Matsumoto A, Nonaka K, Takahashi Y, Ōmura S, Nakashima T (2018) Dipyrimicin A and B, microbial compounds isolated from Amycolatopsis sp. K16-0194. *J Antibiot* 71:535-537.

Jayasuriya H, Herath K, Ondeyka JG, Zhang C, Zink DL, Brower M, Gailliot FP, Greene J, Birdsall G, Venugopal J, Ushio M, Burgess B, Russotti G, Walker A, Hesse M, Seeley A, Junker B, Connors N, Salazar O, Genilloud O, Liu K, Masurekar P, Barrett JF, Singh SB (2007) Isolation and structure elucidation of thiazomycin- a potent thiazolyl peptide antibiotic from *Amycolatopsis fastidiosa. J Antibiot* 60:554-564.

Jefson MR, Bordner J, Reese CP, Whipple EB (1989) UK-69,753, a novel member of the efrotomycin family of antibiotics. II. Structure determination and biological activity. *J Antibiot* 42:1610-1618.

Jiang Y, Li Q, Chen X, Jiang C (2016) Isolation and cultivation methods of Actinobacteria. *Actinobacteria-basics and biotechnological applications*, 39-57.

Jiménez C (2018) Marine natural products in medicinal chemistry. *ACS Med Chem Lett* 9:959-961.

Jin Y, Aobulikasimu N, Zhang Z, Liu C, Cao B, Lin B, Guan P, Mu Y, Jiang Y, Han L, Huang X (2020) Amycolasporins and Dibenzoyls from Lichen-Associated *Amycolatopsis hippodromi* and Their Antibacterial and Anti-inflammatory Activities. *J Nat Prod* 83:3545-3553.

Kanbe K, Naganawa H, Okamura M, Sasaki T, Hamada M, Okami Y, Takeuchi T (1993) Amidenin, a new plant growth-regulating substance isolated from *Amycolatopsis* sp. *Biosci Biotechnol Biochem* 57:1261-1263.

Katiyar C, Gupta A, Kanjilal S, Katiyar S (2012) Drug discovery from plant sources: An integrated approach. *Ayu.* 33(1):10-19.

Keller NP (2019) Fungal secondary metabolism: regulation, function and drug discovery. *Nat Rev Microbiol* 17:167-180.

Keller NP (2019) Fungal secondary metabolism: regulation, function and drug discovery. *Nat Rev Microbiol* 17:167-180.

Kisil OV, Efimenko TA, Efremenkova OV (2021) Looking Back to *Amycolatopsis*: History of the Antibiotic Discovery and Future Prospects. *Antibiotics* 10:1254.

Kumar A, Schweizer HP (2005) Bacterial resistance to antibiotics: active efflux and reduced uptake. *Adv Drug Deliver Rev* 57:1486–1513.

Kunimoto S, Lu J, Esumi H, Yamazaki Y, Kinoshita N, Honma Y, Hamada M, Ohsono M, Ishizuka M, Takeuchi T (2003) Kigamicins, novel antitumor antibiotics. I. Taxonomy, isolation, physico-chemical properties and biological activities. *J Antibiot* 56:1004-1011.

Lacey HJ, Chen R, Vuong D, Fisher MF, Lacey E, Rutledge PJ, Piggott AM (2022) Suertides A-C: selective antibacterial cyclic hexapeptides from *Amycolatopsis* sp. MST-135876v3. *J Antibiot* 75:483-490.

Lade H, Kim JS (2021) Bacterial targets of antibiotics in methicillin-resistant Staphylococcus aureus. *Antibiotics* 10:398.

Lechevalier MP, Prauser H, Labeda DP Ruan JS (1986) Two new genera of nocardioform actinomycetes: *Amycolata* gen. nov. and *Amycolatopsis* gen. nov. *Int J Syst Bacteriol* 36:29–37

Lee LH, Zainal N, Azman AS, Eng SK, Goh BH, Yin WF, Ab Mutalib NS, Chan KG (2014) Diversity and antimicrobial activities of actinobacteria isolated from tropical mangrove sediments in Malaysia. *Sci World J*.

Lee NY, Ko WC, Hsueh PR (2019) Nanoparticles in the treatment of infections caused by multidrug-resistant organisms. *Front pharmacol* 10:1153.

Levine DP (2006) Vancomycin: a history. *Clin Infect Dis* 42:S5-12.

Li XM, Li XM, Lu CH (2017) Abscisic acid-type sesquiterpenes and ansamycins from Amycolatopsis alba DSM 44262. *J Asian Nat Prod Res* 19:946-953.

Lin J, Du F, Long M, Li P (2022) Limitations of Phage Therapy and Corresponding Optimization Strategies: A Review. *Molecules* 27:1857.

Lin P, Fu Z, Liu X, Liu C, Bai Z, Yang Y, Li Y (2023) Direct Utilization of Peroxisomal Acetyl-CoA for the Synthesis of Polyketide Compounds in *Saccharomyces cerevisiae*. *ACS Synth Biol* 12:1599-1607.

Llor C, Bjerrum L (2014) Antimicrobial resistance: risk associated with antibiotic overuse and initiatives to reduce the problem. *Ther Adv Drug Saf* 5:229-241.

Loomba PS, Taneja J, Mishra B (2010) Methicillin and Vancomycin Resistant *S. aureus* in Hospitalized Patients. *J Glob Infect Dis* 2:275-283.

Lu CH, Ye FW, Shen YM (2015) Siderochelins with anti-mycobacterial activity from *Amycolatopsis* sp. LZ149. *Chin J Nat Med* 13:69-72.

Ma SY, Xiao YS, Zhang B, Shao FL, Guo ZK, Zhang JJ, Jiao RH, Sun Y, Xu Q, Tan RX, Ge HM (2017) Amycolamycins A and B, Two Enediyne-Derived Compounds from a Locust-Associated Actinomycete. *Org Lett* 19:6208-6211.

Matsumoto N, Tsuchida T, Umekita M, Kinoshita N, Iinuma H, Sawa T, Hamada M, Takeuchi T (1997) Epoxyquinomicins A, B, C and D, new antibiotics from Amycolatopsis. I. Taxonomy, fermentation, isolation and antimicrobial activities. *J Antibiot* 50:900-5.

McCormick MH, McGuire JM, Pittenger GE, Pittenger RC, Stark WM (1955) Vancomycin, a new antibiotic. I. Chemical and biologic properties. *Antibiot annu* 3:606-611.

McCormick MH, McGuire JM, Pittenger GE, Pittenger RC, Stark WM (1955) Vancomycin, a new antibiotic. I. Chemical and biologic properties. *Antibiot annu*, 3:606-611.

McGuire JM, Bunch RL, Anderson RC, Boaz HE, Flynn EH, Powell HM, Smith JW (1952) Ilotycin, a new antibiotic. *Antibiot Chemother (Northfield)* 2:281-293.

Medema MH, Kottmann R, Yilmaz P, Cummings M, Biggins JB, Blin K, de Bruijn I, Chooi YH, Claesen J, Coates RC, Cruz-Morales P, et. al. (2015) Minimum information about a biosynthetic gene cluster. *Nat Chem Biol* 11:625-631.

Miyanaga A, Kudo F, Eguchi T (2018) Protein–protein interactions in polyketide synthase–nonribosomal peptide synthetase hybrid assembly lines. *Nat Prod Rep* 35:1185-1209.

Mizuno CM, Kimes NE, López-Pérez M, Ausó E, Rodriguez-Valera F, Ghai R (2013) A hybrid NRPS-PKS gene cluster related to the bleomycin family of antitumor antibiotics in Alteromonas macleodii strains. *PLoS One* 8:e76021.

Mocek U, Zeng Z, O'Hagan D, Zhou P, Fan LD, Beale JM, Floss HG (1993) Biosynthesis of the modified peptide antibiotic thiostrepton in *Streptomyces azureus* and *Streptomyces laurentii*. *J Am Chem Soc* 115:7992-8001.

Monciardini P, Iorio M, Maffioli S, Sosio M, Donadio S (2014) Discovering new bioactive molecules from microbial sources. *Microb Biotechnol* 7:209-20.

Montalbán-López M, Scott TA, Ramesh S, Rahman IR, Van Heel AJ, Viel JH, Bandarian V, Dittmann E, Genilloud O, Goto Y, Burgos MJ (2021) New developments in RiPP discovery, enzymology and engineering. *Nat Prod Rep* 38:130-239.

Mulani MS, Kamble EE, Kumkar SN, Tawre MS, Pardesi KR (2019) Emerging Strategies to Combat ESKAPE Pathogens in the Era of Antimicrobial Resistance: A Review. *Front Microbiol* 10:539.

Munita JM, Arias CA (2016) Mechanisms of antibiotic resistance. *Virulence mechanisms of bacterial pathogens* 22:481-511.

Murakami R, Fujita Y, Kizuka M, Kagawa T, Muramatsu Y, Miyakoshi S, Takatsu T, Inukai M (2007) A-102395, a new inhibitor of bacterial translocase I, produced by Amycolatopsis sp. SANK 60206. *J Antibiot* 60:690-695.

Murray CJ, Ikuta KS, Sharara F, Swetschinski L, Aguilar GR, Gray A, Han C, Bisignano C, Rao P, Wool E, Johnson SC (2022) Global burden of bacterial antimicrobial resistance in 2019: a systematic analysis. *The Lancet* 399:629-655.

Nadkarni SR, Patel MV, Chatterjee S, Vijayakumar EK, Desikan KR, Blumbach J, Ganguli BN, Limbert M (1994) Balhimycin, a new glycopeptide antibiotic produced by *Amycolatopsis* sp. Y-86,21022. Taxonomy, production, isolation and biological activity. *J Antibiot* 47:334-341.

Nagarajan R, Merkel KE, Michel KH, Higgins HM, Hoehn MM, Hunt AH, Jones ND, Occolowitz JL, Schabel AA, Swartzendruber JK, (1988) M43 antibiotics: methylated vancomycins and unrearranged CDP-I analogs. *J Am Chem Soc* 110:7896-7897.

Nivina A, Yuet KP, Hsu J, Khosla C (2019) Evolution and diversity of assembly-line polyketide synthases: focus review. *Chemical reviews* 119:12524-12547.

Pan C, Kuranaga T, Liu C, Lu S, Shinzato N, Kakeya H (2020) Thioamycolamides A-E, Sulfur-Containing Cycliclipopeptides Produced by the Rare Actinomycete *Amycolatopsis* sp. *Org Lett* 22:3014-3017.

Parenti F, Beretta G, Berti M, Arioli V (1978) Teichomycins, new antibiotics from *Actinoplanes teichomyceticus* nov. Sp I. Description of the producer strain, fermentation studies and biological properties. *J Antibiot* 31:276-283.

Parenti F, Pagani H, Beretta G (1975) Lipiarmycin, a new antibiotic from Actinoplanes I. Description of the producer strain and fermentation studies. *J Antibiot* 28:247-252.

Parra J, Beaton A, Seipke RF, Wilkinson B, Hutchings MI, Duncan KR (2023) Antibiotics from rare actinomycetes, beyond the genus *Streptomyces. Curr Opin Microbiol.* 76:102385.

Pfeifer Y, Cullik A, Witte W (2010) Resistance to cephalosporins and carbapenems in Gram-negative bacterial pathogens. *Int J Med Microbiol* 300:371–379.

Piddock LJ (2006) Clinically relevant chromosomally encoded multidrug resistance efflux pumps in bacteria. *Clin Microbiol Rev* 19:382–402.

Poole K (2005) Efflux-mediated antimicrobial resistance. *J Antimicrob Chemother* 56:20–51.

Prestinaci F, Pezzotti P, Pantosti A (2015) Antimicrobial resistance: a global multifaceted phenomenon. *Pathog Glob Health* 109:309-318.

Ramirez MS, Tolmasky ME (2010) Aminoglycoside modifying enzymes. *Drug Resist Update* 13:151–171.

Redgrave LS, Sutton SB, Webber MA, Piddock LJ (2014) Fluoroquinolone resistance: mechanisms, impact on bacteria, and role in evolutionary success. *Trends Microbiol* 22:438–445.

Reygaert WC (2009) Methicillin-resistant *Staphylococcus aureus* (MRSA): molecular aspects of antimicrobial resistance and virulence. *Clin Lab Sci* 22:115–119.

Reygaert WC (2018) An overview of the antimicrobial resistance mechanisms of bacteria. *AIMS microbiology* 4:482.

Robbel L, Marahiel MA (2010) Daptomycin, a bacterial lipopeptide synthesized by a nonribosomal machinery. *J Biol Chem* 285:27501-27508.

Roberts MC (2004) Resistance to macrolide, lincosamide, streptogramin, ketolide, and oxazolidinone antibiotics. *Mol Biotechnol* 28:47–62

Roberts MC (2005) Update on acquired tetracycline resistance genes. *FEMS Microbiol Lett* 245:195–203.

Robicsek A, Strahilevitz J, Jacoby GA, Macielag M, Abbanat D, Park CH, Bush K, Hooper DC (2006) Fluoroquinolone-modifying enzyme: a new adaptation of a common aminoglycoside acetyltransferase. *Nat Med.* 12:83–88

Rolston KV, Nguyen H, Messer M (1990) In vitro activity of LY264826, a new glycopeptide antibiotic, against gram-positive bacteria isolated from patients with cancer. *Antimicrob Agents Chemother.* 34:2137-2141.

Ross JI, Eady EA, Cove JH, Cunliffe WJ, Baumberg S, Wootton JC (1990) Inducible erythromycin resistance in staphylococci is encoded by a member of the ATP-binding transport super-gene family. *Mol Microbiol* 4:1207–1214

Ruekit S, Srijan A, Serichantalergs O, Margulieux KR, Mc Gann P, Mills EG, Stribling WC, Pimsawat T, Kormanee R, Nakornchai S, Sakdinava C, Sukhchat P, Wojnarski M, Demons ST, Crawford JM, Lertsethtakarn P, Swierczewski BE (2022) Molecular characterization of multidrug-resistant ESKAPEE pathogens from clinical samples in Chonburi, Thailand (2017-2018). *BMC Infect Dis* 22:695.

Ruiz B, Chávez A, Forero A, García-Huante Y, Romero A, Sánchez M, Rocha D, Sánchez B, Rodríguez-Sanoja R, Sánchez S, Langley E (2010) Production of microbial secondary metabolites: regulation by the carbon source. *Crit Rev Microbiol* 36:146-67.

Salomon CE, Magarvey NA, Sherman DH (2004) Merging the potential of microbial genetics with biological and chemical diversity: an even brighter future for marine natural product drug discovery. *Nat Prod Rep* 21:105-121.

Sánchez-Hidalgo M, González I, Díaz-Muñoz C, Martínez G, Genilloud O (2018) Comparative Genomics and Biosynthetic Potential Analysis of Two Lichen-Isolated *Amycolatopsis* Strains. *Front Microbiol* 9:369.

Sangal V, Goodfellow M, Blom J, Tan GYA, Klenk HP, Sutcliffe IC (2018) Revisiting the taxonomic status of the biomedically and industrially important genus *Amycolatopsis*, using a phylogenomic approach. *Front. Microbiol*. 9:2281.

Santajit S, Indrawattana N (2016) Mechanisms of Antimicrobial Resistance in ESKAPE Pathogens. *Biomed Res Int* 2016:2475067.

Sasaki T, Otani T, Matsumoto H, Unemi N, Hamada M, Takeuchi T, Hori M (1998) MJ347-81F4 A & B, novel antibiotics from *Amycolatopsis* sp.: taxonomic characteristics, fermentation, and antimicrobial activity. *J Antibiot* 51:715-721.

Selim MSM, Abdelhamid SA, Mohamed SS (2021) Secondary metabolites and biodiversity of actinomycetes. *J Genet Eng Biotechnol* 19:72.

Sensi P (1983) History of the development of rifampin. *Rev Infect Dis* 5:S402-S416.

Sensi P, AM G, Ballotta R (1959) Rifomycin. I. Isolation and properties of rifomycin B and rifomycin complex. *Antibiot annu* 7:262-270.

Shen B (2003) Polyketide biosynthesis beyond the type I, II and III polyketide synthase paradigms. *Curr Opin Chem Biol* 7:285-295.

Sheng Y, Fotso S, Serrill JD, Shahab S, Santosa DA, Ishmael JE, Proteau PJ, Zabriskie TM, Mahmud T (2015) Succinylated Apoptolidins from *Amycolatopsis* sp. ICBB 8242. *Org Lett* 17:2526-2539.

Sheng, Y., Fotso, S., Serrill, J. D., Shahab, S., Santosa, D. A., Ishmael, J. E., ... & Mahmud, T. (2015). Succinylated apoptolidins from Amycolatopsis sp. ICBB 8242. Organic letters, 17(10), 2526-2529.

Shimanaka K, Kinoshita N, Iinuma H, Hamada M, Takeuchi T (1994) Novel antibiotics, amythiamicins. I. Taxonomy, fermentation, isolation, physico-chemical properties, and antimicrobial activity. *J Antibiot* 47:668-674.

Song Z, Xu T, Wang J, Hou Y, Liu C, Liu S, Wu S (2021) Secondary metabolites of the genus *Amycolatopsis:* Structures, bioactivities and biosynthesis. *Molecules* 26:1884.

Song Z, Xu T, Wang J, Hou Y, Liu C, Liu S, Wu S (2021) Secondary Metabolites of the Genus *Amycolatopsis*: Structures, Bioactivities and Biosynthesis. *Molecules.* 26:1884.

Sun W, Sanderson PE, Zheng W (2016) Drug combination therapy increases successful drug repositioning. *Drug Discov Today* 21:1189-1195.

Süssmuth RD, Mainz A (2017) Nonribosomal peptide synthesis—principles and prospects. *Angew Chem Int Ed* 56:3770-3821.

Tang KWK, Millar BC, Moore JE (2023) Antimicrobial Resistance (AMR). *Br J Biomed Sci.* 80:11387.

Taylor PW (2013) Alternative natural sources for a new generation of antibacterial agents. *Int J Antimicrob Agents* 42:195-201.

Tedesco KL, Rybak MJ (2004) Daptomycin. *Pharmacotherapy.* 24:41-57.

Tiwari K, Gupta RK (2012) Rare actinomycetes: a potential storehouse for novel antibiotics. *Crit Rev Biotechnol* 32:108-132.

Tong SY, Davis JS, Eichenberger E, Holland TL, Fowler VG Jr (2015) *Staphylococcus aureus* infections: epidemiology, pathophysiology, clinical manifestations, and management. *Clin Microbiol Rev* 28:603-661.

Tsuchida T, Sawa R, Takahashi Y, Iinuma H, Sawa T, Naganawa H, Takeuchi T (1995) Azicemicins A and B, new antimicrobial agents produced by Amycolatopsis. II. Structure determination. *J Antibiot* 48:1148-1152.

Tsuchida T, Umekita M, Kinoshita N, Iinuma H, Nakamura H, Nakamura K, Naganawa H, Sawa T, Hamada M, Takeuchi T (1996). Epoxyquinomicins A and B, new antibiotics from Amycolatopsis. *J Antibiot* 49:326-328.

Tsuji N, Kamigauchi T, Kobayashi M, Terui Y (1988) New glycopeptide antibiotics: II. The isolation and structures of chloroorienticins. *J Antibiot* 41:1506-1510.

Tsunakawa M, Tenmyo O, Tomita K, Naruse N, Kotake C, Miyaki T, Konishi M, Oki T (1992) Quartromicin, a complex of novel antiviral antibiotics. I. Production, isolation, physico-chemical properties and antiviral activity. *J Antibiot* 45:180-188.

Ueno M, Iijima M, Masuda T, Kinoshita N, Iinuma H, Naganawa H, Hamada M, Ishizuka M, Takeuchi T (1992) Dethymicin, a novel immunosuppressant isolated from an Amycolatopsis. Fermentation, isolation, physico-chemical properties and biological activities. *J Antibiot* 45:1819-1826.

Van Acker H, Van Dijck P, Coenye T (2014) Molecular mechanisms of antimicrobial tolerance and resistance in bacterial and fungal biofilms. *Trends Microbiol* 22:326–333.

Van der Meij A, Worsley SF, Hutchings MI, van Wezel GP (2017) Chemical ecology of antibiotic production by actinomycetes. *FEMS Microbiol Rev 41:*392-416.

Veeresham C (2012) Natural products derived from plants as a source of drugs. *J Adv Pharm Technol Res* 3:200.

Ventura M, Canchaya C, Tauch A, Chandra G, Fitzgerald GF, Chater KF, van Sinderen D (2007) Genomics of Actinobacteria: tracing the evolutionary history of an ancient phylum. *Microbiol Mol Biol* 71:495-548.

Vézina C, Kudelski A, Sehgal SN (1975) Rapamycin (AY-22, 989), a new antifungal antibiotic I. taxonomy of the producing streptomycete and isolation of the active principle. *J. Antibiot* 28:721.

Wang H, Fewer DP, Holm L, Rouhiainen L, Sivonen K (2014) Atlas of nonribosomal peptide and polyketide biosynthetic pathways reveals common occurrence of nonmodular enzymes. *Proc Natl Acad Sci USA* 111:9259-9264.

Wang NJ, Han BL, Yameshita N, Sato M (1994) 31-Homorifamycin W, a novel metabolite from Amycolatopsis mediterranei. *J Antibiot* 47:613.

Weinstein MJ, Luedemann CM, Oden EM, Wagman CH (1963) Gentamicin, a new broad spectrum antibiotic complex. *Antimicrob Agents Chemother (Bethesda)* 161:1-7.

Wertheim HF, Melles DC, Vos MC, van Leeuwen W, van Belkum A, Verbrugh HA, Nouwen JL (2005) The role of nasal carriage in Staphylococcus aureus infections. *Lancet Infect Dis* 5:751-762.

Woodruff HB (2014) Selman A. Waksman, winner of the 1952 Nobel Prize for physiology or medicine. *Appl Environ Microbiol* 80:2-8.

Worthington RJ, Melander C (2013) Combination approaches to combat multidrug-resistant bacteria. *Trends Biotechnol* 31:177-84.

Wright GD (2019) Unlocking the potential of natural products in drug discovery. *Microb Biotechnol* 12:55-57.

Xiao YS, Zhang B, Zhang M, Guo ZK, Deng XZ, Shi J, Li W, Jiao RH, Tan RX, Ge HM (2017) Rifamorpholines A-E, potential antibiotics from locust-associated actinobacteria *Amycolatopsis* sp. Hca4. *Org Biomol Chem* 15:3909-3916.

Yi HY, Chowdhury M, Huang YD, Yu XQ (2014) Insect antimicrobial peptides and their applications. *Appl Microbiol Biotechnol* 98:5807-22

Zhang C, Herath K, Jayasuriya H, Ondeyka JG, Zink DL, Occi J, Birdsall G, Venugopal J, Ushio M, Burgess B, Masurekar P, Barrett JF, Singh SB (2009) Thiazomycins, thiazolyl peptide antibiotics from *Amycolatopsis fastidiosa. J Nat Prod* 72:841-847.

Zhang F, Cheng W (2022) The mechanism of bacterial resistance and potential bacteriostatic strategies. *Antibiotics* 11:1215.

Zhao L, Chang WC, Xiao Y, Liu HW, Liu P (2013) Methylerythritol phosphate pathway of isoprenoid biosynthesis. *Annu Rev Biochem* 82:497-530.

Zorzet A (2014) Overcoming scientific and structural bottlenecks in antibacterial discovery and development. *Ups J Med Sci* 119:170-175.

Chapter 2

Screening and identification of bioactive compound producing actinobacteria

Screening and identification of bioactive compound producing actinobacteria

Abstract

Actinobacteria are believed to be a potential source of novel compounds to tackle the antimicrobial resistance challenge. The present study aimed to screen the bioactive compound producing actinobacteria in search of novel antimicrobial molecule. In this regard, previously isolated actinobacteria cultures from the Western Ghats, were screened for antimicrobial activity under shaking and static condition using three fermentation media. Out of 57 isolates, 21 displayed antimicrobial bioactivity against at least one of the test strains i.e., *E. coli* NCIM 2065, *S. aureus* NCIM 2127 or *C. albicans* NCIM 3102. Identification by 16S rRNA gene sequencing showed 20 of culture belongs to *Streptomyces* genus whereas one isolate was a rare actinobacteria from *Amycolatopsis* genus. *Amycolatopsis* sp. WGS_07 showed potent activity against *S. aureus* only under static condition and was closely related to *A. silviterrae* for which no bioactivity was reported. The genome sequencing analysis of *Amycolatopsis* sp. WGS_07 displayed presence of biosynthetic gene clusters associated with diverse secondary metabolites.

Graphical abstract
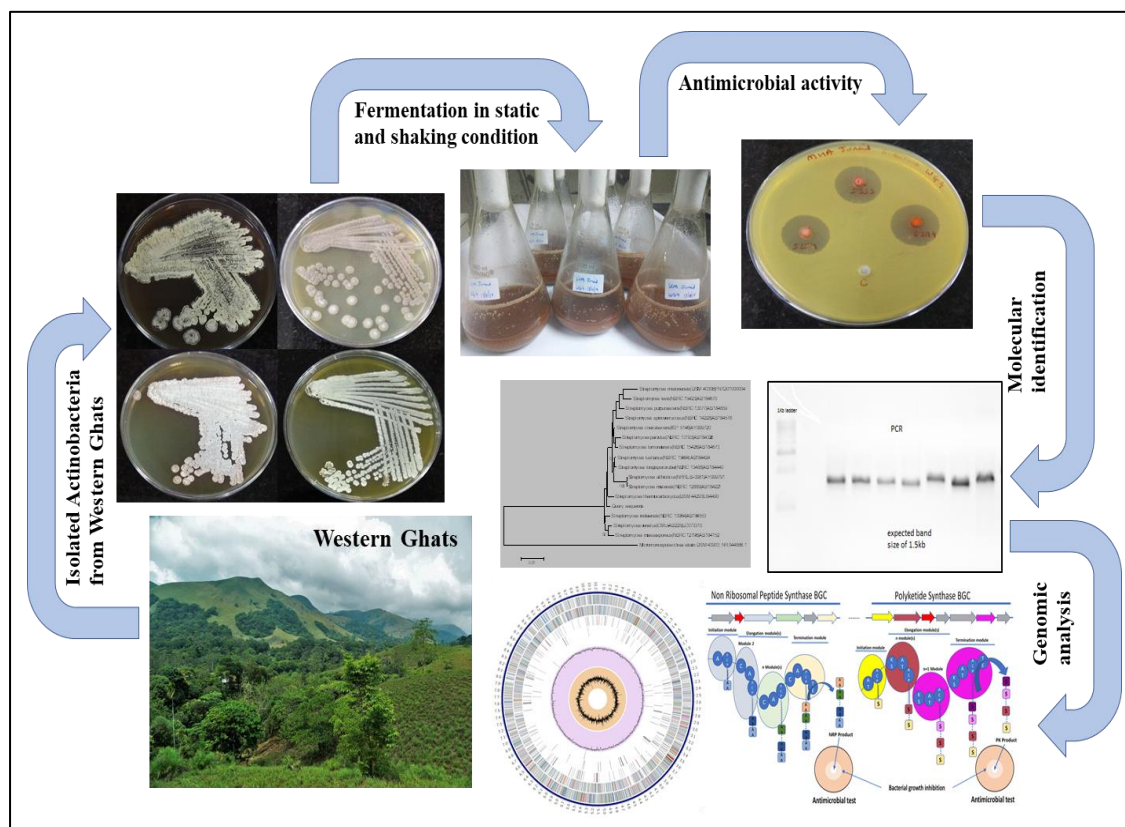
1. Introduction

Antimicrobial resistance (AMR) has become a significant global healthcare issue. The rise of antibiotic-resistant bacteria has led to a situation where antibiotics are no longer effective against the simplest of infections (Ventola, 2015). The resistance to antibiotics are rising by the overuse, misuse and lack of novel antibiotic development (Christaki et al. 2020)**.** Due to the rapid spread of diseases and emergence of antibiotic-resistant pathogens spread, there is an urgent and significant market demand for new antibiotics. Even with the progress in the field of chemical synthesis, nature still remains the most diverse source for novel antimicrobials (Katz and Baltz, 2016). Over the past few decades, the development of antimicrobial drugs has been greatly aided by the use of microbial natural products (Schneider, 2021). Among the microbes, actinobacteria group are the excellent source for antibiotics. They have played a significant role in antimicrobial screening programs because of their diversity and demonstrated capacity to produce new metabolites of therapeutic significance **(**De Simeis and Serra, 2021; Hui et al. 2021). Actinobacteria are spore forming filamentous bacteria widely distributed in natural ecosystems producing approximately two-thirds of existing antibiotics (Barka et al. 2016). Actinobacteria member *Streptomyces* is the prominent producer of bioactive compounds accounting for nearly 75% (Berdy, 2005). However in recent years, with rediscovery of existing compounds from *Streptomyces* species, the programs for screening antimicrobials are focused towards the non-*Streptomyces* group commoly known as rare actinobacteria. Currently, around 50 taxa of rare actinobacteria are known to produce about 2500 bioactive molecules. In the past two decades, the percentage of antibiotics produced by rare actinobacteria has risen to 25–30% of all antibiotics (Ding et al. 2019; Ezeobiora et al. 2022). Rare actinobacteria are crucial in the battle towards multidrug resistant pathogens.

The genome sequencing of actinobacteria indicates the biosynthetic potential of many actinobacteria strains are much higher than actual compounds isolated by fermentation. The cryptic biosynthetic pathways expression in actinobacteria can be elicited using cultivation based approaches in enhancing the chemical diversity (Pettit, 2011). One strain many compounds (OSMAC) approach is a simple aas well as effective method for eliciting metabolic pathways to maximize the secondary metabolite diversity (Romano et al. 2018). The basic concept of this approach is that, while each microbe has the capacity to produce variety of molecules, only specific compounds are produced under particular growth

condition. So, multiple growth conditions can be used to activate new bioactive compounds production by varying the growth parameters such as nutrients, incubation condition, time, temperature, pH, aeration (Yao et al. 2021; Pan et al. 2019; Bode et al. 2002). The cultivation condition of microbe including static or dynamic can directly affect their chemical metabolic process. There are various reports in which fungus have produced various novel metabolites under static condition which was not produced under standard shaking condition (Table 1). The static liquid condition fermentation of marine fungus strain *Aspergillus versicolor* ZLN-60 led to isolation of 4 new prenylated diphenyl ethers and two novel cyclic pentapeptides (Gao et al. 2013; Zhou et al. 2011). The fermentation of fungus *Penicillium* sp. F23-2 under static condition in sea water based medium produced new meleagrin alkaloids, diketopiperazines, and terpenoids (Du et al. 2009).

Table 1. New compounds under static condition fermentation

Culture	New compounds	References
Spicaria elegans KLA03	Nine cytochalasins Z7-Z15, one spicochalasin, five aspochalasins, and three aspochalasin derivatives	Pan et al. 2019; Liu et al. 2006
Aspergillus terreus	Lovastatins and 7-desmethylcitreoviridin	Adpressa and Loesgen, 2016
Rhytidhysteron sp. AS21B	Three spironaphthalenes, rhytidones A–C	Pudhom et al. 2014
Aspergillus versicolor ZLN-60	Four prenylated diphenyl ethers and two cyclic pentapeptides	Gao et al. 2013; Zhou et al. 2011
Penicillium sp. F23-2	Diketopiperazines, terpenoids, and meleagrin alkaloids	Du et al. 2009
Lentinus strigellus	One indole alkaloid echinuline, two prenyl phenols and one anthraquinone fiscione	Zheng et al. 2009
Sphaeropsidales sp. F-24' 707	cladospirones B to I	Bode et al. 2000
Streptomyces sp. CHQ-64	One hybrid isoprenoid alkaloid drimentine I	Che et al. 2016

There is one report in which marine-derived *Streptomyces* sp. CHQ-64 strain under static condition produced one novel hybrid isoprenoid alkaloid other than the polyene-polyols made in liquid shaking condition (Che et al. 2016). The actinobacteria morphologically resembles fungi because of their mycelium and spore forming ability (Reponen et al. 1998). Since the fungi growth in static condition has led to various new secondary metabolites, the screening of actinobacteria under static growth condition can lead to novel molecules.

2. Materials and methods

2.1 Reagents and Kits

The media ingredients used for cultivation and fermentation were purchased from Hi-Media, Mumbai. Ethyl acetate HPLC grade (Hi-media, Mumbai), DNeasy Powersoil pro kit (Qiagen), Qubit® dsDNA HS Assay Kit (Life Technologies), Ligation sequencing kit SQK-LSK 109 and Native barcoding kit NBD114 (Oxford Nanopore Technologies).

2.2 Isolation, maintenance and preservation of actinobacteria

Actinobacteria cultures were previously isolated from the collected soil of Western Ghats, Kerala, India. For the isolation of actinobacteria, a traditional serial dilution method was followed (Siddharth et al. 2020). The dilutions from 10^{-3} to 10^{-9} were spread on different ISP (International *Streptomyces* Project) medium plates with 1.8% agar and incubated at 28°C for 10-15 days. The isolates were further sub-cultured and maintained on ISP-2 (0.4% dextrose, 1% malt extract, 0.4% yeast extract, pH 7.0) plates with 1.8% agar. The glycerol stocks of 25% were made from the cultured actinobacteria in ISP-2 broth and stored at -80°C.

2.3 Screening of the actinobacteria strains for antimicrobial activity

2.3.1 Metabolite production

Actinobacteria cultures were grown on MGYP agar plates (0.3% malt extract, 1% dextrose, 0.3% yeast, 0.5% peptone, and 1.8% agar, pH 7.0) for 7 days at 28°C. The media used for the inoculum preparation i.e. LCM (liquid cultivation medium) and the metabolite production medium i.e. 5333, 5254 and 5294 were adapted from the Compendium of Actinobacteria designed by Dr. Joachim Wink at Sanofi-Aventis (Table 2). For the inoculum preparation, a loopful culture was inoculated in 250 mL Erlenmeyer flask with 50 mL of liquid cultivation medium and incubated at 28ºC for 3 days at 150 rpm on rotary shaker. The inoculum was

check for sterility by light microscopy and 10% v/v was transferred in a 250 mL Erlenmeyer flask, each with 50 ml of fermentation media. The fermentation media used were 5333, 5254 and 5294 and the flasks were incubated in both static and shaking conditions (on a rotary shaker at 150 rpm) for 7 days at 28 °C. The whole broth was extracted by 100 mL of ethyl acetate for 1 hour and the extracted organic phase was separated. Further, it was concentrated under reduced pressure by rotary evaporator at 40ºC temperature. The concentrated crude extract was dissolved to 1.0 mL of ethyl acetate (HPLC grade) for further antimicrobial screening studies.

Table 2. Media used in production of secondary metabolites

Media		Composition (g/L) in distilled water
Liquid cultivation		Soymeal 15.0, Mannitol 15.0, Glucose 4.0, pH 7.0
Metabolite production medium	**5333**	Starch 15.0, Yeast extract 4.0, $MgSO_4$ 0.5, K_2HPO_4 1.0, pH 7.0
	5254	Glucose 15.0, Soymeal 15.0, Corn steep liquor 5.0, $CaCO_3$ 2.0, NaCl 5.0, pH 7.0
	5294	Starch 10.0, Glucose 10.0, Glycerol 10.0, Yeast extract 2.0 , Corn steep liquor 2.5, , Peptone 2.0, $CaCO_3$ 3.0, NaCl 1.0, pH 7.2

https://www.dsmz.de/bacterial-diversity/compendium-of-actinobacteria.html

2.3.2 Antimicrobial activity

Antimicrobial activity of the ethyl acetate crude extract was examined by agar well diffusion method (Balouiri et al. 2016). The bacterial strains of *Escherichia coli* (NCIM 2065)*, Staphylococcus aureus* (NCIM 2127) and yeast strain of *Candida albicans* (NCIM 3102) were used as test organisms for antimicrobial potential of the crude extracts. The $O.D._{625}$ of the test organisms were adjusted to 0.1 with respective broths and 100µl of freshly prepared bacterial test strains were spread on Muller Hinton agar plates and *Candida albicans* on MGYP agar plates. Wells with diameter of 6 mm were punched with sterile borer followed by addition of 50µl of the crude extract and 100µl of cell free supernatant. Ethyl acetate was used as a control. The zone of inhibition was measured after incubating the agar plates with bacteria for 24 hours at 37ºC and with yeast for 48 hours at 30ºC.

2.4 Molecular identification of bioactive actinobacteria

Nucleic acid isolation was done by standard CTAB (Cetyltrimethylammonium bromide) method (Cheng et al. 2006). The culture were streak on ISP-2 agar plates and after 4-6 days of growth a loopful of culture was transferred in 560μl of 1X TE buffer in 2ml eppendorf tube and vortex for 5 minutes. After vortexing, sonication was done and 20μl of lysozyme added, then incubated for one hour at 37°C. Proteinase K and 10% SDS was added, then incubated at 55°C for 2 hours. 5M NaCl and CTAB was added and incubated at 65°C for 10 minutes following with extraction by phenol:chloroform:isoamyl alcohol (25:24:1). Isopropanol used for precipitation of nucleic acid followed by washing of pellet with 70% ethanol. The pellet was dried after centrifugation, and resuspended in 50μl of 1X TE buffer.

Amplification of 16S rRNA gene was performd by PCR (polymerase chain reaction) by universal primer of 27F (5'-AGAGTTTGATCCTGGCTCAG-3') and 1492R (5'-TACCTTGTTACGACTT-3') in a final volume of 50μl, which consisted of genomic DNA: 1μl, molecular grade water: 19μl, Taqara mastermix: 25μl and 2.5μl of forward and reverse primer each (concentration 3.2 picomole). The PCR was conducted with the subsequent cycling parameters: 5 min initial denaturation at 94°C, followed by 34 cycles of denaturation at 94°C for 45 s, annealing at 55°C for 60 s, extension at 72°C for 90 s, and final 10 min extension at 72°C. 5μl of PCR product was examined on 1% agarose gel in 1X TBE buffer. For the purification, equal volume of PEG-NaCl (20% PEG-8000 and 2.5 M NaCl) was mixed with PCR product and incubated for 30 minutes at 37ºC. The incubated PCR product centrifuged at 13000 rpm for 30 min and received pellet was added with 70% of ethanol, then centrifuged at 10000 rpm for 10 min. The pellet was dried and dissolved in 10μl of 1X TE buffer (Cheng et al. 2015). The DNA sequencing was performed on ABI 3500XL genetic analyser. The 16S rRNA gene sequence obtained was searched for closely related species from EzBioCloud database (Yoon et al. 2017).

2.5 Whole genome sequencing, assembly, and annotation

The genomic DNA was isolated from the freshly grown *Amycolatopsis* sp. WGS_07 by using DNeasy Power soil pro kit (Qiagen) as per the manufacturer protocol. The concentration and quality of isolated DNA was examined using 1% agarose gel electrophoresis and NanoDrop Lite spectrophotometer (ThermoFisher Scientific, Q32853) followed by Qubit® fluorometer (ThermoFisher Scientific) by dsDNA high sensitivity (HS) Qubit® assay kit. Afterward, extracted DNA was prepared for Nanopore sequencing. A DNA library was prepared by using 100 ng of extracted DNA with a ligation sequencing kit SQK-LSK 109 and indexed

using Native barcoding kit NBD114. DNA concentration was determined during library preparation with Qubit® dsDNA HS Assay Kit (Life Technologies). The process includes enzymatic steps with minimal magnetic bead-based clean-ups. Further to create 'end-repaired, 5'-phosphorylated, 3'-dA-tailed ds DNA fragments, end repair with A-tailing was carried out. Subsequently, each end-repaired DNA was given a unique identifier with the native barcodes. These indexed samples are then pooled to proceed with the adapter ligation step, followed by the library loading onto the MinION flow cell (FLO-MIN-106D) in an MK1C sequencing platform. The basecalling was performed with high accuracy mode by Guppy v5.0.11 in parallel to the sequencing. The adapters were removed by utilizing Porechop v0.2.4 (https://github.com/rrwick/Porechop) and quality was checked by NanoPlot (De Coster et al., 2018). The genome assembly was done by Flye v2.8.1-b1676 (Kolmogorov et al., 2019). The assembled genome was analysed and annotated by a PATRIC server (Davis et al. 2020) using RAST tool kit (Brettin et al. 2015) pipeline with default setting. Biosynthetic gene cluster related to secondary metabolites were identified by the antiSMASH v7.0 (https://antismash.secondarymetabolites.org) (Blin et al. 2023).

3. Result and Discussion

3.1 Screening of actinobacteria strains for antimicrobial activity

Actinobacteria is considered as the store house of novel antimicrobial compounds (Amaning Danquah et al. 2022). The growth condition like shaking or static incubation and the change in growth media components affects the biosynthesis of secondary metabolites in actinobacteria. The different growth conditions can lead to activation of cryptic biosynthetic gene cluster resulting in production of molecules absent in one growth condition (Romano et al. 2018; Begani et al. 2018). So the screening of actinobacteria plays important role in the selection of potential culture for the fermentation and purification of bioactive compound. In the present screening strategy, the actinobacteria were grown in three different liquid medium under static and shaking incubation condition as well as the antimicrobial activity was screened from both the ethyl acetate extract and the broth supernatant. The antimicrobial activity of the actinobacteria culture was examined by the measurement of zone of inhibition in millimetre (mm).

Table 3. Molecular identification of the isolates and antimicrobial activity of supernatant and crude extract in static and shaking condition fermentation by well diffusion method

Isolate	Identification		S. aureus ATCC 9144						E. coli ATCC 8739						C. albicans ATCC 9028					
			Static			Shaking			Static			Shaking			Static			Shaking		
			M1	M2	M3	M1	M2	M3	M1	M2	M3	M1	M2	M3	M1	M2	M3	M1	M2	M3
WGS_02	*S. badius*	*S	-	-	-	-	10	-	-	-	-	-	-	-	-	-	-	-	-	-
		#E	-	-	-	-	10	-	-	-	-	-	-	-	22	-	-	-	-	-
WGS_03	*S. aureofaciens*	S	30	18	21	23	10	19	13	-	-	11	-	-	-	-	-	-	-	-
		E	22	16	23	26	14	22	-	-	-		-	-	-	-	-	-	-	-
WGS_04	*S. venetus*	S	10	+	-	20	18	20	-	-	-	-	-	-	-	-	-	+	-	-
		E	15	15	13	26	26	23	-	-	-	-	-	-	-	-	-	15	-	-
WGS_06	*S. parvulus*	S	11	25	-	20	14	10	-	-	-	-	-	-	-	-	-	-	-	-
		E	20	26	22	27	26	19	-	-	-	-	-	-	-	-	-	-	-	-
WGS_07	*A. silviterrae*	**S**	**-**	**11**	**23**	**-**	**-**	**-**	**-**	**-**	**-**	**-**	**-**	**-**	**-**	**-**	**-**	**-**	**-**	**-**
		E	**-**	**26**	**34**	**-**	**-**	**-**	**-**	**-**	**-**	**-**	**-**	**-**	**-**	**-**	**-**	**-**	**-**	**-**
WGS_14	*S. roietensis*	S	-	-	-	-	-	-	-	-	-	-	-	-	-	-	cover	-	-	-
		E	-	-	15	-	-	16	-	-	-	-	-	-	-	-	-	-	-	-
WGS_17	*S. daghestanicus*	S	-	-	-	-	-	-	-	-	-	-	-	-	-	16	17	17	15	15
		E	-	-	15	-	-	-	-	-	-	-	-	-	15	16	17	12		13
WGS_21	*S. rochei*	S	12	16	11	-	17	-	14	20	12	-	21	14	-	-	-	-	12	-
		E	-	-	-	-	-	-	-	-	-	-	-	-	-	-	-	-	-	-
WGS_27	*S. ardesiacus*	S	12	15	20	-	10	19	17	17	22	-	-	19	-	11	17	-	-	13
		E	-	-	-	-	-	-	-	-	-	-	-	-	-	-	-	-	-	-
WGS_39	*S. althioticus*	S	-	-	-	-	-	-	-	-	-	-	-	-	-	-	-	-	-	-
		E	-	-	-	-	14	-	-	-	-	-	22	-	15	14	12	-	15	-
WGS_44	*S. roseofaciens*	S	10	10	-	-	-	-	-	-	-	-	-	-	13	14	17	12	14	17
		E	-	-	18	-	-	-	-	-	-	-	-	-	-	11	-	13	12	14
WGS_54	*S. griseus*	S	21	23	19	24	19	28	-	-	-	-	-	-	-	-	-	-	-	-
		E	18	10	13	29	12	26	-	-	-	-	-	-	-	-	-	-	-	-

*S= Supernatant used for antimicrobial activity; #E=Extract used for antimicrobial activity; M1= 5333 media; M2= 5254 media; M3= 5294 media; the numbers in Table 3 represents the antimicrobial activity i.e., Zone of inhibition in millimetre (mm)

Out of the 57 strains screened for antimicrobial activity, 21 were showing inhibition of at least one of the test organisms (Table 3). The strain WGS_07 was interestingly showing maximum zone of inhibition against S. aureus only at static condition in 5254 (26mm) and 5294 (34mm) medium. The antimicrobial activity or the production of bioactive compound from actinobacteria was displaying differences with the change in media or growth condition. The results of antimicrobial screening signify the use of different growth condition can elicit certain silent chemical biosynthetic pathways in actinobacteria.

3.2 Molecular identification

The molecular identification of the bioactive strains of actinobacteria was carried out by the analysis of 16S rRNA gene sequence. From 21 bioactive strains, 20 belong to *Streptomyces* genus whereas one of the strains WGS_07 was identified as a species of *Amycolatopsis* genus. The 16S rRNA gene sequence of *Amycolatopsis* sp. WGS_07 was submitted to NCBI with the GenBank No. MZ824481.
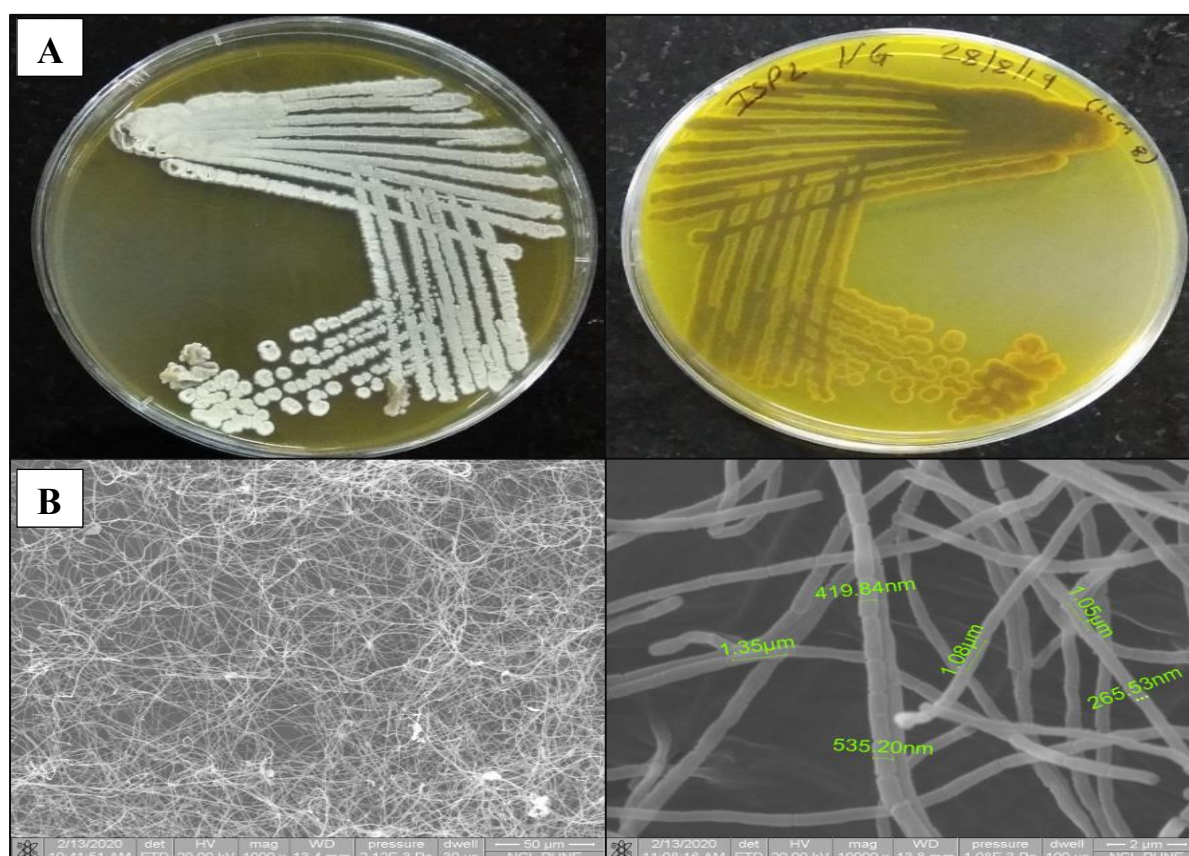
Figure 1. *Amycolatopsis* sp. WGS_07 morphology (**A**) *Amycolatopsis* sp. WGS_07 growth on ISP-2 media (**B**) SEM imaging of aerial mycelia at resolution of 50 and 2 μm.
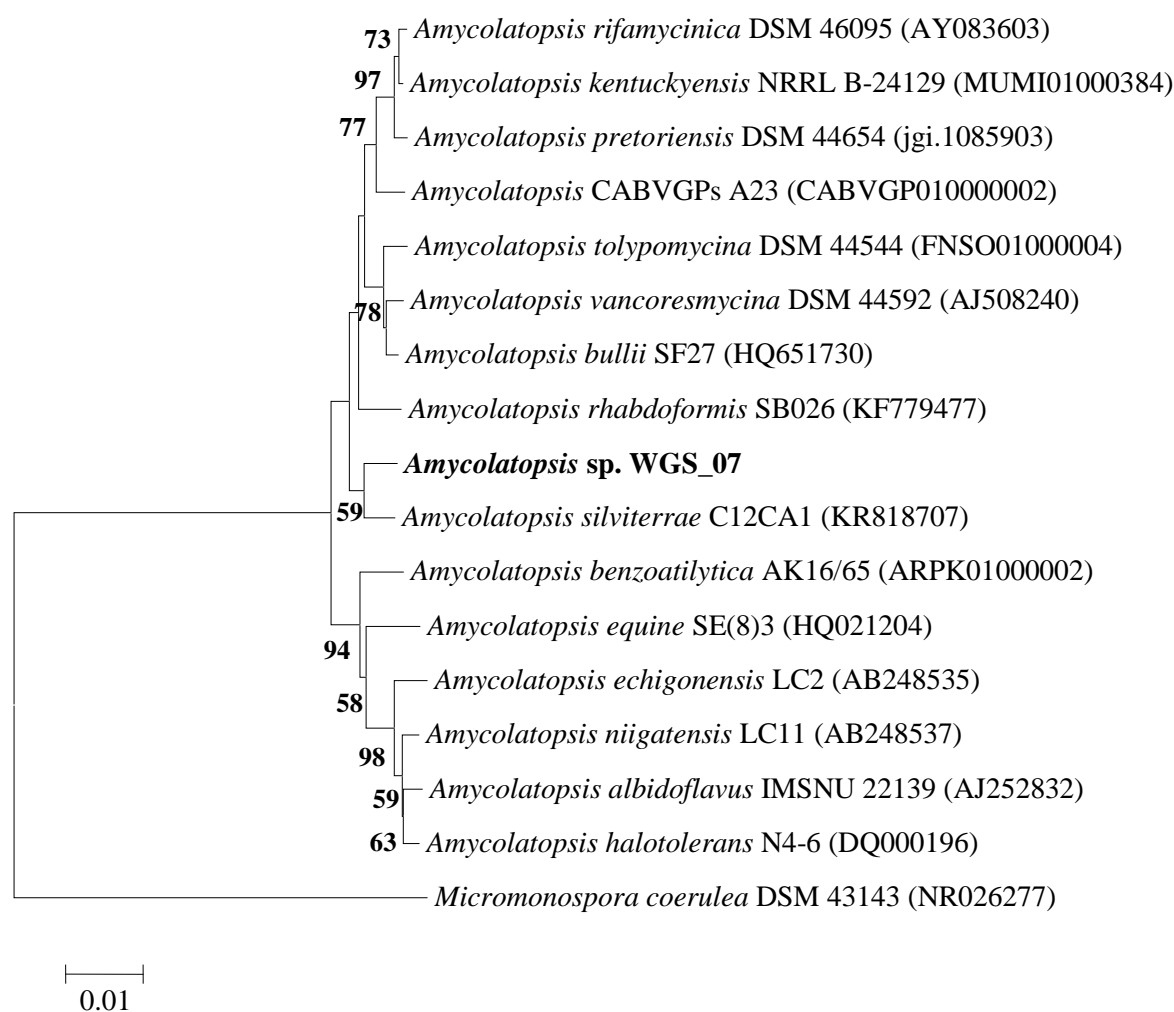
Figure 2. Phylogeny tree by Neighbour Joining method based on 16S rRNA gene sequences displaying the relationship between the strain WGS_07 and species of *Amycolatopsis* genus. *Micromonospora coerulea* DSM 43143 was used as an outgroup. The strain WGS_07 showed phylogenetically close relationship with *Amycolatopsis silviterrae.* Bootstrap values more than 50 % are shown at branch nodes based on 1000 replicates. Bar value 0.01 shows substitutions per nucleotide position.

Amycolatopsis sp. WGS_07 showed 99.24% similarity to the strain *Amycolatopsis silviterrae* (GenBank No. KR818707) and 99.1% similarity to *Amycolatopsis vancoresmycina* (GenBank No. NR_025565). The top closest 15 cultures from the EZ-Biocloud database were used for the phylogeny tree construction by the Neighbour-Joining method using 1000 bootstrap values by Mega 6.0 software. The *Amycolatopsis* sp. WGS_07 was forming a clade with *Amycolatopsis silviterrae,* of which no antibacterial activity was reported so far.

The scanning electron microscopy of the *Amycolatopsis* sp. WGS_07 was also performed to visualize the surface of the mycelium and spore. The figure 1 shows the mesh of mycelium network and aerial mycelia differentiates into long straight chain of spores like structure with smooth surfaces. The substrate mycelia displays yellow to green colour and the aerial mycelia with spore mass have white which later turns to greenish on ISP2 agar plate. The morphological features resemble the closely related *Amycolatopsis silviterrae* (Jamjan et al. 2018). The strain *Amycolatopsis* sp. WGS_07 was deposited at National Centre for Microbial Resource, Pune, India, under accession No. MCC 0218. *Amycolatopsis* genus belongs to the group of rare actinobacteria and is a producer of well-known antibiotics vancomycin and rifamycin. There are many novel molecules reported from *Amycolatopsis* genus in the last few years. Exploring the bioactive potentials for isolation of novel molecules from the *Amycolatopsis* sp. WGS_07 would be of great benefit to microbial natural product drug discovery programs.

3.3 Whole genome sequencing, assembly, and gene prediction

To further characterize the strain *Amycolatopsis* sp. WGS_07 and to look for the biosynthetic gene cluster, whole-genome sequencing (WGS) was carried out using Oxford Nanopore Technology. The comprehensive genome analysis of the assembled genome by PATRIC server yielded 1 contigs with total genome size of 10,225,713 bp as shown in Table 4. . The whole genome sequencing produced 573,457,618 of read length with mean coverage of 55. The assembled genome GC content 69.52% was in consistency with *Amycolatopsis* genus and the read length N_{50} value was 10,225,713.

Table 4. Genome summary of *Amycolatopsis* sp. WGS_07

Assembly and annotation of genome	
Contig	1
GC Content	69.52%
Genome Length	10,225,713 bp
Contig N50	10,225,713
Contig L50	1
Plasmids / Chromosomes	0
CDS	9,952
tRNA	55
rRNA	12

The genome annotation using RAST tool kit (RASTtk) by PATRIC server identified a 9,952 CDS (CoDing sequences) of which 4,095 are hypothetical proteins and 5,857 are functional assigned proteins whereas there are 55 tRNA and 12 rRNA. Among the functional assigned proteins 1,333 proteins were mapped to KEGG pathways, 1,476 had Gene Ontology assignments, and 1,678 proteins had Enzyme Commission (EC) numbers. The PATRIC annotation comprises two categories of protein families, and present genome possesses 8,203 proteins with cross genus protein families (PGFams) and 7,691 proteins with genus-specific protein families (PLFams). This Whole Genome sequence has been submitted at NCBI GenBank under BioProject ID PRJNA1020392 with the biosample accession number of SAMN37521466.
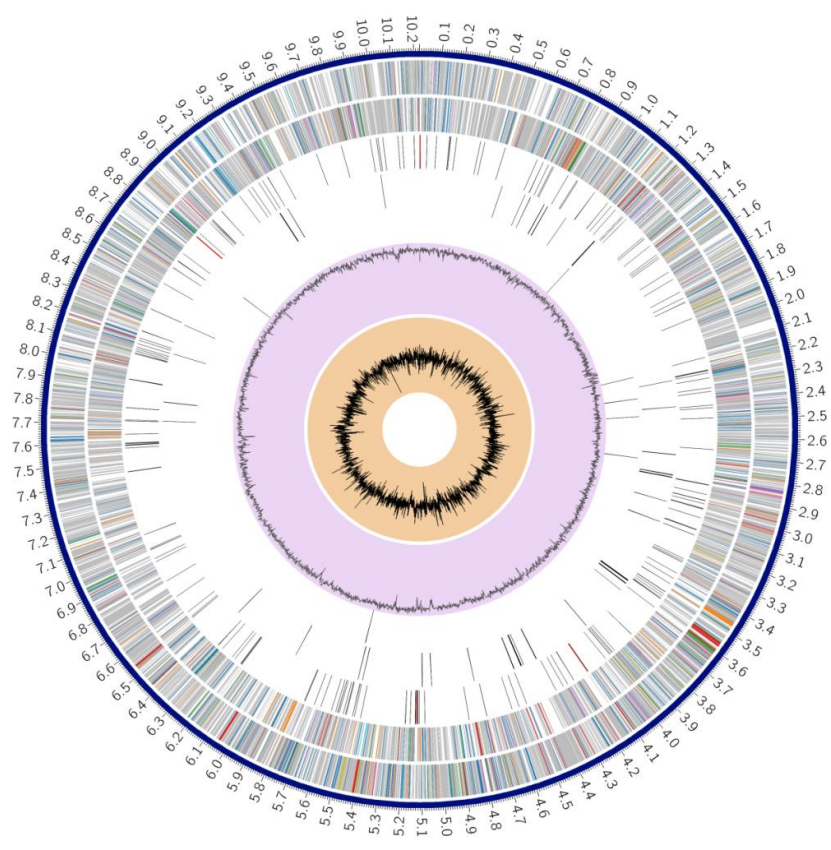
Figure 3. A circular graphical display by Circos plot representing the genome of *Amycolatopsis* sp. WGS_07 in a single contig. The genome *of Amycolatopsis* sp. WGS_07 is represented in Circos plot (Figure 3), and the outermost ring represents the contig. From the outermost to inner rings, the second ring represents the CDS on the forward strand followed by CDS on the reverse strand. The third ring represents the RNA genes followed by the CDS of known antimicrobial genes and CDS of known virulence factors. The last two innermost rings are for GC content and GC skew.

Table 5. Biosynthetic gene clusters of *Amycolatopsis* sp. WGS_07

Most similar BGCs / Type	From (bp)	To (bp)	Similarity
Macrotermycins / T1PKS	522,160	637,378	96%
Mutaxanthene / T2PKS	1,124,639	1,195,629	92%
Lassopeptide	1,442,586	1,465,081	75%
Ulleungdin / lassopeptide	1,582,671	1,630,496	6%
Ectoine	1,940,005	1,950,397	75%
Fortimicin / lanthipeptide	3,202,031	3,230,899	9%
Geosmin / terpene	4,273,351	4,294,505	100%
Ishigamide/ NRPS	4,374,626	4,521,306	61%
Isorenieratene / terpene	5,288,412	5,308,622	42%
Nactins / Siderophore	5,692,005	5,703,798	33%
SF2575/ terpene	5,827,990	5,847,744	4%
Hexacosalactone A / hglE-KS	6,003,717	6,051,017	9%
Cycloserine / RRE-containing	6,143,180	6,165,428	31%
Hopene / terpene	6,312,115	6,336,698	38%
Mirubactin / NNRPS	6,406,759	6,493,308	78%
Thiolutin / NRPS	6,583,166	6,622,907	32%
2-methylisoborneol / NRPS	6,736,643	6,844,272	100%
Ery-6-9 / lanthipeptide	6,852,832	6,875,369	75%
Uncialamycin / T1PKS	6,960,404	7,003,942	18%
Hormaomycins / NRPS	7,311,332	7,386,558	26%
Rhizomide A/ B/ C / RRE-containing	7,475,917	7,491,965	100%
Homopiloquinone / T2PKS	7,580,655	7,651,678	52%
Calicheamicin / T1PKS	7,937,700	7,980,021	12%
Lankacidin C / redox-cofactor	8,508,466	8,530,505	20%
ε-Poly-L-lysine / NAPAA	8,774,987	8,808,246	100%
Stenothricin / NRP	9,054,984	9,089,472	13%
Lipopolysaccharide / lanthipeptide	9,419,440	9,443,671	5%
Chlortetracycline / T2PKS	10,127,982	10,200,533	45%

Microbial natural products are diverse in chemical structure; however they have highly conserved biosynthetic machineries. The genomic data can be screened for the identification of biosynthetic genes since enzymes responsible of secondary metabolite biosynthesis are highly similar in amino acid sequence. The most important secondary metabolites synthesized from biosynthetic assembly includes polyketides, ribosomally synthesized and post translationally modified peptides (RiPPS), non-ribosomally synthesized peptides, and terpenes (Scherlach and Hertweck, 2021; Hertweck, 2009)).

The genome analysis for the biosynthetic potential of secondary metabolites by *Amycolatopsis* sp. WGS_07 led to detection of 28 biosynthetic gene clusters (BGCs) using antiSMASH annotation (Table 5). The putative BGCs related to secondary metabolites includes 7 non-ribosomal peptide synthetases (NRPSs), 3 type 1 PKS (polyketide synthase), 3 type 2 PKS, 4 terpenes, 3 lanthipeptide, 2 lassopeptide, 1 siderophore and 5 other types of BGCs. The presence of putative polyketide BGCs related to bioactive molecules like macrotermycins, chlortetracycline, mutaxanthene, uncialamycin and homopiloquinone displays the potential of *Amycolatopsis* sp. WGS_07 strain in isolation of novel bioactive compounds.

Conclusion:

Fifty seven actinobacteria isolates were screened for antimicrobial activity under shaking and static conditions using three fermentation media. 21 out of 57 isolates, displayed antimicrobial activity towards at least one of the three test strains. Twenty isolates belonged to *Streptomyces* genus whereas one isolate was a rare actinobacteria from *Amycolatopsis* genus. *Amycolatopsis* sp. WGS_07 was closely related to *A. silviterrae* of which no bioactivity has been reported. *Amycolatopsis* sp. WGS_07 showed potent activity against *S. aureus* only under static condition. Genome sequencing of *Amycolatopsis* sp. WGS_07 showed diversity of secondary metabolite associated biosynthetic gene clusters.

References

Adpressa DA, Loesgen S (2016) Bioprospecting chemical diversity and bioactivity in a marine derived *Aspergillus terreus*. *Chem Biodivers* 253-259.

Amaning Danquah C, Minkah PAB, Osei Duah Junior I, Amankwah KB, Somuah SO (2022) Antimicrobial Compounds from Microorganisms. *Antibiotics* 11:285.

Balouiri M, Sadiki M, Ibnsouda SK (2016) Methods for in vitro evaluating antimicrobial activity: A review. *J Pharm Anal* 6:71-79.

Barka EA, Vatsa P, Sanchez L, Gaveau-Vaillant N, Jacquard C, Meier-Kolthoff JP, Klenk HP, Clément C, Ouhdouch Y, van Wezel GP (2015) Taxonomy, Physiology, and Natural Products of Actinobacteria. *Microbiol Mol Biol Rev* 80:1-43.

Begani J, Lakhani J, Harwani D (2018) Current strategies to induce secondary metabolites from microbial biosynthetic cryptic gene clusters. *Ann Microbiol* 68:419-432.

Berdy J (2005) Bioactive microbial metabolites. *J antibiot* 58:1

Blin K, Shaw S, Augustijn HE, Reitz ZL, Biermann F, Alanjary M, Fetter A, Terlouw BR, Metcalf WW, Helfrich EJN, van Wezel GP, Medema MH, Weber T (2023) antiSMASH 7.0: new and improved predictions for detection, regulation, chemical structures and visualisation. *Nucleic Acids Res.* 51:W46-W50.

Bode HB, Bethe B, Höfs R, Zeeck A (2002) Big effects from small changes: possible ways to explore nature's chemical diversity. *Chembiochem* 3:619-627.

Bode HB, Walker M, Zeeck A (2000) Cladospirones B to I from Sphaeropsidales sp. F-24′ 707 by Variation of Culture Conditions. *Eur J Org Chem* 2000:3185-3193.

Brettin T, Davis JJ, Disz T, Edwards RA, Gerdes S, Olsen GJ, Olson R, Overbeek R, Parrello B, Pusch GD, et al, 2015. RASTtk: a modular and extensible implementation of the RAST algorithm for building custom annotation pipelines and annotating batches of genomes. *Sci Rep* 5:8365.

Che Q, Li J, Li D, Gu Q, Zhu T (2016) Structure and absolute configuration of drimentine I, an alkaloid from Streptomyces sp. CHQ-64. *J Antibiot* 69:467-469.

Cheng C, Jia JL, Ran SY (2015). Polyethylene glycol and divalent salt-induced DNA reentrant condensation revealed by single molecule measurements. *Soft matter* 11:3927-3935.

Cheng HR, Jiang N (2006) Extremely rapid extraction of DNA from bacteria and yeasts. *Biotechnol Lett* 28:55-59.

Christaki E, Marcou M, Tofarides A (2020) Antimicrobial Resistance in Bacteria: Mechanisms, Evolution, and Persistence. *J Mol Evol* 88:26-40.

Davis JJ, Wattam AR, Aziz RK, Brettin T, Butler R, Butler RM, Chlenski P, Conrad N, Dickerman A, Dietrich EM, Gabbard JL, Gerdes S, Guard A, Kenyon RW, Machi D, Mao C, Murphy-Olson D, Nguyen M, Nordberg EK, Olsen GJ, Olson RD, Overbeek JC, Overbeek R, Parrello B, Pusch GD, Shukla M, Thomas C, VanOeffelen M, Vonstein V, Warren AS, Xia F, Xie D, Yoo H, Stevens R (2020) The PATRIC Bioinformatics Resource Center: expanding data and analysis capabilities. *Nucleic Acids Res.* 48:D606-D612.

De Simeis D, Serra S (2021) *Actinomycetes*: A Never-Ending Source of Bioactive Compounds-An Overview on Antibiotics Production. *Antibiotics (Basel)* 10:483.

Ding T, Yang LJ, Zhang WD, Shen YH (2019) The secondary metabolites of rare actinomycetes: chemistry and bioactivity. *RSC Adv* 9:21964-21988.

Du L, Li D, Zhu T, Cai S, Wang F, Xiao X, Gu Q (2009) New alkaloids and diterpenes from a deep ocean sediment derived fungus Penicillium sp. *Tetrahedron* 65:1033-1039.

Ezeobiora CE, Igbokwe NH, Amin DH, Enwuru NV, Okpalanwa CF, Mendie UE (2022) Uncovering the biodiversity and biosynthetic potentials of rare actinomycetes. *Future J Pharm Sci* 8:1-9.

Gao H, Zhou L, Cai S, Zhang G, Zhu T, Gu Q, Li D (2013) Diorcinols BE, new prenylated diphenyl ethers from the marine-derived fungus *Aspergillus versicolor* ZLN-60. *J Antibiot* 66:539-542.

Hertweck C (2009) The biosynthetic logic of polyketide diversity. *Angew Chem Int Ed* 48:4688-4716.

Hui ML, Tan LT, Letchumanan V, He YW, Fang CM, Chan KG, Law JW, Lee LH (2021) The Extremophilic Actinobacteria: From Microbes to Medicine. *Antibiotics (Basel).* 10:682.

Jamjan W, Suriyachadkun C, Tanasupawat S, Sakai K, Tashiro Y, Okugawa Y, Tongpim S (2018) *Amycolatopsis silviterrae* sp. nov., isolated from forest soil. *Int J Syst Evol Microbiol* 68:1455-1460.

Katz L, Baltz RH (2016) Natural product discovery: past, present, and future. *J Ind Microbiol Biotechnol* 43:155-76.

Kolmogorov M, Yuan J, Lin Y, Pevzner PA (2019) Assembly of long, error-prone reads using repeat graphs. *Nat Biotechnol* 37:540-546.

Liu R, Gu Q, Zhu W, Cui C, Fan G, Fang Y, Zhu T, Liu H (2006) 10-Phenyl-[12]-cytochalasins Z7, Z8, and Z9 from the Marine-Derived Fungus *Spicaria elegans. J. Nat. Prod* 69:871-875.

Pan R, Bai X, Chen J, Zhang H, Wang H (2019) Exploring Structural Diversity of Microbe Secondary Metabolites Using OSMAC Strategy: A Literature Review. *Front Microbiol* 10:294.

Pettit RK (2011) Small-molecule elicitation of microbial secondary metabolites. *Microb Biotechnol* 4:471-478.

Pudhom K, Teerawatananond T, Chookpaiboon S (2014) Spirobisnaphthalenes from the mangrove-derived fungus *Rhytidhysteron* sp. AS21B. *Mar Drugs* 12:1271-1280.

Reponen TA, Gazenko SV, Grinshpun SA, Willeke K, Cole EC (1998) Characteristics of airborne actinomycete spores. *Appl Environ Microbiol* 64:3807-3812.

Romano S, Jackson SA, Patry S, Dobson ADW (2018) Extending the "One Strain Many Compounds" (OSMAC) Principle to Marine Microorganisms. *Mar Drugs* 16:244.

Schneider YK (2021) Bacterial Natural Product Drug Discovery for New Antibiotics: Strategies for Tackling the Problem of Antibiotic Resistance by Efficient Bioprospecting. *Antibiotics (Basel)* 10:842.

Siddharth S, Vittal RR, Wink J, Steinert M (2020) Diversity and Bioactive Potential of Actinobacteria from Unexplored Regions of Western Ghats, India. *Microorganisms* 8:225.

Ventola CL (2015) The antibiotic resistance crisis: part 1: causes and threats. *P T* 40:277-283.

Yao FH, Liang X, Qi SH (2021) Eight new cyclopentenone and cyclohexenone derivatives from the marine-derived fungus *Aspergillus* sp. SCSIO 41501 by OSMAC strategy. *Nat Prod Res* 35:3810-3819.

Yoon SH, Ha SM, Kwon S, Lim J, Kim Y, Seo H, Chun J (2017) Introducing EzBioCloud: a taxonomically united database of 16S rRNA gene sequences and whole-genome assemblies. *Int J Syst Evol* 67:1613-1617.

Zheng Y, Zhao B, Lu C, Lin X, Zheng Z, Su W (2009) Isolation, structure elucidation and apoptosis-inducing activity of new compounds from the edible fungus *Lentinus striguellus. Nat Prod Commun* 4:501-506.

Zhou LN, Gao HQ, Cai SX, Zhu TJ, Gu QQ, Li DH (2011) Two New Cyclic Pentapeptides from the Marine-Derived Fungus *Aspergillus versicolor. Helvetica Chimica Acta* 94:1065-1070.

Chapter 3

Production, purification and structural elucidation of the purified bioactive compounds

Production, purification and structural elucidation of the purified bioactive compounds

Abstract

Based on the antimicrobial activity and the genomic analysis for the biosynthetic gene clusters, the *Amycolatopsis* sp. WGS_07 strain was investigated further for the production of bioactive molecules. The culture showed antibacterial activity under static and plate-based incubation condition. The major bioactive molecule was of similar type based on the TLC and bio-autography. The 50L fermentation of the *Amycolatopsis* sp. WGS_07 under static condition yielded 52g of crude extract. Bioactivity-guided purification by silica-gel column chromatography and semi-preparative HPLC resulted in isolation of four bioactive molecules. The chemical structure and configurations were elucidated by 1D and 2D NMR spectroscopy, high-resolution mass spectrometry and single-crystal X-ray crystallography. The isolated bioactive molecules were characterized as three new furo-naphthoquinone-derived Enceleamycins A-C (**1-3**) along with one novel *N*-hydroxypyrazinone acid (**4**). Enceleamycin A (**1**) possesses a complex unprecedented pentacyclic oxeto-furo-furo-naphthoquinone skeleton. Enceleamycin B (**2**) features dihydroxylated naphthoquinone segment, whereas Enceleamycin C (**3**) is a furo-furo-naphthoquinone skeleton possessing hydroxy-aldehyde functionalities.

Graphical abstract
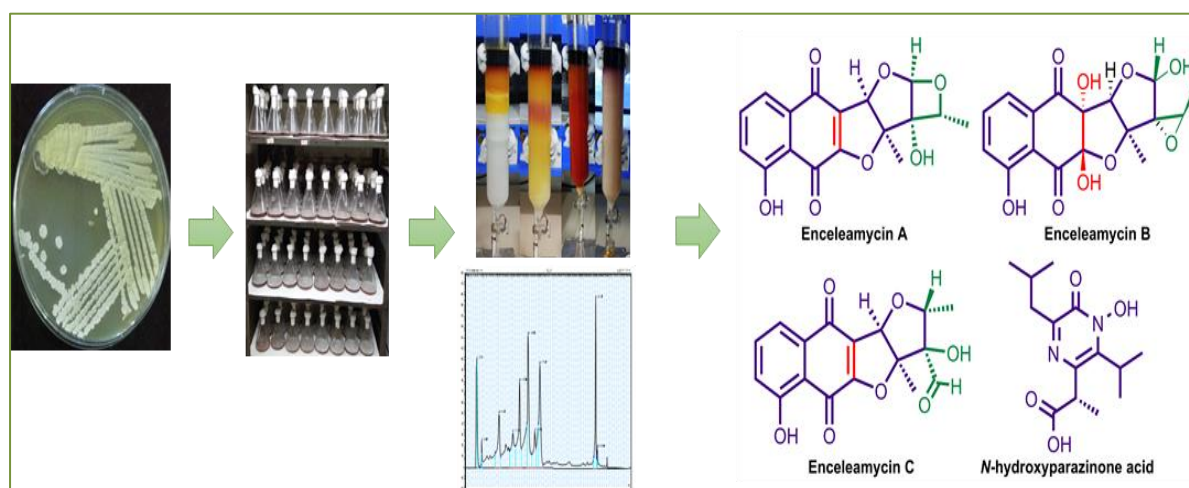
1. Introduction

Natural products from plants, animals and microbes contribute to more than half of the pharmaceutical drugs (Sekurova et al. 2019; Newman and Cragg, 2016). Ever since Alexander Fleming discovered penicillin in 1928, microbes have become an important source for the isolation of bioactive molecules (Fleming, 1929). In recent years with the surge of antimicrobial resistance towards the present antibiotics, novel antibacterial chemicals are required. The species of *Amycolatopsis* genus are potential source for the isolation of novel secondary metabolites. They are producer of two important antibiotics rifamycin and vancomycin used in healthcare (Sangal et al. 2018). There have been reports of numerous new molecules like saalfelduracins, amycolasporins, thioamycolmides, dibenzoyls, thioalbamide A, and pradimicin isolated from different species of *Amycolatopsis (*Kisil et al. 2021*)*. A broad range of biosynthetic gene clusters are present in *Amycolatopsis* species as shown by the whole genome sequences data, suggesting the potential ability to produce new antibiotics by this genus (Adamek et al. 2018).

The microbial natural product drug-discovery aims for novel therapeutic secondary metabolites with unique bioactivity for the medicinal, industrial or agricultural needs (Mushtaq et al. 2018). The process for microbial natural product drug-discovery involves the screening and identification of the bioactive compound producing strains, large scale production of the bioactive compound under optimal growth condition, purification of the desired bioactive compound, and structure elucidation of the active molecule and bioactivity assays for its application in healthcare sector. The present chapter deals with production, purification and structural elucidation of bioactive molecules.

1.1 Production and purification of bioactive compounds

Production of bioactive compounds is performed after the screening and identification of the potential culture. The growth parameters of microorganisms like nutrient, temperature, pH and oxygen levels are critical for the controlled growth and yield of the bioactive compound (Rusu et al. 2023; Romano et al. 2018). The purification of the bioactive compound from the microorganism starts from the extraction of these metabolites from the whole broth or the culture medium after separation from biomass. The extraction method generally used is solvent extraction based on the compounds polarity and the extracted and concentrated crude material contains mixture of compounds. These extract is fractionated by liquid-liquid

partitioning and column chromatography. The separation is by a liquid chromatography method whereby a mixture of compounds is resolved into individual components by passing through a stationary phase (chromatography column) and carried by a mobile phase (liquid-water/solvent/buffer). The chromatographic separation of bioactive compound by column is based on the size or polarity of the molecules in the mixture (Coskun, 2016). High-performance liquid chromatography (HPLC) and thin-layer chromatography (TLC) are frequently used techniques for purification and qualitative analysis of bioactive compounds. HPLC instruments consist of several modules, which include a pump for efficient movement of the mobile phase, an injector valve for the intake of sample, column for separation of injected sample, and a detector to record the timing and quantity of separated compound. The HPLC instruments in analytical and preparative mode have become an indispensable tool for Natural product drug discovery program (Regnier, 1983; Zhang et al. 2018). Several chromatographic purification steps are involved to isolate stable bioactive compound of sufficient purity for its structural elucidation.

1.2 Characterization of bioactive compounds

The structure elucidation of microbial secondary metabolites is a challenging task. The process often involves multi-disciplinary approach to obtain a comprehensive understanding of the bioactive compound structure. The structure elucidation can be time-consuming however it is essential for the identification of novel bioactive chemicals that may have therapeutic benefits. The nuclear magnetic resonance (NMR) is a vital tool in Natural product structure determination. The discovery of nuclei's magnetic characteristics served as the foundation for nuclear magnetic resonance. Because the nuclei have spin angular momentum and a corresponding magnetic moment, the atoms can absorb certain radio frequency waves when they are in an external magnetic field (Wang et al. 2021). NMR spectroscopy contains the cryogenic probes, high-field magnets and advanced two-dimensional pulse sequences. The structural elucidation by 2D-NMR rely on homonuclear correlation of ^{1}H techniques like Nuclear Overhauser Enhancement Spectroscopy (NOESY) or either Correlation Spectroscopy (COSY) and heteronuclear correlation of ^{1}H and ^{13}C like Heteronuclear Single Quantum Coherence (HSQC) and long-range Heteronuclear Multiple-Bond Coherence (HMBC) (Elyashberg, 2015). In order to determine the molecular formula of a complex organic compound, high-resolution mass spectrometry (HRMS) is crucial. In an effort to complete the structure elucidation of novel molecule along with NMR multiple analytical tools like, ultra-violet and infrared spectra, optical rotation, Circular dichroism (CD) spectra

is used to assemble the structural units (Urban and Dias, 2013). In addition to NMR, X-ray Crystallography is the most reliable technique for structure elucidation of pure bioactive compound. Performing the X-ray Crystallography of crystals can yield detailed and accurate three dimensional molecular structures (Smyth and Martin, 2000).
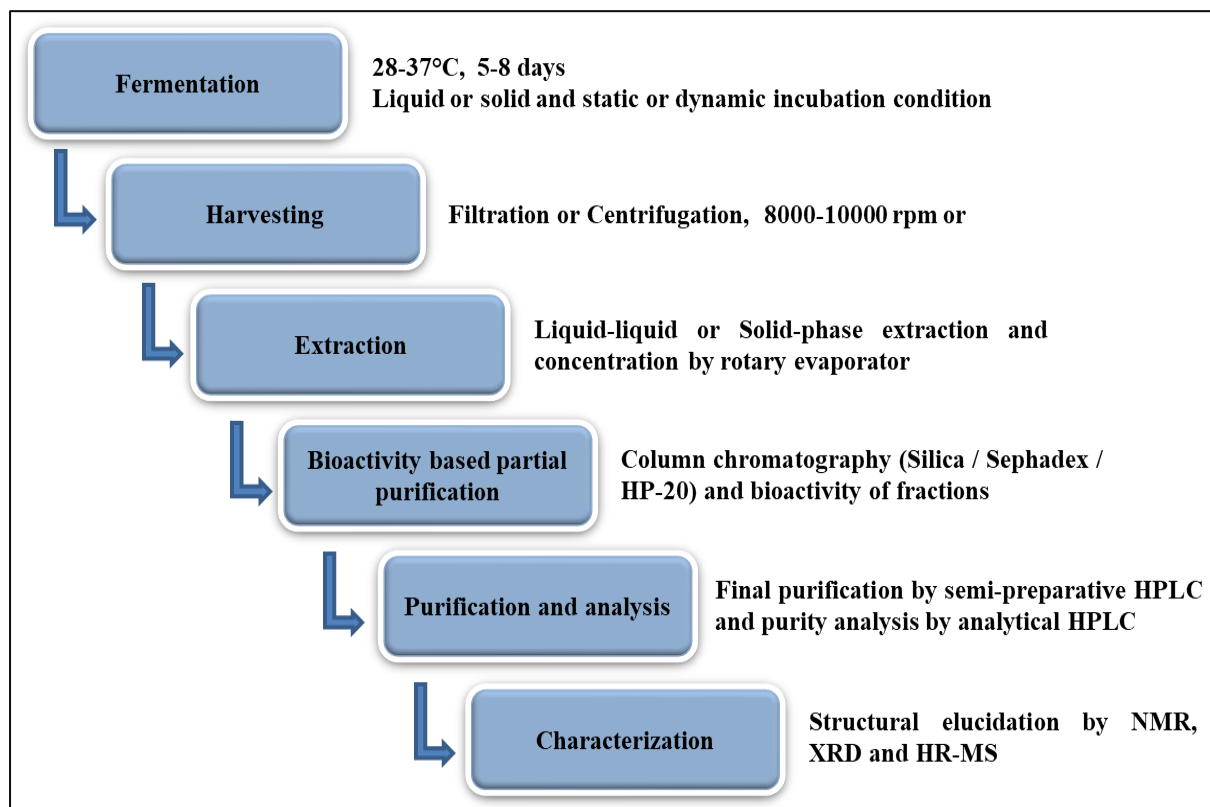
Figure 1. General flowchart for production, purification and characterization of bioactive compound from microorganisms.

2. Materials and Method

2.1 Chemical and media

Growth media components, sterile disc, Silica gel (60–120 mesh and 100–200 mesh), silica TLC plates, Hexane, Pet ether, Ethyl acetate, Methanol, Acetonitrile, Trifluoroacetic acid, CD_3CN, $CDCl_3$ and DMSO-d6. The majority of the media components, solvents and chemicals were ordered by Hi-media and Sigma Aldrich, as aforementioned.

1.1 Antibacterial activity

Amycolatopsis sp. WGS_07 was sub-cultured on MGYP agar plates (0.3% malt extract, 1% dextrose, 0.5% peptone, 0.3% yeast, and 1.8% agar, pH 7.0) for 7 days at 28 °C. A 250 mL Erlenmeyer flask with 50 mL of seed medium was inoculated with a loopful of culture. For three days, the seed culture was incubated at 28°C and 150 rpm on rotary shaker. A 5.0 mL of seed culture was transferred into three different fermentation media in 250 mL Erlenmeyer flask, each with 50 mL media. The seed culture was also streaked on plates contacting the medium used for fermentation with 2% agar. The fermentation media used were 5333, 5254 and 5294. The pH of all three fermentation media was adjusted to 7.0 prior sterilization (autoclaved for 20 min at 121°C). The flasks were incubated in both static and shaking conditions (150 rpm) for 7 days at 28°C. The whole broth and two agar plate with cultures were extracted by 100 mL of ethyl acetate. After extraction, organic phase was separated, and concentrated by rotary evaporator. The extracted and concentrated crude extract was dissolved in 1.0 mL of ethyl acetate (HPLC grade). The antimicrobial activity was carried out by disc-diffusion method using 30μL crude extract against *S. aureus*, *E. coli*, and *C. albicans*.

2.3 TLC and Bio-autography

Bio-autography of the crude extract was done against *S. aureus* to check the major active compound zone from both the static and agar conditions. The bio-autography of crude extract was carried out on a pre-coated Silica Gel 60_{254} TLC plate plates ((8.5×1.5 cm, Merck, Germany). The crude extract from both shaking, static and agar was spotted on silica gel plate, spaced 1.0 cm from baseline. The spotted plate was developed at room temperature in a previously saturated glass chamber with a 5:95 mixture of methanol and dichloromethane (DCM). To examine the spots, the silica plates were dried and inspected at 254 nm in UV chamber. Bioautography of separated bands on TLC was examined against *S. aureus* to track the antibacterial compound. Further, TLC plates were placed in petri dish and UV-sterilized for 30 minutes. Following that, TLC plates in petri dishes were covered with 0.8% semisolid Mueller-Hinton agar that had been mixed with 1.0×10^8 CFU/mL of *S. aureus*. The plates were incubated for 24 hours after solidification and the inhibition zone around active bands were observed.

The day-wise activity of *Amycolatopsis* sp. WGS_07 was performed by using 100μL of cell-free supernatant and for that the fermentation was carried out in 100 ml of 5294 media in 500 mL flask.

2.4 Fermentation, Extraction, and Purification

The large-scale fermentation of 50 litres was carried out for *Amycolatopsis* sp. WGS_07 in 100 mL of 5294 fermentation medium using 500 mL Erlenmeyer flasks. The cultures were incubated in static conditions for 7-8 days at 28 °C. The whole broth was extracted with equal volumes of ethyl acetate three times. Following extraction, organic phase was separated and concentrated by rotary evaporator under lower pressure to get a semi-solid crude extract.

For the purification of bioactive compounds, the crude extract of 52g was employed to silica gel column chromatography. The glass column (45× 7.5 cm) was filled by 100-200 mesh silica gel. The semi-solid crude extract was combined with 60-120 mesh silica bed and uniformly applied from the top of column. The gradient elution of a column was performed using combination of petroleum (pet) ether and ethyl acetate by gradually increasing polarity to give 20 fractions, CF-1 to CF-20 (Column chromatography fraction). Based on the bioactivity profile, CF-9, which was eluted with 70% ethyl acetate/pet ether, was further purified using semi-preparative HPLC by C_{18} column on reverse phase mode. The gradient elution of compound was carried out by water and acetonitrile to yield six fractions. Semi-preparative HPLC was conducted on Thermo Scientific Ultimate 3000 equipped with VWD detector and YMC column (250 × 10 m i.d., 10–20 μm), using flow rate of 4.7 mL/min and column temperature of 28 °C. Fraction CF-9-IV is confirmed as the major compound **1**, and fraction-CF-9-III was further fractionated by semi-preparative HPLC to isolate compound **2**. Based on the TLC profile and bioactivity, column fractions of CF-5 to CF-8 were combined and silica gel CC was performed using pet ether with a gradient increase in ethyl acetate to get fractions I to XII. Fraction VI from CF-5–8 eluted with 30% ethyl acetate/pet ether was separated using semi-preparative HPLC on reverse phase with water and acetonitrile as the mobile phase. The semi-preparative HPLC active fraction (F 26-28) were further separated by preparative TLC (PTLC) on the pre-coated Silica Gel 60_{254} plates (20×20 cm, Merck) in 20:80 mixture of ethyl acetate and pet ether. The desired band was examined under UV light (254 nm) and the silica with band was scratched off the PTLC plate with the help of razor blade. The scratched silica was extracted with 100 ml of ethyl acetate for 30 minutes. The ethyl acetate with compound was separated and concentrated by rotary evaporator. The concentrated compound from PTLC plate was further purified using semi-preparative HPLC

with chiral amylose column in normal phase with an isocratic mobile phase of 30% isopropanol/hexane to yield compound **3**. Fraction V from CF-5–8 eluted with 20% ethyl acetate/pet ether in silica gel CC was purified using semi-preparative HPLC by reversed-phase C_{18} column by gradient mobile phase of acetonitrile and water to get compound **4**.

The fermentation of *Amycolatopsis* sp. WGS_07 was also carried out on the 5294 medium agar plates. Around 400 plates (10L media) were streaked with the culture and incubated for 7-8 days at 28 °C. The plate based culture with agar was cut and extracted by 10L of ethyl acetate for 4-5 h three times. The organic phase after extraction was separated and concenterated by rotary evaporator to get semi-solid crude extract of 10.2g. The crude extract was further purified similar to the static crude extract by silica gel chromatography using pet ether and ethyl acetate as a mobile phase followed by semi-preparative HPLC to get major compound **1** and minor compound **2**.

2.5 Analysis of purified compounds

The four isolated purified compounds were analysed by analytical U-HPLC Thermo Scientific Ultimate 3000 equipped with a VWD detector using reverse phase C-18 Hypersil GOLD having 5 μm particle size with 4.6 × 250 mm dimension (Thermo Scientific, USA) column with the gradient mobile phase of Milli Q Water and Acetonitrile (ACN). The gradient starts from 5% ACN upto 4 minutes and then it increases upto 95% at 17 minutes and maintained at 95% upto 18 min followed by decrease of ACN to 5% at 21 minute and further maintained at 5% upto 25 minute run with flow rate of 1 ml/min.

2.6 Structure elucidation of the purified bioactive compounds

The structure of purified bioactive compounds was determined using nuclear magnetic resonance (NMR) by a Bruker Avance 300 ultra shield NMR apparatus. Using trimethylsilane (0.007) as an internal standard, all chemical shifts (δ) are measured in parts per million (ppm) downfield in CD_3CN (1.94 in ^{1}H and 118.7 ppm in ^{13}C), $CDCl_3$ (7.27 ppm in ^{1}H and 77.00 in ^{13}C), and DMSO-d6 (2.50 in ^{1}H and 39.1 in ^{13}C). The coupling constant *J* is given in hertz (Hz). Spin multiplets were denoted as singlet (s), doublet (d), triplet (t), quartet (q) and multiplets (m). Absorbance spectrum was recorded on ThermoScientific Evolution 201 UV–visible spectrophotometer. An optical rotation was measured on JASCO P-2000 polarimeter. A CD spectrum was obtained from JASCO J-815 CD spectrometer. The melting point was recorded on a Stuart SMP10 (BioCote).

HPLC Prime Infinity II 1260 (800 bar) system coupled to Agilent 6530 Accurate-Mass Quadrupole Time-of-Flight (Q-TOF) mass spectrometer (Agilent, USA) was used for HR-ESIMS analysis. For ionizatio, a dual electrospray ionization (ESI) source was utilized. A Hypersil GOLD C18 (1.9 μm particle size with 2.1 × 150 mm dimension, Thermo Scientific, USA) column was utilized for LC-based metabolite separation. The compound was analysed at 40 °C over the course of 20 min with 0.3 mL/min flow rate using MS grade water (A) and MS grade acetonitrile (B), as a mobile phase. Both mobile phase contains 0.1% formic acid. In the first 0.3 minutes of the LC method, 2% B was used; in the next two minutes, this was increased to 30%. Upto seven minutes the B% was raised from 30% to 45%, then to 98% for sixteen minutes, a level that was maintained for the next one minute. In the final three minutes, the column reached equilibrium with the initial solvent ratio of 98% A and 2% B. The extended dynamic range of 2 GHz was used to collect the MS data. The MS parameters are set to 325 °C for the gas temperature, 10 L/min for the drying gas, 35 psi for the nebulizer and 120 volts for the fragmentor.

Single-crystal XRD was performed on Bruker d8 Advance. High-resolution (0.78 Å) Cu Kα radiation was used to gather crystal XRD data at lower temperature of 100 K. The APEX3 program was employed to monitor the collection of X-ray data.

3. Results and Discussion

3.1 Antibacterial activity

The antibacterial activity of *Amycolatopsis* sp. WGS_07 was evaluated on different growth condition like liquid shaking and static as well as on the agar plate. The crude extract of *Amycolatopsis* sp. WGS_07 showed antibacterial activity in agar plate conditions with zone of inhibition of 20 mm in 5254 medium and 22 mm in 5294 medium, whereas in liquid static conditions the zone of inhibition was 22 mm in 5254 medium and 25 mm in 5294 medium against *S. aureus.* No activity was observed from cultures grown under any of the shaking conditions in the three fermentation media tested (Figure 2).
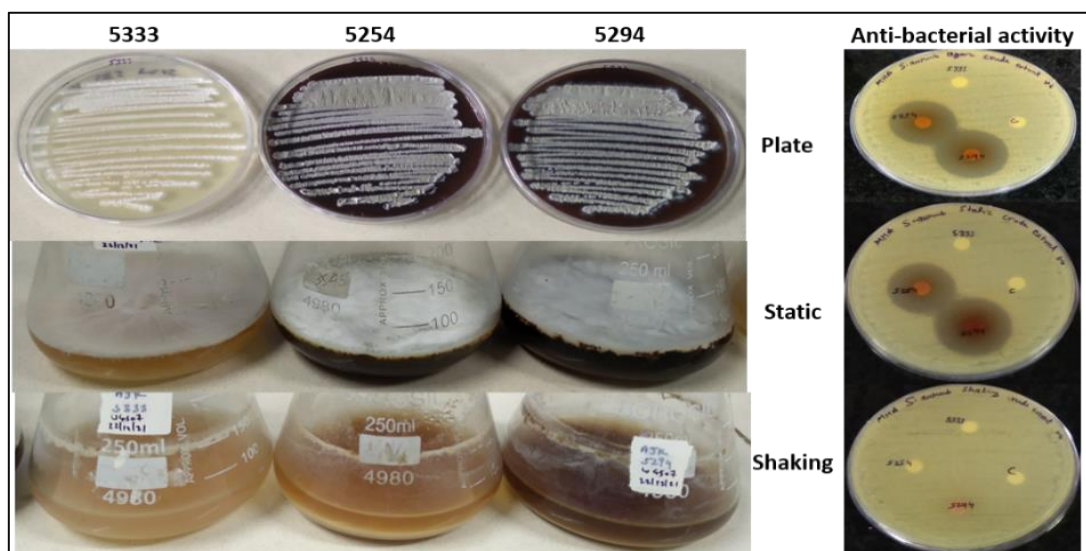
Figure 2. Bioactivity screening against *S. aureus* using three fermentation mediums in plate, static, and shaking conditions.

3.2 TLC and Bio-autography

The crude extracts of *Amycolatopsis* sp. WGS_07 from the three culturing condition were used for TLC analysis. A major yellow pigment was observed in both the static and agar condition whereas there was no yellow pigment band observed in the shaking condition. Later, bio-autography of the crude extract was done against *S. aureus* to check the major active band in the TLC. It was found that the yellow pigment band present in the static and agar plate based incubation showed antibacterial activity. To further confirm, the yellow pigment band cut and used for bio-autography also displayed the zone of inhibition. No yellow pigment or antimicrobial activity was produced in shaking culture conditions (Figure 3 and 4).

Figure 3. Antibactrial activity against *S. aureus* and TLC (mobile phase- 5:95 methanol and DCM) of crude extract of *Amycolatopsis* sp. WGS_07 from shaking, static, and plate-based incubation condition.
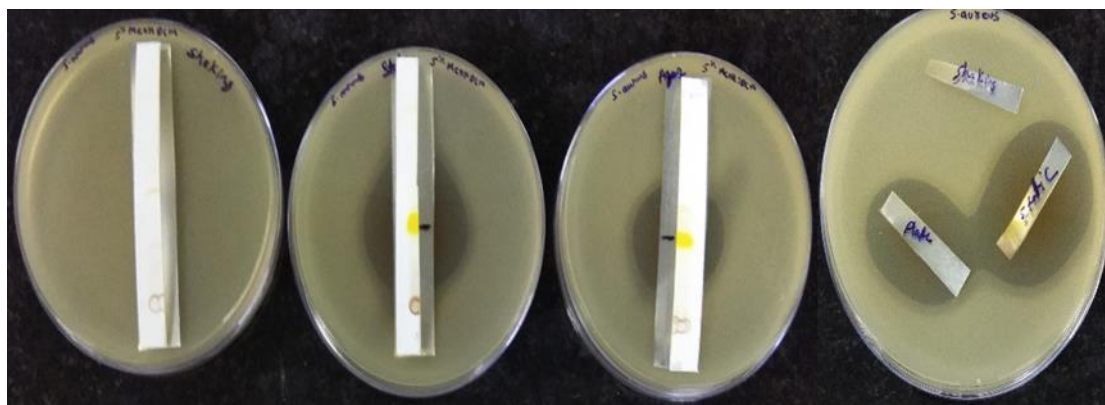
Figure 4. Bio-autography of crude extract in 5:95 of methanol and DCM mobile phase against *S. aureus* from shaking, static, and plate-based incubation condition.
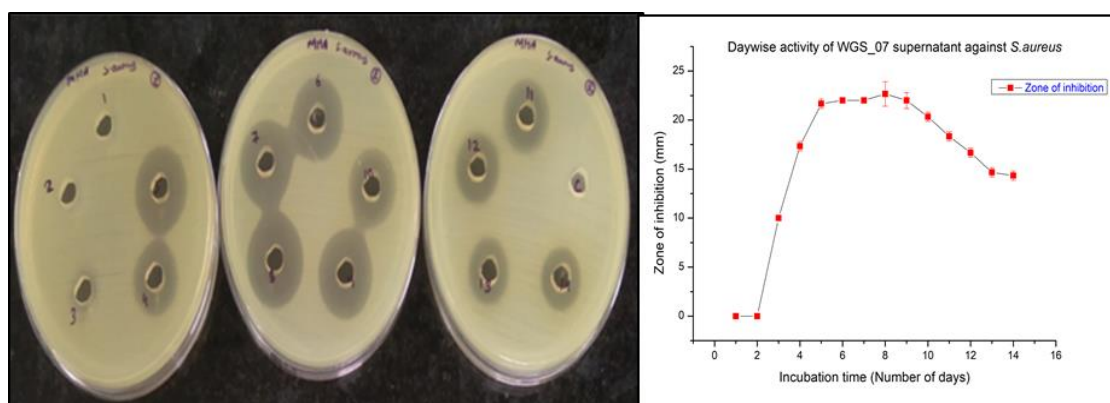
Figure 5. Day-wise activity of *Amycolatopsis* sp. WGS_07 supernatant against *S.aureus.*

The day-wise activity from the culture *Amycolatopsis* sp. WGS_07 was demonstrated using 100 µL of cell-free supernatant using the fermentation media 5294 in 500 mL flask with 100 mL of media. The activity was observed against *S. aureus* from third day of incubation, and maximum activity measured on eighth day of incubation with 22 mm zone of inhibition. The activity was maintained from 5th to 9th day of incubation, however from 10th day there was decline in the activity (Figure 5).

3.3 Fermentation, Purification and analysis of purified bioactive compounds

The *Amycolatopsis* sp.WGS_07 was considered as the potential candidate for novel bioactive compound production. The *Amycolatopsis* are well known producer of antibiotics (Song et al. 2021). Since no bioactive molecules was reported from closely related *Amycolatopsis silviterrae (*Jamjan et al. 2018), we speculated that this strain could be possible source of novel bioactive molecules. The large-scale fermentation of *Amycolatopsis* sp.WGS_07 was

carried out in both the liquid static and plate-based incubation (Figure 6). The fermentation of 50L in 5294 media at liquid static condition yielded 52g of semi-solid crude substance after extraction with ethyl acetate and concentration by rotary evaporator. The plate-based fermentation of 10L (400 plates) in 5294 media followed by extraction and concentration yielded 10.2 g of crude extract. The chromatography techniques like silica gel column chromatography, TLC and semi-preparative HPLC were employed for bioactive compounds purification from the crude extract (Figure 7). The bioactivity-guided purification of semi-solid crude extract from static incubation led to isolation of four bioactive compounds (Figure 8).
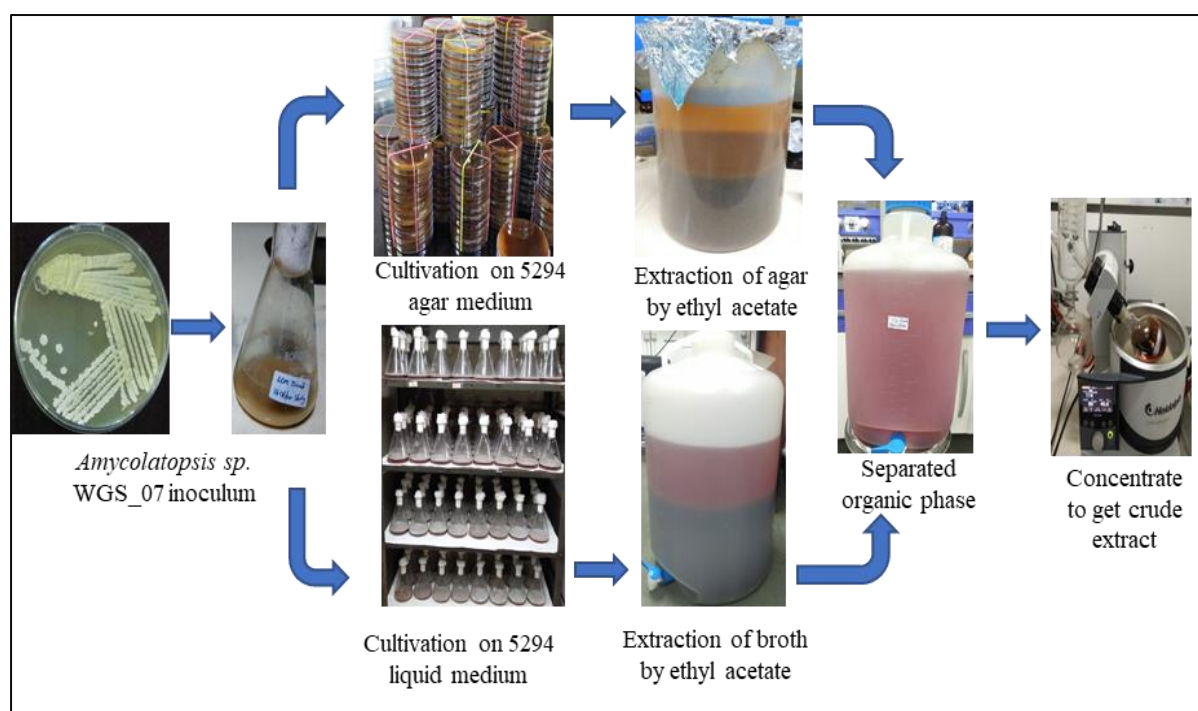
Figure 6. Schematic representation of large scale fermentation and extraction of *Amycolatopsis* sp. WGS_07.

The antibacterial compound-**1** isolated from the column fraction (CF-9) by reverse phase semi-preparative HPLC was major yellow solid compound with the yield of 5250 mg from 50L of fermentation. The isolated compounds after multiple chromatographic separations were analysed for the purity by analytical HPLC. The compound **1** was pure with retention time of 13.22 in the 25 min long run (Figure 15). The congener of compound **1** closely eluted in fraction-3 of CF-9 from semi-preparative HPLC was later separated as compound **2** along with compound **1** (Figure 9 and 10). The purified compound **2** was obtained as a yellow solid with yield of 186 mg and eluted at retention time of 12.66 (Figure 16).
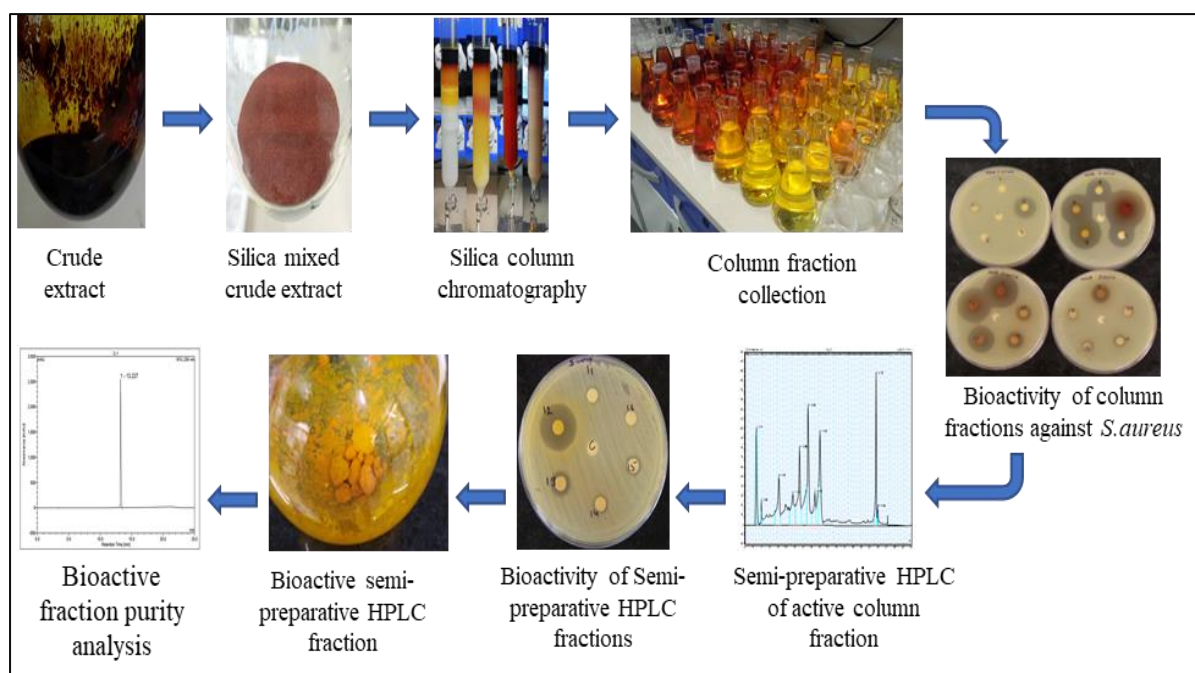
Figure 7. Schematic representation for purification of the crude extract of *Amycolatopsis* sp. WGS_07.

The bioactive compound **3** was isolated from the complex column fraction CF-5-8. Number of chromatography techniques were used to finally purify the compound **3** (Figure 11-13). The compound **3** obtained as yellow solid was similar to compound **1** and **2** but with less polarity. The yield of compound **3** was obtained in least quantity of 32 mg after separation by preparative TLC followed by normal phase semi-preparative HPLC by chiral amylose column. The retention time of compound **3** was 14.55 (Figure 17). The compound-**4** was purified using semi-preparative HPLC by reverse phase mode and was less polar compared to compound **1-3.** The compound **4** obtained as white hairy crystalline solid with yield of 146 mg and eluted at retention time of 15.02 (Figure 18).

The ethyl acetate crude extract from plate-based incubation was separated with the similar purification strategy of column chromatography and semi-preparative HPLC. Like the static condition, similar major compound **1** was obtained with yield of 620 mg from 10L of plate-based incubation of *Amycolatopsis* sp. WGS_07. The compound **2** with yield of 24 mg was also obtained with similar properties. The compound **3** and **4** were not obtained in the plate-based incubation condition may be due to their lower yield. Large-scale fermentation under different growth conditions proved important in isolating novel molecules. Due to their lower yields, these molecules might not be detected under small-scale fermentation.
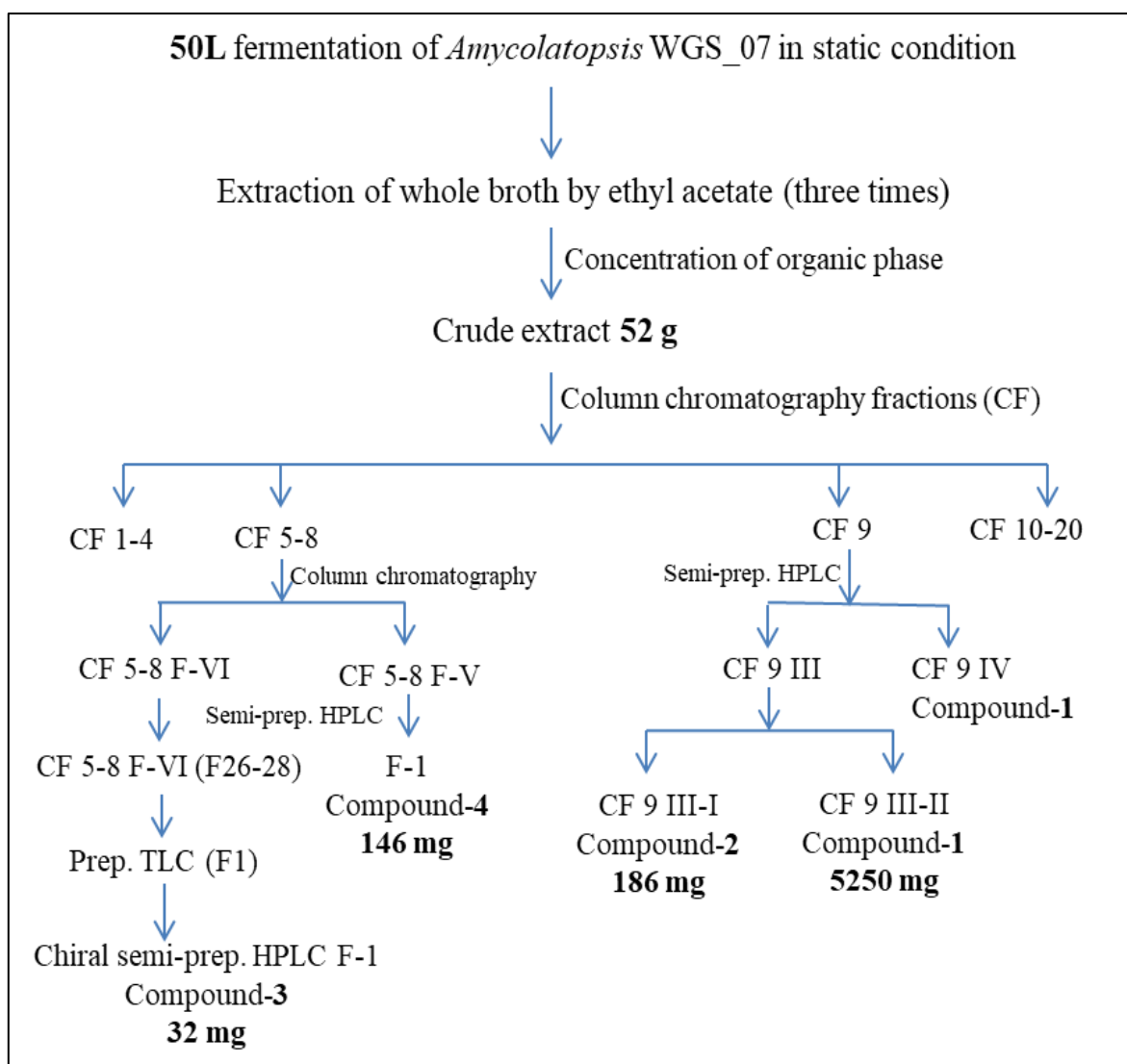
Figure 8. Schematic diagram for the purification of bioactive compounds from crude extract of *Amycolatopsis* sp. WGS_07 incubated under static condition.
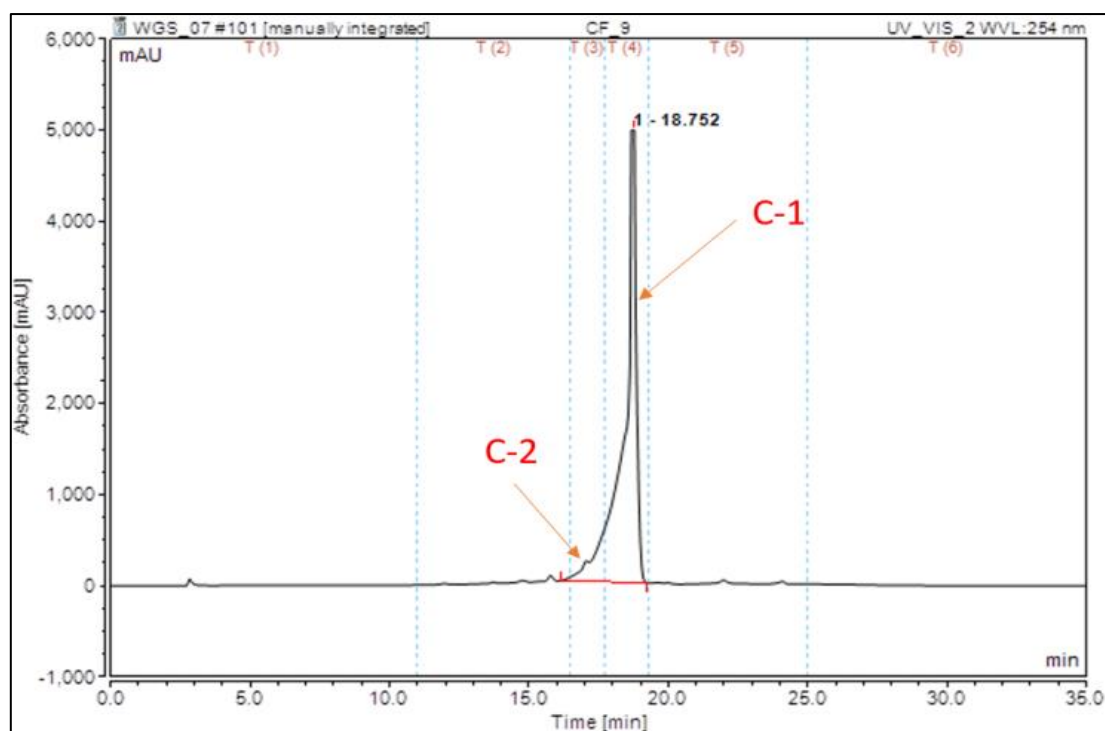
Figure 9. Chromatogram of column fraction (CF-9) with major compound **1** (C-**1**) in fraction-4 and minor compound **2** (C-**2**) in fraction-3 by semi-preparative HPLC.
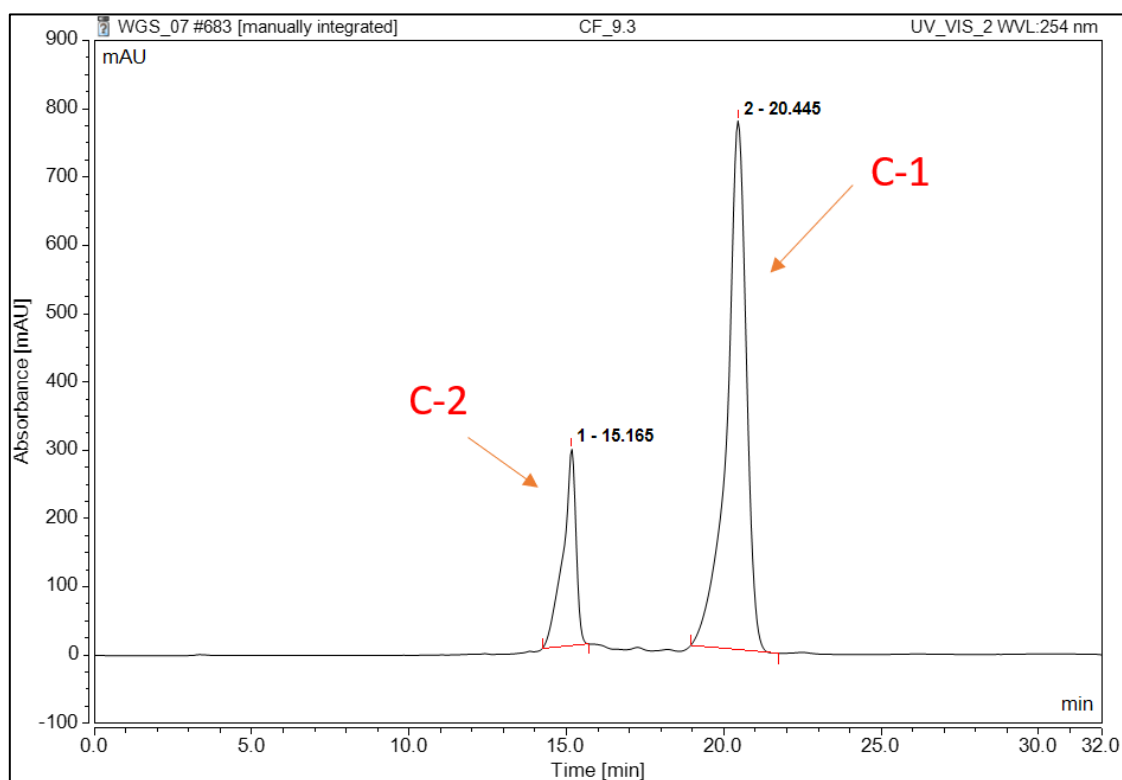
Figure 10. Chromatogram of major compound **1** (C-**1**) and minor compound **2** (C-**2**) after separation from fraction-3 of CF-9 by semi-preparative HPLC.
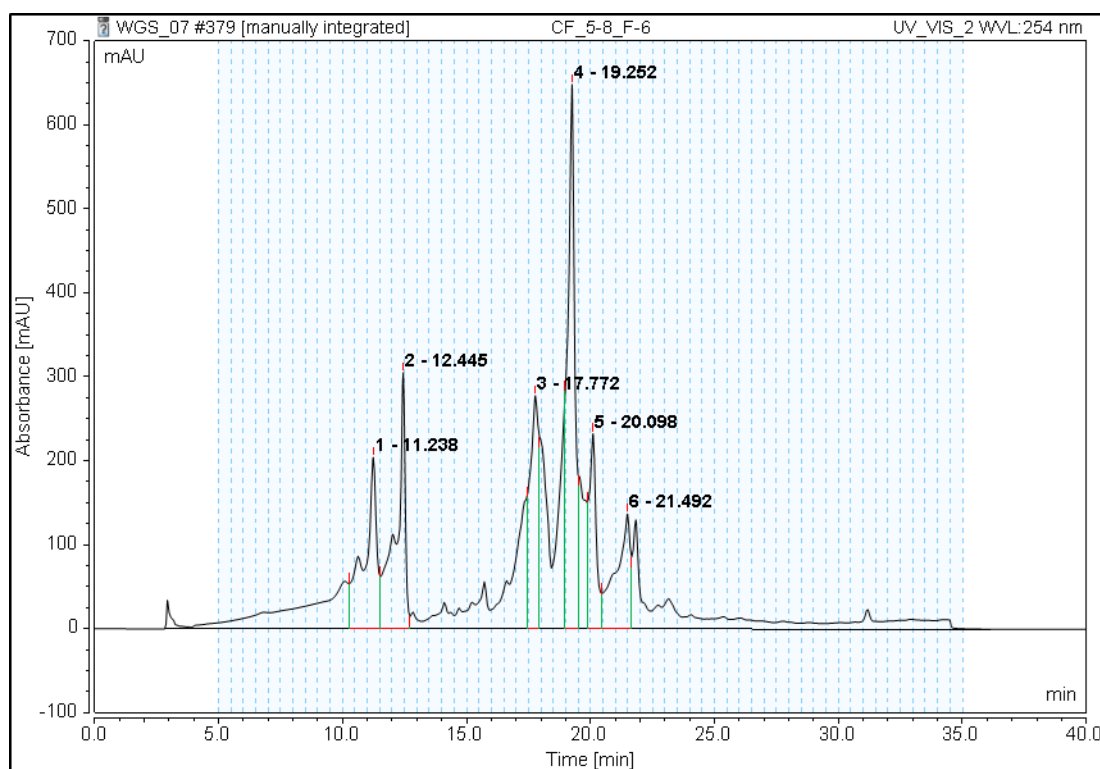
Figure 11. Semi-preparative HPLC (reverse- phase) separation of fraction-6 of the CF 5-8, with bioactivity in eluted fractions 26-28.
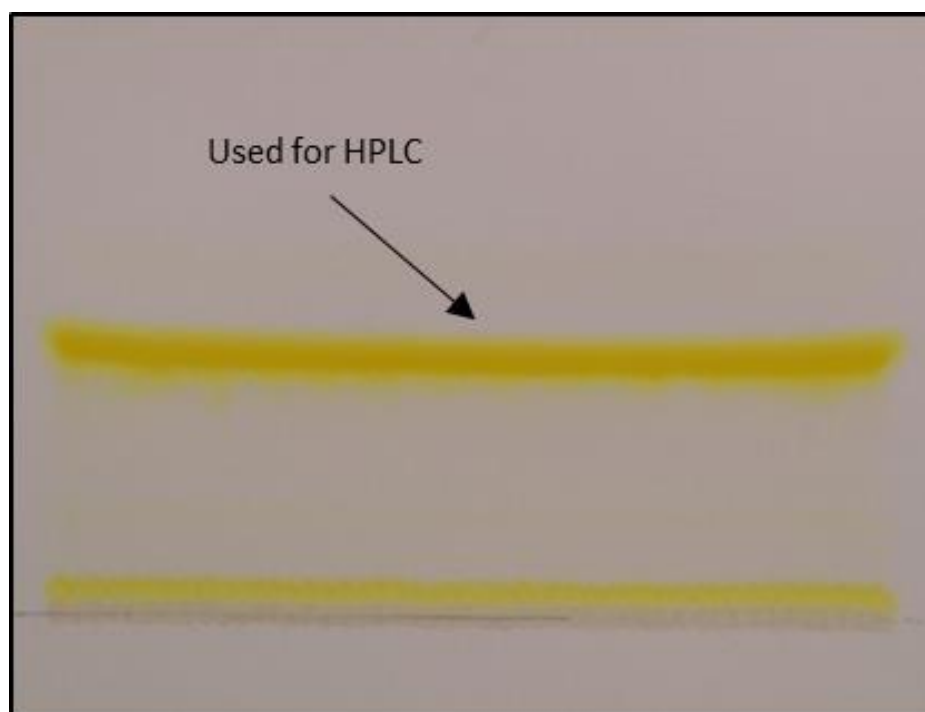
Figure 12. Separation of bioactive semi-preparative HPLC fraction 26-28 by preparative TLC using pet ether : ethyl acetate (80:20).
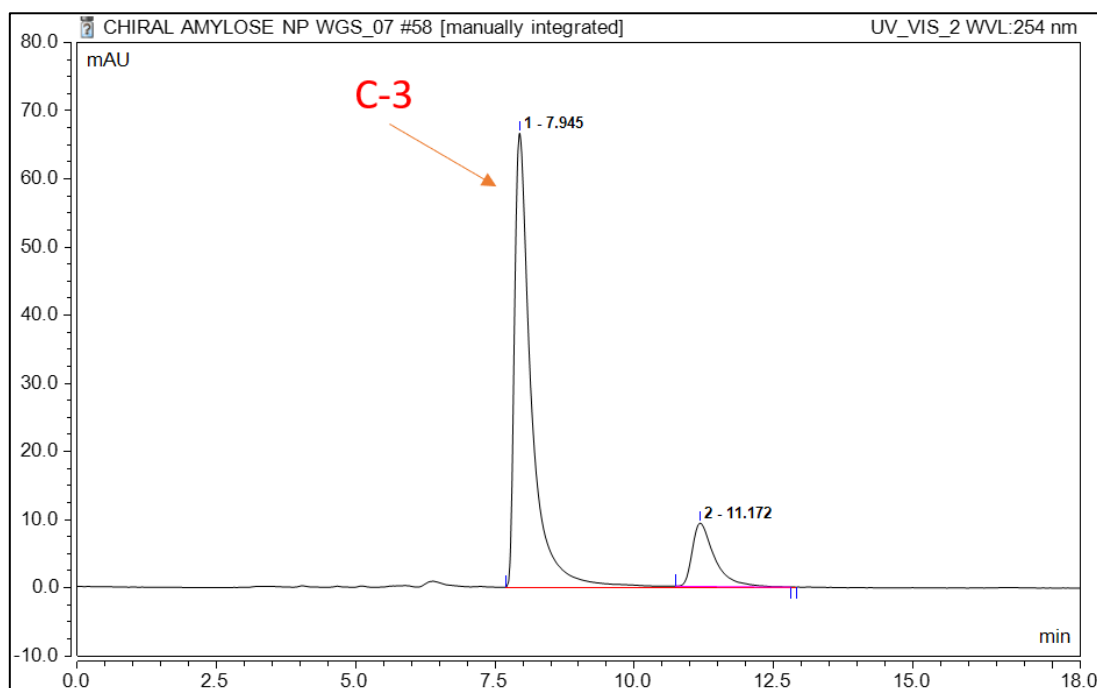
Figure 13. Chromatogram of TLC band after separation of compound **3** (C-**3**) by semi-preparative HPLC using normal phase chiral amylose column.
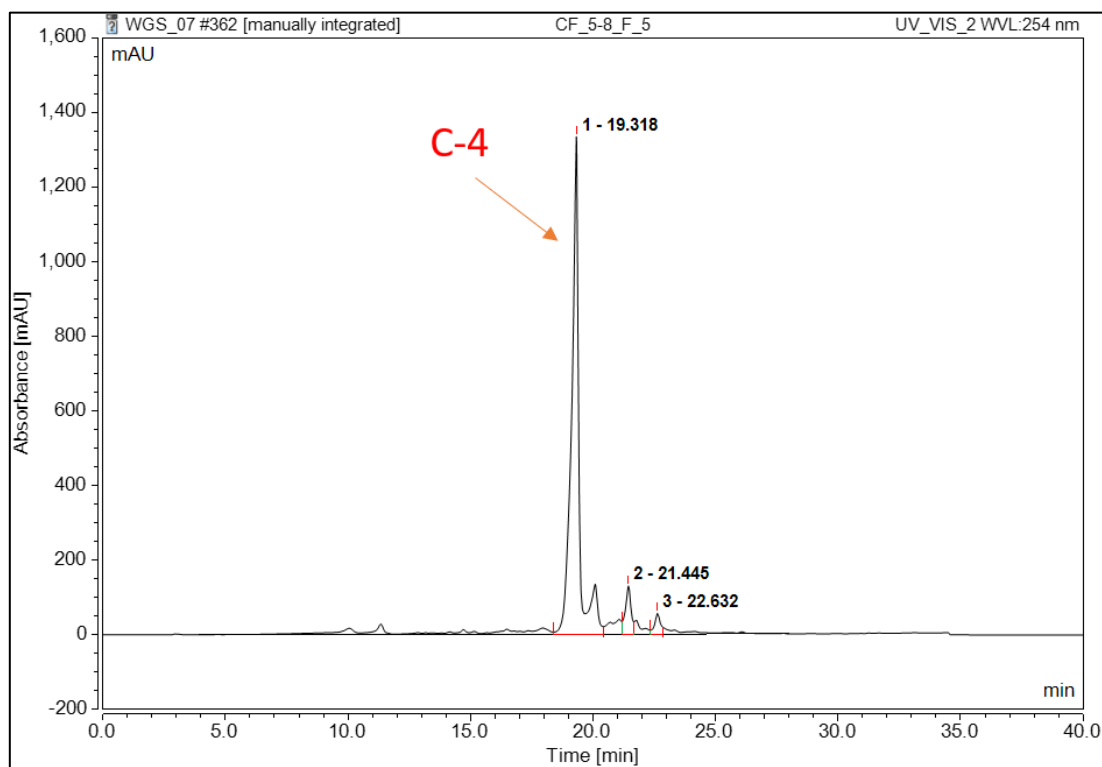
Figure 14. Chromatogram of compound **4** (C-**4**) after separation of column fraction-5 by semi-preparative HPLC.
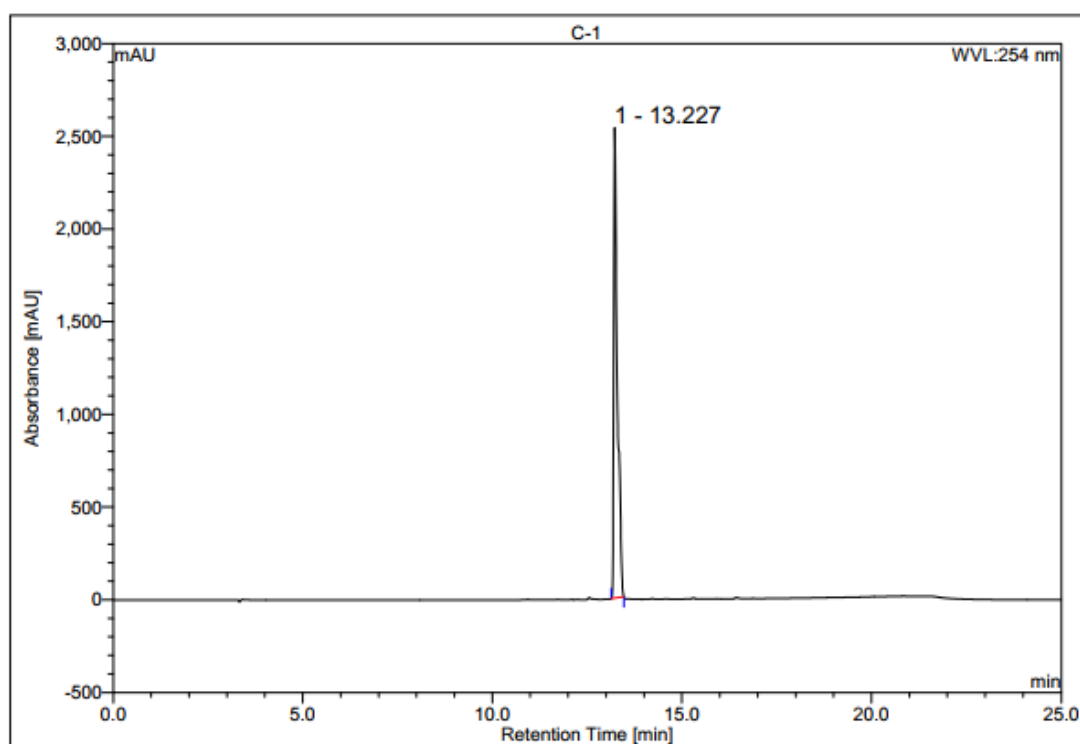
Figure 15. HPLC chromatogram of purified compound-**1** (C-**1**).
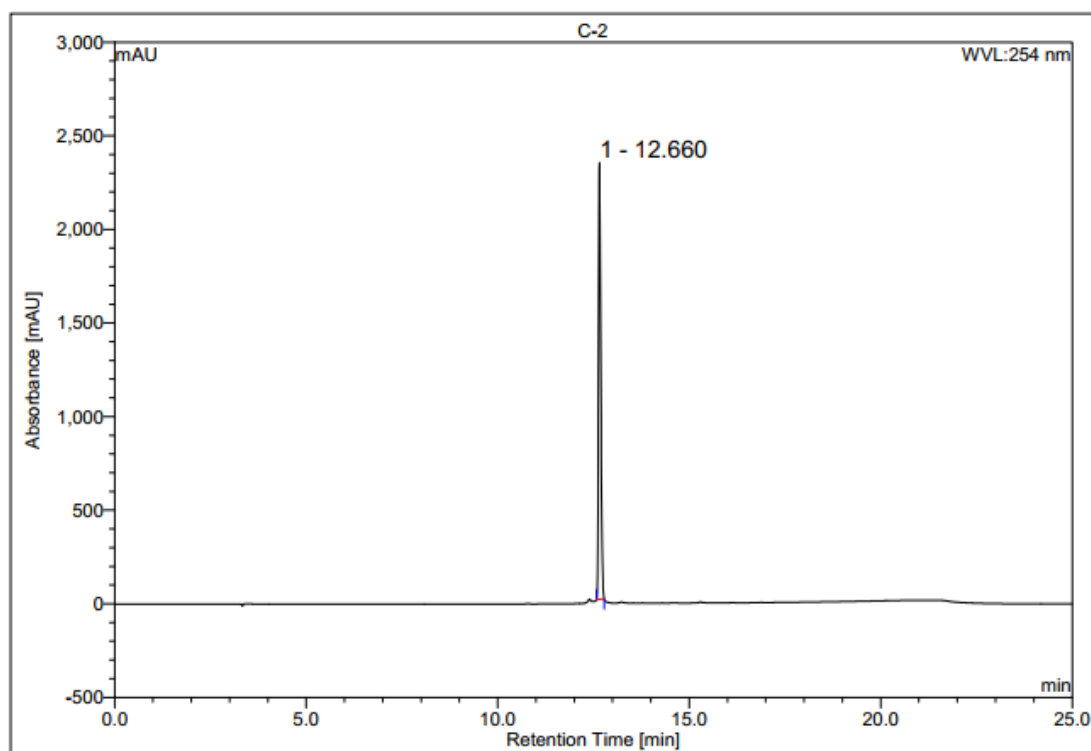
Figure 16. HPLC chromatogram of purified compound-**2** (C-**2**)
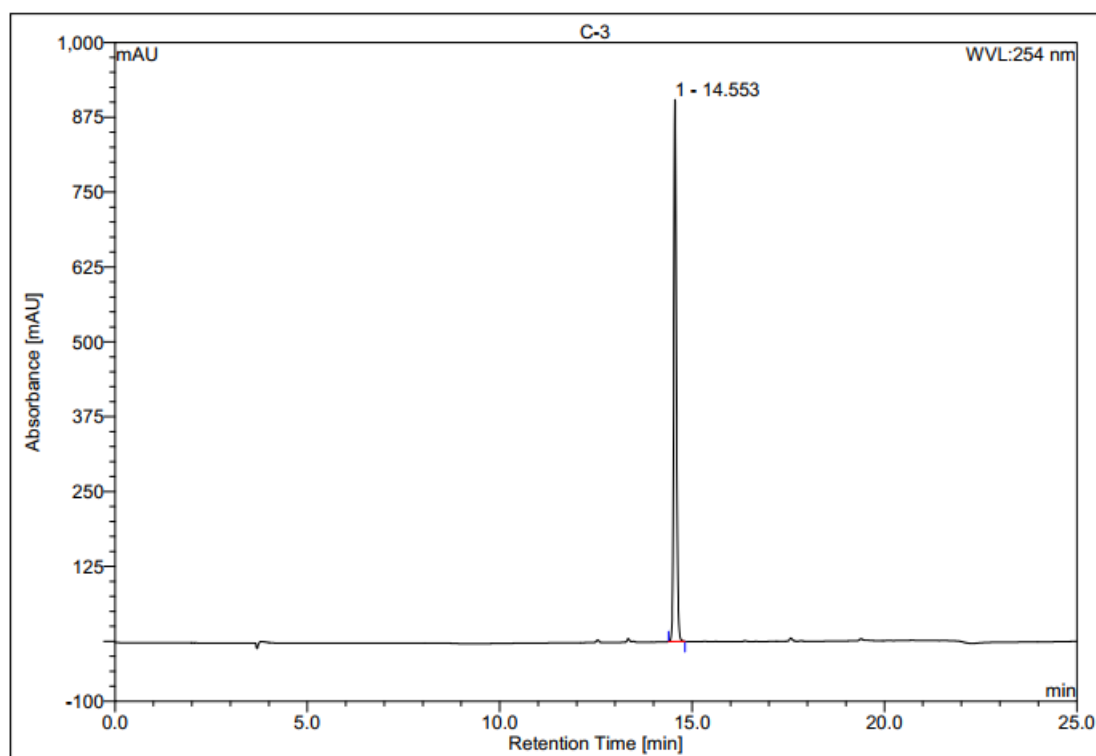
Figure 17. HPLC chromatogram of purified compound **3** (C-**3**).
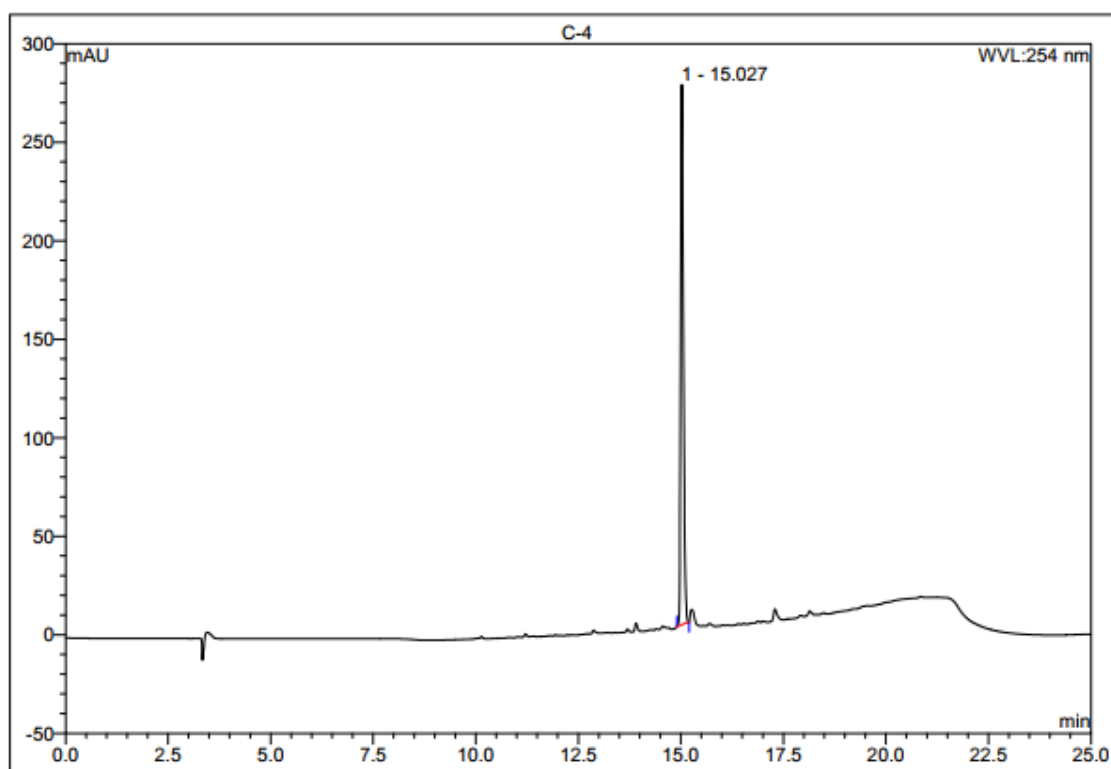
Figure 18. HPLC chromatogram of purified compound-**4** (C-**4**).

3.4 Structure elucidation of the purified bioactive compounds

The four isolated bioactive compounds from the fermentation broth of *Amycolatopsis* sp. WGS_07 were majorly characterized by NMR, HR-MS and X-Ray Crystallography.

3.4.1 Structure elucidation of Compound-1 (Enceleamycin A)

The compound-**1** named as Enceleamycin A (**1**) was isolated as yellow solid. High-resolution mass spectrometry (HRMS) determined the molecular formula of **1** to be $C_{17}H_{14}O_7$, requiring 11 indices of H deficiency. The electronic circular dichroism (ECD) spectrum displayed positive Cotton effect at 249 nm (CD, 0.06 mg/mL, CH_3CN), λ_{max} ($\Delta\varepsilon$) 249 (+23.51), 290 (−8.95) nm. The IR spectrum of **1** exhibits an absorption band at 3437 cm^{-1} for the hydroxy group, and 1641 cm^{-1} for the conjugated enone. The ^1H NMR spectrum of **1** in CD_3CN displayed proton signals for two sp^3 methyls [δ_H 1.34 (d, $J = 6.1$ Hz) and 1.59 (s)], three sp^3 methines [δ_H 5.74 (s), 5.72 (s), and 4.50 (q, $J = 6.4$ Hz)], three sp^2 methines [δ_H 7.25 (d, $J = 8.4$ Hz), 7.73–7.65 (m), and 7.64–7.56 (m)], and a phenolic proton [δ_H 11.51 (br s, 1 H)] (Table 1). The ^{13}C NMR spectra of **1** in CD_3CN had 17 carbon signals. Based on DEPT and HSQC analyses, the presence of two methyls (δ_C 17.9 and 19.7), six methines [three olefinic (δ_C 119.9, 124.9, and 138.6); three oxygenated sp^3 (δ_C 75.9, 92.2, and 111.7)], and nine nonprotonated carbons [three olefinic (δ_C 116.3, 126.0, and 134.4), two olefinic oxygenated (δ_C 161.0 and 162.9), two oxygenated sp^3 (δ_C 87.4 and 100.2), and two carbonyl carbons (δ_C 184.0 and 181.6)] was established. HMBC spectra showed correlations of H-12 (δ_H 7.25 and δ_C 124.9) with C-9 (C=O, δ_C 184.0) and C-10/C-11/C-13/C-14; H-13 (δ_H 7.73–7.65) with C-11/C-14/C-15; and H-14 (δ_H 7.64–7.56 and δ_C 119.9) with C-9 (C=O, δ_C 184.0)/C-10/C-11/C-12/C-13/C-15/C-16 (C=O, δ_C 181.6) and ^1H–^1H COSY cross-correlations of H-12/H-13/H-14, suggesting the presence of a 5-hydroxy-1,4-naphthoquinone ring system (Figure 19).

The HMBC correlation of H-1 [δ_H 5.74 (s), δ_C 92.2)] with C-2/C-3/C-4/C-7/C-8/C-16/C-17; H-7 [δ_H 1.59 (s), δ_C 19.7] with C-1/C-3/C-4; and H-2 [δ_H 5.72 (s), δ_C 111.7)] with C-1/C-3/C-4/C-5 demonstrated presence of two fused tetrahydrofuran moieties (head-to-tail) (Figure 19). ^1H–^1H COSY cross-peaks of H-5 [δ_H 4.50 (q, $J = 6.4$ Hz)] with H-6 [δ_H 1.34 (d, $J = 6.1$ Hz), δ_C 17.9] and HMBC correlation of H-5 with C-2/C-3/C-4, in combination with an unusual downfield shift of the C-2 signal (δ_H 5.72, δ_C 111.7, flanked by two oxygens), led us to assign the C-2 and C-3 fused oxetane and in turn provided the skeletal assignment of **1** possessing an unprecedented pentacyclic oxeto-furo-furo-naphthoquinone

(Figure 19, Table 1). Initially, relative stereochemistry of **1** was determined based on NOESY correlations between H-1/H-2/H-6/H-7, which revealed that these protons were cofacial (Figure 19B, Figure 24).
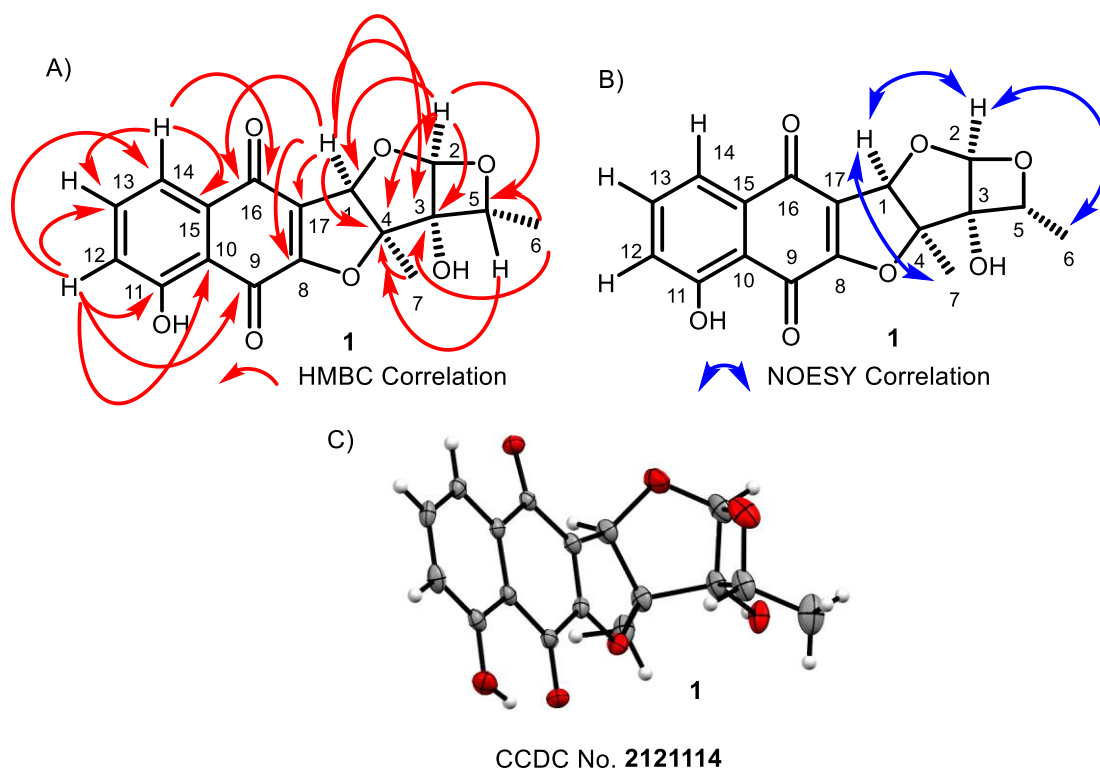
Figure 19. (A) Key HMBC correlations, (B) key NOESY correlations, and (C) ORTEP diagram of compound **1**.

A crystal of Enceleamycin A (**1**) was prepared from cold DMSO and CH_3CN, which led to the establishment of the complete structure and absolute stereochemistry. With 50% of probability level, the displacement ellipsoids were drawn. The hydrogen atoms are depicted as small spheres having arbitrary radii. Through X-ray diffraction tests using Cu radiation, anomalous dispersion effects (Flack parameter, 0.06(18)) determined the absolute configuration. Single-crystal X-ray diffraction data showed that Enceleamycin A (**1**) have R, R, R, S, and R configurations at positions C1, C2, C3, C4, and C5, respectively (Figure 19C). **Enceleamycin A (1):** yellow powder (5.25 g from 50 L, in 10.5% yield); $[\alpha]^{27}_D$ +51.60 (*c* 0.64, CH_3CN); UV (CH_3CN) λ_{max} (log ε) 202 (1.70), 222 (1.36), 289 (0.85), 416 (0.33) nm; IR (neat) (ν_{max}) 3437, 2891, 2821, 2103, 1641, 1443, 1212, 764 cm^{-1}; melting point 171–173 °C; HR-ESI *m/z* [M + H]$^+$ (calculaated for $C_{17}H_{15}O_7$ 331.0810; found 331.0812).
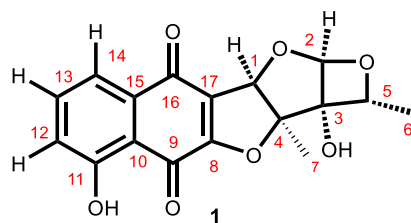
Figure 20. Structure of Compound-1.

Table 1. 1D and 2D NMR (500 MHz) data of Enceleamycin A (**1**) in CD₃CN.

Position	δ_H (*J* in Hz)	δ_C	DEPT	NOESY	COSY	HMBC
1	5.74 (s, 1H)	92.2	92.2 (CH)	H-7, $\delta1.59$		(C-2, $\delta111.7$), (C-3, $\delta87.4$), (C-4, $\delta100.2$), (C-7, $\delta19.7$), (C-8, $\delta161$), (C-16, $\delta181.6$),(C-17, $\delta126.0$),
2	5.72 (s, 1H)	111.7	111.7 (CH)	H-6, $\delta1.34$		(C-1, $\delta92.2$), (C-3, $\delta87.4$) (C-4, $\delta100.2$), (C-5, $\delta75.9$),
3		87.4				
4		100.2				
5	4.50 (q, *J* = 6.4 Hz, 1H)	75.9	75.9 (CH)	H-6, $\delta1.34$	H-6, $\delta1.34$	(C-2, $\delta111.7$), (C-3, $\delta87.4$), (C-4, $\delta100.2$)
6	1.34 (d, *J* = 6.1 Hz, 3H)	17.9	17.9(CH₃)	H-2, $\delta5.72$	H-5, $\delta4.50$	C-2, $\delta111.7$),(C-3, $\delta87.4$), (C-4, $\delta100.2$)
7	1.59 (s, 3H)	19.7	19.7(CH₃)	H-1, $\delta5.74$		(C-1, $\delta92.2$), (C-3, $\delta87.4$), C-4, $\delta100.2$)
8		161.0				
9		184.0				
10		116.3				
11		162.9				
12	7.25 (d, *J* = 8.4 Hz 1H)	124.9	124.9(CH)		H-12 $\delta7.73$-7.65	(C-9, $\delta184.0$),(C-10, $\delta116.3$), (C-11, $\delta162.9$), (C-13, $\delta138.6$), (C-14, $\delta119.9$)
13	7.73-7.65 (m, 1H)	138.6	138.6(CH)		H-12, $\delta7.25$, H-14, $\delta7.64$-7.56	(C-11, $\delta162.9$), (C-14, $\delta119.9$),(C-15, $\delta134.4$),
14	7.64-7.56 (m, 1H)	119.9	119.9(CH)		H-13, $\delta7.73$-7.65	(C-9, $\delta184.0$), (C-10, $\delta116.3$), (C-11, $\delta162.9$), (C-12, $\delta124.9$), (C-13, $\delta138.6$),(C15, $\delta134.4$) (C-16, $\delta181.6$),
15		134.4				
16		181.6				
17		126.0				
OH (C-11)	11.51 (br.s, 1H)					(C-10, δ 116.3), (C-11, δ 162.9), (C-12, $\delta124.9$)
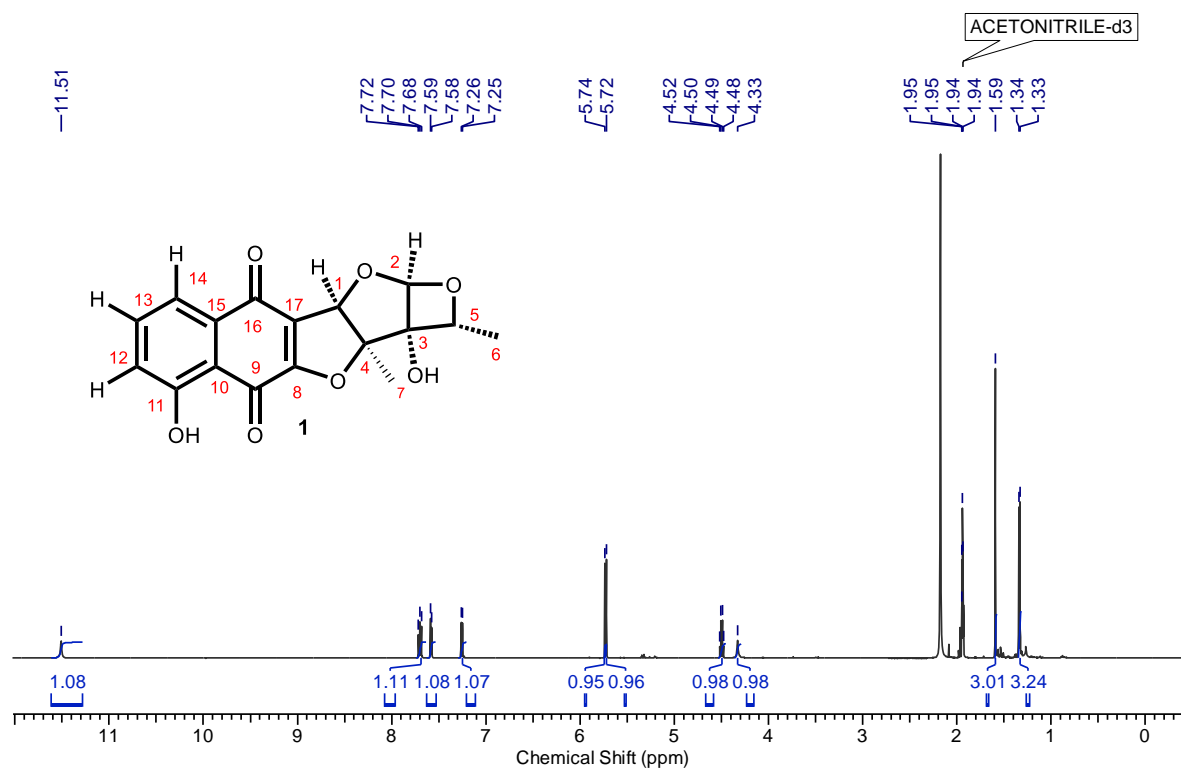
Figure 21. ^{1}H NMR spectrum (500 MHz) of **Compound-1** in CD$_3$CN.
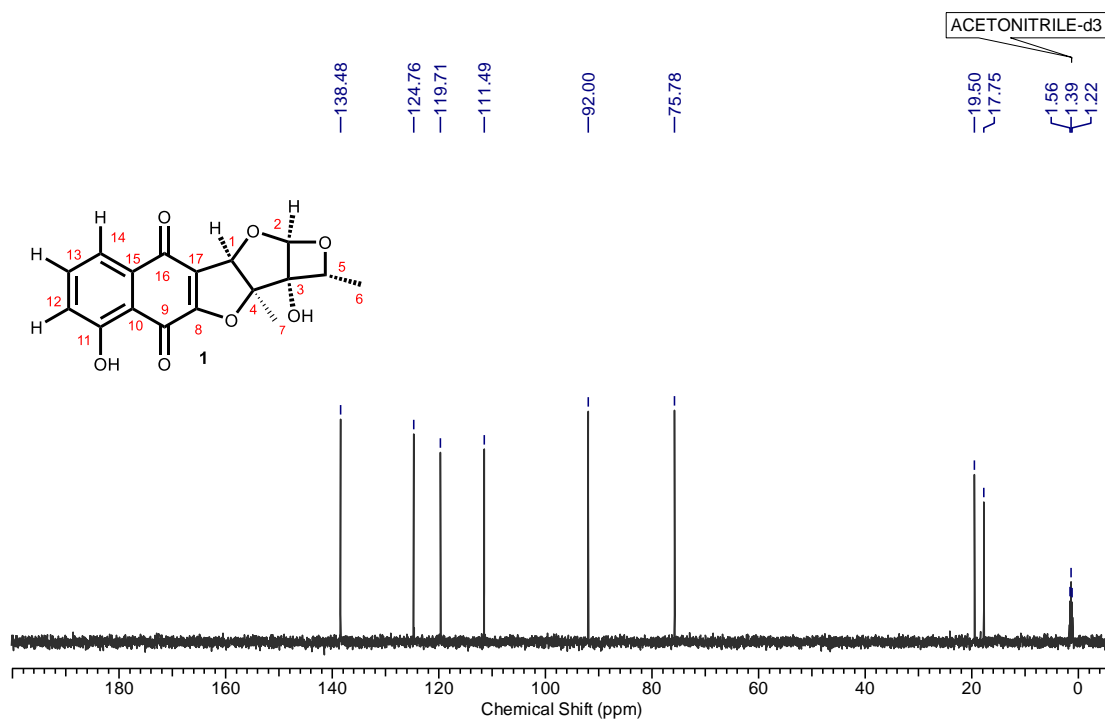
Figure 22. DEPT NMR spectrum (125 MHz) of **Compound-1** in CD$_3$CN.
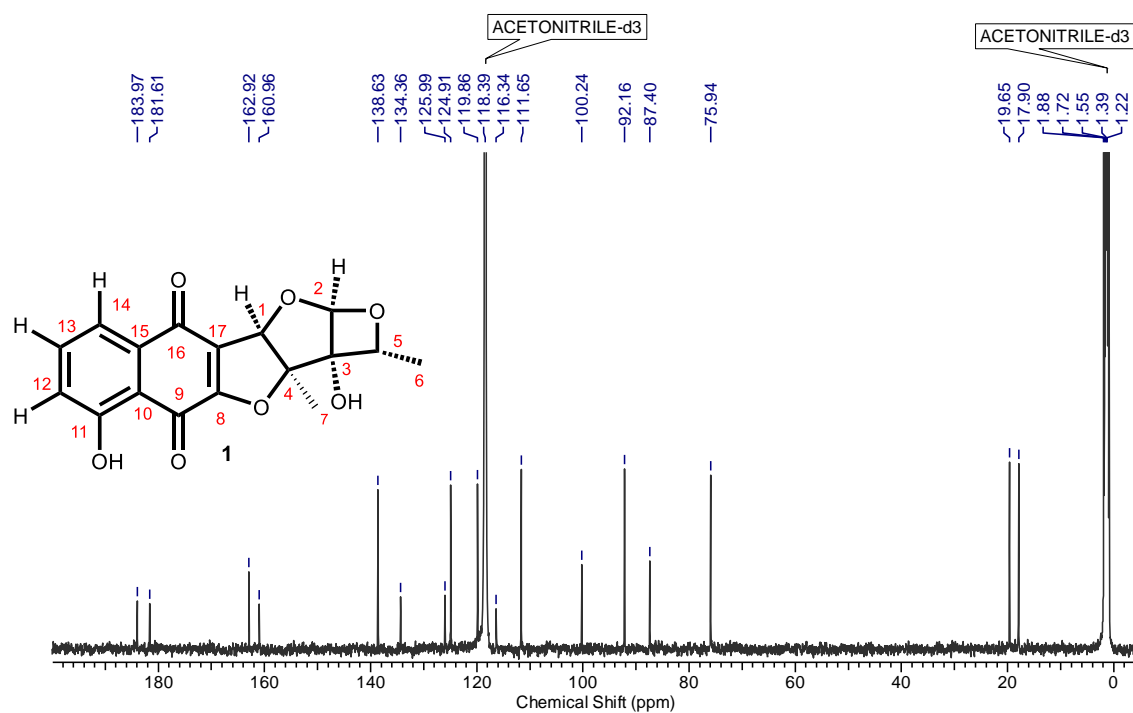
Figure 23. ^{13}C NMR spectrum (125 MHz) of **Compound-1** in CD$_3$CN.
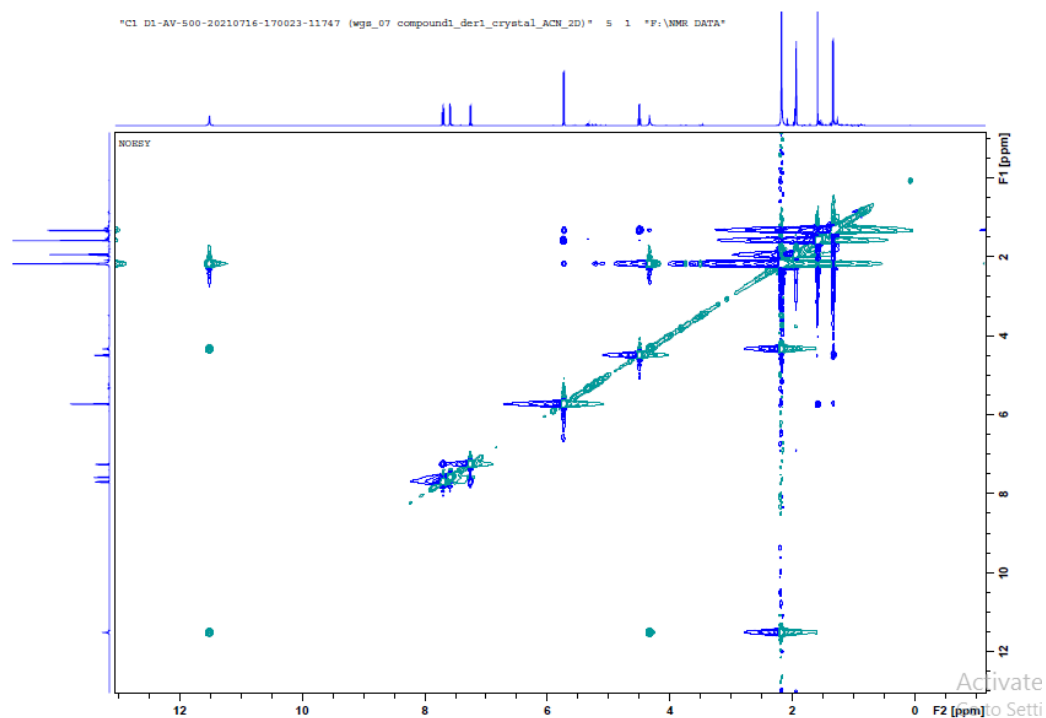
Figure 24. NOESY NMR spectrum (500 MHz) of **Compound-1** in CD$_3$CN.
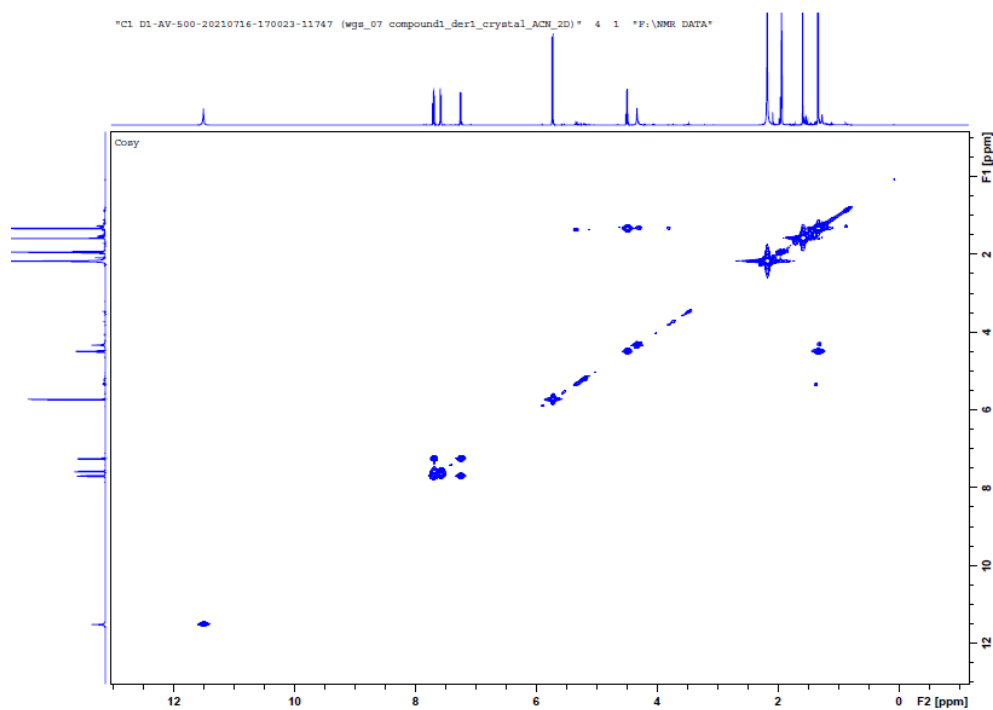
Figure 25. COSY NMR spectrum (500 MHz) of **Compound-1** in CD$_3$CN.
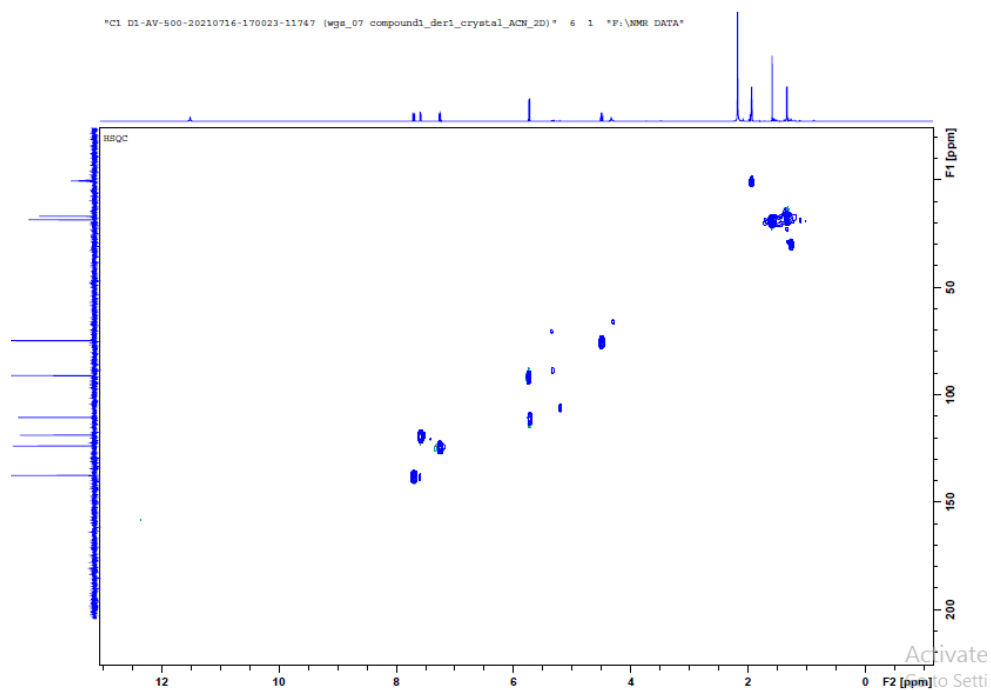
Figure 26. HSQC NMR spectrum (500 MHz) of **Compound-1** in CD$_3$CN.
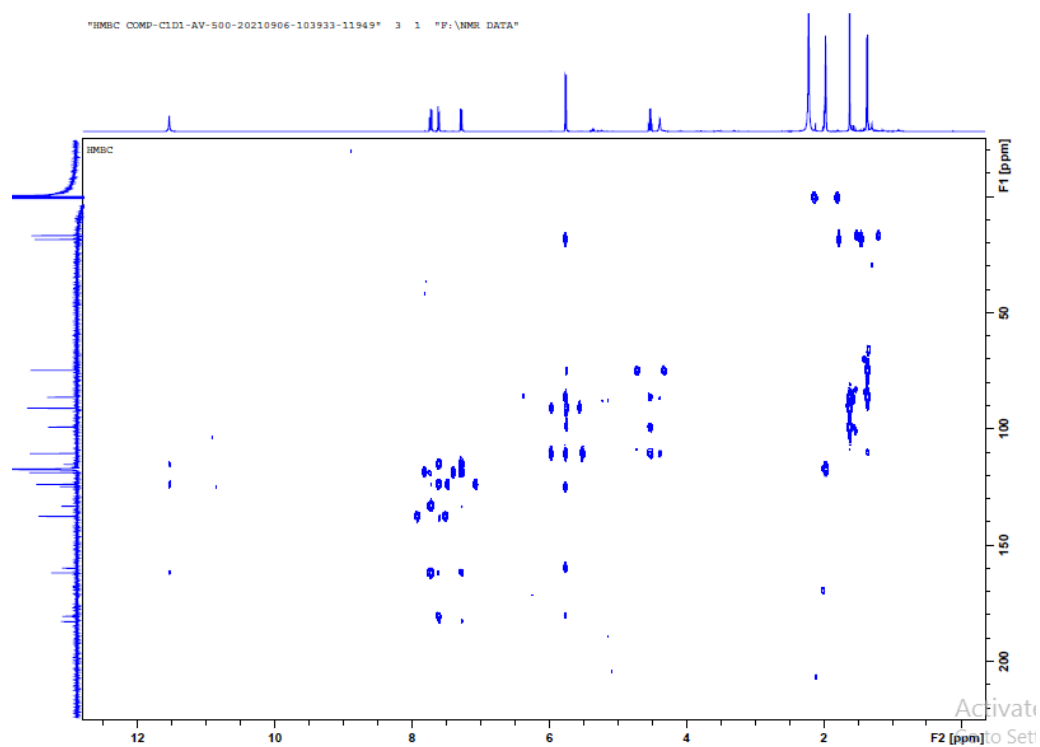
Figure 27. HMBC NMR spectrum (500 MHz) of **Compound-1** in CD$_3$CN.
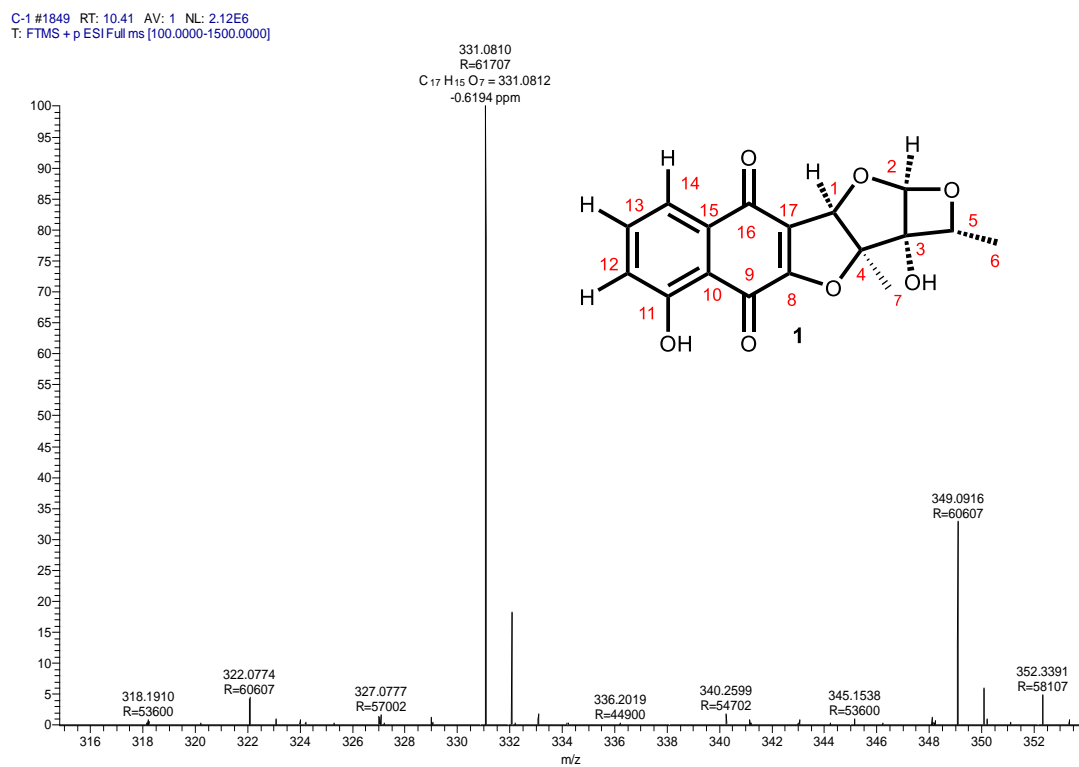
Figure 28. HR-ESIMS of Compound -1.
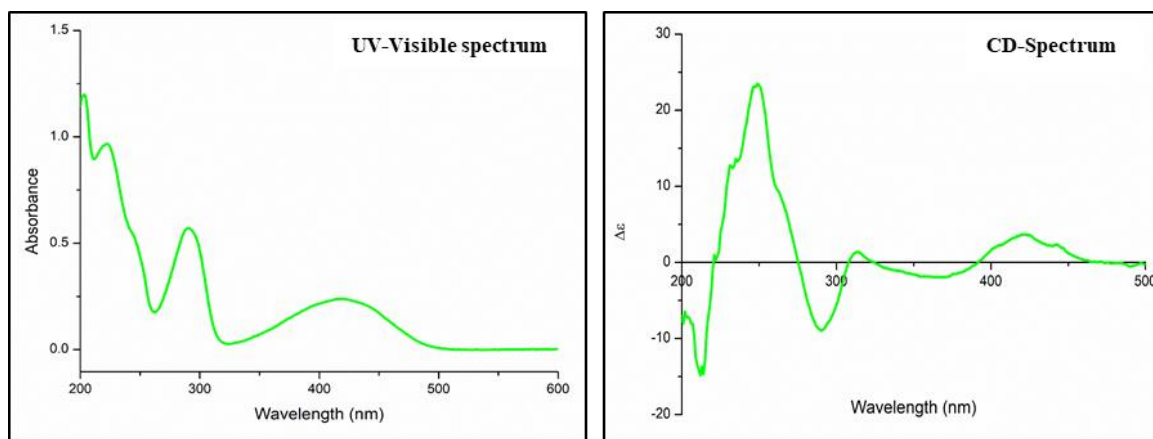
Figure 29. UV-Visible and CD spectrum of **Compound-1.**
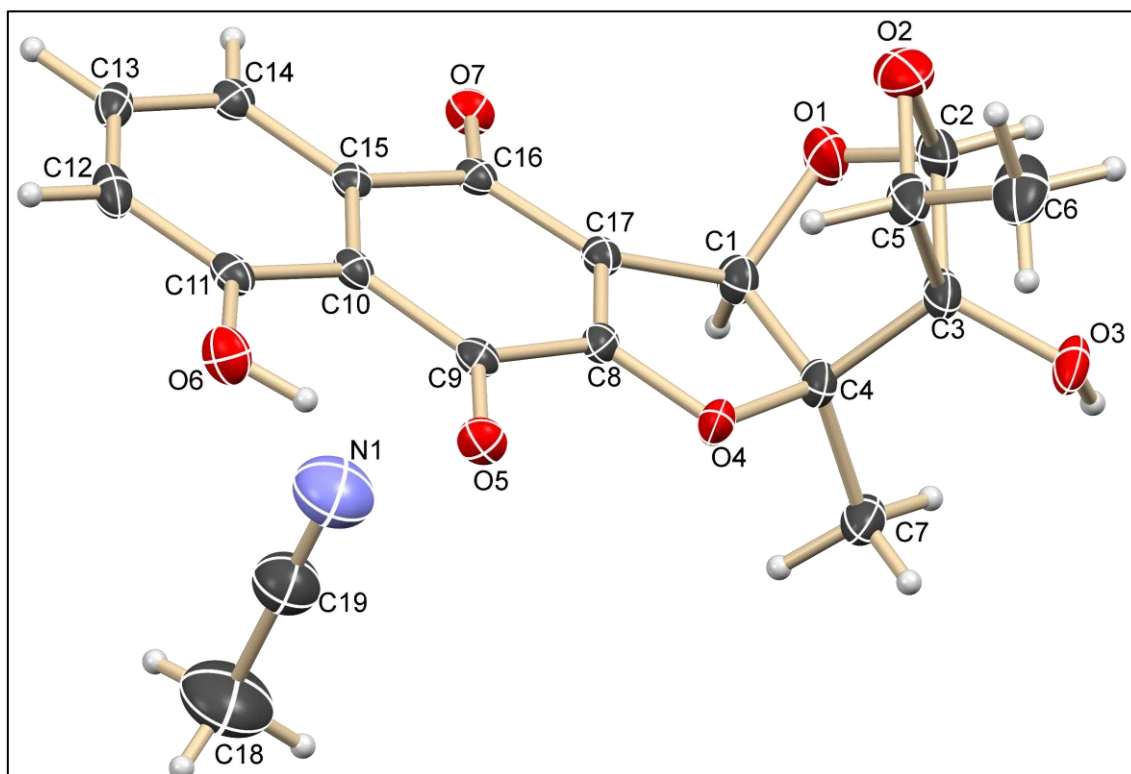
Figure 30. ORTEP view of Compound 1.

3.4.2 Structure elucidation of Compound-2 (Enceleamycin B)

The compound-**2** named as Enceleamycin B (**2**) isolated as a yellow powder. The molecular formula was found to be $C_{17}H_{16}O_9$ based on HRMS (ESI) analysis, requiring 10 indices of H deficiency. The ECD spectrum showed negative Cotton effect at 273 nm (CD, 0.053 mg/mL, CH_3CN), λ_{max} ($\Delta\varepsilon$) 273 (−43.54), 243 (26.11) nm. The 1D and 2D NMR spectrum of compound **2** was overall close to compound **1**, with few exceptions. The ^1H NMR data for **2** (Table 2) in DMSO-d_6 show two methyls (δ_H 1.01 (d, J = 6.6 Hz) and 1.58 (s)), six methines [three oxygen-attached sp^3 (δ_H 3.94 (q, J = 6.6 Hz), 4.34 (s), and 5.01 (d, J = 4.3 Hz) and three sp^2 (δ_H 7.32 (dd, J = 0.83, 7.48 Hz), 7.56 (dd, J = 0.85, 7.48 Hz), and 7.75 (m)], one phenolic [δ_H 10.96 (br s, 1H)] proton, and three hydroxy protons [δ_H 6.93 (d, J = 4.3 Hz) for C2-OH, 5.04 (s) for C8-OH, and 7.09 (s) for C-17-OH]. The ^{13}C NMR spectrum (Table 2) of **2** in DMSO-d_6 had 17 carbon signals. Using DEPT and HSQC analyses established the presence of two methyls [δ_C 14.0 (C-6), 18.7 (C-7)], six methines [three oxygenated sp^3 δ_C 3.94 (C-5), 86.5 (C-1), and 96.3 (C-2) and three olefinic sp^2 δ_C 123.4, 136.9, and 119.3], and four carbons [with oxygenated δ_C 80.1 (C-3), 82.2 (C-17), 91.2 (C-4), and 102.9 (C-8)]. The existence of two new oxygenated carbon signals (δ_C 102.9 for C-8 and δ_C 82.2 for C-17) and a downfield resonance of carbonyl carbons C-9 (δ_C 188.5) and C-16 (δ_C 191.4) compared to compound **1** [C-9 (δ_C 184.0) and C-16 (δ_C 181.6)] led to tentative assignment of structure of **2** as the 8,17-dihydroxylated naphthoquinone segment of **1** (Figure 31, Table 2).
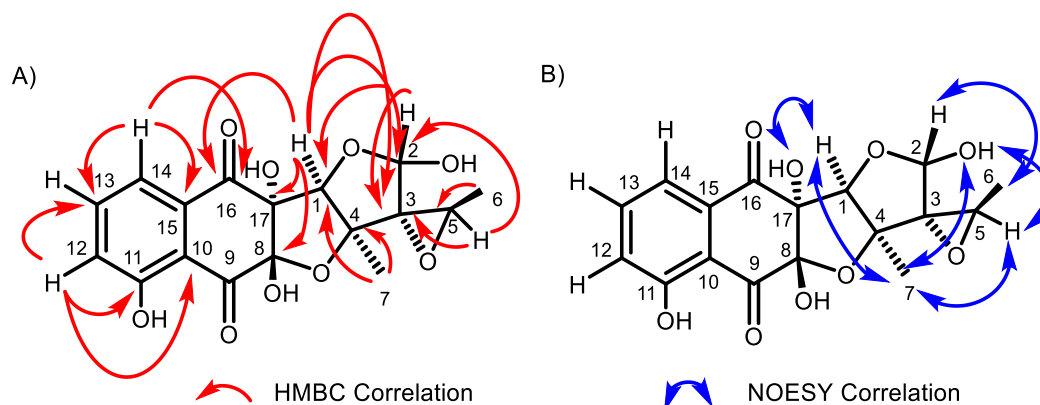
Figure 31. (A) Key HMBC correlations; (B) key NOESY correlations of compound **2**.

The HSQC data determined all ^1J (^1H–^{13}C) connectivities. COSY and HMBC analyses in DMSO-d_6 confirmed the remaining skeletal connectivities. Particularly, HMBC correlation of H-1 (δ_H 4.43) with C-2/C-3/C-4/C-7/C-8/C-16 and H-7 (δ_H 1.58) with C-1/C-3/C-4 validated

the right-side furo-furan segment. In contrast to compound **1**, ^{1}H NMR data (in DMSO-d_6) of compound **2** showed a doublet for H-2 (δ_H 5.01, J = 4.3 Hz) via coupling with the C-2-OH proton (δ_H 6.93, J = 4.3 Hz), which led to the proposition of a cyclic hemiacetal right part instead of a furo-oxetane fused system. The formation of a cyclic hemiacetal could be attributed to the enzymatic (Brønsted acid-mediated) opening of the fused furo-oxetane bicyclic ring system of compound **1** followed by subsequent epoxide formation involving C-3 and C-5 hydroxy groups (*vide infra*).

This proposed structure was established through HMBC correlation of C-5–H with C-2/C-3/C-6 and of C-2–H with C-5/C-1/C-3 and subsequently by HSQC and NOESY analyses. NOESY correlation of H-1 with H-7 (methyl) and of H-7 (methyl) with H-1/H-5/C-2–OH indicated the cofacial nature of all these groups. NOESY correlation of H-2 with H-6 (methyl) revealed the *trans* geometry of 1,2-substituents of the right-side tetrahydrofuran (THF) ring. Further, the NOESY correlation of H-1 with C-17–OH indicated the cofacial relation of these groups, which indirectly established the *trans* geometry of the C-8–C-17 vicinal diol. Based on the absolute stereochemistry of compound **1**, NOESY correlations observed, and anticipating the same biosynthetic origin for **1** and **2**, the stereochemistry of compound **2** was assigned as 1*R*, 2*S*, 3*R*, 4*S*, 5*R*, 8*S*, 17*S* (Figure 31).

Enceleamycin B (2): yellow powder (0.186 g from 50 L, in 0.37% yield); $[\alpha]^{27}_D$ +93.35 (CH$_3$CN, *c* 0.53); UV (CH$_3$CN) λ_{max} (log ε) 232 (2.65), 345 (0.60) nm; IR (neat) (ν_{max}) 3435, 2879, 2103, 1640, 1445, 1338, 1200, 1056, 769 cm^{-1} ; melting point 187–189 °C; HR-ESI *m/z* [M+ Na]$^+$ (calcd for C$_{17}$H$_{16}$O$_9$Na 387.0683; found 387.0687).
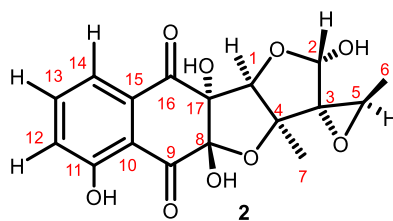
Figure 32. Structure of compound-2.

Table 2. 1D and 2D NMR(500 MHz) data of Enceleamycin B (**2**) in DMSO-d_6.

Position	δ_H (J in Hz)	δ_C	DEPT	NOESY	COSY	HMBC
1	4.43 (s, 1H),	86.5	86.5 (CH)	H-7, 1.58, H-17, 7.09		(C-7, δ18.7), , (C- δ4, 91.1), (C-8, δ102.9), (C-16, δ191.4), (C-17, δ82.2)
2	5.01 (d, J = 4.3 Hz, 1H)	96.3	96.3 (CH)	H-6, 1.01	3 (OH), 6.93	(C-1, δ86.5), (C-2, δ96.3), (C-5, δ71.0)
3		80.1				
4		91.2				
5	3.94 (q, J = 6.6 Hz,1H),	71.0	71.0 (CH)	H-6, 1.01, H-7, 1.58	H-6, 1.01	(C-2, δ96.3), (C-3, δ80.1), (C-6, δ 14.0)
6	1.01 (d, J = 6.6 Hz, 3 H))	14.0	14.0 (CH$_3$)	H-5, 3.94, H-2, 5.01	H-5, 3.94,	(C-3, δ80.1), (C-5, δ71.0),
7	1.58 (s, 3 H)	18.7	18.7 (CH$_3$)	H-1, 4.43		(C-1, δ86.5), (C-4, δ91.1)
8		102.9				
9		188.5				
10		117.1				
11		160.9				
12	7.32 (dd, J = 0.83, 7.48 Hz, 1H),	123.4	123.4 (CH)		H-13, 7.75 (dd, 1H)	(C-10, δ117.1), (C-11, δ160.9)
13	7.75 (t, J = 7.91 Hz 1H)	136.9	136.9 (CH)		H-12, 7.32 (dd, 1H), H-14, 7.56 (dd, 1H),	(C-11, δ160.9), , (C-13, δ136.9), (C-14, δ119.3),(C-15, δ136.4)
14	7.56 (dd, J = 0.85, 7.48 Hz 1H),	119.3	119.3 (CH)		H-13, 7.75 (dd, 1H)	(C-9, δ188.5)(C-10, δ117.1), (C-12, δ123.4), , (C-16, δ191.4)
15		136.4				
16		191.4				
17		82.2				
3 (OH)	6.93 (d, J = 4.3 Hz, 1H)			H-7, 1.58, H-1, 4.43, H-2,5.01	H-2, 5.01	(C-3, δ80.1), (C-17, δ82.2),
8 (OH)	5.04 (s, 1H)					
17 (OH)	7.09 (s, 1H)			H-7,1.58, H-1, 4.43		(C-2, δ96.3), (C-8, δ102.9), (C-9, δ188.5), (C-16, δ191.4)
11(OH)	10.96 (s., 1H)					
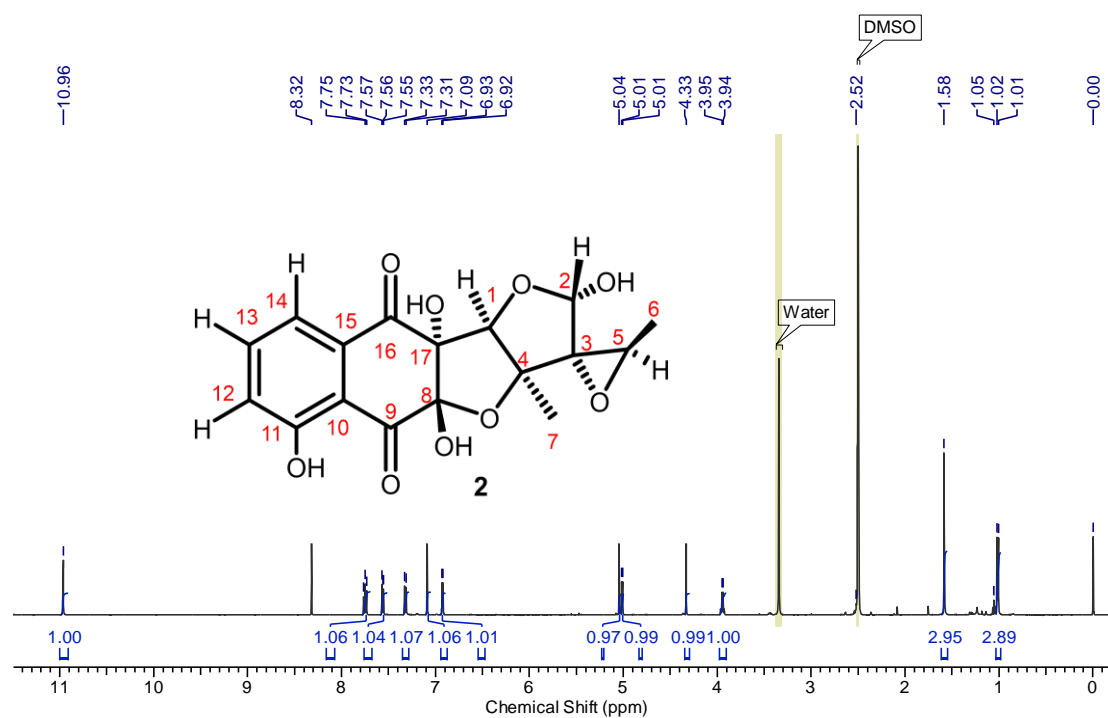
Figure 33.^{1}H NMR spectrum (500 MHz) of **Compound-2** in DMSO-d$_6$.
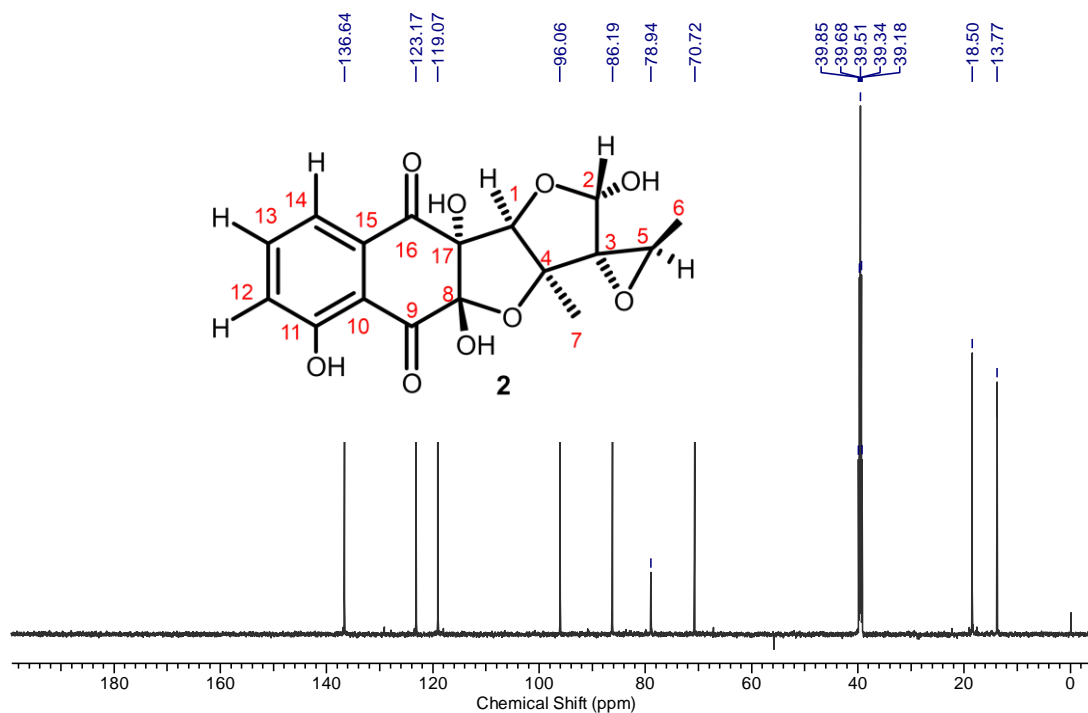
Figure 34. DEPT NMR spectrum (125 MHz) of **Compound-2** in DMSO-d$_6$.
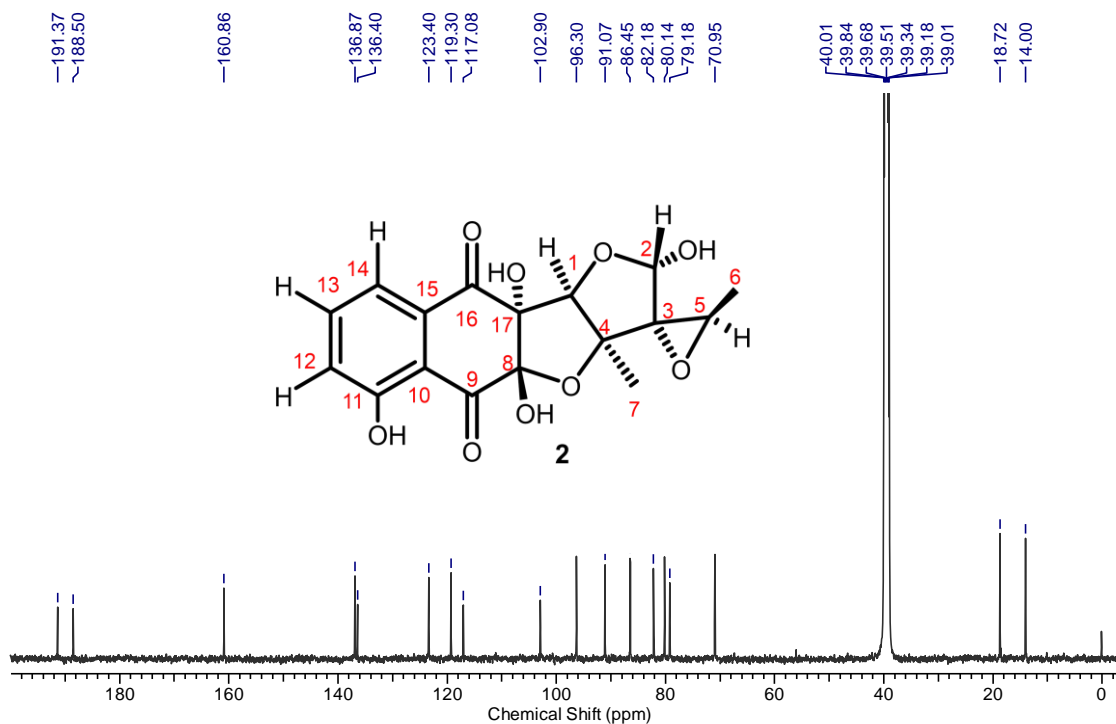
Figure 35. ^{13}C NMR spectrum (125 MHz) of **Compound-2** in DMSO-d6.
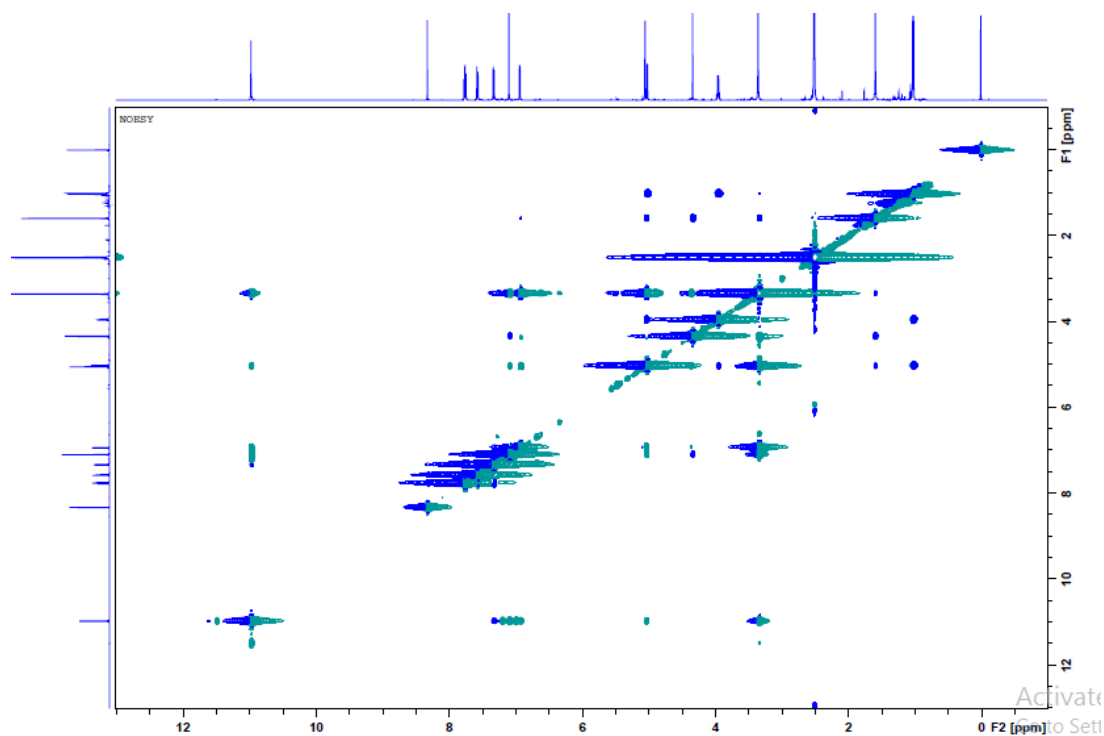
Figure 36. NOESY NMR spectrum (500 MHz) of **Compound-2** in DMSO-d$_6$.
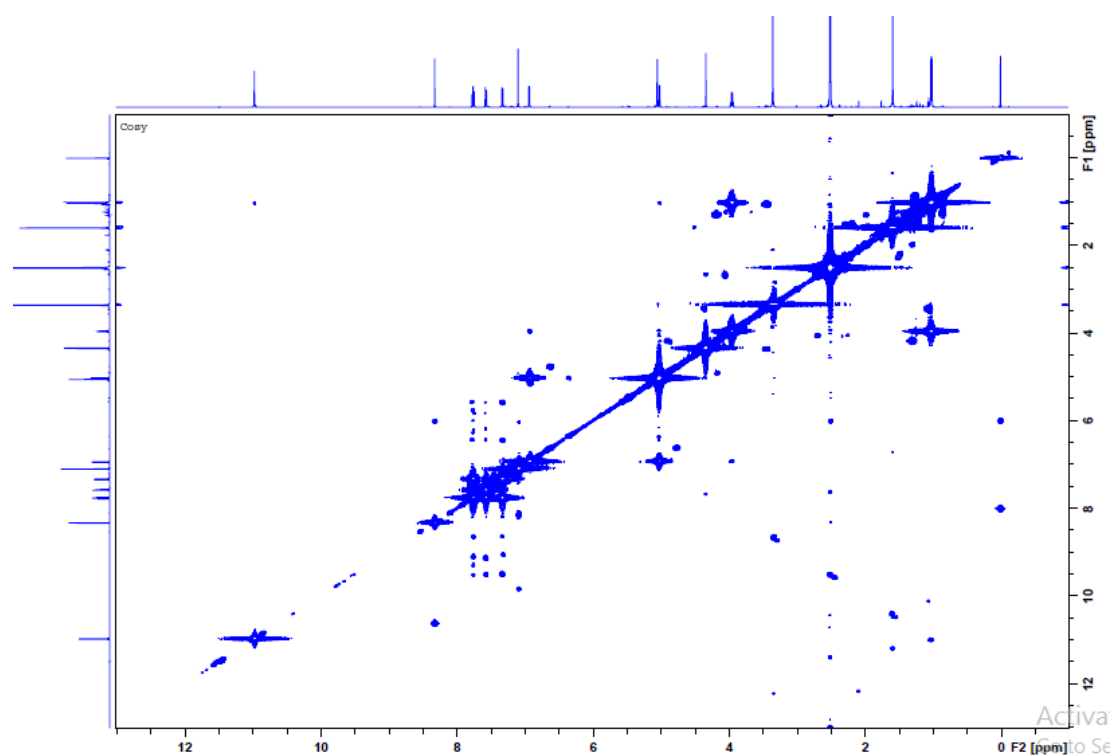
Figure 37. COSY NMR spectrum (500 MHz) of **Compound-2** in DMSO-d$_6$
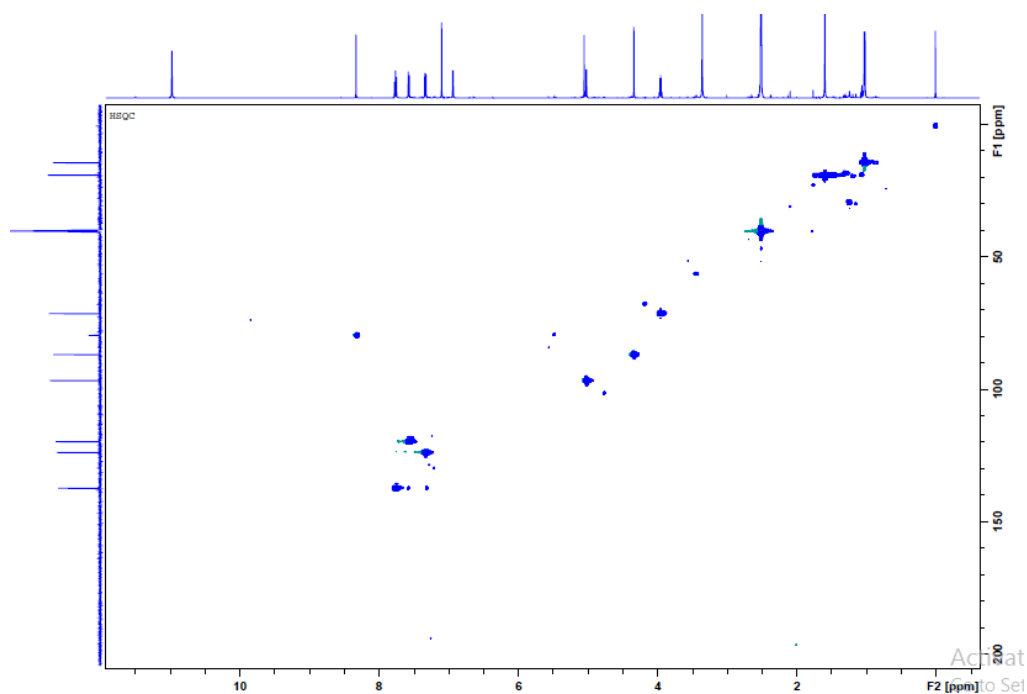
Figure 38. HSQC NMR spectrum (500 MHz) of **Compound-2** in DMSO-d$_6$.
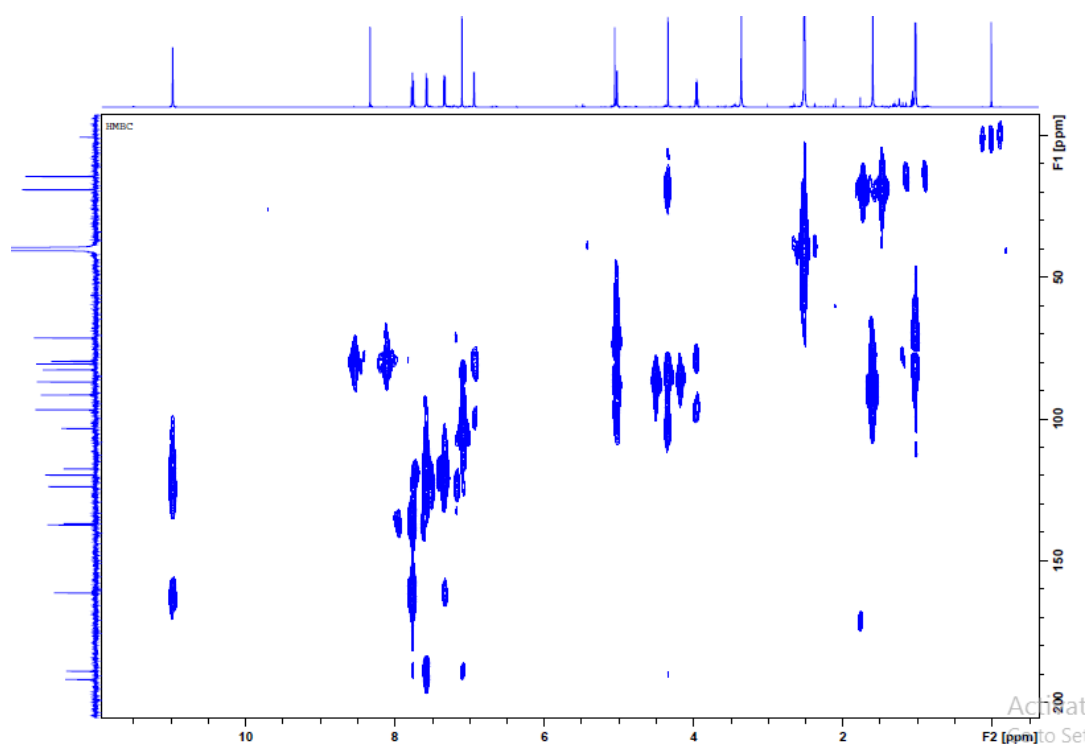
Figure 39. HMBC NMR spectrum (500 MHz) of **Compound-2** in DMSO-d$_6$.
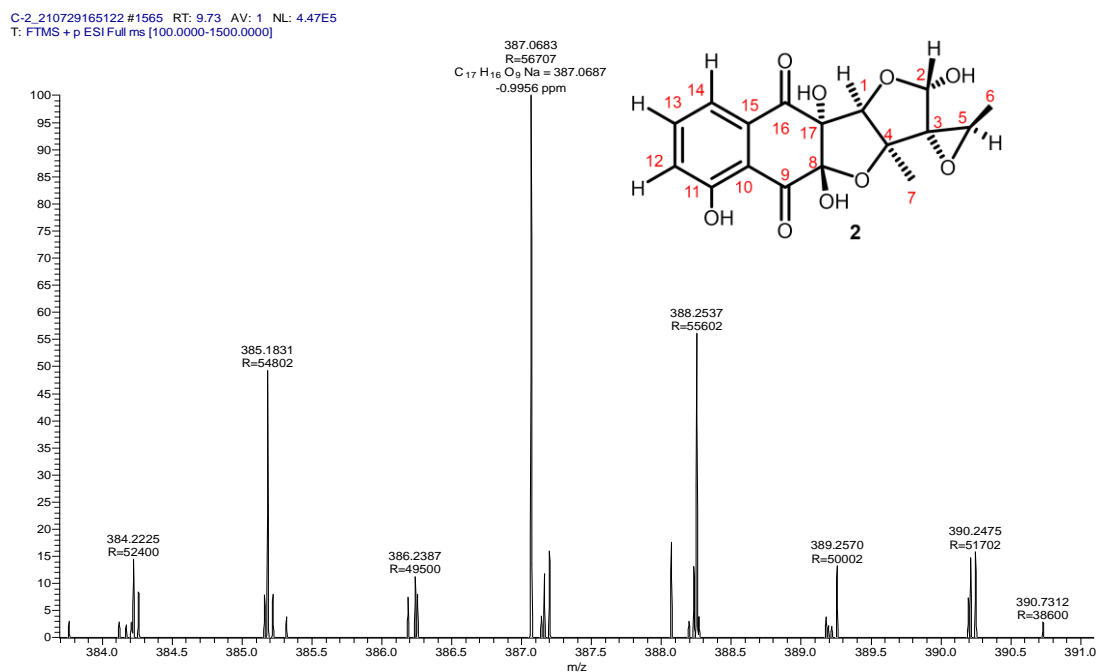
Figure 40. HR-ESIMS of Compound-2.
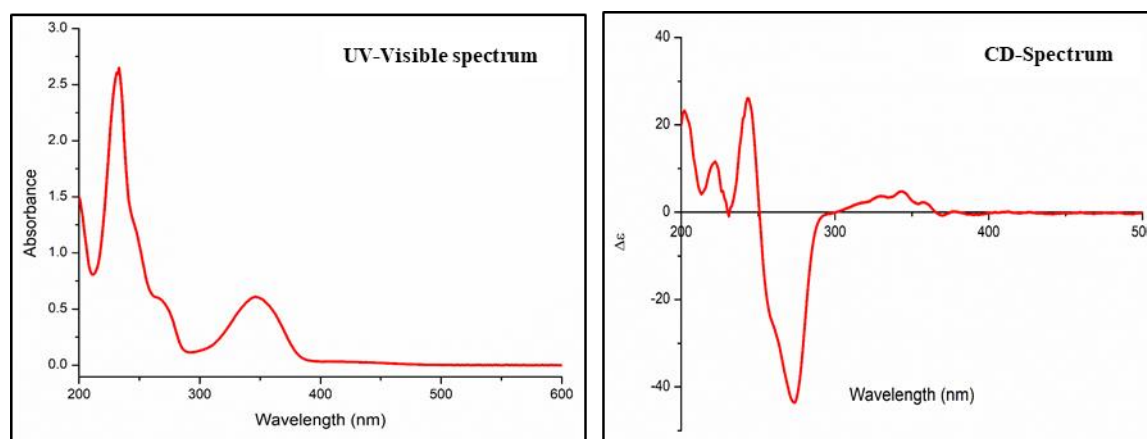
Figure 41. UV-Visible and CD spectrum of **Compound-2.**

3.4.3 Structure elucidation of Compound-3 (Enceleamycin C)

Compound **3** (Enceleamycin C) was purified as yellow powder. The molecular formula of **3** was identified as $C_{17}H_{14}O_7$ through HRMS (ESI) analysis, requiring 11 indices of H deficiency. The ECD spectrum showed negative Cotton effect at 302 nm (CD, 0.026 mg/mL, CH_3CN), λ_{max} ($\Delta\varepsilon$) 302 (−34.63), 276 (18.24) nm. Similar to compound **1**, compound **3** contains a furo-naphthoquinone skeleton, with (Table 3) two methyl groups [δ_H 1.13 (d, $J = 6.9$ Hz) and 1.40 (s)], five methines [two oxygenated (δ_H 3.89 (q, $J = 6.4$ Hz) and 5.54 (s) and three olefinic hydrogens [δ_H 7.27 (dd, $J = 1.1, 8.4$ Hz), 7.72 (dd, $J = 7.6, 8.4$ Hz), and 7.61 (dd, $J = 1.0, 7.4$ Hz)], and one phenolic proton [δ_H 11.51 (br s, 1H)]. ^{13}C NMR (Table 3), DEPT, and HSQC analyses showed 17 carbon signals, including two methyls (δ_C 13.3, 17.7), six methines [three olefinic (δ_C 125.0, 119.9, and 138.7), two sp^3 oxygenated (δ_C 77.7 and 84.5), one aldehyde (δ_C 202.3)], and nine carbons [three olefinic (δ_C 116.5, 123.3, and 134.5), two olefinic oxygenated (δ_C 162.3 and 162.9), two sp^3 oxygenated (δ_C 88.6 and 98.7), and two carbonyl carbons (δ_C 184.0 and 181.8)]. A shielded H-2 signal (δ 3.89) and the presence of an aldehyde group (δ_H 9.74 and δ_C 202.2) led us to anticipate the reorganization (opening) of the strained oxetane ring system in compound **3** compared to **1** (Figure 42).

Next, systematic 2D NMR analyses were performed to elucidate the complete structure and relative stereochemistry of compound **3**. As observed for **1**, HMBC correlations of H-12 with C-10/C-11/C-13/C-14; H-13 with C-11/C-14/C-15; and H-14 with C-10/C-12/C-13/C-15/C-16/C-17 confirmed the presence of the naphthoquinone moiety. HMBC of H-1 with C-2/C-3/C-7/C-8/C-16/C-17; H-2 with C-3/C-5; H-6 with C-2/C-3; H-7 (methyl)

with C-1/C-3/C-4; and H-5 with C-2/C-3/C-4 suggested the furo-furo-naphthoquinone skeleton possessing hydroxy-aldehyde functionalities at C-3.
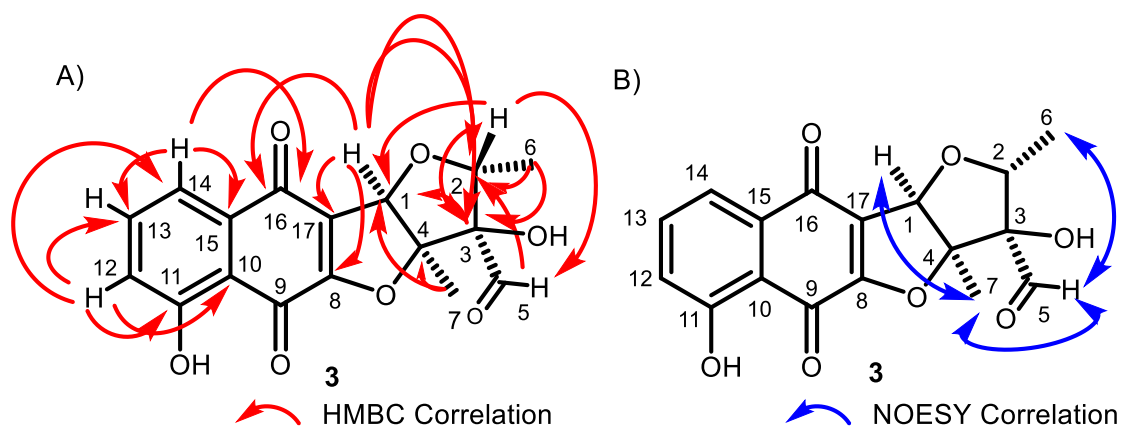
Figure 42. Key HMBC and NOESY correlations of compound **3.**

The presence of NOESY correlation of H-1/H-5/H-6/H-7 revealed the relative stereochemistry of **3** as presented in Figure 42 (B). Based on the absolute stereochemistry of Enceleamycin A (**1**), the absolute stereochemistry for **3** was tentatively assigned as 1*R*, 2*R*, 3*R*, 4*S* (Figure 42).

Enceleamycin C (3): yellow powder (0.032 g from 50 L, in 0.064% yield); $[\alpha]^{27}_D$ +84.26 (*c* 0.26, CH$_3$CN); UV (CH$_3$CN) λ_{max} (log ε) 202 (1.49), 216 (1.31), 288 (0.73), 418 (0.27) nm; IR (neat) (ν_{max}) 3416, 3013, 1522, 1441, 1336, 1214, 1151, 939, 765 cm^{-1} ; melting point 194–197 °C; HR-ESI *m/z* [M + Na]$^+$ (calcd for C$_{17}$H$_{14}$O$_7$Na, 353.0630; found 353.0632).
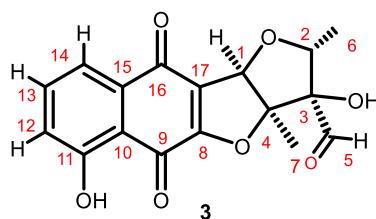
Figure 43. Structure of compound-3.

Table 3. 1D and 2D NMR(500 MHz) data of Enceleamycin C (**3**) in CD$_3$CN.

Position	δ_H (J in Hz)	δ_C	NOESY	COSY	HMBC
1	5.54 (s, 1H)	84.5 (CH)	H-6 δ1.40		(C-2, δ77.7),(C-3, δ88.6), (C-7, δ17.7),(C-8, δ162.3), C-16, δ 181.8),(C-17, δ123.3),
2	3.89 (q, J = 6.4 Hz, 1H)	77.7 (CH)		H-5, δ 1.13	(C-3, δ88.6), (C-5, δ202.3)
3		88.6			
4		98.7			
5	9.74 (s, 1H)	202.3	H-5, δ 1.13, H-6, δ1.40, H-1, δ 5.54		(C-2, δ77.7), (C-3, δ88.6), (C-4, δ98.7)
6	1.13 (d, J = 6.9 Hz, 3H)	13.3 (CH$_3$)	H-2 δ3.89, H-7 δ 9.74	H-2, δ 3.89	(C-2, δ77.7), (C-3, δ88.6)
7	1.40 (s, 3H)	17.7 (CH$_3$)	H-1, δ 5.54, H-7, δ 9.74		(C-1, δ84.5), (C-3, δ88.6), (C-4, δ98.7)
8		162.3			
9		184.0			
10		116.5			
11		162.9			
12	7.27 (dd, J = 1.1, 8.4 Hz, 1H)	125.0 (CH)		H-13, δ 7.72	(C-10, δ116.5), (C-11, δ162.9), (C-13, δ138.7), (C-14, δ119.9)
13	7.72 (dd, J = 7.6, 8.4 Hz, 1H)	138.7 (CH)		H-12, δ 7.27, H-14, δ 7.61	(C-11, δ162.9), (C-14, δ119.9) (C-15, δ134.5),
14	7.61 (dd, J = 1.0, 7.4 Hz, 1H),	119.9 (CH)		H-13, δ 7.72	(C-10, δ116.5), (C-12, δ125.0), (C-13, δ138.7), (C-15, δ134.5), (C-16, δ181.8), (17, δ123.3)
15		134.5			
16		181.8			
17		123.3			
OH (C-11)	11.51 (br. s., 1H)				

Figure 44. ^{1}H NMR spectrum (400 MHz) of **Compound-3** in CD$_3$CN.
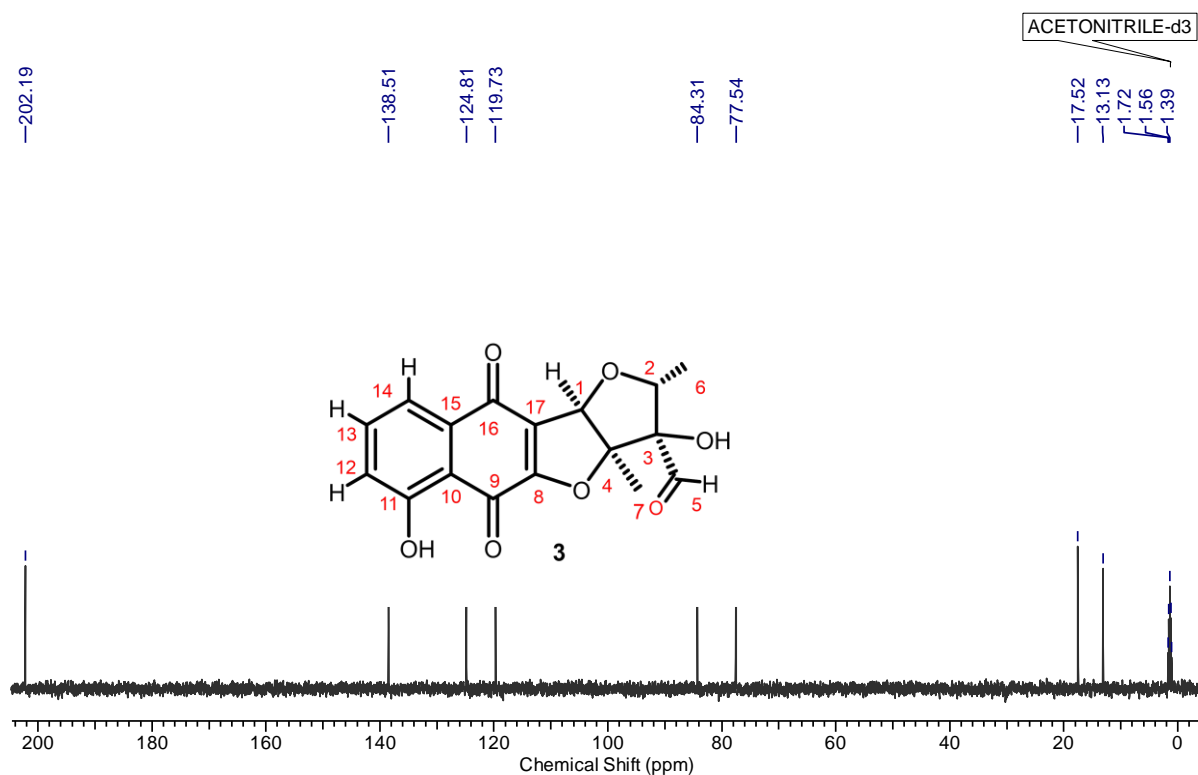
Figure 45. DEPT NMR spectrum (100 MHz) of **Compound-3** in CD$_3$CN.
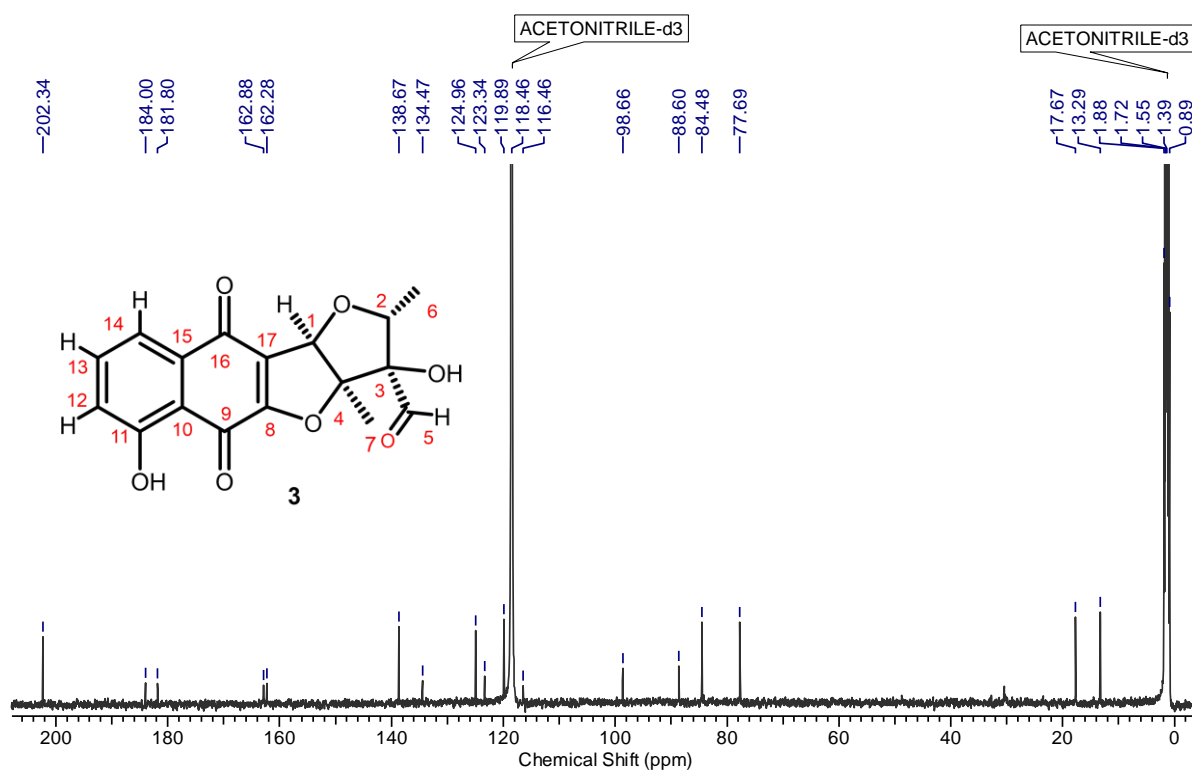
Figure 46. ^{13}C NMR spectrum (100 MHz) of **Compound-3** in CD$_3$CN.
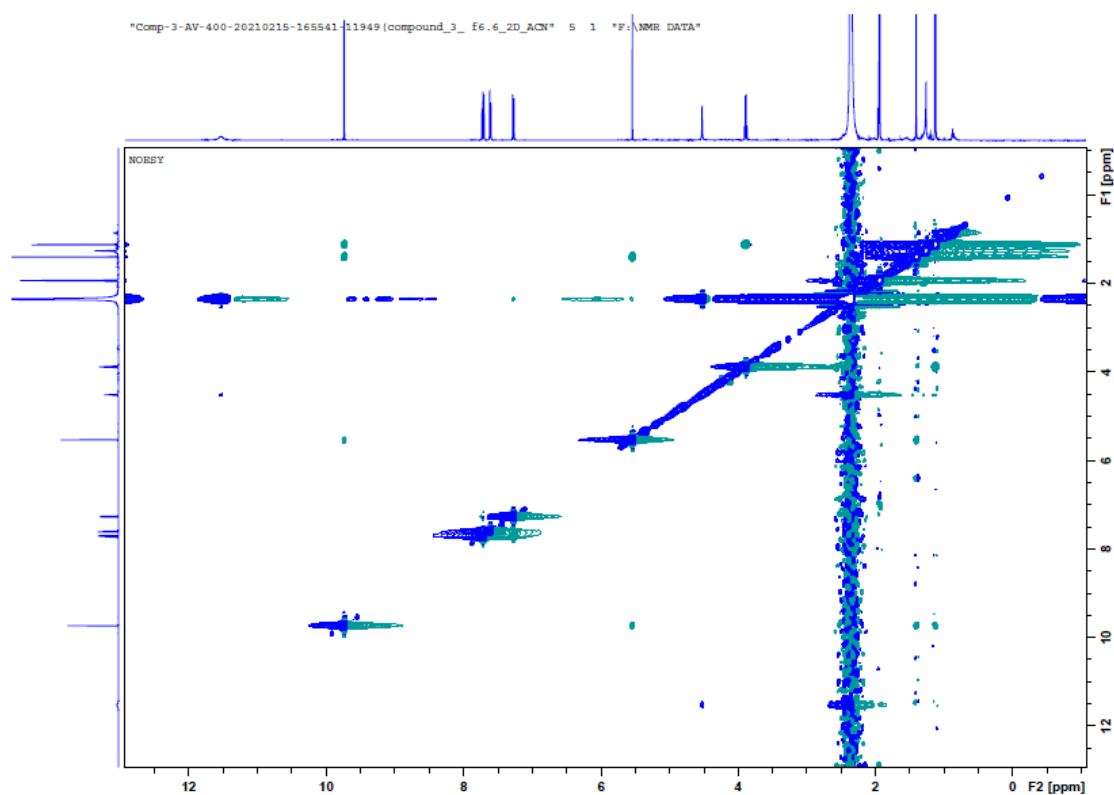
Figure 47. NOESY NMR spectrum (400 MHz) of **Compound-3** in CD$_3$CN.
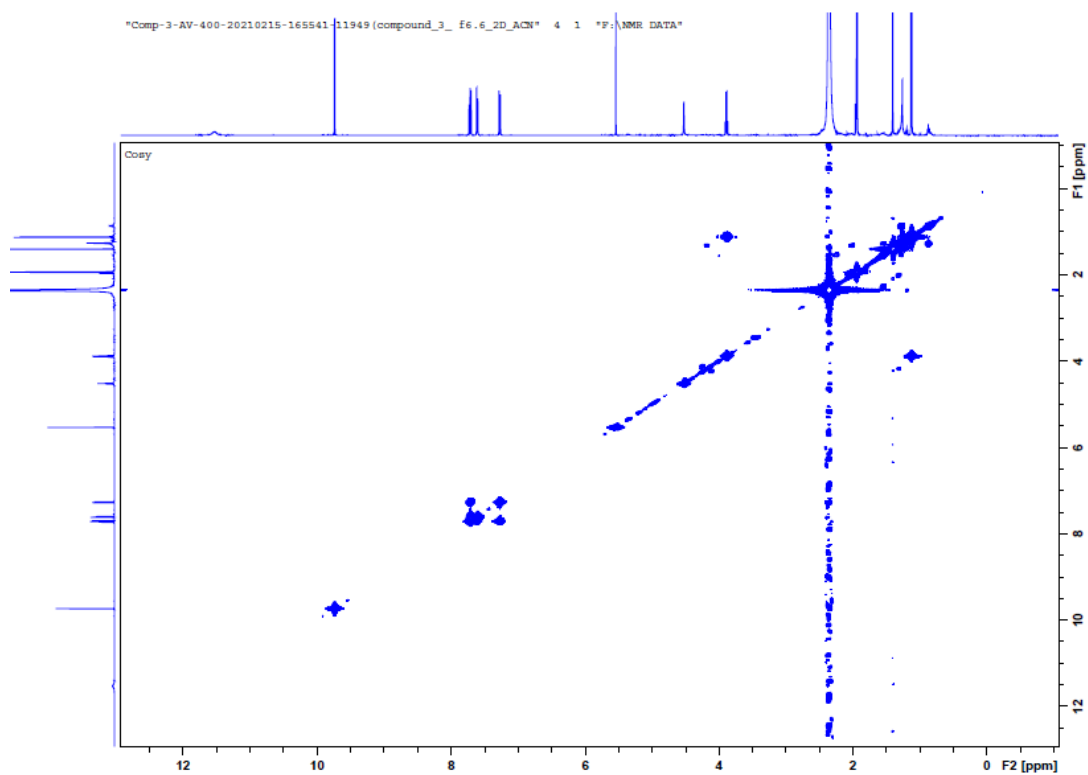
Figure 48. COSY NMR spectrum (400 MHz) of **Compound-3**in CD$_3$CN.
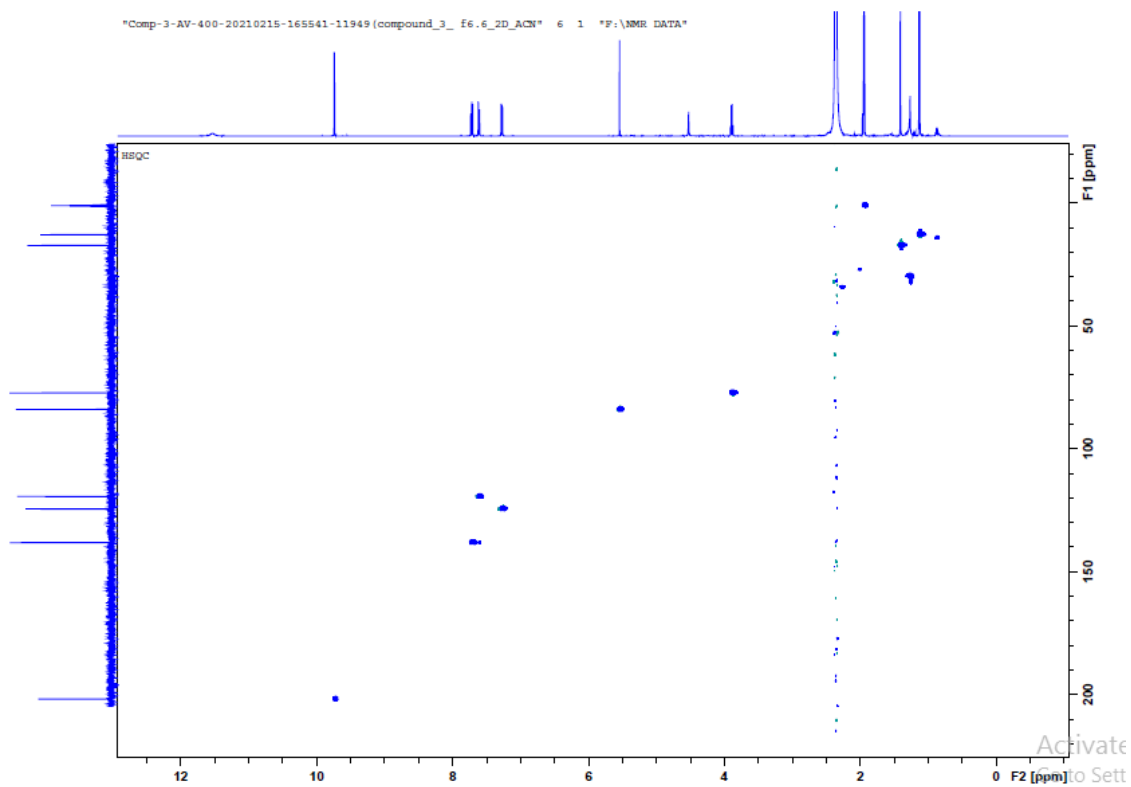
Figure 49. HSQC NMR spectrum (400 MHz) of **Compound-3** in CD$_3$CN.
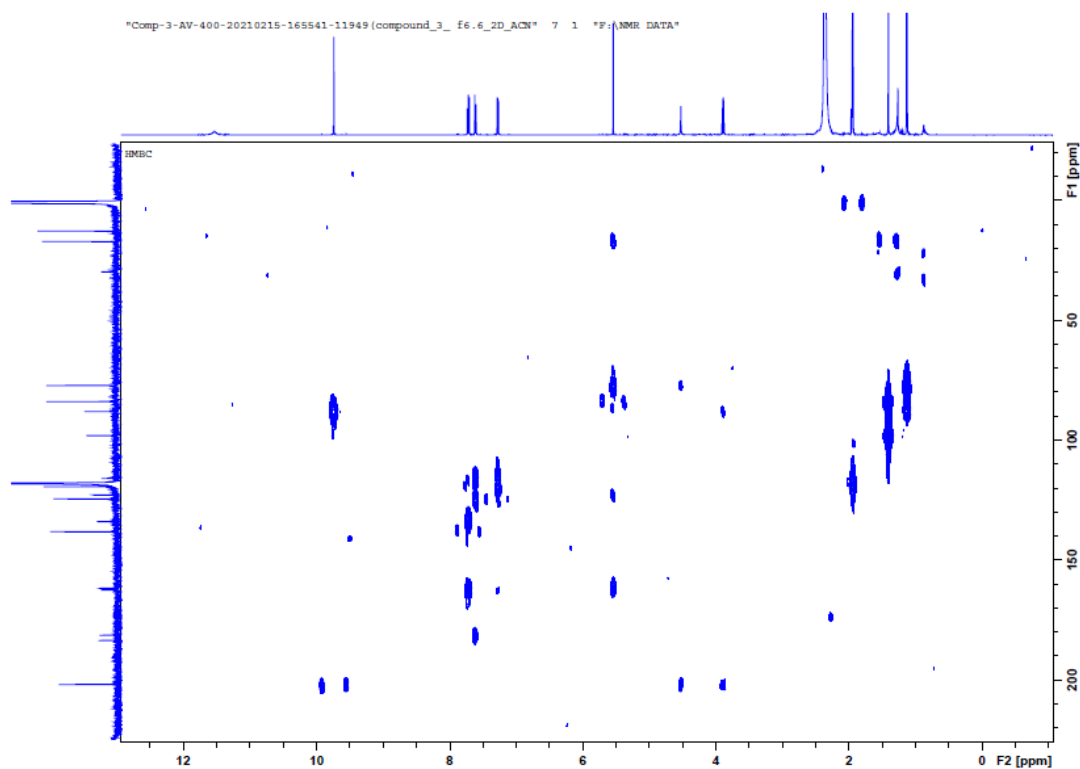
Figure 50. HMBC NMR spectrum (400 MHz) of **Compound-3** in CD₃CN.
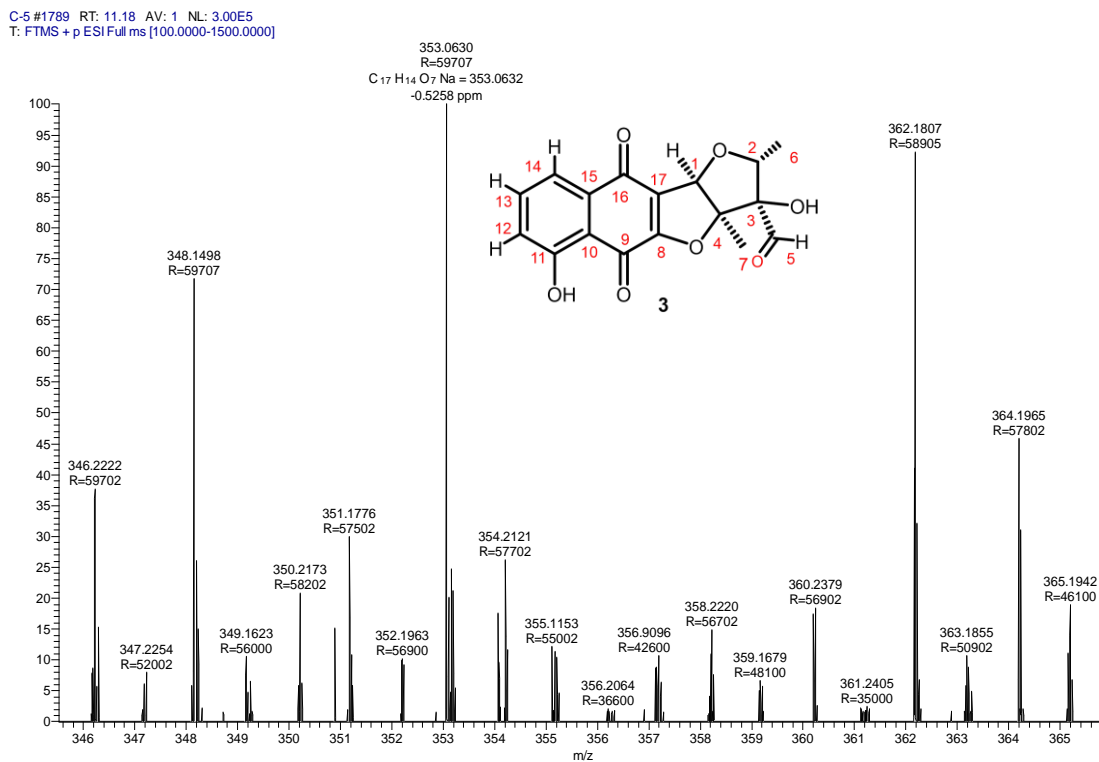
Figure 51. HR-ESIMS of Compound-3.
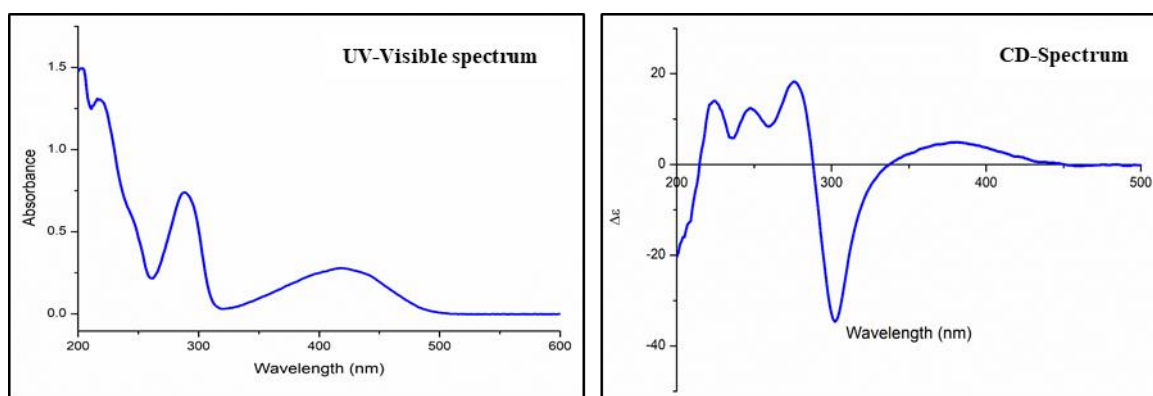
Figure 52. UV-Visible and CD spectrum of **Compound-3.**

Plausible biosynthetic conversion of Enceleamycin A

A plausible biosynthetic conversion of Enceleamycin A (**1**) into its structurally close congeners **2** and **3** is presented in scheme 1. The initial enzymatic (Brønsted acid-mediated) opening of the strained oxetane fused ketal moiety of **1** would deliver the trihydroxy aldehyde **A**, which subsequently undergoes ring-closure via two distinct pathways (paths A and B).
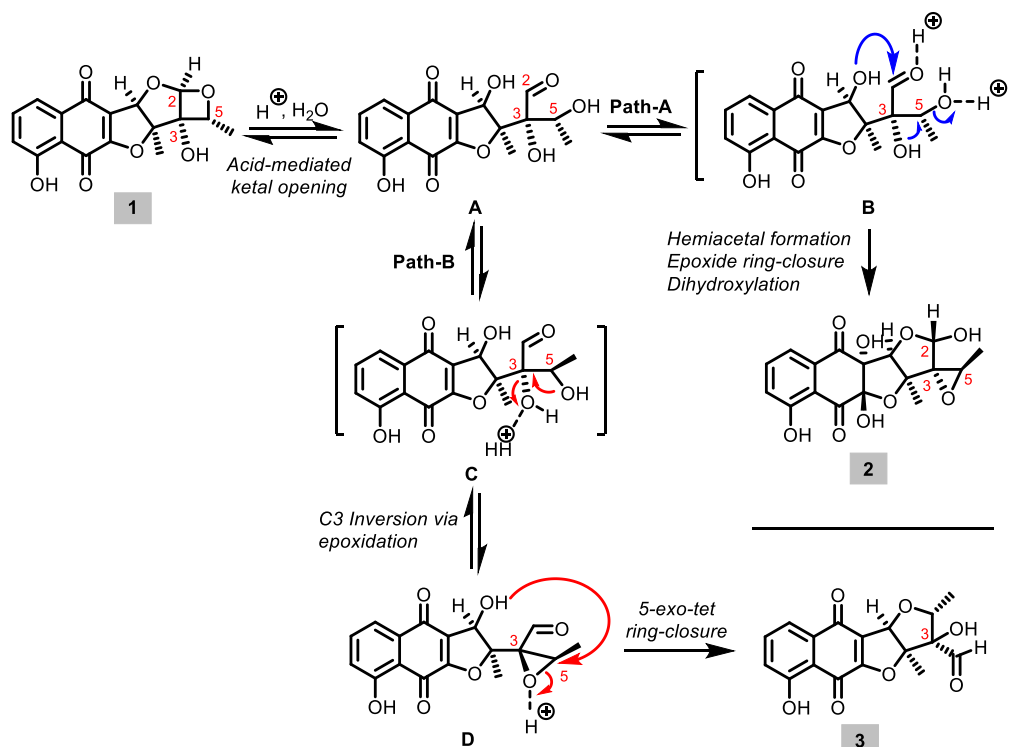
Scheme 1. Plausible Biosynthetic Conversion of Compound **1** into Compounds **2** and **3.**

Acid-mediated intramolecular 1,2-addition (5-*exo*-trig) of the C-1 hydroxy onto the aldehyde, followed by epoxide formation through C-5–OH activation (inversion at C-5), and dihydroxylation of the C-8–C-17 olefinic functionality of **A** would lead to the formation of Enceleamycin B (**2**) (Scheme 1, path A). In an alternative route, intermediate **A** would undergo epoxide formation through C-3–OH activation (inversion at C-3) to give the corresponding epoxy aldehyde intermediate D, which could subsequently undergo 5-*exo*-tet ring-closure with C-1–OH (via epoxide opening) to furnish Enceleamycin C (**3**) (Scheme 1, path B).

3.4.4 Structure elucidation of Compound-4 (*N*-hydroxypyrazinone acid)

A novel *N*-hydroxypyrazinone acid (compound **4**) was isolated from a common ethyl acetate extract as a white hairy crystalline solid, in addition to Enceleamycins A–C (**1**–**3**). Molecular formula of **4** was determined to be $C_{14}H_{22}N_2O_4$ by HRMS, requiring 5 indices of H deficiency. The ECD spectra displayed positive Cotton effect at 241 nm (CD, 0.054 mg/mL, CH_3CN), λ_{max} ($\Delta\varepsilon$) 241 (55.67), 221 (−23.32) nm. ^1H NMR analysis of **4** showed the presence of five methyls [δ_H 0.91 (s, $J = 6.8$ Hz), 0.93 (s, $J = 6.8$ Hz), 1.44 (s, $J = 7.2$ Hz), 1.46 (d, $J = 7.2$ Hz), and 1.51 (d, $J = 7.2$ Hz)], three methines [δ_H 2.17 (m, 1H), 3.42–3.28 (m), and 3.98 (q, $J = 6.8$ Hz)], and a methylene [δ_H 2.69 (d, $J = 6.8$ Hz)]. The ^{13}C and DEPT NMR spectra showed 14 resonating signals, including five methyls (δ_C 17.6, 17.6, 18.9, 19.1, and 22.6), three sp^3 methines (δ_C 28.8, 26.7, and 42.4), one methylene (δ_C 41.5), and five nonprotonated carbons [three olefinic (δ_C 132, 138.2, and 151.3), one amide (δ_C 151.1), and one for a carboxylic acid functionality (δ_C 177.9)]. Combined ^1H and ^{13}C NMR, DEPT, HSQC, and COSY analyses were used to establish all carbon and hydrogen connectivities (Figure 53, Table 4).

COSY (^1H–^1H) correlations of H-5 [δ_H 3.42–3.28 (m, 1H)] with H-6 (methyl)/H-7 (methyl) and HMBC correlation of H-5 with C-2/C-6/C-7 revealed the presence of an isopropyl group. Similarly, COSY correlations of H-11 [δ_H 2.69 (d, $J = 6.8$ Hz, 2H)] with H-12 [δ_H 2.17 (m, 1H)] and of H-12 with H-13 and H-14 suggested the presence of an isobutyl chain. The H-8 [δ_H 3.89 (q, $J = 6.8$ Hz, 1H)] showed a COSY correlation with H-9 (methyl, δ_H 1.51 (d, $J = 7.2$ Hz, 3H)) and HMBC correlations with C-3/C-9/C-10, indicating presence of a propionic acid moiety (Figure 53A). All these correlations led us to conclude that isopropyl, isobutyl, and propionic acid groups were attached to the pyrazinone ring. Further, key NOESY cross-correlations of −O$\underline{H}$/H-6/H-7/H-9/–$CO_2\underline{H}$ and H-11/H-12/H-13/H-14 have strongly supported our structural assignment.
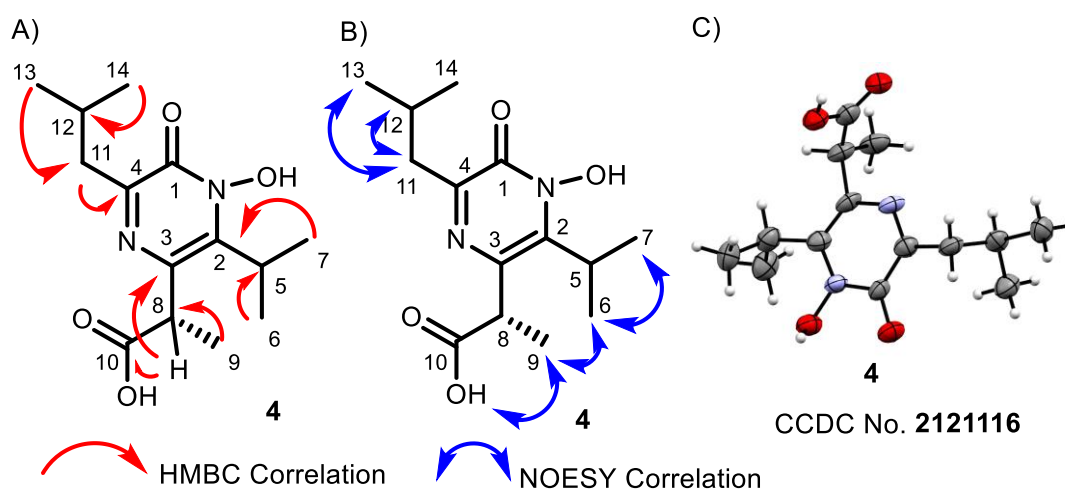
Figure 53. (A) Key HMBC correlations, (B) key NOESY correlations, and (C) ORTEP diagram of compound **4**.

Moreover, the complete structure and absolute stereochemistry of **4** were rigorously established using single-crystal X-ray crystallography analyses (Figure 53). The recrystallization of *N*-hydroxypyrazinone acid (**4**) was carried out in methanol. With the 30% of probability level, the displacement ellipsoids were drawn. The hydrogen atoms are displayed as small spheres with arbitrary radii. Single-crystal X-ray diffraction data analysis determined the *S* configurations at the C8A, C8B, C8C, and C8D positions in four different conformers of compound **4** (Figure 64).

N-Hydroxypyrazinone acid (4): white crystalline solid (0.146 g from 50 L, in 0.29% yield); $[\alpha]^{27}_{D}$ +97.84 (*c* 0.6, CH$_3$CN); UV (CH$_3$CN) λ_{max} (log ε) 205 (1.26), 330 (0.97), 238 (0.97) nm; IR (neat) (ν_{max}) 3423, 2879, 2104, 1639, 1443, 1335, 1212, 1038, 941, 766 cm^{-1}; melting point 108–110 °C; HR-ESI *m/z* [M + H]$^+$ (calcd for C$_{14}$H$_{23}$N$_2$O$_4$, 283.1651; found 283.1652).
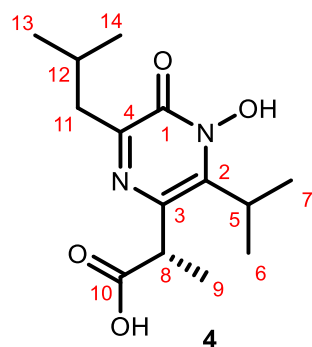
Figure 54. Structure of compound-4.

Table 4. 1D and 2D NMR (500 MHz) data of *N*-Hydroxypyrazinone acid (**4**) in CDCl$_3$.

Position	δ_H (*J* in Hz)	δ_C	NOESY	COSY	HMBC
1		151.1			
2		138.2			
3		132			
4		151.3			
5	3.42-3.28 (m, 1H)	26.7 (CH)	H-17, δ 1.46, H-8, δ 3.98	H-6, δ 1.46	C-2, δ 138), (C-6, δ 19.1), (C-7, δ 18.9)
6	1.46 (d, *J* = 7.2 Hz, 3H)[a]	19.1 (CH$_3$)	H-8, δ 3.98	H-5, δ 3.36	(C-2, δ138.2),(C-6, δ19.1), (C-12, δ28.8),
7	1.44 (s, *J* = 7.2 Hz, 3H)[a]	18.9 (CH$_3$)	H-13, δ 0.93, H-5, δ 3.3,	H-5, δ 3.36	
8	3.98 (q, *J* = 6.8 Hz, 1H)	42.4 (CH)	H-6, δ 1.46, H-5-3.32,	H-9, δ 1.51	(C-3, δ132.0), (C-7, δ18.9), (C-10, δ177.9)
9	1.51(d, *J* = 7.2 Hz, 3H)	22.6 (CH$_3$)	H-8 δ 3.98,	H-8, δ 3.98	(C-3, δ132), (C-10, δ177.9),(C-11, δ41.5)
10		177.9			
11	2.69 (d, *J* = 6.8 Hz, 2H)	41.5 (CH$_2$)	H-13-0.93, H-12-2.17	H-12, δ 2.17	(C-4, δ151.1), (C-5, δ22.6)
12	2.17 (m, 1H)	28.8 (CH)	H-13, δ0.93, H-11, δ 2.69	H-14, δ0.9, H-11, δ 2.69	(C-4, δ151.31),(C-8, δ42.4), (C-9, δ22.6)
13	0.93 (d, *J* = 6.8 Hz, 3H)[b]	17.6 (CH$_3$)		H-12, δ 2.17	(C-8, δ42.4),(C-9, δ22.6), (C-12, δ28.8),
14	0.91 (d, *J* = 6.8 Hz, 3H)[b]	17.6 (CH$_3$)	H-7, δ1.44, H-12 δ2.17, H-11, δ 2.69,	H-12, δ 2.17	(C-8, δ42.4),(C-9, δ22.6), (C-12, δ28.8),
N-OH	10.38 (br. s; 1H)				
COOH	10.48 (br. s., 1H)				
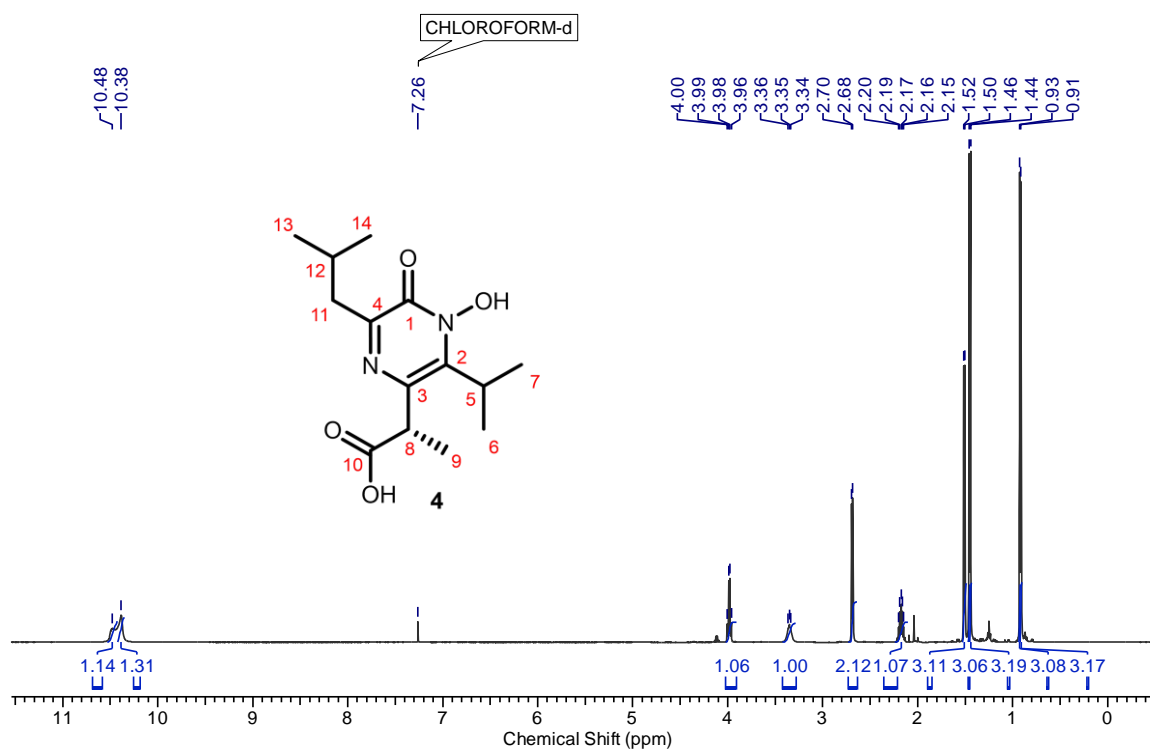
Figure 55. ^{1}H NMR spectrum (400 MHz) of **Compound-4** in CDCl$_3$.
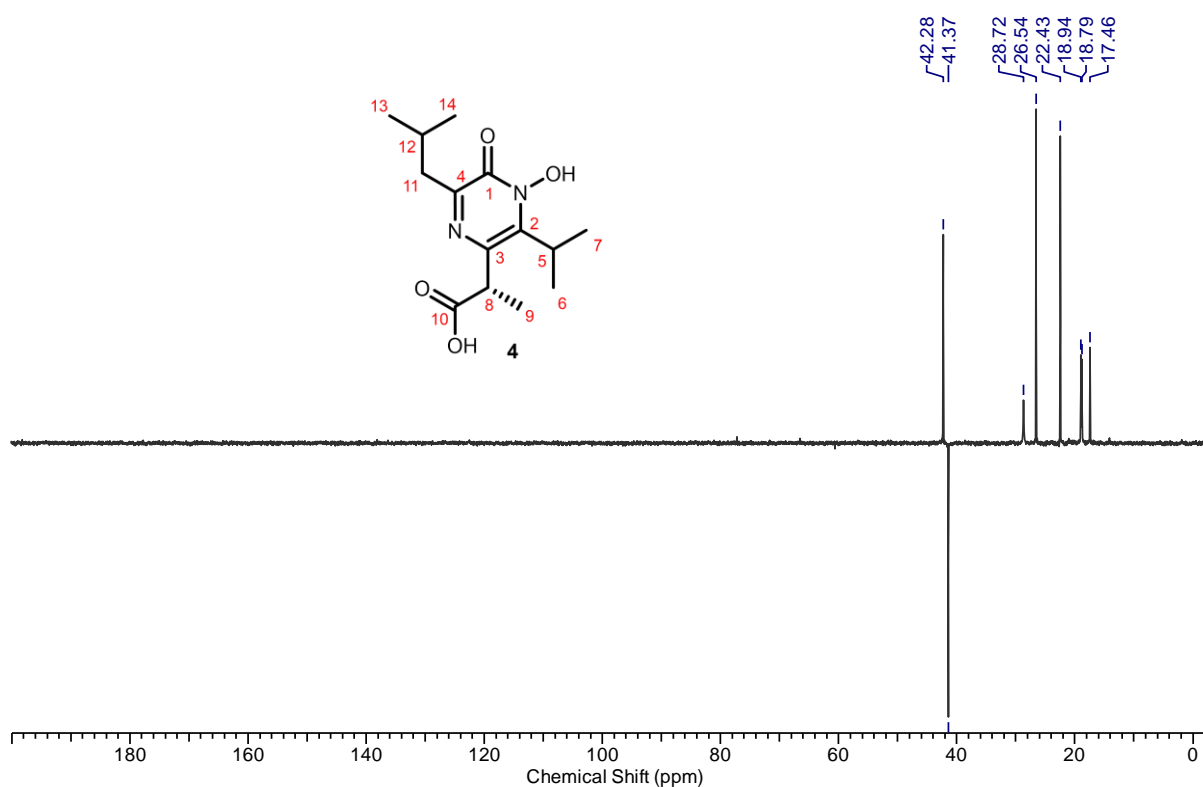
Figure 56. DEPT NMR spectrum (100 MHz) of Compound-4 inCDCl$_3$.
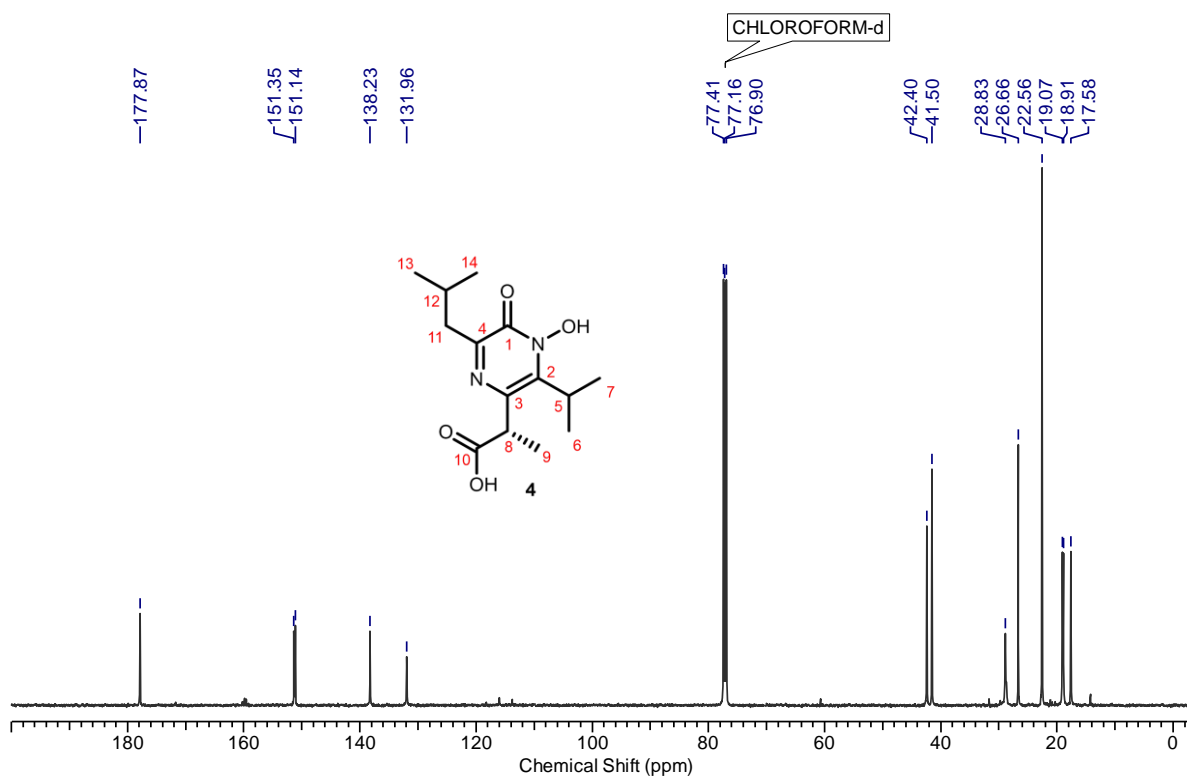
Figure 57. ^{13}C NMR spectrum (100 MHz) of **Compound-4** in CDCl[3].
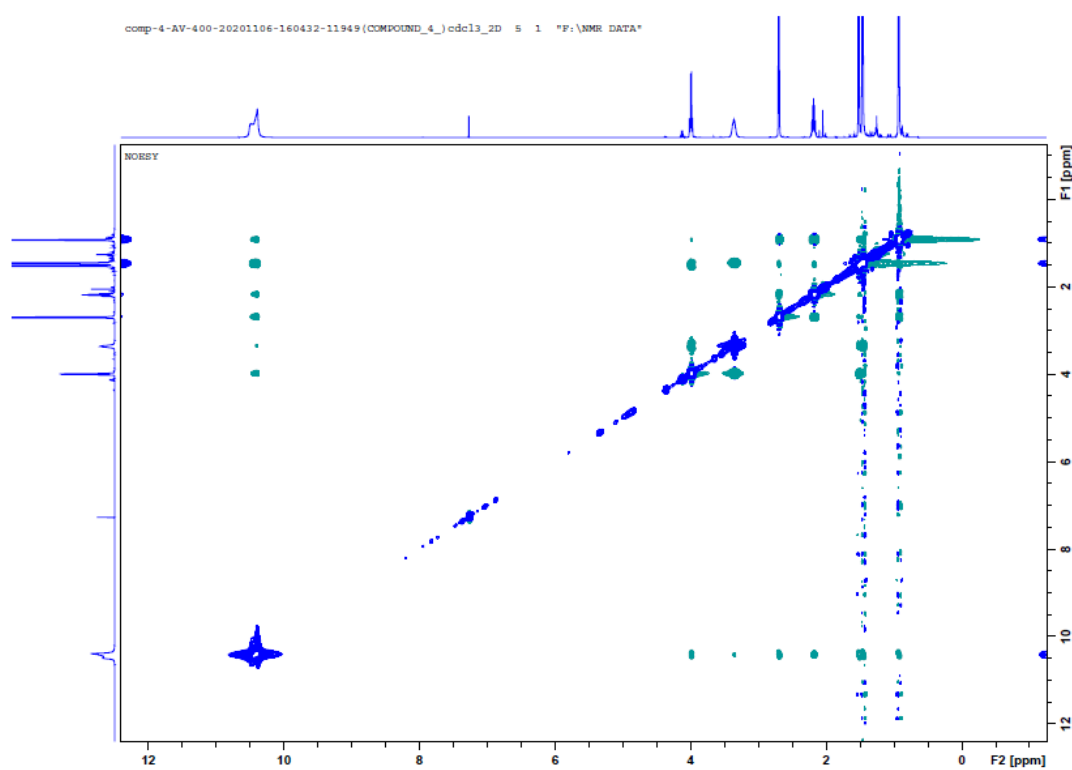
Figure 58. NOESY NMR spectrum (400 MHz) of **Compound-4** in CDCl[3].
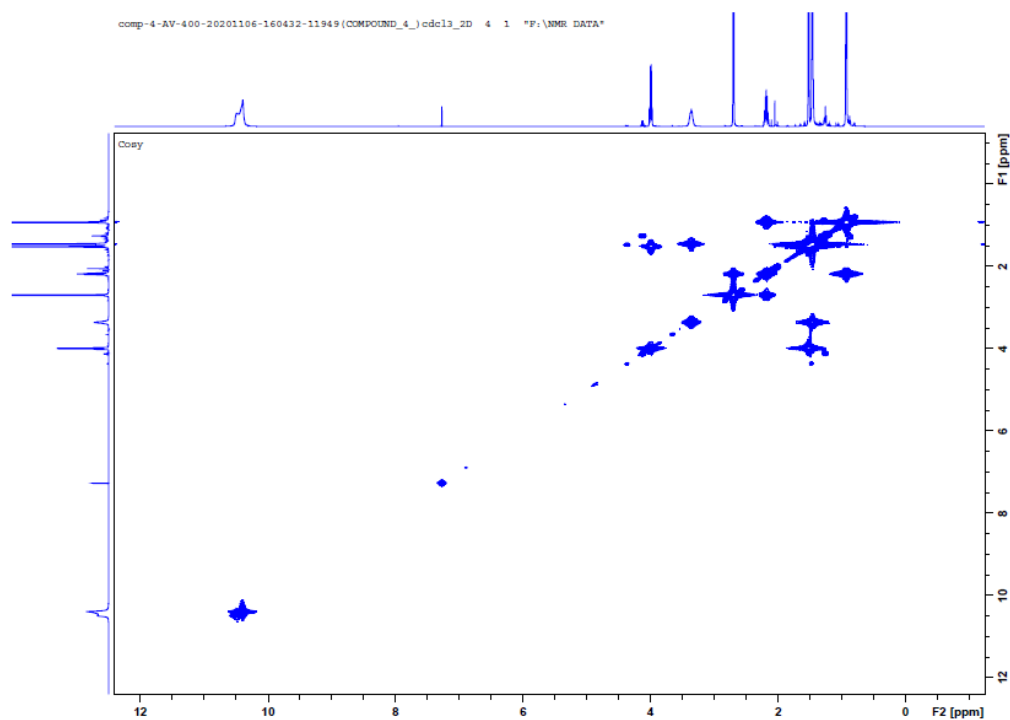
Figure 59. COSY NMR spectrum (400 MHz) of **Compound-4** inCDCl$_3$.
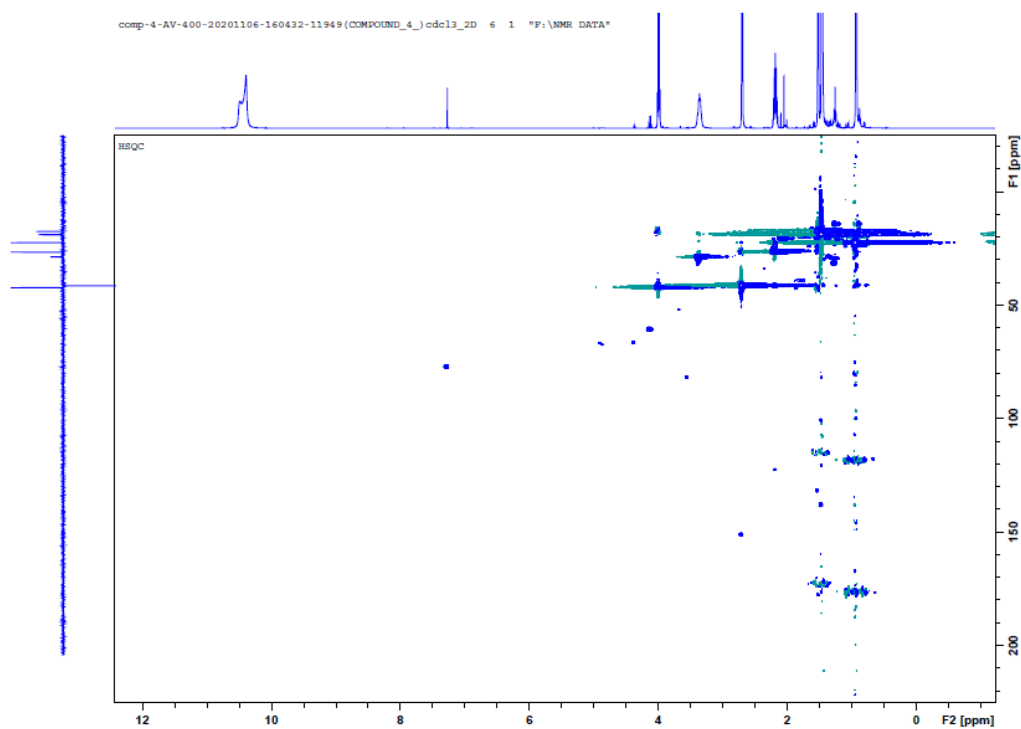
Figure 60. HSQC NMR spectrum (400 MHz) of **Compound-4** in CDCl$_3$.
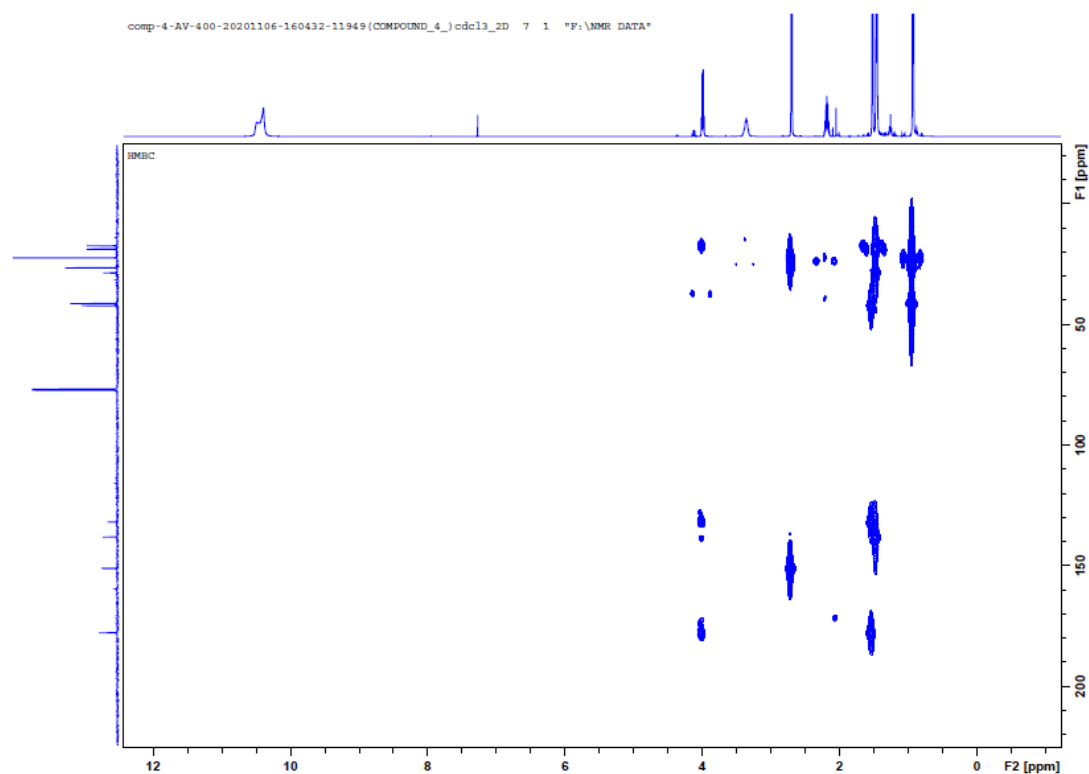
Figure 61. HMBC NMR spectrum (400 MHz) of **Compound-4** in CDCl$_3$.
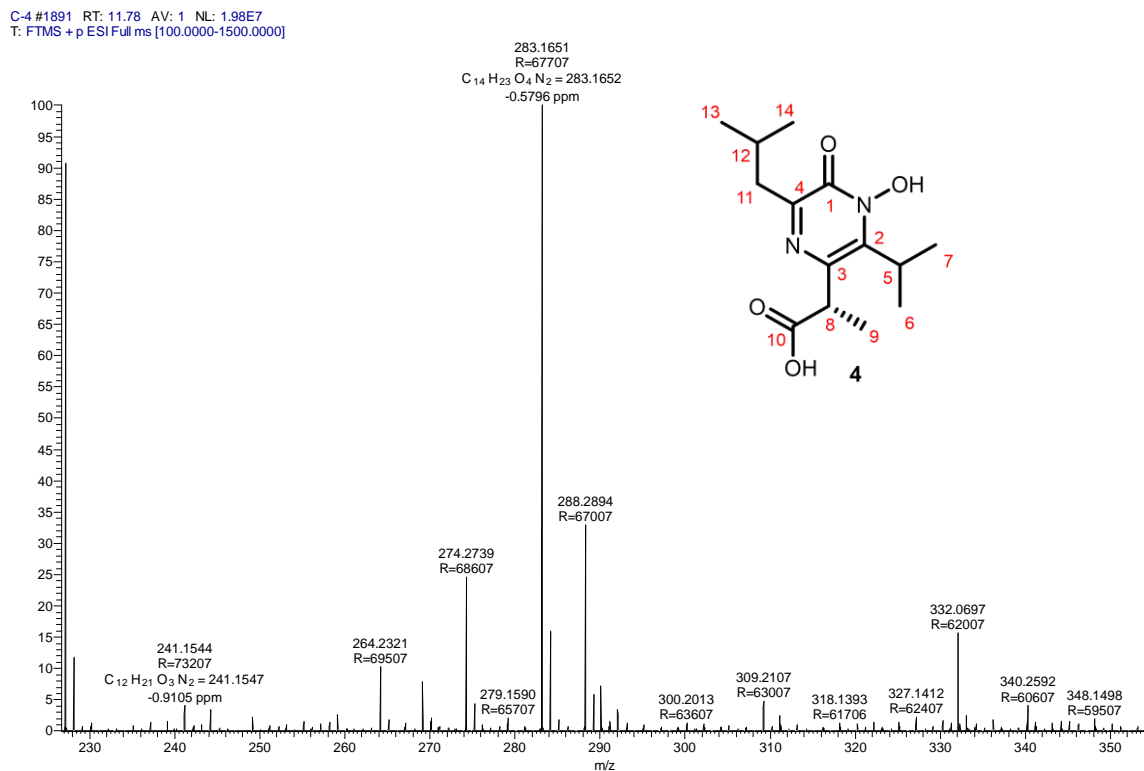
Figure 62. HR-ESIMS of Compound-4.
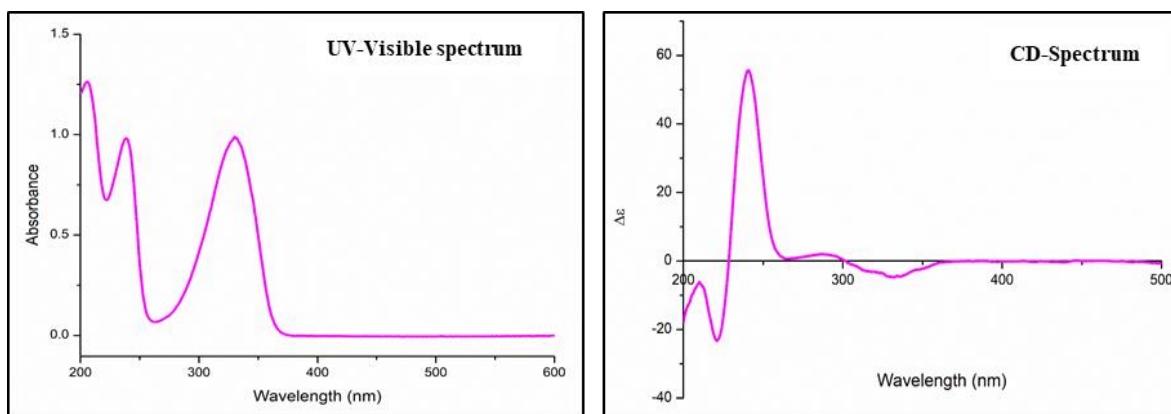
Figure 63. UV-Visible and CD spectrum of **Compound-4.**
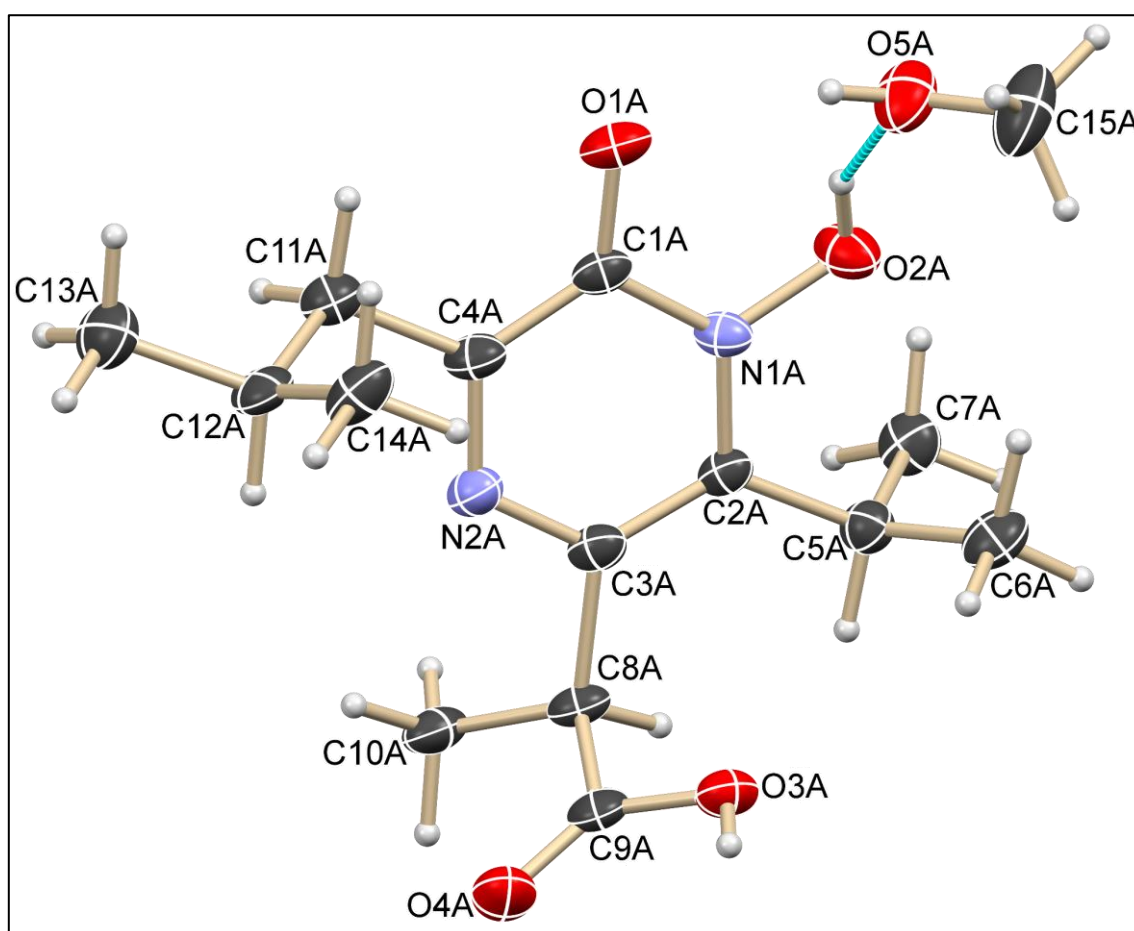
Figure 64. ORTEP view of Compound-4.

Conclusion

Amycolatopsis are rich source of bioactive compounds and its exploitation under different growth condition can help in isolation of novel antimicrobial compounds. The screening under different growth condition showed that the culture produce bioactive compounds under liquid static and agar plate-based incubation condition. The TLC and bio-autography study showed the similar major bioactive yellow pigment compound was present in both the static and plate based crude extract. Large scale fermentation of 50 L was carried out for *Amycolatopsis* sp. WGS_07 under static condition. The bioactivity guided purification of the 52g crude extract led to the discovery of three new furo-naphthoquinone-derived Enceleamycins A-C (**1-3**), and one novel *N*-hydroxypyrazinone acid (**4**). The major compound Enceleamycin A (**1**) along with Enceleamycin B (**2**) was also isolated from the agar plate-based incubation condition. Enceleamycin A (**1**) has a complex unprecedented pentacyclic oxeto-furo-furo-naphthoquinone skeleton. In contrast, Enceleamycins B (**2**) features dihydroxylated naphthoquinone segment, and Enceleamycins C (**3**) has the oxetane rearranged moiety with aldehyde group attached.

References

Adamek M, Alanjary M, Sales-Ortells H, Goodfellow M, Bull AT, Winkler A, Wibberg D, Kalinowski J, Ziemert N (2018) Comparative genomics reveals phylogenetic distribution patterns of secondary metabolites in *Amycolatopsis* species. *BMC Genomics* 19:426.

Coskun O (2016) Separation techniques: Chromatography. *North Clin Istanb* 3:156-160.

Elyashberg M (2015) Identification and structure elucidation by NMR spectroscopy. *Trends Analyt Chem* 69:88-97.

Fleming A (1929) On the antibacterial action of cultures of *Penicillium*, with special reference to their use in the isolation of *B. influenzae*. *Br. J. Exp. Pathol.* 10:226–236.

Jamjan W, Suriyachadkun C, Tanasupawat S, Sakai K, Tashiro Y, Okugawa Y, Tongpim S (2018) *Amycolatopsis silviterrae* sp. nov., isolated from forest soil. *Int J Syst Evol Microbiol* 68:1455-1460.

Kisil OV, Efimenko TA, Efremenkova OV (2021) Looking Back to *Amycolatopsis*: History of the Antibiotic Discovery and Future Prospects. *Antibiotics* 10:1254.

Mushtaq S, Abbasi BH, Uzair B, Abbasi R (2018) Natural products as reservoirs of novel therapeutic agents. *EXCLI J* 17:420-451.

Newman DJ, Cragg GM (2016) Natural Products as Sources of New Drugs from 1981 to 2014. *J Nat Prod* 79:629-61.

Regnier FE (1983) High-performance liquid chromatography of biopolymers. *Science* 222:245-252.

Romano S, Jackson SA, Patry S, Dobson ADW (2018) Extending the "One Strain Many Compounds" (OSMAC) Principle to Marine Microorganisms. *Mar Drugs* 16:244.

Rusu AV, Trif M, Rocha JM (2023) Microbial Secondary Metabolites via Fermentation Approaches for Dietary Supplementation Formulations. *Molecules* 28:6020.

Sangal V, Goodfellow M, Blom J, Tan GYA, Klenk HP, Sutcliffe IC (2018) Revisiting the taxonomic status of the biomedically and industrially important genus *Amycolatopsis*, using a phylogenomic approach. *Front. Microbiol*. 9:2281.

Sekurova ON, Schneider O, Zotchev SB (2019) Novel bioactive natural products from bacteria via bioprospecting, genome mining and metabolic engineering. *Microb Biotechnol* 12:828-844.

Smyth MS, Martin JH (2000) X ray crystallography. *Mol Pathol* 53:8-14.

Song Z, Xu T, Wang J, Hou Y, Liu C, Liu S, Wu S (2021) Secondary Metabolites of the Genus *Amycolatopsis*: Structures, Bioactivities and Biosynthesis. *Molecules* 26:1884.

Urban S, Dias DA (2013) NMR spectroscopy: structure elucidation of cycloelatanene A: a natural product case study. *Methods Mol Biol* 1055:99-116.

Wang ZF, You YL, Li FF, Kong WR, Wang SQ (2021) Research Progress of NMR in Natural Product Quantification. *Molecules* 26:6308.

Zhang QW, Lin LG, Ye WC (2018) Techniques for extraction and isolation of natural products: A comprehensive review. *Chin med* 13:1-26.

Chapter 4

Bioactivity of Enceleamycin A-C and *N*-hydroxypyrazinone acid

Bioactivity of Enceleamycin A-C and *N*-hydroxypyrazinone acid

Abstract

Naphthoquinones are naturally distributed compounds derived from naphthalene ring system containing two carbonyl groups. Naphthoquinones possess several bioactivities especially antibacterial and anticancer. With the rise of resistance both by the bacteria and the cancer cells there is a need of novel molecules to tackle the issue of drug resistance. The presence of bioactivity in several furo-naphthoquinone substructures prompted to examine antibacterial and anticancer activity of isolated compounds.

The first section of chapter deals with antibacterial study of the isolated Enceleamycins A, B, C and *N*-hydroxypyrazinone acid. The study includes the detail antibacterial activity of Enceleamycin A towards methicillin resistant *S. aureus* (MRSA). The experiment includes MIC determination, growth kinetics, synergistic activity and biofilm inhibition in presence of Enceleamycin A. The increase in ROS level in MRSA after treatment with Enceleamycin A showed compounds ability of ROS formation inside the bacterial cells. Overall, the study presents the essential insights of Enceleamycin A for the antibacterial activity against MRSA.

The second section of the chapter involves the anticancer activity of the isolated Enceleamycins A-C and *N*-hydroxypyrazinone acid. As the compound Enceleamycin A displayed potential anticancer activity, particularly against the MDA-MB-231 (TNBC) cells, the detailed anticancer properties were evaluated. The important assays like anti-migration inhibition ability, ROS formation and apoptosis cell death by Enceleamcin A conforms its anticancer potential. The *in silico* molecular docking and MD simulation showed that Enceleamycin A can be a potential AKT2 inhibitor candidate which was also proven by *in vitro* assay. Further the *in silico* physicochemical and ADMET studies showed good bioavailability and drug-likeness of Enceleamycin A. No prominent hemolytic effect showed by Enceleamycin A on human RBCs. Overall, the study presents the essential insights of Enceleamycin A for the anticancer activity particularly against TNBC cells.

1. Introduction

1.1 Naphthoquinones

Quinones represent a class of naturally distributed metabolites in animals, plants, and microorganisms. Quinones are involved in essential phases of living beings, mainly at the levels of photosynthesis (plastoquinones), respiratory chains (ubiquinones), and controlling the action on blood coagulation (naphthoquinones-types of Vitamin K). Interest in quinones has intensified for their crucial roles in energy production of the cells respiratory chain and their prominence in various pharmacological studies (Silva et al. 2003). The bioactivities reported from quinones are anticancer, antifungal, antibacterial, anti-inflammatory, antiviral, and antiparasitic (Sasaki et al. 2002; Huang et al. 1998). Quinones are source of many cytotoxic compounds of the anthracycline group used in cancer therapy, like doxorubicin, daunorubicin, and mitoxantrone (Pereyra et al. 2019). The cytotoxicity of quinones is associated with producing reactive oxygen species (ROS) and hampering human DNA topoisomerase I and II (Song et al. 2000).

Quinones are chemically classified based on the different arrangements of an aromatic system supporting quinone ring, i.e., benzoquinones (benzene ring), naphthoquinones (naphthalene ring), and anthraquinones (anthracene ring, linear or angular). Naphthoquinones are further categorized into two groups based on configurations of carbonyl groups, 1,4-naphthoquinones having spacing of two carbons between carbonyls or 1,2-naphthoquinones that have an adjacent functional group (Sieglar, 1998). The isomers differ in their physicochemical properties because of the difference in their pharmacological actions (Silva et al. 2003).
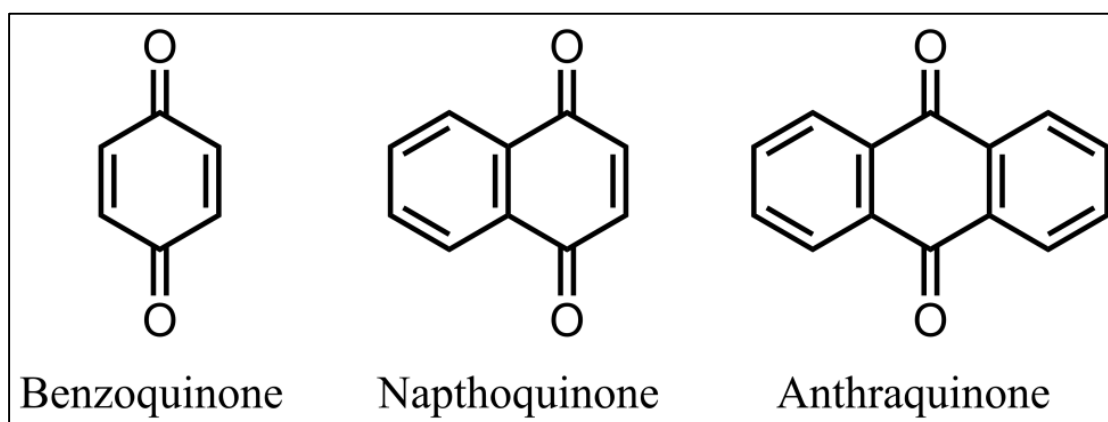
Figure 1. Quinones classification based on the aromatic ring

1.2 Biosynthesis of naphthoquinones

1.2.1 Type II polyketide synthases (PKSs)

The aromatic polyketides in actinobacteria with diverse structures are generally bio-synthesized by type II PKSs. Type II PKSs are complex of monofunctional proteins that contain key elements needed for biosynthesis of polyketides, namely Ketosynthases (KS), acyl carrier protein (ACP) and chain length factor (CLF). The term "minimal PKS" refers to one set of monofunctional proteins (Sattely et al. 2008; Das and Khosla, 2009). A heterodimer of KS and CLF are formed to catalyze the iterative decarboxylative condensation process between acyl-ACP and malonyl-ACP, which results in the synthesis of a polyketide chain. To create a final polyketide product, tailoring enzymes like cyclases and oxidoreductases further modify the formed polyketide chain (Sattely et al. 2008; Katsuyama et al. 2016).

Katsuyama et al. have showed that Isofuranonaphthoquinones (IFNQs) like JBIR-76 and JBIR-77 were purified from *Streptomyces* sp. RI-77. The analysis of genome and gene disruption has demonstrated that JBIR-76 and JBIR-77 are produced by the type II PKS (*ifn* gene cluster). Type II PKS integrates octaketide intermediate from precursors of malonyl CoA. Baeyer-Villiger monooxygenase stimulates critical C–C bond cleavage, resulting in distinctive scaffolds of JBIR-76 and JBIR-77 (Katsuyama et al. 2016).
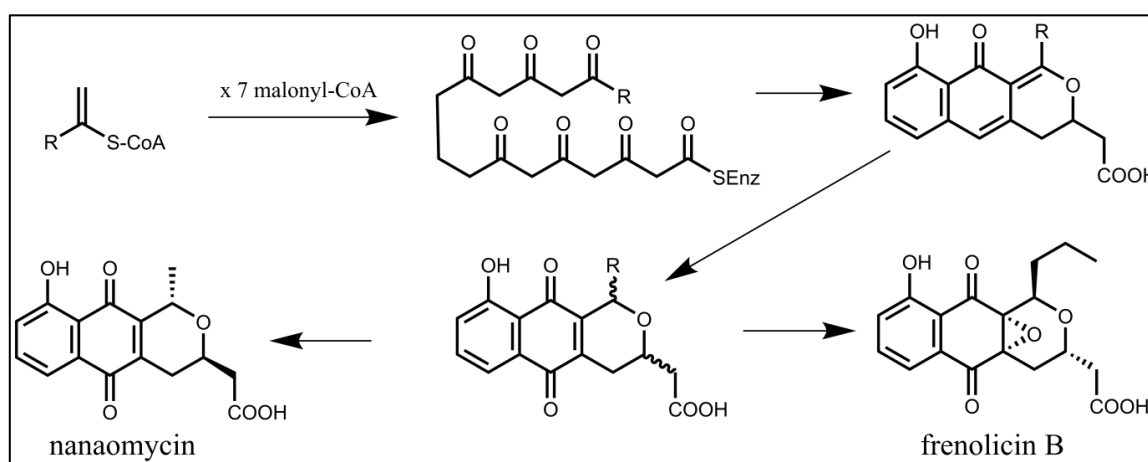
Figure 2. Biosynthesis of naphthoquinones frenolicin B and nanaomycin by PKS-II (Moore and Hertweck, 2002)

1.2.2 Type III polyketide synthases (PKSs)

Meroterpenoid-type naphthoquinones are of mixed biosynthetic origin, i.e., a combination of terpenoid building blocks and polyketides to form various structural analogs (Geris and Simpson, 2009). Several actinomycete strains produce polyketide-isoprenoid hybrid compounds, like naphterpin, furaquinocin, napyradiomycin, flaviogeranin, and marinone, all of which are display various bioactivities (Shen et al. 2020; Kawasaki et al. 2006). The critical aromatic polyketide backbone of these natural products is 1,3,6,8-tetrahydroxynaphthalene (THN), which is biosynthesized by THN synthase, a type III PKS homodimer by the condensation and aromatization of five malonyl coenzyme A subunits (Funa et al. 1999; Austin et al. 2004). THN synthase has been involved in various meroterpenoid biosynthesis, like *Fur*1 in furaquinocins and *Mcl*17 in merchlorins. Prenyltransferase enzymes catalyze the attachment of various prenyl groups to the THN at nucleophilic C-2 and C-4 positions by an electrophilic aromatic substitution reaction. The prenyl moieties, including prenyl, geranyl, and farnesyl pyrophosphates, play an essential role in naphthoquinones structural diversity and bioactivity (Tello *et al.* 2008). Further modifications like halogenation, oxidative dearomatization, hydroxylation, methylation, and hydroxyketone rearrangements by multiple modifying enzymes like vanadium-dependent haloperoxidase (VHPO) further enrich and give molecular architecture to the complex naphthoquinone structure (Winter and Moore, 2009).

In 2006, Kawasaki et al. performed heterologous expression in *Streptomyces lividans* TK23 and identified biosynthetic gene cluster of Furaquinocin A, a polyketide-isoprenoid hybrid compound. The genes function were estimated using sequence similarity with the translated product, *fur1* (THN synthase), f*ur4* (*C*-methyltransferase), *fur6* (*O*-methyltransferase), *fur7* (prenylation enzyme) and *fur8* (P450 enzyme) (Kawasaki *et al.* 2006). Based on their chemical structure, Shen et al. revealed proposed biosynthetic pathway of flaviogeranin congeners isolated from *Streptomyces* sp. B9173. Type III PKS choose malonyl-coenzyme A as starting unit and four additional extensions are carried out to produce pentaketide which ultimately leads to naphthoquinone ring formation. The resulting non-reducing ketide is released, and the pentaketide cyclizes to form THN. Subsequently, intermediate THN oxidizes to produce 2,5,7-trihydroxy-1,4-naphthoquinone, also called flaviolin, and later through modification forms distict flaviogeranin congeners through oxidation, methylation, and prenylations (Shen *et al.* 2020).
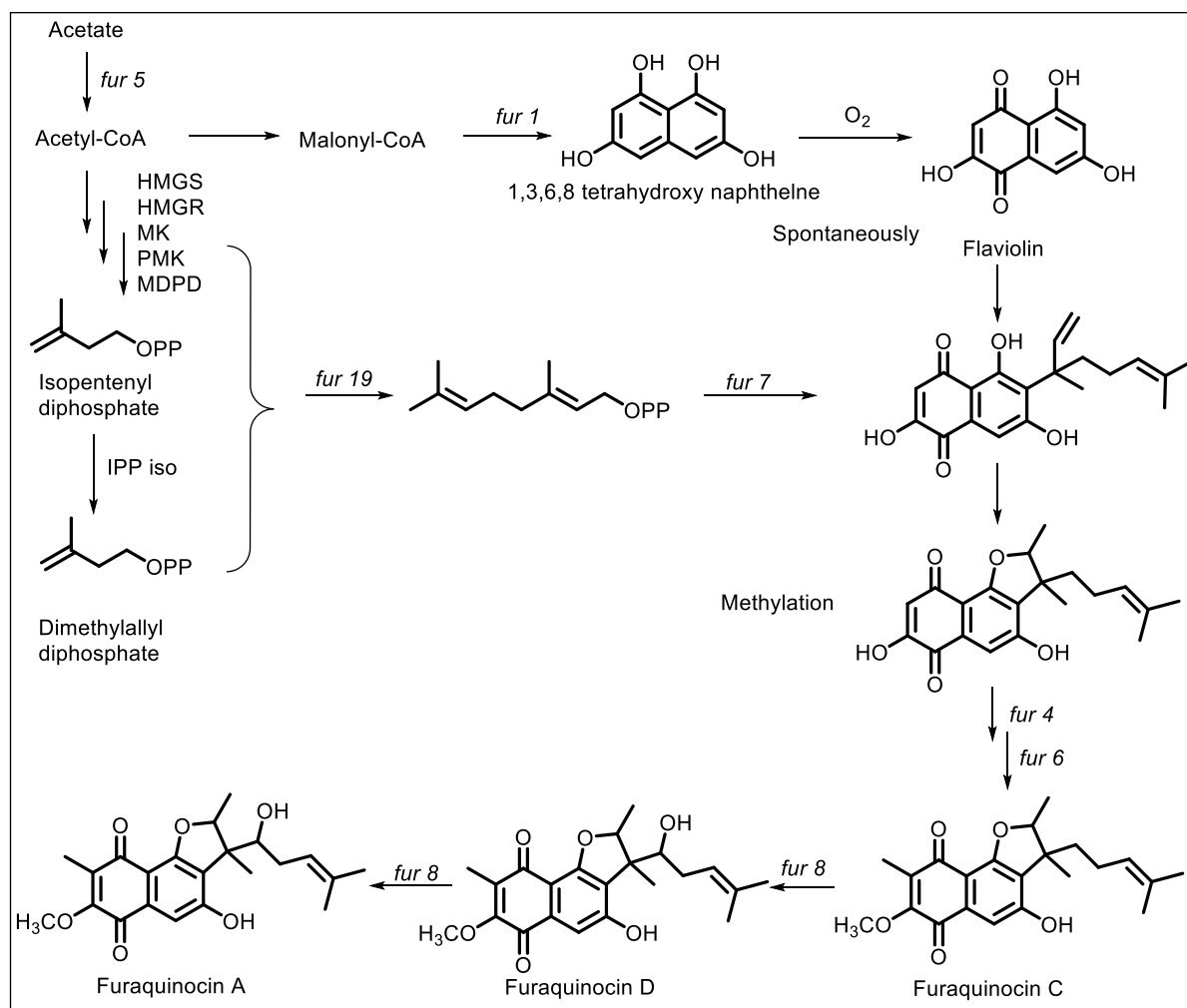
Figure 3. Biosynthetic pathway of a natural polyketide-isoprenoid hybrid compound, Furaquinocin A, a potent antitumor compound, produced by *Streptomyces* sp. strain KO-3988 (Kawasaki *et al.* 2006)

1.3 Bioactive potentials of naphthoquinones from actinobacteria

1.3.1 Antibacterial activity

Naphthoquinones are a class of organic molecules with a promising ability to treat bacterial infections (Ravichandiran et al. 2019). Naphthoquinones are often isolated from actinobacteria and have been investigated for their significant antibacterial activity. Some important antibacterial naphthoquinones investigated from actinobacteria are juglomycin, nanaomycin, medermycin, napyradiomycin, hygrocins, griseusins and flaviogeranin (Table 1). Napyradiomycins isolated from *Streptomyces* sp. SCSIO 10428, exhibited antibacterial activities against Gram-positive bacterial strains (MIC of 0.25 to 32 µg/mL) (Wu et al. 2013). Lactoquinomycins isolated from *Streptomyces bacillaris* strain MBTC38, possess potent

antibacterial activities towards Gram-positive bacteria (MIC of 0.06–4 μg/mL), including MRSA (MIC of 0.25–8 μg/mL) and weak activity towards Gram-negative bacteria (Chung et al. 2021). The antibacterial naphthoquinones' inhibitory activity depends on the structural variation of naphthoquinones and the target bacterial strains. There are also investigations to further enhance the antibacterial activity and lower antibiotic resistance by combining naphthoquinones and other antibiotics (Song et al. 2020).

1.3.2 Possible mechanisms of antibacterial naphthoquinones

The mechanism of action of antibacterial naphthoquinones from actinobacteria is least explored. Naphthoquinones exhibits antibacterial properties by distict mechanisms, which includes generating reactive oxygen species (ROS), disrupting bacterial cell membranes, or causing DNA damage. Reactive oxygen species (ROS) severely affect cell viability because their multiple macromolecule targets, like proteins, lipids, and DNA, are essential building blocks for cell survival. The accumulation of OH− radicals in an uncontrolled manner leads to peroxidation of essential lipids in cells, making bacterial cell survival lethal (Zhao and Drlica, 2014). In the recent study, stress response and mode of action of lapachol were evaluated in *S. aureus* using RNA-seq transcriptomics. The study indicates that the antibacterial effect of lapachol in *S. aureus* is caused by production of ROS, which compromises redox equilibrium and increases protein thiol-oxidation (Linzner *et al.* 2020). The mode of action of plant-derived 1,4-naphthoquinone, i.e., juglone, against *S.aureus*, suggested that juglone upregulated oxidoreductase, thereby enhancing the redox process and creating a per-oxidative environment in the cell. The per-oxidative condition significantly decreases cell membrane and cell wall formation, ultimately leading to cell death (Wang *et al*. 2016). The antibacterial activity of semi-synthesized derivative of lawsone was evaluated, and the study further revealed multifaceted modes of action mediated by disruption of cell membrane, intracellular ROS generation, and intracellular iron ion chelation (Song et al. 2020). The potential use of naphthoquinones for antibacterial is in process, and further studies are needed for a complete understanding of mechanism of action and their efficacy as a drug.

Table 1. Antibacterial naphthoquinones from actinobacteria

Naphthoquinones	Organism	Reference
TMKS8A, a chlorinated α-lapachone	*Streptomyces* sp. TMKS8	Zhang et al. 2021
Vertirhodins A−F	*Streptomyces* sp. B15-008	Sun et al. 2021
Lactoquinomycin A	*Streptomyces* sp. MBTC38	Chung et al. 2021
Flaviogeranin D and C2	*Streptomyces* sp. B9173	Shen et al. 2020
Naphthomevalin	*Streptomyces* sp. CPCC 203577	Li et al. 2020
Napyradiomycin D1	*Streptomyces* sp. CA-271078	Carretero-Molina et al. 2019
Juglomycin A	*S. achromogenes* E91CS4	Ahmad et al. 2020
Rubromycins CA1 and CA2	*S. hyaluromycini* MB-PO13T	Harunari et al. 2019
Beijinchromes C	*Nocardia beijingensis* NBRC 16342	Hoshino et al. 2019
Medermycin and G15-F	*S. albolongus* CA-186053	Lacret et al. 2019
Strepoxepinmycins A−D and medermycin	*Streptomyces* sp. XMA39	Jiang et al. 2018
Qinimycins	*Streptomyces* sp. MBT76	Wu et al. 2017
Isofuranonaphthoquinones IFQ A-G	*Streptomyces* sp. CB01883	Guo et al. 2017
4-dehydro-4a-dechloronapyradiomycin A1 and napyradiomycin A1	*Streptomyces* sp. Strain CA-271078	Lacret et al. 2016
Alnumycin D and granaticin B	*Streptomyces* sp.	Oja et al. 2015
Marfuraquinocins A, C and D	*S. niveus* SCSIO 3406	Song et al. 2013
Three new napyradiomycins	*Streptomyces* sp. SCSIO 10428	Wu et al. 2013
Compound Z-4-2	*S. djakartensis* NW35	Zhang et al. 2013
Cryptosporin	*Streptomyces* sp. SCSIO 03219	Zhang et al. 2013
Griseusins F and G	*Nocardiopsis* sp. YIM DT266	Ding et al. 2012
8 Napyradiomycins	*S. antimycoticus* NT17	Motohashi et al. 2008
Hygrocins A and B	*S. hygroscopicus* ATCC 25293	Cai et al. 2005
Fumaquinone	*S. fumanus*	Charan et al. 2005
Naphthomycins	*Streptomyces* sp. E/784	Hooper & Rickards, 1998
Juglomycin Z	*S. tendae*	Fiedler et al. 1994
A80915 A, B, C, and D	*St. aculeolatus* A80915	Fukuda et al. 1990
SF2415A1, A2, A3, Bl, B2 and B3	*S. aculeolatus*	Gomi et al. 1987
Griseusins A and B	*S. griseus* K-63	Tsuji et al. 1976
Nanaomycins A and B	*S. rosa var. notoensis*	Omura et al. 1974
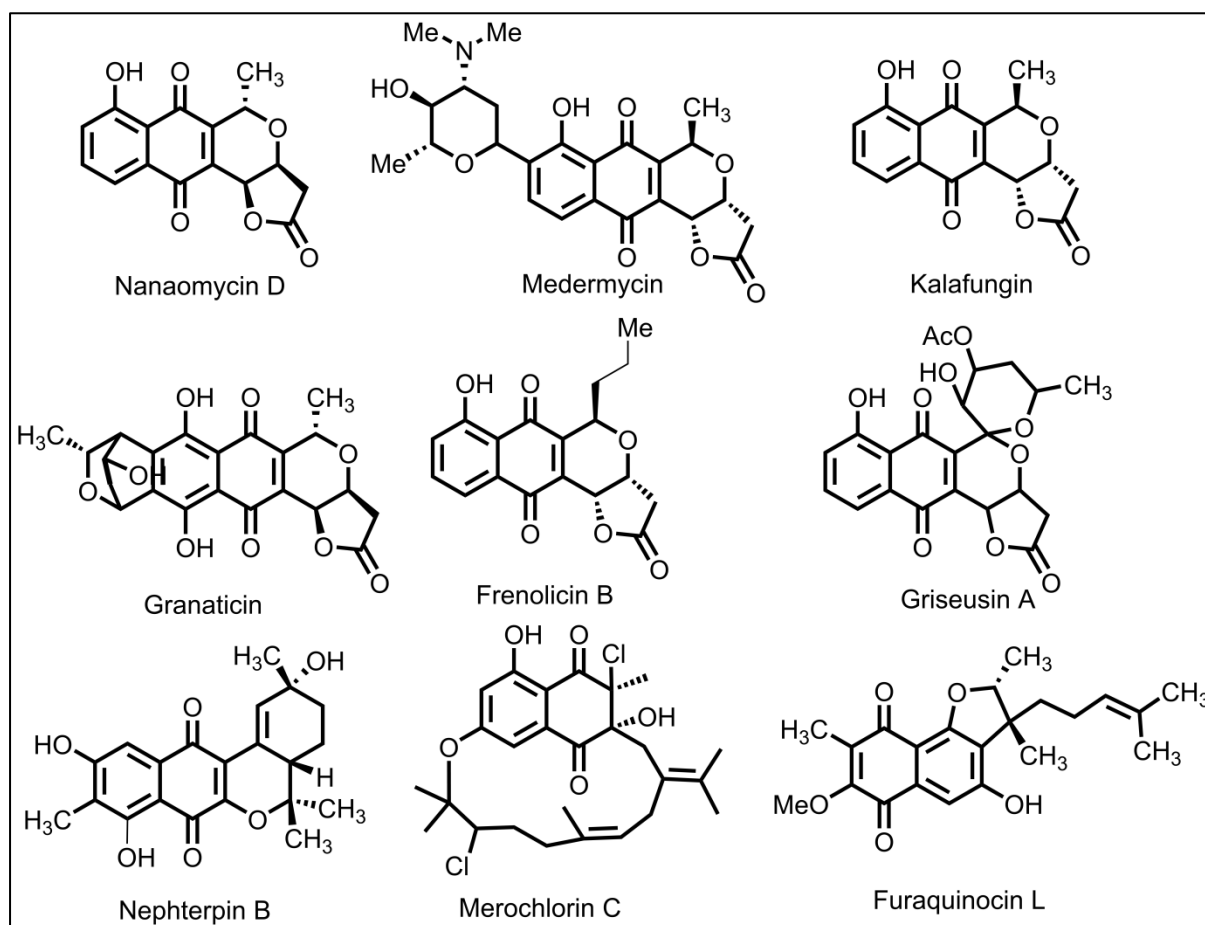
Figure 4. Structural variation of bioactive naphthoquinones isolated from actinobacteria (adapted from Murray et al. 2020)

1.3.3 Anticancer activity of naphthoquinones from actinobacteria

Cancer is a class of non-communicable diseases associated with uncontrollable cell growth. It is the major cause of mortality worldwide, leading to nearly 10 million deaths in 2020. Countries with low- and middle-income accounts for nearly 70% of cancer cases because of poor diagnostic and treatment services. Cancer treatment involves three main approaches, i.e., surgery, radiation, and chemotherapy. The disadvantage of the surgery and radiation is the damage caused to healthy tissues and cells, whereas radiotherapy also leads to fatigue during therapy or even months after. Chemotherapy is the only systemic method inhibiting original and metastasized tumors as the drug reaches through bloodstream circulation to cancer cells throughout the tissue. This approach also has numerous adverse effects that impacts the patient's way of life, and chances of cancer cells developing resistance to these chemotherapeutic drugs are also present (Pereyra et al. 2019, Wellington, 2015).

The National Cancer Institute (NCI-USA) studies showed that quinones possess anticancer activity (Driscoll, 1974). Quinones have been used clinically as an anticancer drug for a long time; some examples are anthracycline antibiotics (doxorubicin, daunorubicin, idarubicin, and mitoxantrone), dactinomycin and mitomycin-C (Zhang et al. 2006; Wellington, 2015). The naphthoquinones from actinobacteria are interesting source of anticancer molecules due to their versatile structural features and potential activity. Table 2 displays the naphthoquinones isolated from actinobacteria such as naphthablin, flaviogeranin, napyradiomycins, griseorhodins, furaquinocins and medermycin have showed significant anticancer activity and are still a source of novel cancer therapeutics.

1.3.4 Possible mechanism of anticancer naphthoquinones

Reactive oxygen species (ROS) are formed as a by-product in mitochondrial metabolism and are necessary in low concentrations for certain functions to generally take place, like folding new proteins in the Endoplasmic reticulum and controlling caspase activity during apoptosis (Veskoukis et al. 2012). ROS also has deleterious effects on cells if found in higher concentrations, leading to oxidative stress and damaging lipids, proteins, DNA, and RNA. DNA damage occurs mainly by strand breakage, base modification, and DNA–protein cross-linkage. Modifying base 2-deoxyguanosine by hydroxyl radical is one of the significant damages that occur, and 8-hydroxy-2-deoxyguanosine derivative is suggested as an oxidative stress biomarker (Valavanidis et al. 2009).

Cancer cells generally have a higher concentration of ROS than normal cells due to the higher metabolic demands. This non-lethal but higher concentration of ROS promotes tumor growth even by damaging DNA, as some damage is beneficial for cancer cells (Poljsak and Fink, 2016). This concentration difference of ROS could be the chemotherapy target since producing even more amount of ROS can lead to cell death. So, this might be the reason for naphthoquinone's actions as an anticancer agent and selectivity towards cancer cells over normal cells (Wellington, 2015). It has been reported that the cytotoxicity of a naturally occurring 2-methoxy-1,4-naphthoquinone in A549 lung cancer cells is stimulated through the generation of ROS, which leads to action on MAPK and JNK signalling pathways (Ong et al. 2015).

Table 2. Anticancer naphthoquinones isolated from actinobacteria

Naphthoquinones	Organism	Reference
Phytohabinone	*Phytohabitans* sp. RD003013	Harunari et al. 2022
Sarubicin A, B, B1 and B2	*Streptomyces* sp. Hu186	Wang et al. 2022
TMKS8A	*Streptomyces* sp. TMKS8	Zhang et al. 2021
Bluemomycin	*Streptomyces* sp. ERINLG-201	Balachandran et al. 2021
Flaviogeranin D and flaviogeranin C2	*Streptomyces* sp. B9173	Shen et al. 2020
Napyradiomycin D1	*Streptomyces* sp. CA-271078	Carretero-Molina et al. 2019
Naquihexcins C, E, and I	*Streptomyces* sp. KIB3133	He et al. 2019
Sekgranaticin, granaticins A, B and methyl granaticinate	*Streptomyces* sp. 166#	Lv et al. 2019
Naphthalenone derivative (C-2)	*Micromonospora* sp. NEAU-gq13	Li et al. 2018
Strepoxepinmycins C-D	*Streptomyces* sp. XMA39	Jiang et al. 2018
Medermycin	*Streptomyces* sp. ZS-A45	Huang et al. 2018
Naphthablin A-C	*Streptomyces* sp. CP26-58	Martucci et al. 2017
Naquihexcins A and BE-52440A	*Streptomyces* sp. HDN-10-293	Che et al. 2016
PM100117 and PM100118	*S. caniferus* GUA-06-05-006A	Pérez et al. 2016
Hygrocins C, D, and F	*Streptomyces* sp. LZ35	Lu et al. 2013
Marfuraquinocins A and C	*Streptomyces niveus* SCSIO 3406	Song et al. 2013
Napyradiomycins	*Streptomyces* sp. SCSIO 10428	Wu et al. 2013
Sacchathridine A	*Saccharothrix* sp. MI559-46F5.	Nakae et al. 2013
Griseusins F and G	*Nocardiopsis* sp. YIM DT266.	Ding et al. 2012
langkolide	*Streptomyces* sp. *Acta* 3062	Helaly et al. 2012
Four new pyranonaphthoquinones	*Streptomyces* sp. IFM 11307	Abdelfattah et al. 2011
Furaquinocins H	*Streptomyces* sp. SN-593	Panthee et al. 2011
Prechrysophanol glucuronide	*Streptomyces* sp. AK 671	Fiedler et al. 2008
Griseusin D	*Nocardiopsis* sp. YIM 80133	Li et al. 2007
4-Dehydro-deacetylgriseusin	*Nocardiopsis* sp. DSM1664	He et al. 2007
Naphthomycins	*Streptomyces* sp. E/784	Hooper & Rickards, 1998
Naphthablin	*Streptomyces aculeolatus*	Umezawa et al. 1995
Griseorhodins A and C	*Streptomyces griseus* (FCRC-57)	Stroshane et al. 1979

1.3.5 Other biological activity

Along with anticancer and antibacterial activity, naphthoquinones possess various biological activities like antifungal, antiparasitic, antivirus, and antioxidant. As shown in Table 3, the naphthoquinones from actinobacteria, such as konamycins and naphterpins possess radical scavenging activity whereas naphthomycins and juglomycins shows antifungal activity.

Table 3. Biological activity of naphthoquinones from actinobacteria other than antibacterial and anticancer

Naphthoquinones	Organism	Bioactivity	Reference
Naquihexcins C, E, I	*Streptomyces* sp. KIB3133	anti-HIV-1 activity	He et al. 2019
Konamycins A	*Streptomyces* sp. MB-PO13T	radical scavenging activity	Harunari et al. 2019
Strepoxepinmycins A−D and medermycin	*Streptomyces* sp. XMA39	Antifungal	Jiang et al. 2018
Naphterpins	*Streptomyces* sp. CNQ-509	Radical scavenging activities	Park and kwon, 2018
Coprisidins A and B	*Streptomyces* sp. SNU607	Coprisidin A inhibit Na+/K+-ATPase activity, coprisidin B induces NAD(P)H:quinone oxidoreductase 1	Um et al. 2016
Langkolide	*Streptomyces* sp. *Acta* 3062	Antifungal, Inhibition of human recombinant phosphodiesterase-4	Helaly et al. 2012
JBIR-85	*Streptomyces* sp. RI-77	antioxidative activity, DPPH radical scavenging activity	Izumikawa et al. 2011
Naphterpins B and C	*Streptomyces* sp. CL190	lipid peroxidation is suppressed in rat homogenate system	Motohashi et al. 2008
Naphthoquinones 1-4	*Streptomyces* sp.	weak activity against cdc25A phosphatase	Kulanthaivel et al. 1999
Naphthomycins	*Streptomyces* sp. E/784	Antifungal	Hooper & Rickards, 1998
Juglomycin Z	*Streptomyces tendae*	Antifungal	Fiedler et al. 1994
WS-5995 A, B and C	*S. auranticolor*	Anti-coccidial activity	Ikushia et al. 1980

Conclusion

The naphthoquinones are interesting chemical structure identified as conjugated cyclic diketones with various biological activities. The review deals with the characterization, biosynthetic pathways and bioactivities of the naphthoquinones isolated from actinobacteria which includes particularly antibacterial and anticancer with its mode of action. Naphthoquinones are surely one of the invaluable chemical entities which should be look upon to tackle the present and future challenges of the drug resistance.

References

Abdelfattah MS, Kazufumi T, Ishibashi M (2011) New pyranonaphthoquinones and a phenazine alkaloid isolated from Streptomyces sp. IFM 11307 with TRAIL resistance-overcoming activity. *J Antibiot* 64:729-734.

Ahmad T, Arora P, Nalli Y, Ali A, Riyaz-Ul-Hassan S (2020) Antibacterial potential of Juglomycin A isolated from *Streptomyces achromogenes*, an endophyte of *Crocus sativus Linn*. *J Appl Microbiol* 128:1366-1377.

Austin MB, Izumikawa M, Bowman ME, Udwary DW, Ferrer JL, Moore BS, Noel JP (2004) Crystal structure of a bacterial type III polyketide synthase and enzymatic control of reactive polyketide intermediates. *J Biol Chem* 279:45162-45174.

Balachandran C, Al-Dhabi NA, Duraipandiyan V, Ignacimuthu S (2021) Bluemomycin, a new naphthoquinone derivative from Streptomyces sp. with antimicrobial and cytotoxic properties. *Biotechnol Lett.* 43:1005-1018.

Cai P, Kong F, Ruppen ME, Glasier G, Carte, GT (2005) Hygrocins A and B, Naphthoquinone Macrolides from *Streptomyces hygroscopicus. J Nat Prod* 68:1736-1742.

Carretero-Molina D, Ortiz-López FJ, Martín J, Oves-Costales D, Díaz C, de la Cruz M, Cautain B, Vicente F, Genilloud O, Reyes F. New Napyradiomycin Analogues from *Streptomyces* sp. Strain CA-271078. *Mar Drugs* 18:22.

Charan RD, Schlingmann G, Bernan VS, Feng X, Carter GT (2005) Fumaquinone, a new prenylated naphthoquinone from *Streptomyces fumanus*. *J antibiot* 58:271-274.

Che Q, Tan H, Han X, Zhang X, Gu Q, Zhu T, Li D (2016) Naquihexcin A, a S-Bridged Pyranonaphthoquinone Dimer Bearing an Unsaturated Hexuronic Acid Moiety from a Sponge-Derived Streptomyces sp. HDN-10-293. *Org let* 18: 3358-3361.

Chung B, Kwon OS, Shin J, Oh KB (2020) Antibacterial Activity and Mode of Action of Lactoquinomycin A from *Streptomyces bacillaris*. *Mar Drugs* 19:7.

Das A, Khosla C (2009) Biosynthesis of aromatic polyketides in bacteria. *Acc Chem Res* 42:631-9

Ding ZG, Zhao JY, Li MG, Huang R, Li QM, Cui XL, Wen ML (2012) Griseusins F and G, spiro-naphthoquinones from a tin mine tailings-derived alkalophilic *Nocardiopsis* species. *J Nat Prod* 75:1994-1998.

Driscoll JS (1974) Quinone structure-antitumor activity relationships. *Cancer Chemother Rep* 4:3-4.

Fiedler HP, Dieter A, Gulder TA, Kajahn I, Hamm A, Brown R, Jones AL, Goodfellow M, Müller WE, Bringmann G (2008) Genoketides A1 and A2, new octaketides and biosynthetic intermediates of chrysophanol produced by Streptomyces sp. AK 671. *J Antibiot* 61:464-473.

Fiedler HP, Kulik A, Schüz TC, Volkmann C, Zeeck A (1994) Biosynthetic capacities of actinomycetes. 2. Juglomycin Z, a new naphthoquinone antibiotic from *Streptomyces tendae*. *J Antibiot* 47:1116-1122.

Fitzgerald JT, Ridley CP, Khosla C (2011) Engineered biosynthesis of the antiparasitic agent frenolicin B and rationally designed analogs in a heterologous host. *J Antibiot* 64:759-762.

Fukuda DS, Mynderse JS, Baker PJ, Berry DM, Boeck LD, Yao RC, Hobbs JN (1990) A80915, A new antibiotic complex produced by Streptomyces aculeolatus discovery, taxonomy, fermentation, isolation, characterization, and antibacterial evaluation. *J Antibiot* 43:623-633.

Funa N, Ohnishi Y, Fujii I, Shibuya M, Ebizuka Y, Horinouchi S (1999) A new pathway for polyketide synthesis in microorganisms. *Nature* 400:897-899.

Geris R, Simpson TJ (2009) Meroterpenoids produced by fungi. *Nat Prod Rep 26*:1063-1094.

Gomi S, Ohuchi S, Sasaki T, Itoh J, Sezaki M (1987) Studies on new antibiotics SF2415. II. The structural elucidation. *J Antibiot* 40:740-749.

Guo Z, Pan G, Xu Z, Yang D, Hindra, Zhu X, Huang Y, Zhao LX, Jiang Y, Duan Y, Shen B (2017) New isofuranonaphthoquinones and isoindolequinones from Streptomyces sp. CB01883. *J Antibiot* 70:414-422.

Harunari E, Imada C, Igarashi Y (2019) Konamycins A and B and rubromycins CA1 and CA2, aromatic polyketides from the tunicate-derived *Streptomyces hyaluromycini* MB-PO13T. *J Nat Prod* 82:1609-1615.

Harunari E, Mae S, Fukaya K, Tashiro E, Urabe D, Igarashi Y (2022) Bisprenyl naphthoquinone and chlorinated calcimycin congener bearing thiazole ring from an actinomycete of the genus Phytohabitans. *J Antibiot* 75:542-551.

He J, Roemer E, Lange C, Huang X, Maier A, Kelter G, Jiang Y, Xu LH, Menzel KD, Grabley S, Fiebig HH, Jiang CL, Sattler I (2007) Structure, derivatization, and antitumor activity of new griseusins from Nocardiopsis sp. *J Med Chem* 50:5168-5175.

He X, Wang Y, Luo RH, Yang LM, Wang L, Guo D, Yang J, Deng Y, Zheng YT, Huang SX (2019) Dimeric Pyranonaphthoquinone Glycosides with Anti-HIV and Cytotoxic Activities from a Soil-Derived *Streptomyces*. *J Nat Prod* 82:1813-1819.

Helaly SE, Kulik A, Zinecker H, Ramachandaran K, Tan GY, Imhoff JF, Süssmuth RD, Fiedler HP, Sabaratnam V (2012) Langkolide, a 32-membered macrolactone antibiotic produced by *Streptomyces* sp. Acta 3062. *J Nat Prod* 75:1018-1024.

Hooper AM, Rickards RW (1998) 3-Amino-5-hydroxybenzoic acid in antibiotic biosynthesis. XI. Biological origins and semisynthesis of thionaphthomycins, and the structures of naphthomycins I and J. *J antibiot* 51:845-851.

Hooper AM, Rickards RW (1998) 3-Amino-5-hydroxybenzoic acid in antibiotic biosynthesis. XI. Biological origins and semisynthesis of thionaphthomycins, and the structures of naphthomycins I and J. *J Antibiot* 51:845-851.

Hoshino S, Awakawa T, Zhang H, Hayashi F, Abe I (2019) Beijinchromes A-D, Novel Aromatic Compounds Isolated from Nocardia beijingensis NBRC 16342. *Chem Pharm Bull* 67:775-777.

Huang LJ, Chang FC, Lee KH, Wang JP, Teng CM, Kuo SC (1998) Synthesis and antiplatelet, antiinflammatory, and antiallergic activities of substituted 3-chloro-5, 8-dimethoxy-1, 4-naphthoquinone and related compounds. *Bioorg Med Chem* 6:2261-2269.

Huang Y, Jiang Q, Chen YH, Zhang DS, Ding WJ, Ma ZJ (2019) A new medermycin analog from the marine-derived actinomycetes *Streptomyces* sp. ZS-A45. *J Asian Nat Prod Res.* 21:826-831.

Ikushima H, Okamoto M, Tanaka H, Ohe O, Kohsaka M, Aoki H, Imanaka H (1980) New anticoccidial antibiotics, WS-5995 A and B. I. Isolation and characterization. *J Antibiot* 33:1107-13.

Izumikawa M, Satou R, Motohashi K, Nagai A, Ohnishi Y, Takagi M, Shin-ya K (2011) Naphthoquinone-like polyketide isolated from Streptomyces sp. RI-77 and its predicted biosynthetic pathway. *J Nat Prod* 74:2588-2591.

Jiang YJ, Zhang DS, Zhang HJ, Li JQ, Ding WJ, Xu CD, Ma ZJ (2018) Medermycin-Type Naphthoquinones from the Marine-Derived Streptomyces sp. XMA39. *J Nat Prod* 81:2120-2124.

Katsuyama Y, Sone K, Satou R, Izumikawa M, Takagi M, Fujie M, Satoh N, Shin-Ya K, Ohnishi Y (2016) Involvement of the Baeyer-Villiger Monooxygenase IfnQ in the Biosynthesis of Isofuranonaphthoquinone Scaffold of JBIR-76 and -77. *Chembiochem* 17:1021-1028.

Kawasaki T, Hayashi Y, Kuzuyama T, Furihata K, Itoh N, Seto H, Dairi T (2006) Biosynthesis of a natural polyketide-isoprenoid hybrid compound, furaquinocin A: identification and heterologous expression of the gene cluster. *J Bacteriol* 188:1236-1244.

Kulanthaivel P, Perun TJ Jr, Belvo MD, Strobel RJ, Paul DC, Williams DC (1999) Novel naphthoquinones from a *Streptomyces* sp. *J Antibiot* 52:256-262.

Lacret R, Oves-Costales D, Pérez-Victoria I, de la Cruz M, Díaz C, Vicente F, Genilloud O, Reyes F (2019) MDN-0171, a new medermycin analogue from *Streptomyces albolongus* CA-186053. *Nat Prod Res.* 33:66-73.

Lacret R, Pérez-Victoria I, Oves-Costales D, de la Cruz M, Domingo E, Martín J, Díaz C, Vicente F, Genilloud O, Reyes F (2016) MDN-0170, a New Napyradiomycin from *Streptomyces* sp. Strain CA-271078. *Mar Drugs.* 14:188.

Li JS, Zhang H, Qi H, Wang JD, Xiang WS (2019) Bioactive naphthoquinone and anthrone derivatives from endophytic *Micromonospora* sp. NEAU-gq13. *J Asian Nat Prod Res* 21:1151-1160.

Li S, Hu X, Li L, Hu X, Wang J, Hu X, Liu H, Yu L, You X, Jiang B, Wu L (2020) 1-hydroxy-7-oxolavanducyanin and $\Delta^{7'',8''}$-6″-hydroxynaphthomevalin from *Streptomyces* sp. CPCC 203577. *J Antibiot* 73:324-328.

Li YQ, Li MG, Li W, Zhao JY, Ding ZG, Cui XL, Wen ML (2007) Griseusin D, a new pyranonaphthoquinone derivative from a alkaphilic Nocardiopsis sp. *J Antibiot* 60:757-761.

Linzner N, Fritsch VN, Busche T, Tung QN, Loi VV, Bernhardt J, Kalinowski J, Antelmann H (2020) The plant-derived naphthoquinone lapachol causes an oxidative stress response in Staphylococcus aureus. *Free Radic Biol Med* 158:126-136.

Lu C, Li Y, Deng J, Li S, Shen Y, Wang H, Shen Y (2013) Hygrocins C–G, cytotoxic naphthoquinone ansamycins from gdmAI-disrupted Streptomyces sp. LZ35. *J Nat Prod* 76:2175-2179.

Lv Q, Fan Y, Tao G, Fu P, Zhai J, Ye B, Zhu W (2019) Sekgranaticin, a SEK34b-Granaticin Hybrid Polyketide from *Streptomyces* sp. 166. *J Org Chem* 84:9087-9092.

Martucci H, Campit SE, Gee SR, Bray WM, Gokey T, Cada AK, Yen TY, Minoura K, Guliaev AB, Lokey RS, Amagata T (2017) Naphthablins B and C, Meroterpenoids Identified from the Marine Sediment-Derived Streptomyces sp. CP26-58 Using HeLa Cell-Based Cytological Profiling. *J Nat Prod* 80:684-691.

Moore BS, Hertweck C (2002) Biosynthesis and attachment of novel bacterial polyketide synthase starter units. *Nat Prod Rep* 19:70-99.

Motohashi K, Irie K, Toda T, Matsuo Y, Kasai H, Sue M, Furihata K, Seto H (2008) Studies on terpenoids produced by actinomycetes. 5-dimethylallylindole-3-carboxylic Acid and A80915G-8″-acid produced by marine-derived *Streptomyces* sp. MS239. *J Antibiot* 61:75-80.

Motohashi K, Sue M, Furihata K, Ito S, Seto H (2008) Terpenoids produced by actinomycetes: Napyradiomycins from *Streptomyces antimycoticus* NT17. *J Nat Prod* 71:595-601.

Murray LAM, McKinnie SMK, Moore BS, George JH (2020) Meroterpenoid natural products from Streptomyces bacteria - the evolution of chemoenzymatic syntheses. *Nat Prod Rep* 37:1334-1366.

Nakae K, Kurata I, Kojima F, Igarashi M, Hatano M, Sawa R, Kubota Y, Adachi H, Nomoto A (2013) Sacchathridine A, a prostaglandin release inhibitor from Saccharothrix sp. *J Nat Prod* 76:720-2.

Oja T, San Martin Galindo P, Taguchi T, Manner S, Vuorela PM, Ichinose K, Metsä-Ketelä M, Fallarero A (2015) Effective Antibiofilm Polyketides against *Staphylococcus aureus* from the Pyranonaphthoquinone Biosynthetic Pathways of *Streptomyces* Species. *Antimicrob Agents Chemother* 59:6046-6052.

Omura S, Tanaka H, Koyama Y, Oiwa R, Katagiri M (1974) Letter: Nanaomycins A and B, new antibiotics produced by a strain of *Streptomyces*. *J Antibiot* 27:363-365.

Ong JY, Yong PV, Lim YM, Ho AS (2015) 2-Methoxy-1,4-naphthoquinone (MNQ) induces apoptosis of A549 lung adenocarcinoma cells via oxidation-triggered JNK and p38 MAPK signaling pathways. *Life Sci* 135:158-64.

Panthee S, Takahashi S, Takagi H, Nogawa T, Oowada E, Uramoto M, Osada H (2011) Furaquinocins I and J: novel polyketide isoprenoid hybrid compounds from Streptomyces reveromyceticus SN-593. . *J Antibiot* 64:509-513.

Park JS, Kwon HC (2018) New Naphthoquinone Terpenoids from Marine Actinobacterium, *Streptomyces* sp. CNQ-509. *Mar Drugs* 16:90.

Pereyra CE, Dantas RF, Ferreira SB, Gomes LP, Silva-Jr FP (2019). The diverse mechanisms and anticancer potential of naphthoquinones. *Cancer Cell Int* 19:1-20.

Pérez M, Schleissner C, Fernández R, Rodríguez P, Reyes F, Zuñiga P, de la Calle F, Cuevas C (2016) PM100117 and PM100118, new antitumor macrolides produced by a marine Streptomyces caniferus GUA-06-05-006A. *J Antibiot* 69:388-394.

Poljšak B, Fink R (2014) The protective role of antioxidants in the defence against ROS/RNS-mediated environmental pollution. *Oxid Med Cell Longev* 671539.

Ravichandiran P, Sheet S, Premnath D, Kim AR, Yoo DJ (2019) 1,4-Naphthoquinone Analogues: Potent Antibacterial Agents and Mode of Action Evaluation. *Molecules* 24:1437.

Sasaki K, Abe H, Yoshizaki F (2002). In vitro antifungal activity of naphthoquinone derivatives. *Biol Pharm Bull* 25:669-670.

Sattely ES, Fischbach MA, Walsh CT (2008) Total biosynthesis: in vitro reconstitution of polyketide and nonribosomal peptide pathways. *Nat Prod Rep* 25:757-93.

Seigler DS (1998) *Plant secondary metabolism*. Springer Science & Business Media.

Shen X, Wang X, Huang T, Deng Z, Lin S (2020) Naphthoquinone-Based Meroterpenoids from Marine-Derived *Streptomyces* sp. B9173. *Biomolecules* 10:1187.

Silva MND, Ferreira VF, de Souza MCB (2003) An overview of the chemistry and pharmacology of naphthoquinones with emphasis on beta-lapachone and derivatives. *Quimica Nova 26*:407-416.

Song GY, Kim Y, Zheng XG, You YJ, Cho H, Chung JH, Sok DE, Ahn BZ (2000) Naphthazarin derivatives (IV): synthesis, inhibition of DNA topoisomerase I and cytotoxicity of 2- or 6-acyl-5,8-dimethoxy-1, 4-naphthoquinones. *Eur J Med Chem* 35:291-298.

Song R, Yu B, Friedrich D, Li J, Shen H, Krautscheid H, Huang SD, Kim MH (2020) Naphthoquinone-derivative as a synthetic compound to overcome the antibiotic resistance of methicillin-resistant *S. aureus*. *Commun Biol* 3:529.

Song Y, Huang H, Chen Y, Ding J, Zhang Y, Sun A, Zhang W, Ju J (2013) Cytotoxic and antibacterial marfuraquinocins from the deep South China Sea-derived *Streptomyces niveus* SCSIO 3406. *J Nat Prod* 76:2263-2268.

Stroshane RM, Chan JA, Rubalcaba EA, Garretson AL, Aszalos AA, Roller PP (1979) Isolation and structure elucidation of a novel griseorhodin. *J Antibiot* 32:197-204.

Sun J, Zhao G, O'Connor RD, Davison JR, Bewley CA (2021) Vertirhodins A–F, C-Linked Pyrrolidine-Iminosugar-Containing Pyranonaphthoquinones from *Streptomyces* sp. B15-008. *Org Lett* 23:682-686.

Tello M, Kuzuyama T, Heide L, Noel JP, Richard SB (2008) The ABBA family of aromatic prenyltransferases: broadening natural product diversity. *Cell Mol Life Sci* 65:1459-1463.

Tsuji N, Kobayashi M, Wakisaka Y, Kawamura Y, Mayama M (1976) New antibiotics, griseusins A and B. Isolation and characterization. *J Antibiot* 29:7-9.

Um S, Bach DH, Shin B, Ahn CH, Kim SH, Bang HS, Oh KB, Lee SK, Shin J, Oh DC (2016) Naphthoquinone-Oxindole Alkaloids, Coprisidins A and B, from a Gut-Associated Bacterium in the Dung Beetle, Copris tripartitus. *Org Lett* 18:5792-5795.

Umezawa K, Masuoka S, Ohse T, Naganawa H, Kondo S, Ikeda Y, Kinoshita N, Hamada M, Sawa T, Takeuchi T (1995) Isolation from *Streptomyces* of a novel naphthoquinone compound, naphthablin, that inhibits Abl oncogene functions. *J Antibiot* 48:604-607.

Valavanidis A, Vlachogianni T, Fiotakis C (2009) 8-hydroxy-2' -deoxyguanosine (8-OHdG): A critical biomarker of oxidative stress and carcinogenesis. *J Environ Sci Health C Environ Carcinog Ecotoxicol Rev* 27:120-39.

Veskoukis AS, Tsatsakis AM, Kouretas D (2012) Dietary oxidative stress and antioxidant defense with an emphasis on plant extract administration. *Cell Stress Chaperones* 17:11-21.

Wang H, Qi H, Zhang SY, Song WS, Zhang LQ, Xiang WS, Wang JD (2022). Sarubicinols A-C, Cytotoxic Benzoxazoles from a *Streptomyces*. *J Nat Prod* 85:1167-1173.

Wang J, Cheng Y, Wu R, Jiang D, Bai B, Tan D, Yan T, Sun X, Zhang Q, Wu Z (2016) Antibacterial Activity of Juglone against *Staphylococcus aureus*: From Apparent to Proteomic. *Int J Mol Sci* 17:965.

Wellington KW (2015) Understanding cancer and the anticancer activities of naphthoquinones –a review. *RSC adv* 5:20309-20338.

WHO Global health (2022) fact sheets. https://www.who.int/news-room/fact-sheets/detail/cancer. Accessed 22 November, 2023.

Winter JM, Moore BS (2009) Exploring the chemistry and biology of vanadium-dependent haloperoxidases. *J Biol Chem* 284:18577-18581.

Wu C, Du C, Ichinose K, Choi YH, van Wezel GP (2017) Discovery of C-Glycosylpyranonaphthoquinones in *Streptomyces* sp. MBT76 by a Combined NMR-Based Metabolomics and Bioinformatics Workflow. *J Nat Prod* 80:269-277.

Wu Z, Li S, Li J, Chen Y, Saurav K, Zhang Q, Zhang H, Zhang W, Zhang W, Zhang S, Zhang C (2013) Antibacterial and cytotoxic new napyradiomycins from the marine-derived *Streptomyces* sp. SCSIO 10428. *Mar Drugs* 11:2113-25.

Zhang G, Fang L, Zhu L, Zhong Y, Wang PG, Sun D (2006) Syntheses and biological activities of 3'-azido disaccharide analogues of daunorubicin against drug-resistant leukemia. *J Med Chem* 49:1792-1799.

Zhang W, Wei S, Zhang J, Wu W (2013) Antibacterial activity composition of the fermentation broth of *Streptomyces djakartensis* NW35. *Molecules* 18:2763-2768.

Zhang Y, Zhou X, Huang H, Tian X, Song Y, Zhang S, Ju J (2013) 03219A, a new Δ(8,9)-pregnene isolated from *Streptomyces* sp. SCSIO 03219 obtained from a South China Sea sediment. *J Antibiot* 66:327-331.

Zhang Z, Sibero MT, Kai A, Fukaya K, Urabe D, Igarashi Y (2021) TMKS8A, an antibacterial and cytotoxic chlorinated α-lapachone, from a sea slug-derived actinomycete of the genus *Streptomyces*. *J Antibiot* 74:464-469.

Zhao X, Drlica K (2014) Reactive oxygen species and the bacterial response to lethal stress. *Curr Opin Microbiol* 21:1-6.

Section 4A: Antibacterial study of Enceleamycins A-C and *N*-hydroxypyrazinone acid

Abstract

Antimicrobial resistance has become a global threat as rapid emergence of antibiotic-resistant bacteria is endangering the efficacy of present antibiotics. Novel antibiotics are required to combat the high level of antimicrobial resistance. In present study, we have explored the antibacterial activity of Enceleamycins A, B, C and *N*-hydroxypyrazinone acid isolated from *Amycolatopsis* sp. WGS_07. Enceleamycin displayed potential antibacterial activity towards clinically isolated MRSA. Enceleamycin A was having a bacteriostatic effect on the growth of MSSA and MRSA. Further we also evaluated the synergistic effect of antibiotics with Enceleamycin A and found that erythromycin was showing a synergistic effect on MRSA. The purified molecule Enceleamycin A also showed significant biofilm inhibition and disruption. Enceleamycin A inhibits the growth of *S. aureus* by the production of intracellular ROS. Altogether, this study presents essential insights into Enceleamycin A possessing potential for bacterial treatment against MRSA.

Graphical abstract
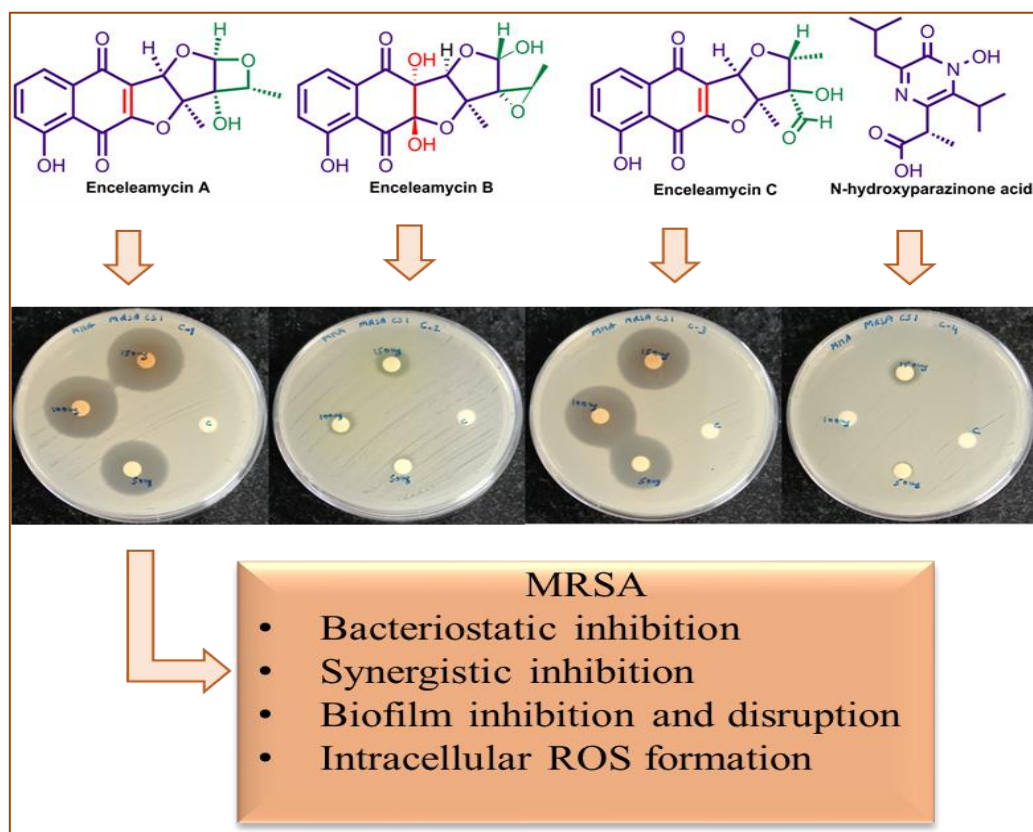
1. Introduction

Antimicrobial resistance (AMR) develops when microorganisms evolve overtime and no longer respond to antimicrobial medications making infections more difficult to cure (Tang et al. 2023). Antibiotic resistance is one of most challenging elements in terms of AMR due to the high rate of resistance towards various antibiotics that were used for bacterial infection treatment. Antibiotic resistance makes infections more difficult to treat, causing treatment delays that could result in prolong sickness and death (Llor and Bjerrum 2014). In 2019, there were estimated 4.95 million deaths linked to bacterial AMR, of which 1.27 million deaths were directly attributed to bacterial AMR (Murray et al. 2022). The second most common bacteria associated with AMR is *Staphylococcus aureus* (*S. aureus*) and it has become one of greatest threats to human health. *S. aureus* is both a commensal bacterium and a human pathogen (Tong et al. 2015; Wertheim et al. 2005). It is one of the major causes of healthcare associated bacteraemia. It leads to skin and soft tissue infections, infective endocarditis, osteoarticular infection and device-related infections (Tong et al. 2015). Treating these infections has become challenging due to rise of multidrug resistance strains over past few decades. MRSA (methicillin-resistant *S. aureus*) is one of the most prevalent antimicrobial-resistant organisms found in nearly every region of the world. Hospital-associated MRSA is associated with increased risk of morbidity and mortality (Loomba et al. 2010).

To successfully treat bacterial infections in the near future, novel class of antibiotics are urgently needed. Since the emergence of resistance to any antibiotic is unavoidable, in addition to discovering new antibiotics, combination antibiotic therapy is a further approach to minimize the drug resistance development (Worthington et al. 2013). Synergistic activity might exhibit comparable effectiveness at lower, non-toxic levels and combinatorial therapy may prevent the emergence of resistance brought on by monotherapy (Sun et al. 2016). Naphthoquinones comprise a naphthalene ring system bearing two carbonyl groups, naturally distributed in bacteria, fungi, and plants. They display various biological activities, like antibacterial, antifungal, anticancer, antimalarial, antiviral, antitrypanosomal, and anti-inflammatory (Rahmoun et al. 2012; Leyva et al. 2017; Inagaki et al. 2015, Rahman et al. 2022; de Sena Pereira et al. 2018; Khraiwesh et al. 2012). The presence of a furo-naphthoquinone substructure in several bioactive natural products isolated from terrestrial and marine organisms prompted to study antibacterial activity of the isolated compounds. The bioactivity of naphthoquinones is associated with reactive oxygen species (ROS)

production (Ravichandiran et al.2019) and it would be interesting to study the antibacterial activity and its mechanisms of action of novel furo-naphthoquinone structure.

In the present section of the chapter we have displayed the antibacterial activity of Enceleamycins A-C and *N*-hydroxypyrazinone acid. Based on the potential antibacterial activity, further the MIC of Enceleamycin A towards the MSSA and MRSA was evaluated and compared with standard antibiotics. The Enceleamycin A activity in combination with standard antibiotics was determined to identify potential synergistic activity against MRSA. The mechanism of Enceleamycin A was studied based on the growth inhibition, time kill assay, cell leakage assay and ROS detection. The biofilm inhibition and disruption was also evaluated for Enceleamycin A.

2. Materials and method

2.1 General materials

The test strains were obtained from NCIM resource centre, Pune. The clinical strains of MRSA were obtained from Hospital, Dharwad, Karnataka. Antibiotics and sterile disc were purchased from Hi-Media, Mumbai. H_2-DCFDA dye obtained from Sigma. Media components used for growth and bioactivity were obtained from Hi-Media, Mumbai.

2.2 Anti-bacterial activity of purified compounds 1-4 against MSSA and MRSA

The anti-bacterial activity of the novel furano-naphthoquinones, Enceleamycin A-C and *N*-hydroxypyrazinone acid was evaluated against Methicillin-sensitive *S. aureus* (MSSA*)* and clinically isolated Methicillin-resistant *S. aureus* (MRSA) by disc diffusion method. In brief, the overnight grown culture of test bacteria was adjusted to 0.5 McF in 0.85% saline and 100 µL of suspension was spread on Mueller-Hinton agar plates. The compounds were loaded in three different concentrations (50, 100, and 150 µg) on a sterile disc along with DMSO as a control. To determine the antibiotic susceptibility and resistance in MSSA and MRSA, antibiotics like ampicillin, kanamycin, vancomycin, and Enceleamycin-A were loaded at a concentration of 50 and 100µg per disc. The zone of inhibition was observed after 20 hours of incubation at 37°C.

2.3 Determination of minimum inhibitory concentration (MIC)

After the preliminary anti-bacterial activity, the MICs of the purified compounds were performed according to CLSI guidelines (Humphries et al. 2021) using Mueller Hinton broth (Hi-media, Mumbai) against a panel of six Gram-positive bacteria, *S. aureus*, *B. cereus, S. epidermidis*, *B. subtilis, L. monocytogenes,* and *M. luteus*, two Gram-negative bacteria, *P. aeruginosa,* and *E. coli* and four MRSA clinical strains. The stock solution of compounds was made at 10 mg/mL in DMSO. The compounds (highest concentration 128 μg/mL) were serially diluted in 50 μL of Mueller-Hinton broth, and 50 μL bacterial suspensions were added to reach final desired cell density of 5×10^5 CFU mL^{-1} in each well of 96-well microtiter plate except for media control. Media, untreated culture, DMSO, ampicillin, and kanamycin were used as controls. The plates were observed for MIC after an incubation of 18 h at 37 °C in shaking conditions. The MIC for *M. smegmatis* was examined following above method in Middlebrook 7H9 medium, and the growth inhibition was observed after 48 h. The MICs were defined as lowest concentration of molecule that inhibited the visible growth of bacteria.

2.4 Effect of purified compounds on the growth of MSSA and MRSA

The growth curve of MSSA and MRSA was observed in compound's presence. The bacterial culture with a cell density of 5×10^5 CFU/mL was grown in MHB in a compound at different concentrations. The 96-well microtitre plate was incubated at 37°C in shaking condition for 24 hours in Synergy Microtek H1, and absorbance at 600 nm was measured every 2 hours.

2.5 Time kill assay

The Time-kill assay was conducted on MSSA and MRSA_CS1. The bacterial culture in the early exponential phase (1×10^5 CFU/mL) was treated with C-1 at different concentrations (1/2×MIC, 1×MIC, 2×MIC, 4×MIC, and 8×MIC) and standard antibiotics ampicillin, vancomycin, and kanamycin (16 μg/ml). The culture was incubated at 37 °C and 180 rpm of shaking. Number of viable bacteria (CFU/mL) was counted at predetermined intervals of 4, 8, 12, 16, 20, and 24 hours, by serially diluting treated suspension of bacterial cells and plating it on a tryptic soy agar (Song et al. 2020).

2.6 Checkerboard assay

To determine the additive or synergistic impact of C-1 (Enceleamycin A) with common antibiotics, the checkerboard experiment was performed. In brief, along the row-axis, C-1 was serially diluted two-fold. To generate a matrix where each well combines at a distinct concentration, the antibiotics were serially diluted two-fold along the column axis. MRSA_CS1 was added to each well to yield around 5×10^5 CFU/mL with final volume of 100µL. The wells were then incubated for 20 hours at 37 °C, and MIC was determined by looking for visibility. The fractional inhibitory concentration (FIC) of the C-1 was determined by dividing the MIC of C-1 in presence of antibiotic by the MIC of the C-1 alone. Similarly, the fractional inhibitory concentration (FIC) of the antibiotic was determined by dividing the MIC of antibiotics in the presence of C-1 by MIC when antibiotic was employed alone. The summation of the FIC value of C-1 and antibiotic was used to compute the FIC index. The FIC index was defined as indifferent, additive, or synergistic for values of $1 < x \geq 4$, $0.5 < x < 1$, and $x \leq 0.5$, respectively.

2.7 Cell leakage analysis

The bacterial culture was grown to the logarithmic stage (10^8 CFU/mL) and splitted into six aliquots of 5 mL each. These samples were centrifuged and suspended in 5 ml of Phosphate buffer saline. The suspension was added with PBS, 8X MIC C-1, and 0.05% Triton X-100 respectively. The aliquots were then cultivated at 37°C with shaking and sampled after 2, 4, and 6 hours, respectively. Next, using an ultra-micro UV-Vis spectrophotometer (ThermoFisher Scientific), supernatant's absorbance was measured at 260/280 nm and the quantities of leaked nucleic acids and proteins from bacterial cells was determined (Tao et al., 2023).

2.8 Biofilm inhibition and Biofilm disruption assay

The biofilm inhibition assay was examined in six-well plate. A culture of *S. aureus* was incubated with the compound in a six-well plate containing a sterile coverslip for 24 hours at 37 °C. After incubation, coverslip was washed with 0.85% saline twice and stained with 0.5% crystal violet for 5 min. The coverslip was washed with saline, and ethanol was used to destain the coverslip. 100µL of the destained solution was used for reading at 570 nm. For the

biofilm disruption, the culture was grown initially for 24 hours to form a biofilm, followed by treatment with a compound (Rogers et al. 2005).

2.9 Measurements of intracellular ROS

The production of intracellular levels of ROS in bacterial cells was evaluated by the 2′,7′-dichlorofluorescein diacetate (H$_2$-DCFDA) method. In brief, the culture of *S. aureus* and 6B_MRSA (2×10^8 CFU/mL) solution was prepared in MHB medium. Enceleamycin A (1× MIC, 2× MIC, and 4× MIC) was added to the culture at different concentrations and left for one hour at 37 °C with 180 rpm of agitation. After centrifuging the bacterial solution for 10 minutes at 5000 rpm, it was resuspended in PBS. After adding the H$_2$-DCFDA (20 μM) in suspension, the mixture was incubated for 30 minutes at 37 °C in the dark. The solutions of 100 μL were then transferred to a 96-well microtitre plate. A microplate reader was used to measure the relative fluorescence units (RFU) of the 100 μL of solutions at 495/529 (excitation/emission). Using the agar plate counting method, the number of viable bacteria (CFU/ml) in the solution was determined. Number of viable bacteria was used to normalize the RFU value (Po et al. 2021).

3. Result and discussion

3.1 Anti-bacterial activity of purified compounds 1-4 against MSSA and MRSA

The antibacterial activity of Enceleamycin A-C and *N*-hydroxypyrazinone acid was determined with disc diffusion method by measuring zone of inhibition (ZOI) against *S. aureus*. Enceleamycin A displayed maximum activity followed by the Enceleamycin C whereas Enceleamycin B and *N*-hydroxypyrazinone acid showed weak activity against Gram positive *S. aureus* bacteria (Figure 1 and Table 1). Further the antibacterial activity was performed against clinically isolated strain of MRSA. Similar results were observed with Enceleamycin A and C displaying potent activity whereas Enceleamycin B and *N*-hydroxypyrazinone acid showed weak activity against MRSA.

To determine the activity and resistance of MRSA_CS1 the bioactivity was performed using standard antibiotics ampicillin, vancomycin and kanamycin along with compound 1. There was clear reduction in the bioactivity of ampicillin against MRSA (ZOI: 15mm) compared to MSSA (ZOI: 40mm). In case of kanamycin no activity was observed against

MRSA_CS1. Vancomyin and compound 1 (C-1) was not showing much difference in the activity against MRSA compared to MSSA (Figure 2 and Table 2).
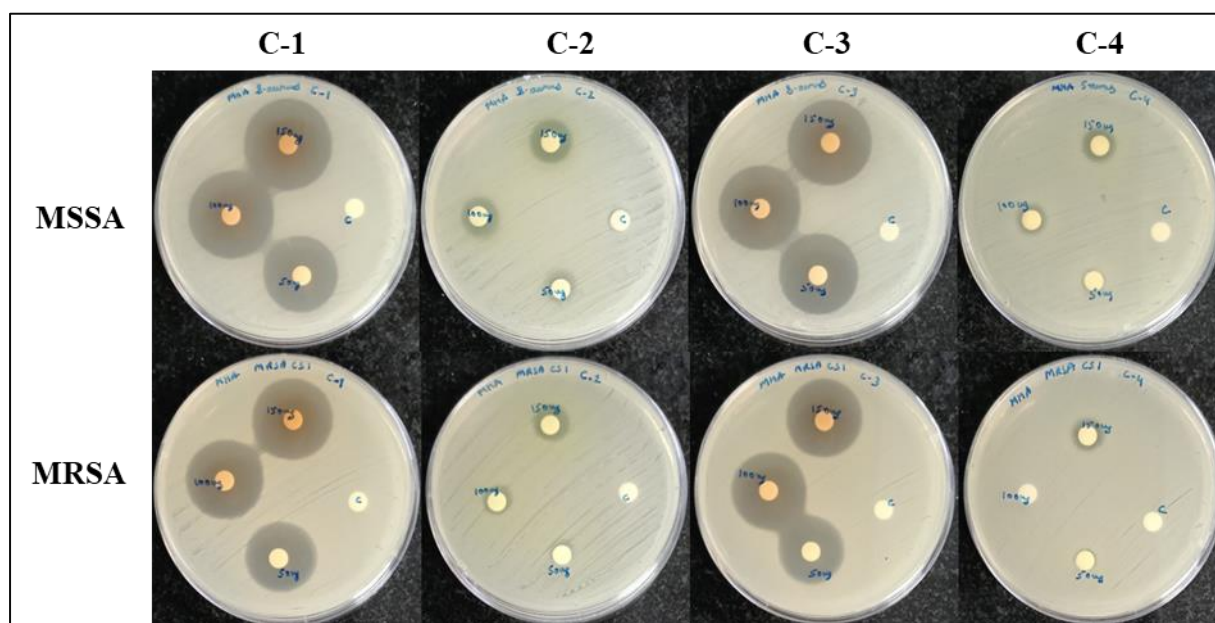
Figure 1. Antibacterial activity of purified compounds **C1-C4** performed by disc diffusion method against methicillin-sensitive *S. aureus* (MSSA) and methicillin-resistant *S. aureus* (MRSA) MRSA at different concentrations (150, 100 and 50 µg per disc)

Table 1. Antibacterial activity of compounds **1-4** performed by disc diffusion method against methicillin-sensitive *S. aureus* (MSSA) and methicillin-resistant *S. aureus* (MRSA)

Concentration (µg)	Zone of inhibition (in mm)							
	C1		C2		C3		C4	
	MSSA	MRSA	MSSA	MRSA	MSSA	MRSA	MSSA	MRSA
150	29	27	14	11	28	26	12	10
100	28	26	11	10	27	25	10	-
50	24	23	10	-	24	23	-	-
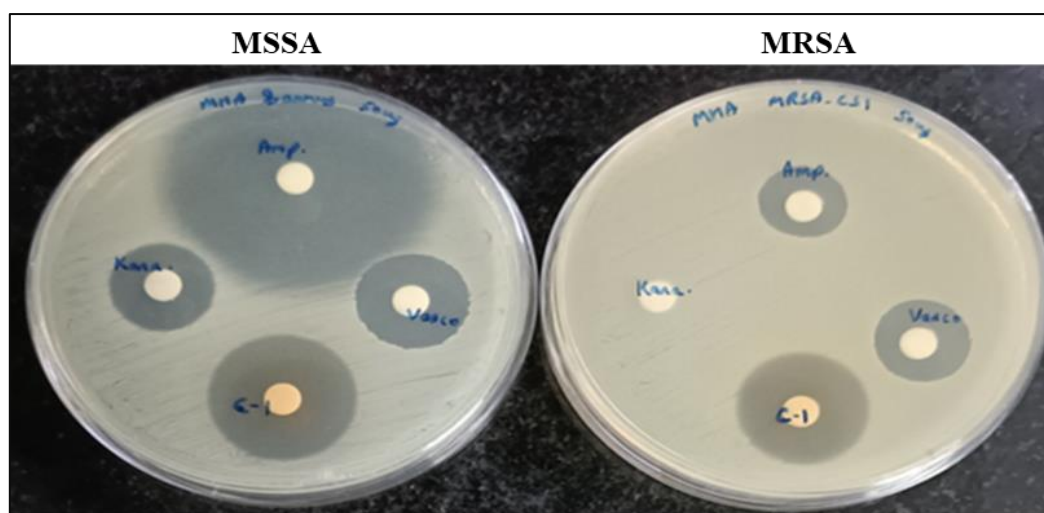
Figure 2. Antibacterial activity of **C-1** and antibiotics performed by disc diffusion method against MSSA and MRSA at concentration of 50 µg per disc

Table 2. Antibacterial activity of **C-1** and antibiotics performed by disc diffusion method against MSSA and MRSA

Test strain	Concentration (µg)	Zone of inhibition (in mm)			
		Amp	**Kan**	**Vanco**	**C-1**
MSSA	50	40	18	18	24
MRSA	50	15	-	17	23
MSSA	100	40	19	19	28
MRSA	100	19	-	19	26

[a]Ampicillin (Amp), [b]Kanamycin (Kan), [c]Vancomycin (Van) used as a reference standard, C-1 refers to compound-1 (Enceleamycin A)

3.2 Determination of minimum inhibitory concentration (MIC)

The isolated compounds showed selective inhibition toward the Gram-positive bacteria (Table 3). Compounds **1** and **3** have antibacterial activity against tested Gram-positive bacteria (MIC values of 2 to 32 µg/mL), whereas compounds **2** and **4** were less active (MIC value of 64 to 128 µg/mL). These compounds also inhibited the growth of four different clinically isolated methicillin-resistant *S. aureus*.

Table 3. MIC determination of Compounds **1–4**

Bacterial strain	MIC (µg/mL)					
	C-1	C-2	C-3	C-4	Amp [a]	Kan [b]
S. aureus ATCC 9144	2	128	8	128	0.03	8
S. epidermidis ATCC 12228	2	64	8	64	1	1
B. cereus ATCC 11778	8	>128	16	128	16	2
B. subtilis ATCC 6633	4	>128	16	128	0.03	0.5
M. luteus ATCC 9341	8	>128	32	64	0.03	8
L. monocytogenes ATCC19111	2	128	8	128	0.03	1
M. smegmatis ATCC 607	64	>128	64	>128	64	0.25
MRSA_CS1	4	>128	16	128	8	>128
MRSA_CS2	4	>128	8	128	8	>128
MRSA_CS2	4	>128	16	128	16	128
MRSA_CS4	4	128	8	128	4	>128
E. coli ATCC 8739	>128	>128	>128	>128	2	8
P. aeruginosa ATCC 9027	>128	>128	>128	>128	2	8

[a]Ampicillin (Amp) used as a reference standard.

[b]Kanamycin (Kan) used as a reference standard. C refers to the compounds.

The MIC was determined for both the MSSA and MRSA against different class of antibiotics and Enceleamycin A (Table 4). The MIC fold difference was evaluated between the MSSA and MRSA strain and was found that all the class of antibiotics showed higher MIC value except the vancomycin. The beta lactam class of antibiotic ampicillin and amoxicillin displayed around >1000 times MIC value against MRSA compared to the MSSA. Other than this the antibiotic kanamycin, gentamycin and nalidixic acid did not show inhibition upto 128 µg/mL. In the MIC determination, the C-**1** displayed 2 and 4 µg/mL MIC value against MSSA and MRSA respectively, better than all other compounds. The 2 fold increase in MIC of Enceleamycin A (C-**1**) value might be because of difference in strain level.

Table 4. Comparison of MIC for antibiotics and compounds against MSSA and MRSA_CS1

Antibiotics	MIC (µg/mL)		MIC difference
	MSSA	**MRSA_CS1**	**fold increase**
Ampicillin	0.03	32	1066
Amoxicillin	0.03	32	1066
Vancomycin	1.0	1.0	1.0
Bacitracin	64	128	2.0
Kanamycin	8.0	>128	>16
Gentamycin	2.0	>128	>64
Erythromycin	0.5	128	256
Chloramphenicol	2.0	8.0	4.0
Ciprofloxacin	0.125	16	128
Nalidixic acid	32	>128	>2.0
Tetracycline	0.06	0.125	2.0
Trimethoptrin	0.5	2.0	4.0
Enceleamycin A (C**1**)	2.0	4.0	2.0
Enceleamycin B (C**2**)	128	>128	>1.0
Enceleamycin C (C**3**)	8.0	16.0	2.0
N-hydroxypyrazinone acid (C**4**)	128	128	1.0

Figure 3. MIC of Ampicillin and Amoxicillin against MSSA and MRSA_CS1

3.3 Effect of the purified Compounds on the growth of MRSA

The effect of Enceleamycin A-C and *N*-hydroxypyrazinone on the growth of MSSA and MRSA was determined for 24 hours. Enceleamycin A showed complete growth inhibition of *S. aureus* (MRSA and MSSA) at 4 μg/mL in 24 hours. However, at lower concentrations of 2 μg/mL the culture was showing growth at the later stage of incubation which shows its bacteriostatic effect (Figure 4). Similar results were observed for Enceleamycin C at 8 μg/mL. Enceleamycin B inhibits the growth of MSSA at 128 μg/mL but in MRSA case growth was observed after 8-10 hours. The compound **4** completely inhibited the growth of MSSA at 128 μg/mL but against MRSA slight growth was found only after 20 hours of incubation.

3.4 Time kill assay

Upon identifying Enceleamycin A as the most potent antibacterial candidate against MSSA and MRSA, antibacterial activity of Enceleamycin A was evaluated using time-kill assay against MSSA and MRSA. The time-kill assay determines the interaction between the antimicrobial agents and the microbes. It displays the time or concentration-dependent effect of antibiotics on the growth of bacteria and determines its bacteriostatic or bactericidal nature (Balouiri et al. 2016, Adusei et al. 2019). Bactericidal activity is considered when the CFU/ml of bacteria is decreased by greater than 3 $\log_{10}$ –fold which corresponds to 99.9% of the inoculum being killed. To confirm the bacteriostatic nature of Enceleamycin A, time-kill assay was evaluated against MSSA and MRSA_CS1 at MIC values of 0.5X, 1X, 2X, 4X and 8X. It was found that in the presence of Enceleamycin A, the CFU/ml of both the MSSA and MRSA was not completely reduced even at concentration of 8X MIC which shows a bacteriostatic effect against both MSSA and MRSA (Figure 5). All the three antibiotics were bactericidal against MSSA however against MRSA only vancomycin was active and showing bactericidal effect.
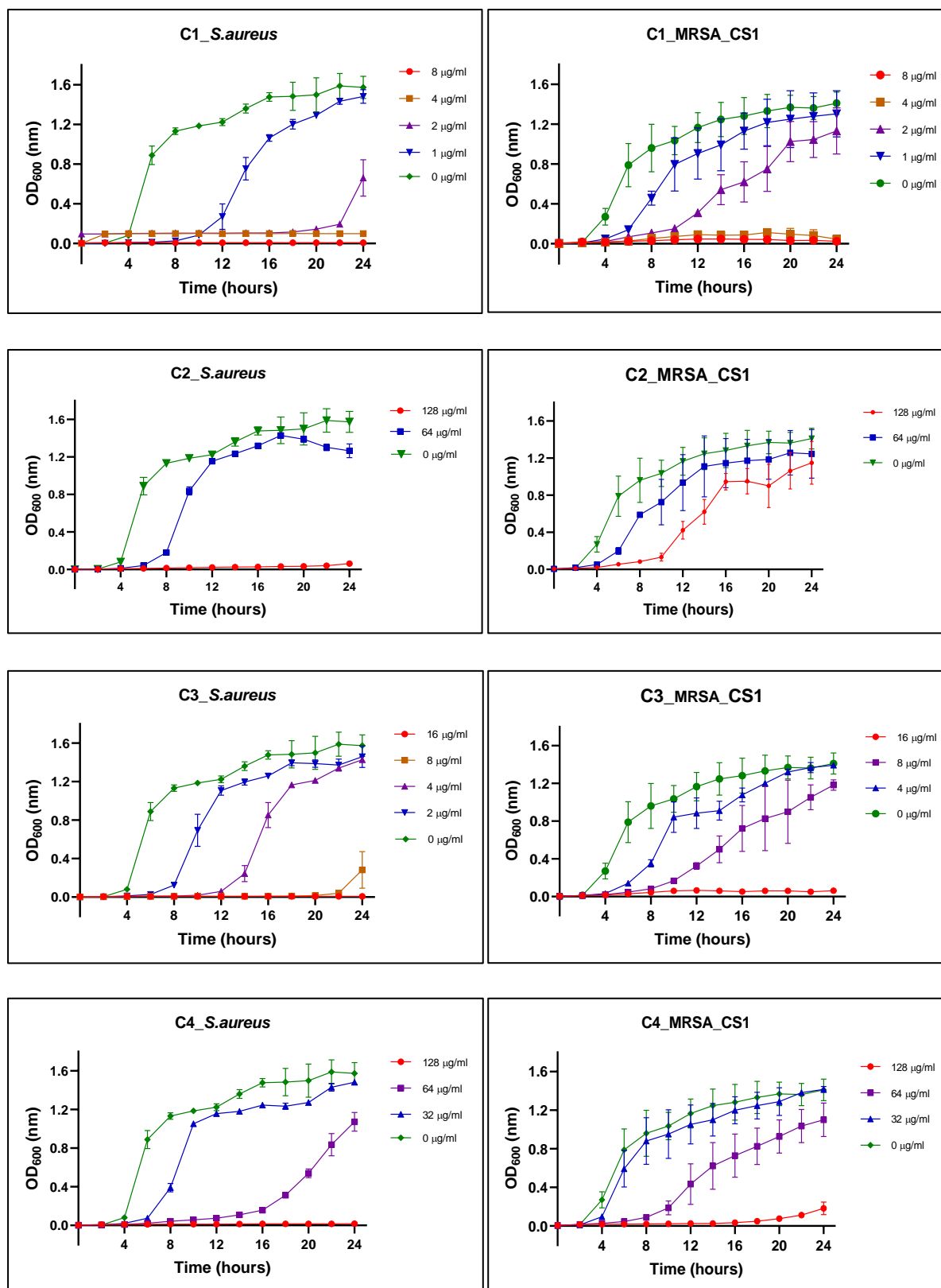
Figure 4. The effect on the growth of *S. aureus* (MSSA and MRSA) at different concentrations of compound C**1**, C**2**, C**3** and C**4**
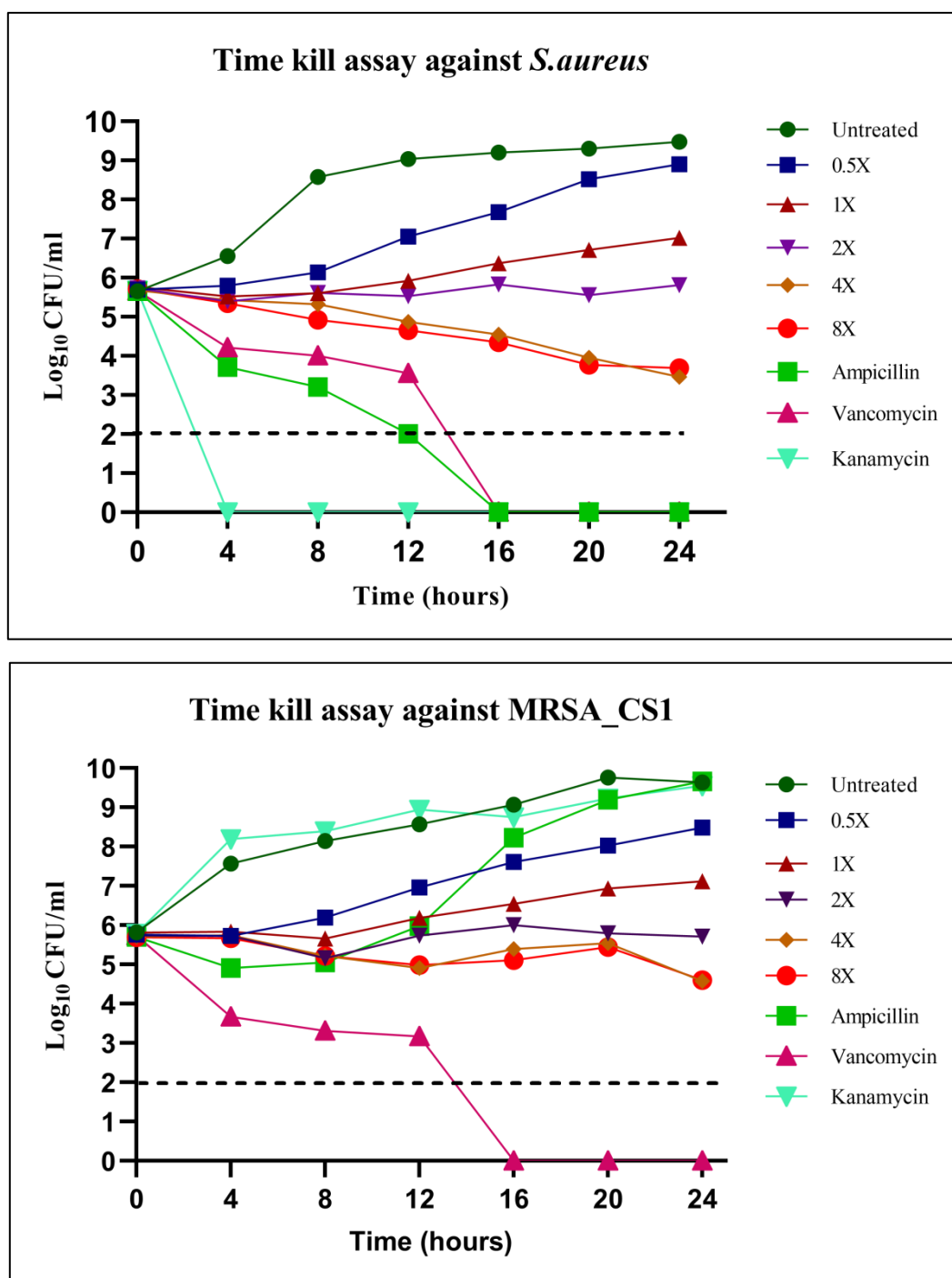
Figure 5. Time kill assay against MSSA and MRSA_CS1 in presence of **C-1** and antibiotics

3.5 Checkerboard assay

The checkerboard assay was used to investigate the synergistic or additive effect of Enceleamycin A in combination with standard antibiotics. The combination antibiotic therapy is used for better inhibitory activity at non-toxic lower concentration and also to minimize the

development of drug resistance (Worthington et al. 2013, Sun et al. 2016). In the checkerboard assay, MIC of erythromycin alone was determined to be 128 μg/mL and combined treatment of 1/4 MIC of Enceleamycin A resulted in reduced MIC of erythromycin to 32 μg/mL against MRSA_CS1 (Figure 6). The fractional inhibitory concentration (FIC) index for erythromycin and Enceleamycin A was 0.5, suggesting the synergistic effect of erythromycin and Enceleamycin A (Table 5). In addition, Enceleamycin A also displayed additive effect in combination with ampicillin, vancomycin and ciprofloxacin with FIC index of 1, 0.625 and 0.725 respectively. The synergistic and additive effect of Enceleamycin A could result in a shorter course of antibiotic treatment, a quicker clearance of the illness, and consequently less dose-related toxicity.
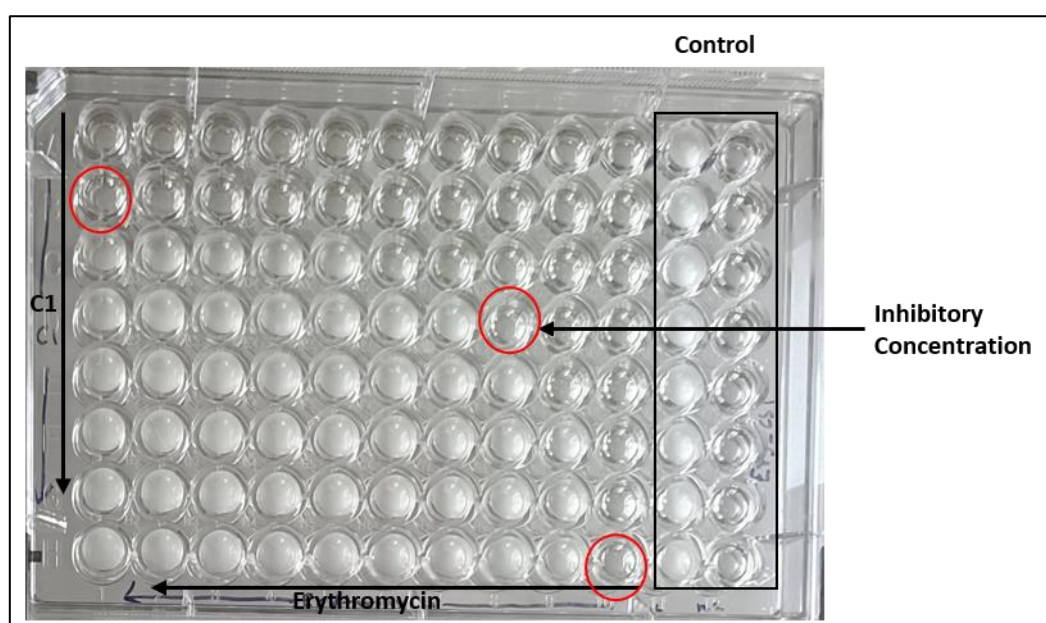
Figure 6. Effect of erythromycin and **C-1** (Enceleamycin A) in combination against MRSA_CS1

Table 5. Effect of antibiotics and **C-1** (Enceleamycin A) in combination against MRSA_CS1

Antibiotic	FIC Antibiotic	FIC C-1	FIC index	Interpretation
Ampicillin	0.5	0.5	1	Additive
Vancomycin	0.5	0.125	0.625	Additive
Erythromycin	0.25	0.25	0.5	Synergistic
Ciprofloxacin	0.25	0.5	0.725	Additive
Trimethoptrin	1	1	2	Indifference

3.6 Cell leakage analysis

To determine the cell leakage of MRSA by detecting the contents of nucleic acids and proteins leaked after treatment with Enceleamycin A, absorbance of cell-free supernatant was measured at 260 and 280 nm. Significant cell leakage was observed only after 4 and 6 hours of treatment compared to untreated. The leakage of nucleic acid and proteins were comparatively less than the positive control Triton-X.
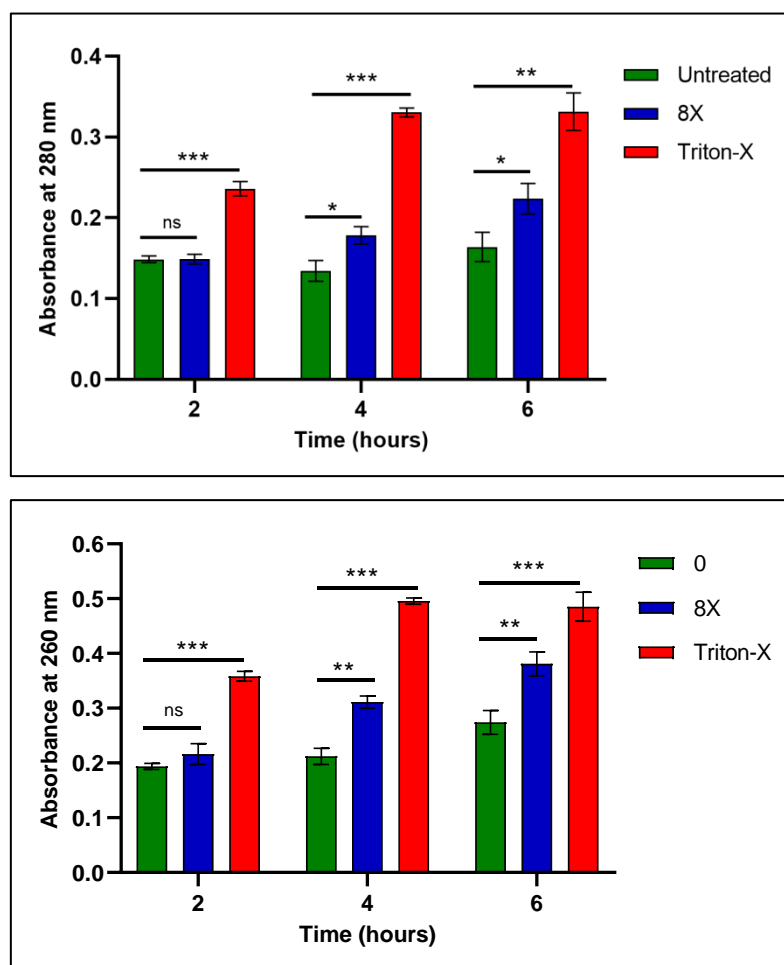
Figure 8. Nucleic acid leakage analysis after treatment with Enceleamycin A

3.7 Biofilm inhibition and Biofilm disruption assay

The bacterial infections caused by the biofilm formation are challenging to eradicate and can cause major complications. The bacterial biofilm structures adhere to living or inert surfaces and comprised of extracellular polymeric matrix made up of proteins, polysaccharides and various organic components (Di Ciccio et al. 2015). Most common biofilm associated infections are caused by *S. aureus*. They adhere to various surfaces to form biofilms like human tissues or medical devices (Arciola et al. 2018). The biofilms are more resistant to

antimicrobial compounds compared to planktonic cells resulting in immune system evading and prolonged infection (Koo et al. 2017). The naphthoquinone and their derivatives have displayed inhibitory activity against wide range of bacterial biofilm and can be vital in dealing with biofilm related infections (Novais et al. 2020, Song et al. 2020, Novais et al. 2018). Considering this, in addition to the inhibitory activity of Enceleamycin A towards planktonic bacterial cells, the biofilm inhibition and its disruption was also performed. The inhibition and disruption of the biofilm formed by *S. aureus* was clearly visible in the microscopic images (Figure 7A and 7B). The biofilm formation by *S. aureus* was significantly inhibited by Enceleamycin A at all concentration tested starting from 1/2X MIC i.e. 1μg/ml or above (Figure 7C). However, Enceleamycin A required higher concentration of 1X MIC i.e. 2 μg/ml or above for the significant disruption of already formed biofilm (Figure 7D).
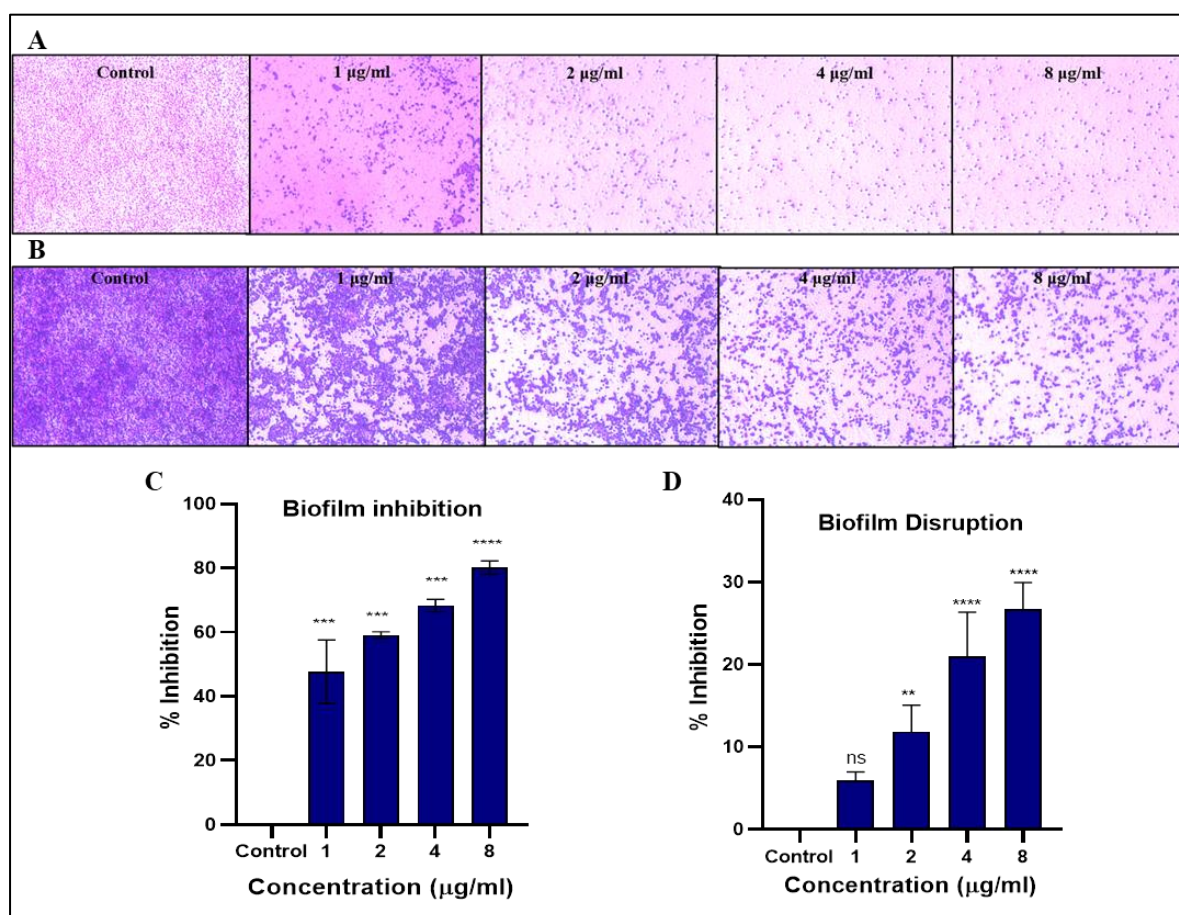
Figure 7. Biofilm inhibition and biofilm disruption of *S.aureus* in presence of **C-1** (Enceleamycin A), (**A**) Microscopic image of biofilm inhibition (**B**) Microscopic image of biofilm disruption (**C**) Percentage of biofilm inhibition (**D**) Percentage of biofilm disruption

3.8 Measurements of the intracellular ROS

The presence of quinone moiety in naphthoquinones is known for producing intracellular ROS and is responsible for the antibacterial activity (Paul et al. 2021). We examined the intracellular ROS production in MRSA after treatment with Enceleamycin A by $2',7'$-dichlorofluorescein diacetate (H2-DCFDA). As shown in Figure 9A, the cellular esterase deacetylates the cell-permeable dye (H2-DCFDA) to a non-fluorescent molecule, which upon oxidation by ROS, transforms into highly fluorescent $2',7'$-dichlorofluorescein (DCF) (Ng and Ooi 2021). The intracellular ROS formation after treatment with Enceleamycin A was detected after 1 hour and analysed by normalizing the RFU and number of viable bacteria (CFU/mL). The graph in Figure 9B displayed concentration-dependent significant increase in the ROS production after treatment with Enceleamycin A at all concentration starting from 1X MIC i.e. 2 μg/mL or above. It is well-known that excessive ROS formation within the cell leads to growth inhibition of bacteria and is one of the primary reasons of the naphthoquinones bioactivity against bacteria.
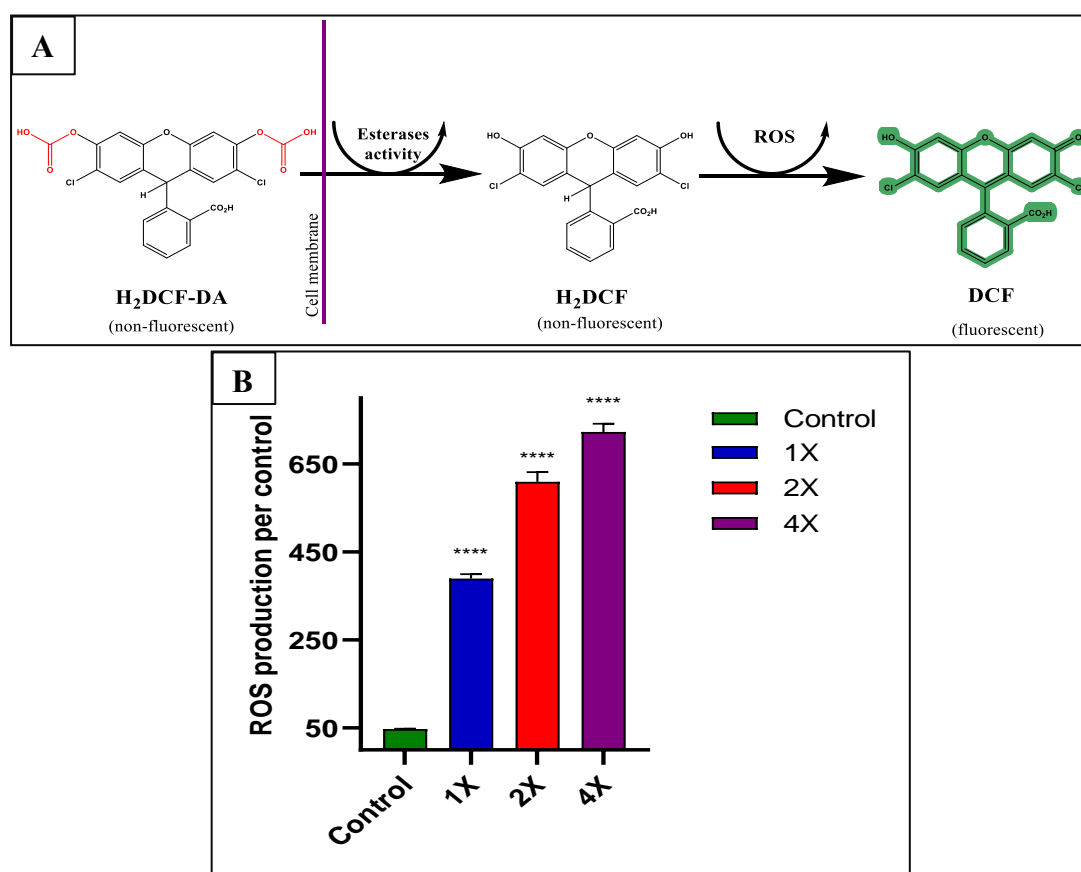
Figure 9. ROS detection by H$_2$DCF-DA dye (**A**) Process of cell permeable H$_2$-DCFDA conversion to a highly fluorescent 2',7'-dichlorofluorescein (DCF), (**B**) ROS production in *S. aureus* after treatment with Enceleamycin A at concentration of 1X, 2X and 4X MIC

Conclusion

The isolated compounds showed antibacterial activity against various Gram-positive bacteria including clinically isolated MRSA. The novel Enceleamycin A (**1**) and C (**3**) displayed potent antibacterial activity whereas Enceleamycin B and *N*-hydroxypyrazinone acid were weakly active. Enceleamycin A showed bacteriostatic inhibition of MSSA and MRSA. It also displayed synergistic activity against MRSA in combination with erythromycin. Enceleamycin A displayed significant inhibition of biofilm formation by MRSA and also disrupt the formed MRSA biofilm. The preliminary study shows that ROS produced by Enceleamycin A (**1**) might be the reason for inhibition of bacterial growth. Considering activity of Enceleamycin A, it can be a candidate molecule to tackle the antimicrobial resistance related to MRSA.

References

Adusei EBA, Adosraku RK, Oppong-Kyekyeku J, Amengor CDK, Jibira Y (2019) Resistance Modulation Action, Time-Kill Kinetics Assay, and Inhibition of Biofilm Formation Effects of Plumbagin from *Plumbago zeylanica* Linn. *J Trop Med* 2019:1250645.

Arciola CR, Campoccia D, Montanaro L (2018) Implant infections: adhesion, biofilm formation and immune evasion. *Nat Rev Microbiol* 16:397–409.

Balouiri M, Sadiki M, Ibnsouda SK (2016) Methods for *in vitro* evaluating antimicrobial activity: A review. *J Pharm Anal* 6:71-79.

Barka EA, Vatsa P, Sanchez L, Gaveau-Vaillant N, Jacquard C, Meier-Kolthoff JP, Klenk HP, Clément C, Ouhdouch Y, van Wezel GP (2016) Taxonomy, Physiology, and Natural Products of Actinobacteria. *Microbiol Mol Biol Rev* 80:1-43.

Bérdy J (2005) Bioactive microbial metabolites. *J Antibiot* 58:1-26.

Das S, Lyla PS, Ajmal Khan S (2008) Distribution and generic composition of culturable marine actinomycetes from the sediments of Indian continental slope of Bay of Bengal. *Chin J Oceanol Limnol* 26:166-77.

de Sena Pereira VS, da Silva Emery F, Lobo L, Nogueira F, Oliveira JIN, Fulco UL, Albuquerque EL, Katzin AM, de Andrade-Neto VF (2018) In vitro antiplasmodial activity, pharmacokinetic profiles and interference in isoprenoid pathway of 2-aniline-3-hydroxy-1.4-naphthoquinone derivatives. *Malar J* 17:482.

Di Ciccio P, Vergara A, Festino AR, Paludi D, Zanardi E, Ghidini S, Ianieri A (2015) Biofilm formation by *Staphilococcus aureus* on food contact surfaces: Relationship with temperature and cell surface hydrophobicity. *Food Control* 50:930–936.

Greco I, Molchanova N, Holmedal E, Jenssen H, Hummel BD, Watts JL, Håkansson J, Hansen PR, Svenson J (2020) Correlation between hemolytic activity, cytotoxicity and systemic in vivo toxicity of synthetic antimicrobial peptides. *Sci Rep* 10:13206.

Humphries R, Bobenchik AM, Hindler JA, Schuetz AN (2021) Overview of changes to the clinical and laboratory standards institute performance standards for antimicrobial susceptibility testing, M100. *J Clin Microbiol* 59:10-128.

Inagaki R, Ninomiya M, Tanaka K, Koketsu M (2015) Synthesis, Characterization, and Antileukemic Properties of Naphthoquinone Derivatives of Lawsone. *ChemMedChem* 10:1413-1423.

Khraiwesh MH, Lee CM, Brandy Y, Akinboye ES, Berhe S, Gittens G, Abbas MM, Ampy FR, Ashraf M, Bakare O (2012) Antitrypanosomal activities and cytotoxicity of some novel imido-substituted 1,4-naphthoquinone derivatives. *Arch Pharm Res* 35:27-33.

Koo H, Allan RN, Howlin RP, Stoodley P, Hall-Stoodley L (2017) Targeting microbial biofilms: current and prospective therapeutic strategies. *Nat Rev Microbiol* 15:740–755.

Kumar N, Afjei R, Massoud TF, Paulmurugan R (2018) Comparison of cell-based assays to quantify treatment effects of anticancer drugs identifies a new application for Bodipy-L-cystine to measure apoptosis. *Sci Rep* 8:16363.

Kumar, Nita, Rayhaneh Afjei, Tarik F. Massoud, and Ramasamy Paulmurugan. *Scientific reports* 8, no. 1 (2018): 16363.

Lee LH, Zainal N, Azman AS, Eng SK, Goh BH, Yin WF, Ab Mutalib NS, Chan KG (2014) Diversity and antimicrobial activities of actinobacteria isolated from tropical mangrove sediments in Malaysia. *ScientificWorldJournal* 2014:698178.

Leyva E, López LI, de la Cruz RF, Espinosa-González CG (2017) Synthesis and studies of the antifungal activity of 2-anilino-/2, 3-dianilino-/2-phenoxy-and 2, 3-diphenoxy-1, 4-naphthoquinones. *Res Chem Intermed* 43:1813-27.

Llor C, Bjerrum L (2014) Antimicrobial resistance: risk associated with antibiotic overuse and initiatives to reduce the problem. *Ther Adv Drug Saf* 5:229-241.

Loomba PS, Taneja J, Mishra B (2010) Methicillin and Vancomycin Resistant S. aureus in Hospitalized Patients. *J Glob Infect Dis* 2:275-283.

Luo C, Wang Y, Wei C, Chen Y, Ji Z (2020) The anti-migration and anti-invasion effects of Bruceine D in human triple-negative breast cancer MDA-MB-231 cells. *Exp Ther Med* 19:273-279.

Murray CJ, Ikuta KS, Sharara F, Swetschinski L, Aguilar GR, Gray A, Han C, Bisignano C, Rao P, Wool E, Johnson SC (2022) Global burden of bacterial antimicrobial resistance in 2019: a systematic analysis. *The Lancet* 399:629-655.

Novais JS, Carvalho MF, Ramundo MS, Beltrame CO, Geraldo RB, Jordão AK, Ferreira VF, Castro HC, Figueiredo AMS (2020) Antibiofilm effects of N,O-acetals derived from 2-amino-1,4-naphthoquinone are associated with downregulation of important global virulence regulators in methicillin-resistant Staphylococcus aureus. *Sci Rep* 10:19631.

Novais JS, Moreira CS, Silva ACJA, Loureiro RS, Sá Figueiredo AM, Ferreira VF, Castro HC, da Rocha DR (2018) Antibacterial naphthoquinone derivatives targeting resistant strain Gram-negative bacteria in biofilms. *Microb Pathog* 118:105-114.

Orhan G, Bayram A, Zer Y, Balci I (2005) Synergy tests by E test and checkerboard methods of antimicrobial combinations against *Brucella melitensis*. *J Clin Microbiol* 43:140-143.

Paul P, Chakraborty P, Chatterjee A, Sarker RK, Dastidar DG, Kundu T, Sarkar N, Das A, Tribedi P (2021) 1,4-Naphthoquinone accumulates reactive oxygen species in Staphylococcus aureus: a promising approach towards effective management of biofilm threat. *Arch Microbiol* 203:1183-1193.

Po KH, Chow HY, Cheng Q, Chan BK, Deng X, Wang S, Chan EW, Kong HK, Chan KF, Li X, Chen S (2021) Daptomycin exerts bactericidal effect through induction of excessive ROS production and blocking the function of stress response protein Usp2. *Nat Sci* 1:e10023.

Rahman MM, Islam MR, Akash S, Shohag S, Ahmed L, Supti FA, Rauf A, Aljohani ASM, Al Abdulmonem W, Khalil AA, Sharma R, Thiruvengadam M (2022) Naphthoquinones and derivatives as potential anticancer agents: An updated review. *Chem Biol Interact* 368:110198.

Rahmoun NM, Boucherit-Otmani Z, Boucherit K, Benabdallah M, Villemin D, Choukchou-Braham N (2012) Antibacterial and antifungal activity of lawsone and novel naphthoquinone derivatives. *Med Mal Infect.* 42:270-275.

Ravichandiran P, Masłyk M, Sheet S, Janeczko M, Premnath D, Kim AR, Park BH, Han MK, Yoo DJ (2019) Synthesis and Antimicrobial Evaluation of 1,4-Naphthoquinone Derivatives as Potential Antibacterial Agents. *ChemistryOpen* 8:589-600.

Rogers SA, Melander C (2008) Construction and screening of a 2-aminoimidazole library identifies a small molecule capable of inhibiting and dispersing bacterial biofilms across order, class, and phylum. *Angew Chem Int Ed Engl* 47:5229-5231.

Salomon CE, Magarvey NA, Sherman DH (2004) Merging the potential of microbial genetics with biological and chemical diversity: an even brighter future for marine natural product drug discovery. *Nat Prod Rep* 21:105-121.

Song R, Yu B, Friedrich D, Li J, Shen H, Krautscheid H, Huang SD, Kim MH (2020) Naphthoquinone-derivative as a synthetic compound to overcome the antibiotic resistance of methicillin-resistant *S. aureus*. *Commun Biol* 3:529.

Sun W, Sanderson PE, Zheng W (2016) Drug combination therapy increases successful drug repositioning. *Drug Discov Today* 21:1189-1195

Tao Z, Geng D, Tao J, Wang J, Liu S, Wang Q, Xu F, Xiao S, Wang R (2023) Synergistic Antibacterial Effect and Mechanism of Allicin and an *Enterobacter cloacae* Bacteriophage. *Microbiol Spectr* 11:e03155.

Tong SY, Davis JS, Eichenberger E, Holland TL, Fowler VG Jr (2015) *Staphylococcus aureus* infections: epidemiology, pathophysiology, clinical manifestations, and management. *Clin Microbiol Rev* 28:603-661.

Ventura M, Canchaya C, Tauch A, Chandra G, Fitzgerald GF, Chater KF, van Sinderen D (2007) Genomics of Actinobacteria: tracing the evolutionary history of an ancient phylum. *Microbiol Mol Biol Rev* 71:495-548.

Wertheim HF, Melles DC, Vos MC, van Leeuwen W, van Belkum A, Verbrugh HA, Nouwen JL (2005) The role of nasal carriage in *Staphylococcus aureus* infections. *Lancet Infect Dis* 5:751-762.

Worsley CM, Veale RB, Mayne ES (2022) Inducing apoptosis using chemical treatment and acidic pH, and detecting it using the Annexin V flow cytometric assay. *PLoS One* 17:e0270599.

Worthington RJ, Melander C (2013) Combination approaches to combat multidrug-resistant bacteria. *Trends Biotechnol* 31:177-184.

Section 4B: Anticancer study of Enceleamycins A-C and *N*-hydroxypyrazinone acid

Abstract

It has become more crucial than ever to find novel anticancer compounds due to the rise in cancer mortality and resistance to the present chemotherapeutic drugs. The isolated novel molecules Enceleamycins A-C and *N*-hydroxypyrazinone were examined for their anti-cancer potential. Enceleamycin A demonstrated considerable cytotoxicity for triple-negative breast cancer (TNBC) MDA-MB-231 cells with an IC_{50} value of 1.25 µg/mL (3.78 µM). It also showed its ability to inhibit MDA-MB-231 cell migration. Enceleamycin A raises intracellular ROS levels in TNBC cells, ultimately leading to apoptotic cell death, as demonstrated by Annexin V/PI staining. The molecular docking and simulation investigation revealed better binding affinity of Enceleamycin A with AKT2, which plays a vital role in breast cancer's invasiveness and chemo-resistance. Enceleamycin A inhibits the AKT2 enzyme in vitro with an IC_{50} value of 0.736 µg/ml, further validating the docking study. The *in silico* physicochemical and pharmacokinetics characteristics of Enceleamycin A demonstrated its drug-likeness. Intriguingly, Enceleamycin A was non-hemolytic in nature. Taken together, Enceleamycin A could be a candidate molecule for treating TNBC cells by targeting the AKT2 signaling pathway.

Graphical Abstract
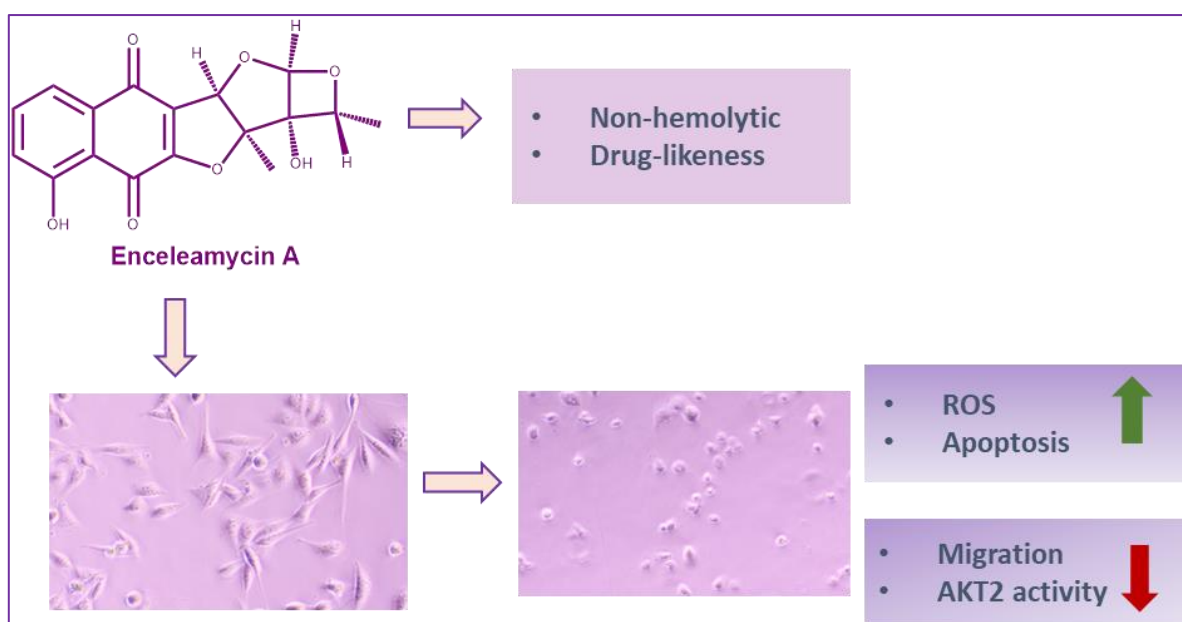
1. Introduction

Cancer is a non-communicable disease and is associated with a rapid and uncontrolled cell growth (Wellington 2015). Cancer is the second largest cause of mortality globally, with approximately twenty million new cases and ten million fatalities in the year 2020. With a projected 2.3 million new cases, breast cancer has now surpassed lung cancer, as the most frequently detected cancer (Rashid et al. 2019; Sung et al. 2021). Among all breast cancer, triple-negative breast cancer (TNBC) counts for 10–15% of cases and is considered more aggressive with a low survival rate. TNBCs does not express the three receptors, namely, progesterone (PR), estrogen (ER), and human epidermal growth factor receptor-2 (HER2) (Karakaş et al. 2019; yin et al. 2020). There are limited options for specific and effective therapy against TNBC due to the absence of validated biomarkers. So, chemotherapy is generally considered as the standard TNBC treatment, however prognosis remains poor (Yao et al. 2017; Le et al. 2022; Mock et al. 2015). Considering this, developing new anticancer molecules with increased potency and high specificity is essential.

In several kinds of human cancer, an aberration in the PI3K-AKT-mTOR signaling pathway promotes development of tumor (Testa and Bellacosa 2001). AKT, also referred as protein kinase B (PKB), belongs to a serine-threonine kinase family and is essential for the smooth functioning of this pathway. Among the three AKT isomers, AKT2 is closely associated with cancer cell metabolism, metastasis, proliferation, angiogenesis, and drug resistance (Rychahou et al. 2008; Liu et al. 2020). Elevated AKT2 expression is frequently detected in various human tumors, including breast, lung, pancreatic, colorectal, prostate, and ovarian. Overexpression of AKT2 is correlated with cancer aggressiveness and poor survival rates (Rychahou et al. 2008; Riggio et al. 2017; Bellacosa et al. 1995). Inhibition of AKT2 in breast cancer effectively reduces the colony formation abilities and invasion of non-cancer stem cells and Cancer Stem Cells (Gener et al. 2019). All these vital PI3K-AKT-mTOR signalling function, makes AKT2 signaling molecule a promising target for cancer therapy.

Naphthoquinone-like structures have been approved by FDA and are used in various cancer chemotherapy (Figure 1). Mitomycin (a benzoquinone) is used to treat bladder and anal cancer (Milla et al. 2014; Vinayan et al. 2016). Anthraquinones, such as Doxorubicin, daunorubicin, idarubicin, mitoxantrone, and epirubicin, are commonly used to treat various solid and hematologic cancers (Hortobagyi, 1997). Thus, these molecules continue to attract in developing new drugs for cancer therapy.
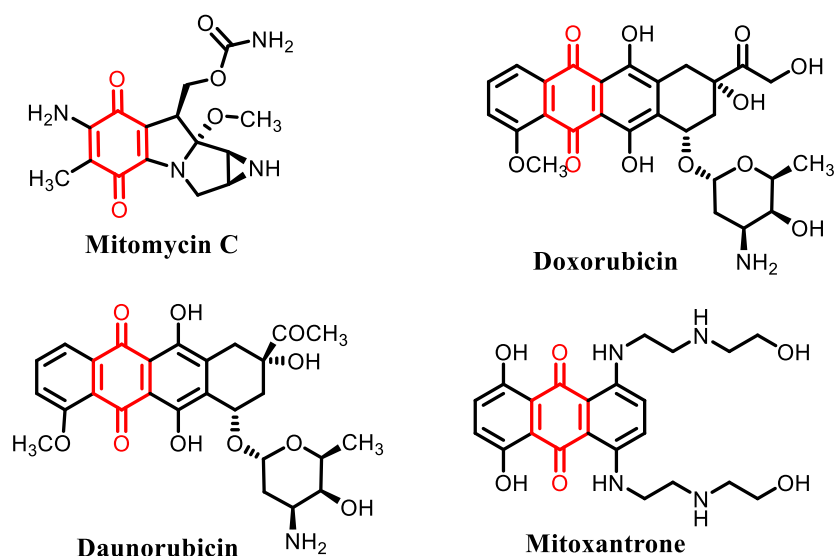
Figure 1. Structure of anticancer drugs with quinone moiety (adapted from Vinayan et al. 2016; Hortobagyi, 1997)

The primary mechanism of the naphthoquinones is suggested to be Reactive oxygen species (ROS) formation in the cell. Cancer cells often have a higher concentration of ROS than normal cells because of the higher metabolic demands; producing even higher amounts of ROS by naphthoquinones in cells can lead to cell death (Wellington 2015; Kumagai et al. 1997). Also, the pyrano-naphthoquinone molecules like lactoquinomycin, frenolicin B, and kalafungin were found to have selective inhibition towards the serine-threonine kinase AKT (Salaski et al. 2009). Therefore, the dual-action molecule with the ability to produce ROS and inhibit the AKT2 signaling pathway would result in potent anticancer drug with higher specificity and low resistance.

In present study, anticancer activity of the isolated compounds was demonstrated. With the potent activity, Enceleamycin A was considered for the ROS formation ability and apoptosis assay in the MDA-MB-231 cells. Moreover, Enceleamycin A displayed binding affinity to the serine-threonine kinase AKT2, determined by the molecular docking and molecular dynamic (MD) simulation, which was further validated *in vitro*. The molecule's physicochemical and pharmacokinetic characteristics were examined *in silico*, and its hemolytic effect was also established. The findings from our research can stimulate interest in exploring the microbial naphthoquinones as potential anticancer medication by targeting AKT2 kinase signalling pathway.

2. Materials and method

2.1 Materials

Heat-inactivated FBS (Fetal bovine serum) and DMEM (Dulbecco's modified eagle's medium) were obtained from GIBCO. 3-(4,5-Dimethylthiazol-2-yl)-2,5-diphenyl tetrazolium bromide (MTT), and Trypsin EDTA were purchased from Hi-media. Standard Doxorubicin and H_2-DCFDA dye was purchased from Sigma. MDA-MB-231, A549, HeLa, HFF and Vero cells were procured from NCCS (National Center for Cell Science), Pune.

2.2 Cell viability assay

The MTT assay, which measures cellular metabolic activity, was used to examine cell viability (Mosmann 1983). The cell lines used for the study were MDA-MB-231, A549, HeLa, HFF and Vero. DMEM with 10% FBS was the media used for the growth and assay of all the cells. The seeding of 10,000 cells/well was done of these cells in 96-well plate and incubated at 37º C with 5% CO_2 for 20 hours. Stock solution of 20 mg/ml was made of compounds Enceleamycin A, B, C and *N*-hydroxy pyrazinone acid in Dimethyl sulfoxide (HiMedia). Stock solution of compounds were diluted to 1 mg/ml in complete medium (DMEM + 10% FBS) and was again diluted to 100 µg/ml and 10 µg/ml working solution in DMEM media. The final DMSO concentration at the highest concentration tested at 100 µg/ml was 0.5% i.e. below toxicity level and was used as a negative control. The stock solution of 20 mg/mL of the standard drug doxorubicin was made in MQ water, filter sterilized and further diluted to working solution in complete media. The adhered cells were treated with various concentration of compounds in range of 0.1 to 100 µg/mL for 48 hours. 100 µL of MTT solution (0.5 mg/mL) was added after media was removed, and solution was incubated for 4h at 37 °C in dark. Subsequently, the MTT solution was decanted, and the solubilization of formazan crystals was done by adding 100 µl DMSO. Biotek synergy H1 microplate reader was used to capture the reading at 570 nm. In addition, inhibition of MDA-MB-231 cells was examined for Enceleamycin A at 4, 24, and 48h for the time point study.

2.3 Anti-migration Assay

To estimate the anti-migration impact of Enceleamycin A on MDA-MB-231 cells, a scratch assay was conducted (Justus et al. 2014; Luo et al. 2020). In a 24-well plate, 1.5×10^5 cells/well were seeded in DMEM (10% FBS). After the confluency, linear gaps were

scratched at the bottom of the plate by a sterile micropipette tip (200 μL), and detached cells were subsequently eliminated by 1X phosphate buffer saline (PBS). The adherent cells were incubated with Enceleamycin A (0.5, 1, and 2 μg/ml) in serum-free DMEM media for 24 hours at 37° C with 5% CO_2 to eliminate interference of cell proliferation. The wound images were obtained using an inverted microscope at 0 and 24 h, respectively, and the % of cell migration was calculated with reference to scratch width (SW) at 0 h and 24 h : (SW at 0 h – SW at 24 h/SW at 0 h) × 100.

2.4 Measurement of intracellular ROS

The intracellular level of ROS production was assessed by 2′,7′-dichlorofluorescein diacetate (H2-DCFDA) dye (Ng and Ooi 2021). In brief, seeding 1×10^4 cells/well of MDA-MB-231 cells was done in 96-well plate and kept for 24 hours. After being washed with DPBS, cells were incubated at $37\,°C$ in dark for $30\,minutes$ with H2-DCFDA ($20\,μM$) in DMEM complete media. The culture was treated with a varying concentration of Enceleamycin A (2, 10, 20, and 50 μg/mL) in DMEM complete media for 24 and 48 h. After incubation, RFU was measured at 485/535 (Excitation/Emission) in a micro-plate reader.

2.5 Apoptosis detection in MDA-MB-231 cell line

The apoptotic-like features in MDA-MB-231 cells after treatment with Enceleamycin A were estimated by Alexa Fluor® 488 Annexin V/Dead Cell Apoptosis Kit (ThermoFisher Scientific) (Worsley et al. 2022). In brief, seeding of 3.5×10^5 cells/well of MDA-MB-231 cells was done in a 6-well plate and enable to grow overnight. The culture was treated with Enceleamycin A (2, 4, and 8 μg/mL) for 48 h. After being washed with binding buffer (1X), the cells were stained for 30 min by Alexa Flour Annexin V and Propidium iodide at 37 °C in dark. Stained cells were assessed for percentage of apoptotic cells relative to the untreated and unstained cells by flow cytometry.

2.6 Docking analysis

Canonical Smiles of the novel ligand, Enceleamycin A, were converted to protein data bank format using Open Babel software. The 3-dimensional structure of the PI3K-AKT-mTOR pathway receptors was obtained from Protein Data Bank. Native ligands, water molecules, and other heteroatoms from protein were removed using PyMOL (v.1.74) before docking. Molecular docking was performed using Autodock 4.2.6 (Azam and Abbasi 2013; Morris et al. 2009). The final DLG file contained important details, viz., top ten conformations for

every run consisting of rank, free binding energy (Kcal/mol), mean RMSD, and inhibitory constant (µM). The docking parameter was analyzed based on the lowest binding energy of the ligand-protein complex. Autodock tools 4.2.6, Discover Studio v20.1.0.19295 from Biovia, and PyMOL v.1.74 were used in molecular docking to visualize and study the two-dimensional, three-dimensional and surface annotation of Enceleamycin A interaction with the protein (Umar et al. 2022; Gao and Huang 2011). The docked complex was validated by redocking of AKT2 with native ligand, and the RMSD value was calculated from the DockRMSD (Bell and Zhang 2019) and LS-align web tool (Hu et al. 2018).

2.7 Molecular dynamics simulations

MD simulation of the docking complex was carried out with reading biomolecular coordinates, solvation of desired protein, setting periodic boundary conditions, and generating the input files for equilibration and production using the Gromacs v 2020.6 and visualization and analysis using VMD v 1.9.3 and PyMOL v 1.7.4.5 software. The novel ligand bound to the AKT2 receptor was analyzed using the GROMOS 54A7 force field of the GROMACS simulation software. With the help of MODELLER9 v 14, (Webb and Sali 2016) the missing residues from the crystal structure's 1O6L (Ile450, Thr451, Pro452, Pro453, Asp454, Arg455, Tyr456, Asp457, Ser458, Leu459, Gly460, Leu461, Leu462, Glu463, Leu464, Asp464, Gln464, Arg464, Glu465, Glu466) were put back together. By using the Automated Topology Builder (ATB) repository, force fields of ligand were created (Malde et al. 2011). Hydrogen was added to heavy atoms using the GROMACS module pdb2gmx. The structure were then solvated within cubic periodic box by water stretching 2 Å on all sides outside protein by applying the simple point charge (SPCE) water model (Clifford and Wight 1976). After that, system was maintained with a suitable 0.15 M salt concentration by introducing sufficient concentration of Na^+ and Cl^- ions to the system for neutralization. The steepest descent method was subsequently employed to minimize the energy of all systems in the solvated state over a time frame of 2000 steps.

To carry out equilibrium in NVT (No. of atoms, Volume, and Temperature) ensemble, system was then heated gradually to temperature of 310 K by a V-rescale thermostat having 0.1 ps coupling constant (Gangadharappa et al. 2020). Further to achieve equilibration in the NPT (No. of atoms, pressure, and temperature) ensemble, the Parrinello-Rahman barostat was implemented to maintain solvent density at 1 bar and 310 K having 0.1 ps coupling constant. To check the stability of protein and ligand complex, each structure generated from

equilibration phase of NPT was utilized for final NPT ensemble production run for 100 ns simulation (Chandan et al. 2022).

Molecular mechanics Poisson–Boltzmann surface area (MM-PBSA), is an approach for determining binding free energy of protein–ligand complexes. MM-PBSA technique was employed via g_mmpbsa (Kumari et al. 2014) tool. For the evaluation of stability of the simulated systems, trajectories produced after simulations were analysed to determine RMSD for backbone atom, Root mean square fluctuation (RMSF) for C-alpha, Radius of gyration (Rg) and interacting hydrogen bonds.

2.8 ADP-Glo Kinase Assay

AKT2 kinase activity was measured in presence of Enceleamycin A by employing ADP-Glo kinase assay and the AKT2 Kinase enzyme system (Promega). The assay is based on quantifying ADP produced during the kinase reaction. The reaction was done in 96-well plates in which 10 µL of AKT2 (10 ng), 5 µL of Modified AKT substrate (1µg), 5 µL of ATP (50 µM), and 5 µL of inhibitor was added followed by an hour-long incubation at ambient temperature. To terminate the kinase reaction, 5 µL of the ADP-Glo reagent was applied for 40 min. At last, 10 µL of kinase detection reagent was added and left for 30 min. Biotek synergy H1 microplate reader detected the luminescence. The relative activity (%) of kinase was calculated compared to control without an inhibitor (Zegzouti et al. 2009).

2.9 Physicochemical and Pharmacokinetics Analysis

In silico physicochemical and pharmacokinetic properties were detected for Enceleamycins using the SwissADME online program (Daina and Zoete 2017). The SMILES notations generated from ChemDraw 20.0 was submitted as an input file to the SwissADME web tool, which provides a reliable prediction of physicochemical (TPSA, number of hydrogen bond acceptor and donor, and Solubility), pharmacokinetics (GI absorption, BBB permeability, and CYP inhibitor) and drug-likeness (Lipinski's rule of five and Veber's rule) properties. In addition, toxicity profile, like the Ames test, skin sensitivity, and hepatotoxicity, was generated by the pkCSM web tool (Pires et al. 2015).

2.10 Hemolysis assay

Hemolytic activity of Enceleamycin A was performed on the RBCs of human blood sample. The blood sample of 5 ml was decanted after being centrifuged at 5000 rpm for 10 min. RBCs were suspended in Phosphate buffer saline (PBS), then washed three times by

centrifugation for 10 min at 5000 rpm, and the pelleted RBCs were resuspended in 25 ml of PBS. The compound was twofold diluted in PBS and mixed with RBCs suspension to achieve concentrations varying from 1 to 512 µg/mL. Triton X-100 (1% v/v) and DMSO (0.5%) in PBS were considered positive and negative controls, respectively. The treated suspensions were kept for 60 min at 37 °C and centrifuged at 5000 rpm for 10 minutes. The resultant supernatant was added to 96-well plate with a flat bottom. At 570 nm, absorbance was measured, and relative percent of hemolysis was estimated compared to suspension treated with 1% Triton X-100. The following equation calculates the percent of hemolysis: % hemolysis = [absorbance of the sample (treated with Enceleamycin A)] ÷ [absorbance of the positive control (treated with 1% Triton X-100)] × 100 (Ali et al. 2014; Sæbø et al. 2023).

3. Results and discussion

3.1 Cell Viability Assay

Previous studies have shown that naphthoquinones exhibit anticancer effects on different types of cancer (Inagaki et al. 2015; Rahman et al. 2022; Leyva et al. 2017). In order to investigate anticancer activity of furo-naphthoquinones, the cytotoxicity of Enceleamycins along with N-hydroxy pyrazinone was evaluated against triple-negative breast cancer cells (MDA-MB-231), cervical cancer cells (HeLa), lung cancer cells (A549), HFF cells (non-cancer human Foreskin Fibroblasts) and Vero (non-cancer monkey kidney epithelial cells) by the MTT assay (Mosmann 1983).

The results indicated that Enceleamycin A has potential activity towards the MDA-MB-231 (TNBC cells) with an EC_{50} value of 1.25 µg/mL (3.78 µM), followed by HeLa and A549 cells with an EC_{50} value of 1.51 (4.57 µM), and 1.98 µg/mL (5.99 µM), respectively. The EC_{50} value of Enceleamycin A was better than the standard anticancer drug doxorubicin in all the cell lines tested. Furthermore, Enceleamycin A displayed better inhibitory activity towards the cancer cells compared to the non-cancer HFF cells with selectivity index (SI) in the range of 2.0 to 3.17. The selectivity index of Enceleamycin A against cancer cells with respect to non-cancer Vero cells was in range of 2.35 to 3.73 (Figure 2 and Table 1). Enceleamycin A exhibited strong anticancer activity, followed by Enceleamycin C, whereas Enceleamycin B and N-hydroxy pyrazinone acid showed moderate activity. The potential bioactivity of Enceleamycin A and C may be due to the presence of double bond in the second naphthalene ring, which acts as an electron acceptor and results in formation of semiquinone or hydroquinone. The subsequent reduction of Enceleamycin A and C may

result in ROS formation and thereby leading to cell death (Wellington et al. 2015; Kumagai et al. 1997).

Table 1. The viability of cancer and non-cancer cells in presence of Enceleamycin A, B, C, *N*-hydroxypyrazinone acid and doxorubicin by MTT method and their selectivity index (SI) with respect to non-cancer cells.

	HFF	Vero	MDA-MB-231			A549			HeLa		
	CC_{50} [a]	CC_{50} [a]	EC_{50} [b]	SI [c]	SI [d]	EC_{50} [b]	SI [c]	SI [d]	EC_{50} [b]	SI [c]	SI [d]
A	3.97 ±0.41	4.66 ±0.66	1.25 ±0.31	3.1	3.7	1.98 ±0.27	2.0	2.3	1.51 ±0.14	2.6	3.0
B	70.95 ±6.85	27.05 ±5.8	23.49 ±3.13	3.0	1.1	46.68 ±3.29	1.5	0.5	30.53 ±3.84	2.3	0.8
C	7.60 ±0.7	6.93 ±0.34	2.59 ±0.26	2.9	2.6	3.51 ±0.35	2.1	1.9	7.27 ±1.8	1.0	0.9
D	91.30 ±10.33	64.97 ±7.15	44.77 ±5.1	2.0	1.4	97.69 ±8.85	0.9	0.6	60.67 ±7.85	1.5	1.0
Std	8.96 ±0.57	2.96 ±0.54	3.28 ±0.59	2.7	0.9	2.68 ±0.87	2.8	1.1	1.69 ±0.27	4.4	1.7

A, B, C : Enceleamycin A, B, C; D : *N*-hydroxy pyrazinone acid; Std. : Doxorubicin

[a] CC_{50} is the concentration that achieved 50% cytotoxicity;

[b] EC_{50} is effective concentration that achieved 50% inhibition

[c] SI is the selectivity index for the cancer cells with respect to the non-cancer HFF cells

[d] SI is the selectivity index for the cancer cells with respect to the non-cancer Vero cells

With the selectivity and maximum activity of Enceleamycin A against the MDA-MB-231 cells, the dose-response viability at 4h, 24h, and 48h was determined as shown in Figure 3. Interestingly, the MDA-MB-231 cell growth was inhibited within 4 hours of treatment by Enceleamycin A with an EC_{50} value of 7.7 μg/mL. The difference in inhibition after 24 and 48 h of treatment was not much at lower concentrations upto 2 μg/mL; however, at 4 μg/mL and above, maximum inhibition was observed at 48 hours of treatment.
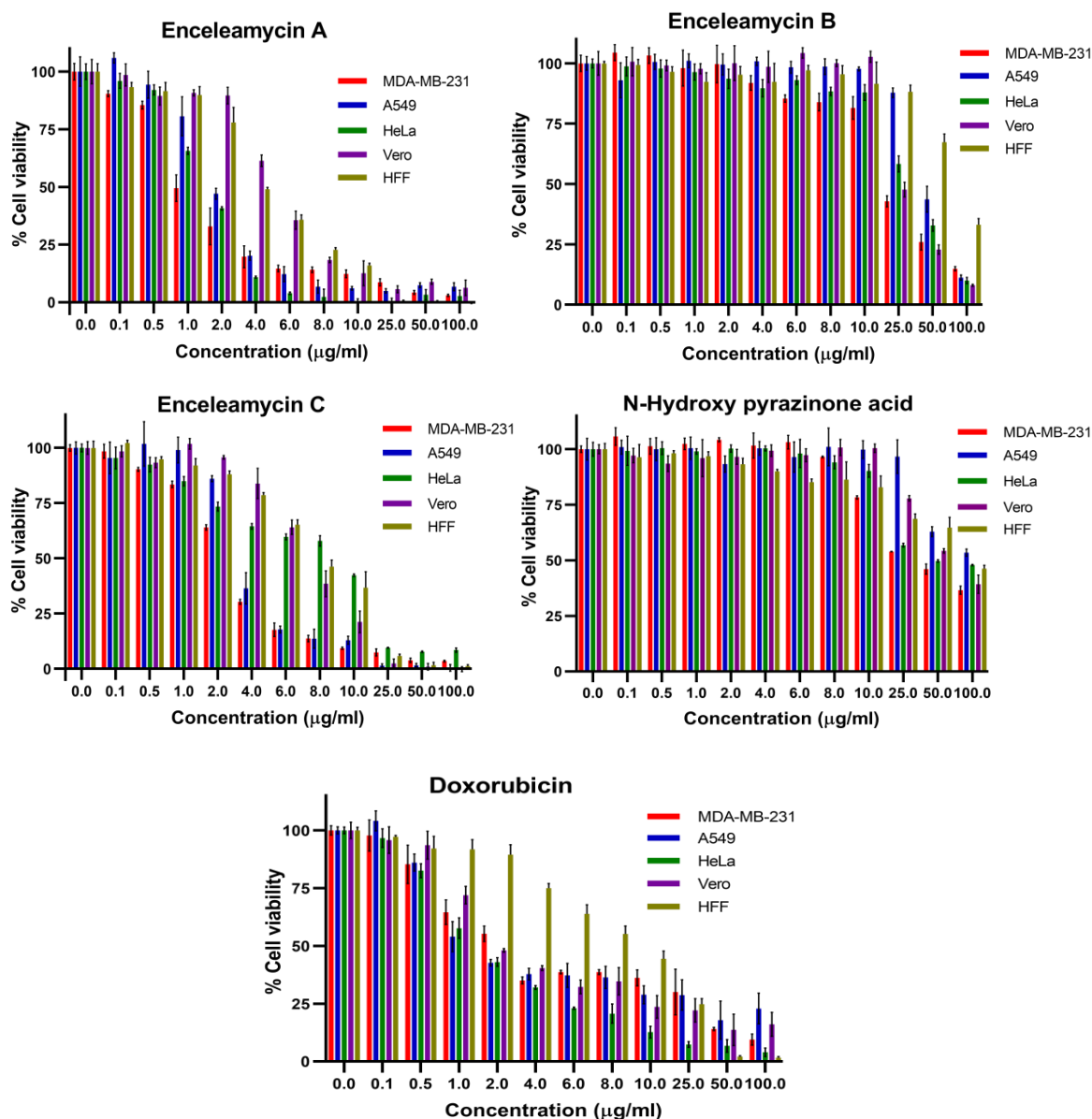
Figure 2. Dose-dependent viability of cancer cells (MDA-MB-231, A549 and HeLa) and non-cancer (Vero and HFF) cells in presence of Enceleamycin A-C, N-hydroxy pyrazinone acid and doxorubicin at concentrations varying from 0.1 to 100 µg/ml.
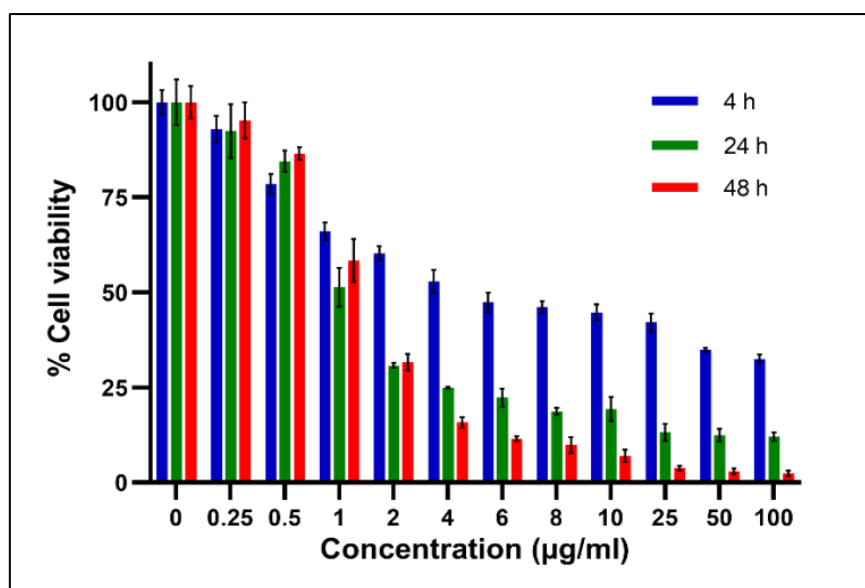
Figure 3. Cell viability of MDA-MB-231 cells at 4, 24 and 48 h treatment with Enceleamycin A

Enceleamycin A was isolated in reasonable quantity compared to other compounds and was further used for the *in vitro* anticancer activity by Anticancer Drug screening facility (ACDSF) at ACTREC, Navi Mumbai, India. The anticancer activity was performed by the Sulforhodamine B (SRB) assay at one dose of 10 μg/ml against nine human cancer cell lines originating from breast, liver, colon, oral, cervical, lung, prostate, ovarian, and leukemia (Figure 4). The data analysis (Table 2) was based on growth percent (GP), where a lower GP value displays a higher growth inhibition percentage (GI%) calculated as (GI% =100-GP). The GP value in negative corresponds to lethal activity, whereas the increased negative value corresponds to the higher activity of the tested compound.

Enceleamycin A displayed lethal activity to all tested cancer cell lines and showed maximum cytotoxicity towards breast cancer cells with GP value of -90.6, followed by lung cancer. Similar to the results of MTT assay, Enceleamycin A showed better lethal activity than the anticancer drug adriamycin against most cancer cell lines tested. Furthermore, we selected Enceleamycin A for the evaluation of the probable mode of action against MDA-MB-231 cells and its drug-likeness because of its specific potent activity towards the MDA-MB-231 cells, high yield compared to Enceleamycin C, (Khan et al. 2022) and lack of treatment options for TNBC cells (Yin et al. 2020; Yao et al. 2017).
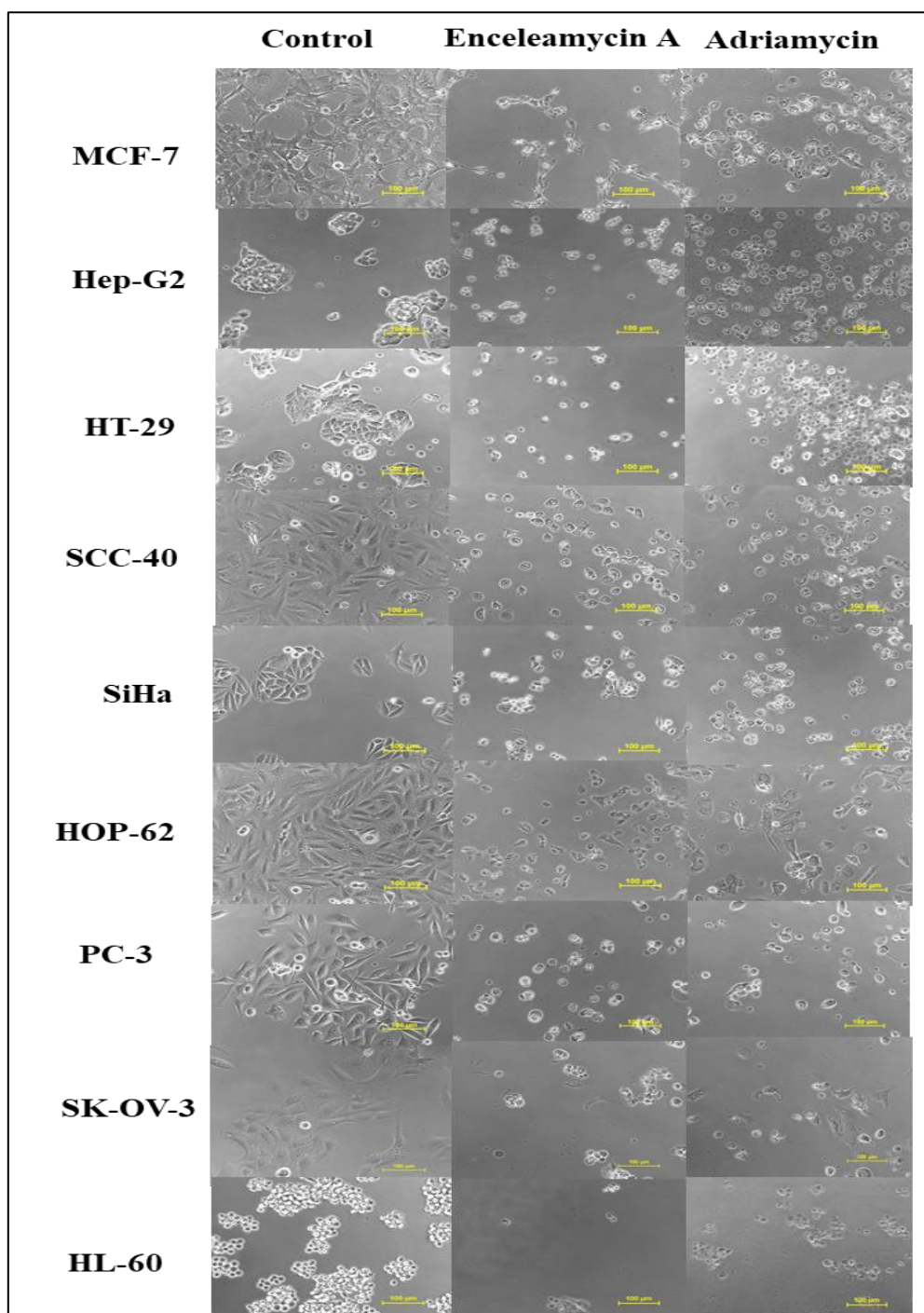
Figure 4. Morphological change in various cancer cell lines after treatment with Enceleamycin A and Adriamycin at 10 μg/ml.

Table 2. The percentage growth inhibition (%GI) or lethality of Enceleamycin A and Adriamycin against cancer cell line at 10 µg/ml

Human cancer type	Cell line name	Enceleamycin A	Adriamycin
Breast	MCF-7	-90.6	-81.3
Liver	Hep-G2	-64.6	-39.1
Colon	HT-29	-32.0	97.1 [a]
Oral	SCC-40	-32.5	-73.7
Cervical	SiHa	-31.2	-59.4
Lung	Hop-62	-85.5	98.9 [a]
Prostate	PC-3	-76.4	-25.3
Ovarian	SK-OV-3	-78.7	-25.5
Leukemia	HL-60	-36.7	-9.3

[a] Percentage growth inhibition (%GI) = 100 - GP (Growth percentage). [b] Negative values correspond to the lethality of respective cancer cell line.

3.2 Anti-migration Assay

Cell migration is crucial during the whole process of cancer development. Cancer cells have the ability to migrate, which is essential to invade surrounding tissues and cause tumor metastasis. The study of cell migration inhibition is appealing as metastatic progression is considered the major cause of death in cancer patients (Justus et al. 2014). To examine the inhibitory impact of Enceleamycin A on MDA-MB-231 cell migration, an *in vitro* anti-migration assay was conducted by a scratch/wound healing assay (Luo et al. 2020). The images of cell migration (Figure 5A) were recorded in Olympus CKX53 inverted microscope at 0 and 24 hours of treatment and the migration of cells was measured in micrometers using MagVision software. The rate of relative migration for MDA-MB-231 cells treated with Enceleamycin A was 45.25%, 43.01%, 25.55%, and 6.99% at 0 µg/mL, 0.5 µg/mL, 1.0 µg/mL and 2.0 µg/mL respectively. The migration ability of MDA-MB-231 cells was significantly inhibited with 1.0 and 2.0 µg/mL concentrations of Enceleamycin A (Figure

5B). These results demonstrated that Enceleamycin A suppresses the MDA-MB-231 cell's ability to migrate in a concentration-dependent manner.
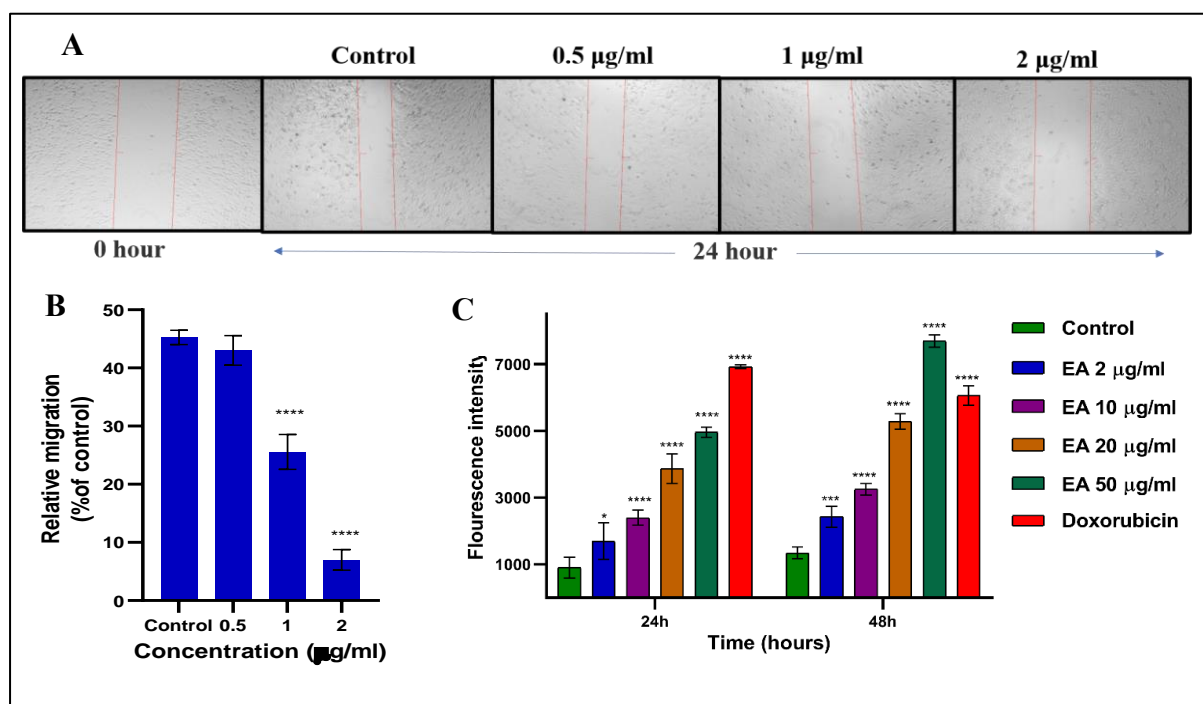
Figure 5. Enceleamycin A effect on the migration and ROS formation ability in MDA-MB-231 cells (**A**) Migration of MDA-MB-231 cells in presence of Enceleamycin A at 0, 0.5, 1 and 2 μg/mL after 24 hours (**B**) Statistical data analyses for MDA-MB-231 cells mobility in presence of Enceleamycin A at 0 (control), 0.5, 1 and 2 μg/mL after 24 hours. One-way ANOVA Dunnett test was used to determine statistical significance; ****$p < 0.0001$ (**C**) Statistical data analyses of ROS formation by MDA-MB-231 cells after treatment with Enceleamycin A (EA) at 24 and 48 hours. Two-way ANOVA Dunnett test was used to determine statistical significance; *$p < 0.05$, **$p < 0.01$, ***$p < 0.001$, ****$p < 0.0001$

3.3 Measurements of intracellular reactive oxygen species (ROS)

Since naphthoquinones are known for producing intracellular ROS, we quantified the ROS production after treatment with Enceleamycin A by 2′,7′-dichlorofluorescein diacetate (H2-DCFDA). The ROS at lower concentration plays a vital role in the homeostasis of cells; however, when in excess, it leads to the death of cells through apoptosis (Sun et al. 2014; Redza-Dutordoir and Averill-Bates 2016). In the ROS assay, the MDA-MB-231 cells in

presence of Enceleamycin A demonstrated a relative increase in fluorescence intensity at 24 and 48 hours as the concentration was raised from 2 to 50 µg/ml compared to the untreated control. The graph (Figure 5C) displayed MDA-MB-231 cells after treatment with Enceleamycin A resulted in concentration and time-dependent increase in intracellular levels of ROS. It is known that excessive ROS formation within the cell can induce apoptosis and results in cell death.

3.4 Apoptosis detection in MDA-MB-231 cells

To examine whether the ROS production by Enceleamycin A in MDA-MB-231 cells results in apoptotic cell death, we perform the apoptosis assay using flow cytometry. The apoptotic analysis in cancer cells is based on the movement of phosphatidylserine from inner membrane to outer membrane, which eventually recognizes by Annexin V. The scatter plot (Figure 6A) for control and treated cells was demonstrated with four distinct populations of unstained for viable cells, Annexin V-Alexa flour for early apoptotic cells, and for late apoptotic cells dual stained with Annexin V/Propidium iodide (Worsley et al. 2022). The early/late apoptosis ratio was 25.8%/2.45%, 49.7%/10.7%, 58.4%/14.85, and 60.65%/ 19.2% at the concentration 0, 2, 4, and 8 µg/mL respectively, after 48 hours of treatment with Enceleamycin A (Figure 6B). These observations demonstrated the concentration-dependent apoptosis in the MDA-MB-231 cells by Enceleamycin A.

3.5 Molecular Docking

The inhibitory activity of the novel ligand Enceleamycin A against the intended protein target of the PI3K-AKT-mTOR pathway was examined using molecular docking. The protein target considered for molecular docking were PI3Kα (4TV3), AKT1 (3O96), AKT2 (1O6L), mTOR (1E7U), and S6K1 (3A62). The top rank from the cluster of a receptor with the lowest binding energy and 0 RMSD was considered appropriate for visualizing the interactions between the protein and ligand complex. The details of the best molecular fit conformations were displayed by Autodock 4.2.6 (Azam and Abbasi 2013) and the best molecular fit pose was visualized by Biovia discovery studio v20.1.0.19295 (Umar et al. 2022).
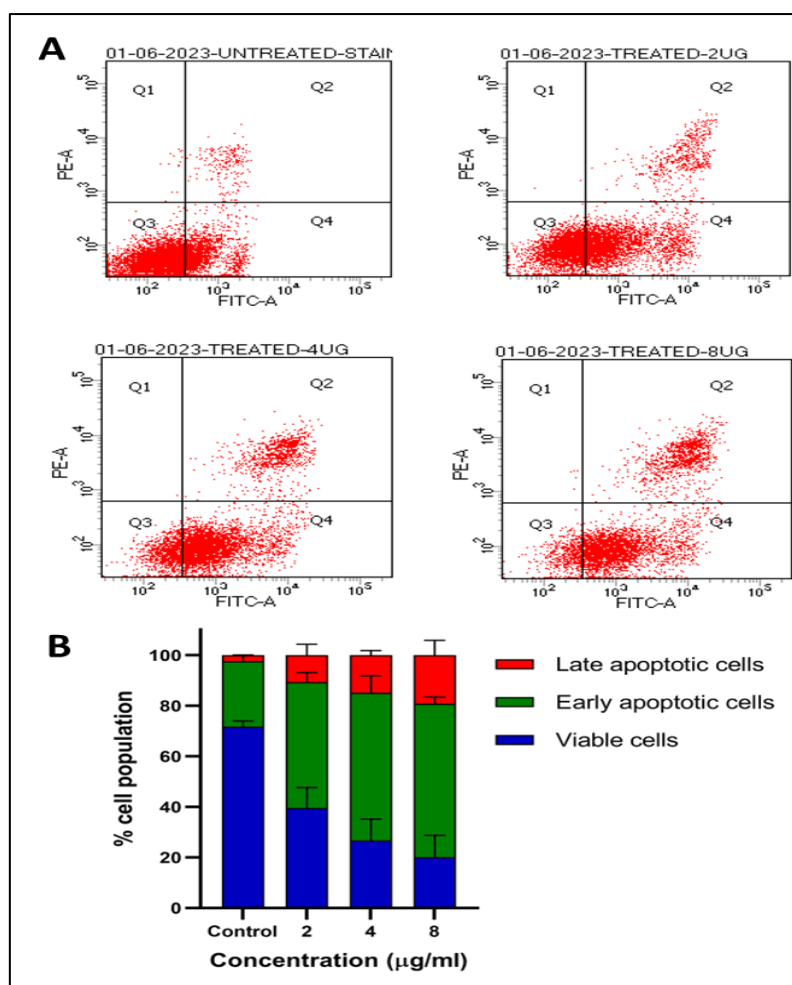
Figure 6. Apoptosis detection in MDA-MB-231 cells in presence of Enceleamycin A. (**A**) Enceleamycin A effect on apoptosis of MDA-MB-231 cells using Annexin V-Alexa flour-488 and PI staining. The cell stages were given as viable-Q3, early apoptotic-Q4 and late apoptotic-Q2 (**B**) Percentage of viable, early and late apoptotic cells in the population based on Flow cytometry data analysis.

Enceleamycin A displayed better binding affinity with AKT2 compared to the other proteins of PI3K-AKT pathway shown in Table 3 and Figure 7. The binding energy calculated was -7.14 Kcal/mol for the docked complex. The non-bond interactions gave us information about active sites, the nature of bonding, the distance between the native ligand and the protein, and the donor and acceptor atoms. The active sites of the interacting Enceleamycin A and AKT2 displayed in Figure 7C and Table 4, were Lys 181, Glu 200, Gly 295, Asp 293, Glu 193, Phe 163, Leu 183, Lys 191, which signifies that the novel ligand is interacting with the A polypeptide chain of AKT2 protein. The interaction distance of active site Lys 181 and Glu 200 was of 2.2 and 2.0 Å, respectively (Figure 8D) by conventional

hydrogen bonding. The other interactions include the carbon hydrogen bond for Gly 295 and Asp 293, electrostatic pi-anion for Glu 193, hydrophobic pi-pi stacked for Phe 163, hydrophobic alkyl for Leu 183 and hydrophobic pi-alkyl for Lys 191. Figure 7E and Table 4 displays the H-bond donor and acceptor details of interacting complex of Enceleamycin A and AKT2 in which Lys 181 acts as a H-bond donor and Glu 200 as an H-bond acceptor.

Table 3. Binding affinity of Enceleamycin A with proteins associated with PI3K-AKT-mTOR pathway using molecular docking

Receptor PDB ID	Receptor Name	Binding affinity (Kcal/mol)
4TV3	PI3Kα	-6.87
3O96	AKT1	-6.58
1O6L	AKT2	**-7.14**
1E7U	mTOR	-6.65
3A62	S6K1	-6.34

Binding Energy = - 7.14 Kcal/mol

Ligand Efficiency = - 0.3

Inhibitory constant = 5830nM

Intermolar energy = - 7.74 Kcal/mol

Vander Waal and desolvation energy = - 7.32 Kcal/mol

Electrostatic energy = - 0.42 Kcal/mol

Total internal energy = 0.46 Kcal/mol

Torsional energy = 0.6 Kcal/mol

Figure 7. Conformation of the best molecular fit of Enceleamycin A and AKT2 (PDB ID1O6L)
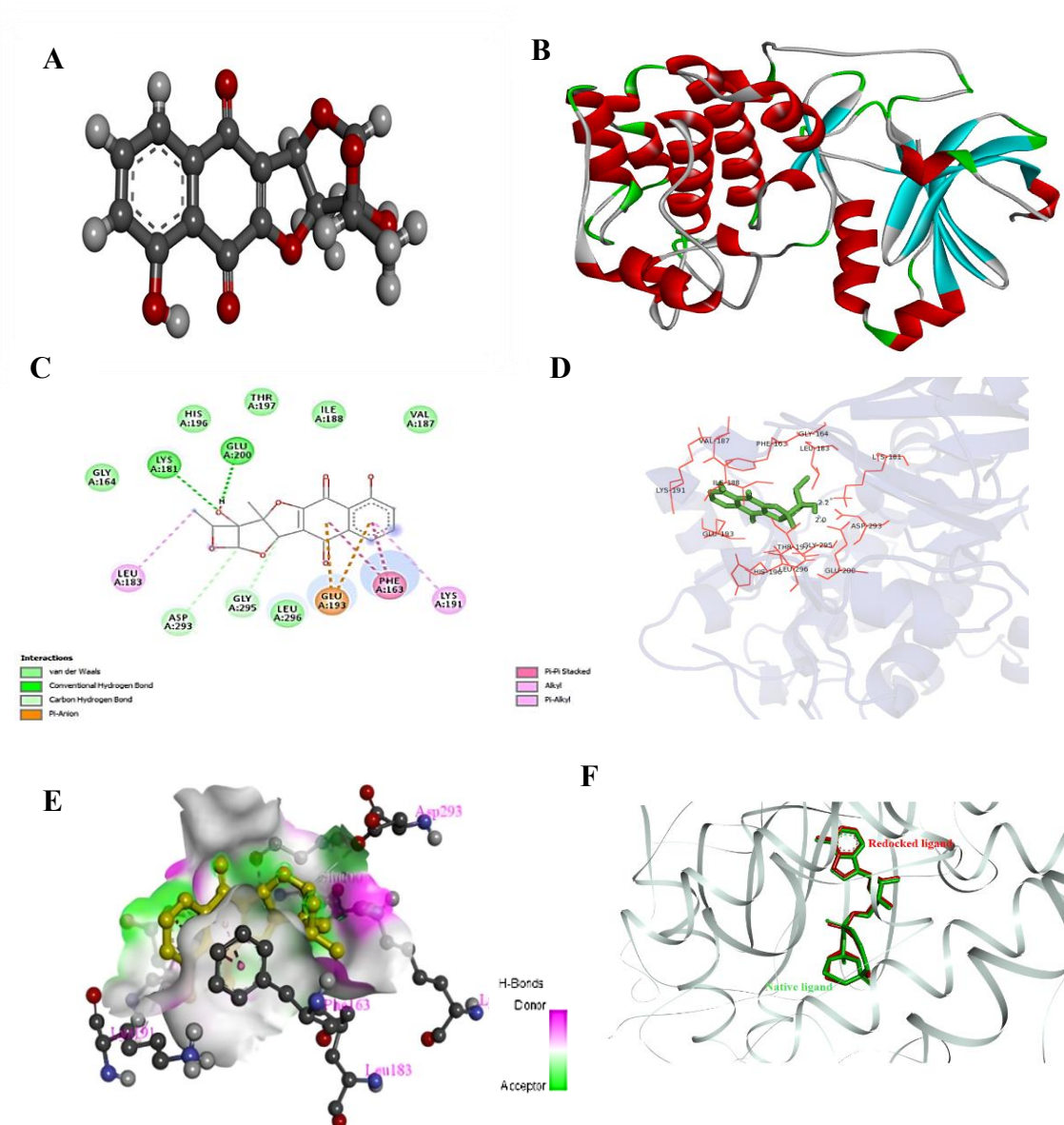
Figure 8. Molecular docking of Enceleamycin A with AKT2 protein and docking validation (**A**) Enceleamycin A in protein databank (pdb) format where red indicates oxygen atom, light grey represents hydrogen atom and dark grey represents carbon atom, (**B**) AKT2 (1O6L) receptor, where α-helices are denoted in red, β-sheets in yellow, and turns & loops in green. (**C**) Two-dimensional diagram of the docked complex (AKT2 and Enceleamycin A) showing the active sites and the type of interactions (**D**) Three-dimensional diagram displaying the interaction of active site Lys 181 and Glu 200 with distance of 2.2 and 2.0 Å, respectively (**E**) Three-dimensional diagram with H-bond display of the interacting complex, where the pink shade represent H-bond donor and green shade represents H-bond acceptor (**F**) Docking validation of native ligand AMP-PNP to AKT2 (1O6L) and displaying the super-imposition of the redocked native ligand protein complex.

Table 4. Non-bond interactions between AKT2 protein and Enceleamycin A (EA)

Name	Distance (Å)	Category	Types	From (Donor)	To (Acceptor)
LYS A: 181: HZ1 - EA: O	2.20784	Hydrogen Bond	Conventional Hydrogen Bond	LYS A:181: HZ1	EA: O
EA: H - GLU A: 200: OE1	2.04415	Hydrogen Bond	Conventional Hydrogen Bond	EA: H	GLU A: 200: OE1
EA: C – GLY A: 295: O	3.41985	Hydrogen Bond	Carbon Hydrogen Bond	EA: C	GLY A: 295: O
EA: C – ASP A: 293: OD1	3.69348	Hydrogen Bond	Carbon Hydrogen Bond	EA: C	ASP A: 293: OD1
GLU A: 193: OE1 - EA	4.00257	Electrostatic	Pi-Anion	GLU A: 193: OE1	EA
PHE A: 163 - EA	3.61776	Hydrophobic	Pi-Pi Stacked	PHE A: 163	EA
EA:C – LEU A: 183	4.55503	Hydrophobic	Alkyl	EA: C	LEU A: 183
EA – LYS A: 191	5.27434	Hydrophobic	Pi-Alkyl	EA	LYS A: 191

To further validate the docking method, the AKT2 (1O6L) protein was re-docked with the native ligand AMP-PNP (Phosphoaminophosphonic Acid-Adenylate Ester). Both re-docked, and native ligands interacted with the protein AKT2 with significant overlap and resemblance (Figure 8F). The RMSD (root mean square deviation) value of the interactions was computed by the DockRMSD and found to be 1.262 Å, considered a reliable docking procedure since the value was <2.0 Å (Bell and Zhang 2019). The RMSD value calculated for the superimposed ligand conformation using LS-align was 0.684 Å, which is <1 Å denotes strongly aligned atom pairs (Hu et al. 2018).

3.6 Molecular dynamics (MD) simulation analysis

Molecular dynamics (MD) is commonly used computational simulation technique for predicting mode of interactions in drug development. It is extensively used to investigate how the molecules shift their form and interact with species of other molecules in variety of environment (De Vivo et al. 2016). To confirm the structural stability of docked complex of Enceleamycin A and AKT2, MD simulations were run for 100 ns using GROMACS package.

Molecular mechanics Poisson–Boltzmann surface area (MM-PBSA), technique displays the binding energy of -10.481 ± 3.398 Kcal/mol during the run of 100 ns demonstrating the potential affinity between the Enceleamycin A and AKT2.
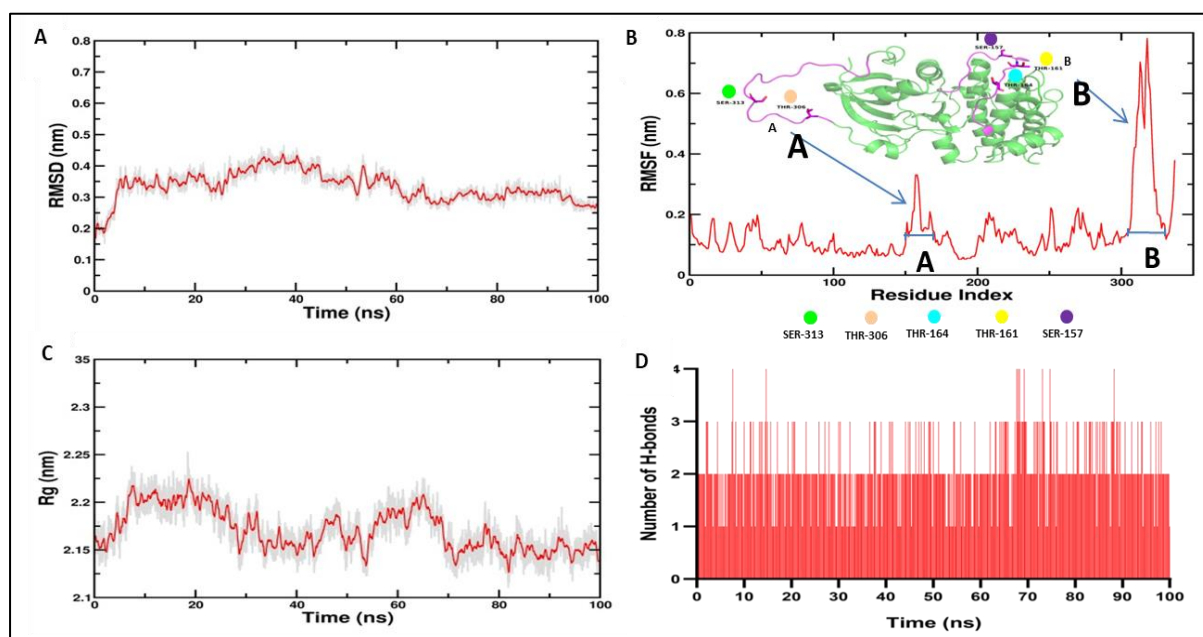
Figure 9. Plots displaying the MD simulation data of simulated complex (Enceleamycin A with AKT2 protein) for the 100 ns simulation (**A**) Plot displaying the RMSD values of simulated complex for 100 ns (**B**) Plot displaying the RMSF value of simulated complex for 100 ns where labeling in the residue index region ranging from 150-170 and 305-325 correlates with the designated A and B loop in pink colour. These loops contain serine and threonine residues responsible for phosphorylation that shows the higher fluctuation (**C**) Plot displaying the radius of gyration (Rg) of simulated complex for 100 ns (**D**) Plot displaying number of H-bonds interacting within simulated complex for 100 ns

RMSD calculates the variation between the protein's starting location and final structure. The RMSD values displayed low fluctuation throughout the 100 ns period, and were almost constant from around 70 to 100 ns demonstrating the structural stability of protein-ligand complex in Figure 9A. The interactions of protein-ligand appear energetically advantageous and contribute to complexes' stability based on low RMSD values. RMSF evaluates flexibility of each residue over-time and used to determine the variations in the protein residues. The RMSF score estimates protein-ligand complexes stability with larger values suggesting less stability and greater flexibility. The major fluctuation was observed only in the designated A (150-170) and B (305-325) region of protein loop which is conserved structurally and functionally for the serine and threonine kinase family (Yang et al.

2002) shown in Figure 9B. This major fluctuation might be due to the inhibition of AKT2 by Enceleamycin A affecting the phosphorylation responsible for protein functionality. The understanding of radius of gyration (Rg) of protein complex is essential to comprehend effect of inhibitors on the compactness of protein. In our simulation, the radius of gyration was found to be 2.17 and displayed lesser deviation throughout the 100 ns run as depicted in Figure 9C. The intermolecular H-bonds between interacting atom pairs impacts molecular recognition process and stability of protein-ligand complex's. To ascertain dynamic stability of complex, H-bonds interacting with the ligand and receptor protein were measured over the 100 ns run. In Figure 9D, Hydrogen bond interaction was observed throughout the 100 ns run and the interaction was increased from 70 ns onwards. Hydrogen bond occupancy was similar to results inferred from molecular docking, with Lys 181 occupying 16.08%, followed by Glu 200 occupying 10.79% during the MD run. Thus, it appears that predicted system is stable.

3.7 ADP-Glo Kinase Assay

An in vitro assay using the AKT2 kinase enzyme system was conducted to confirm further the *in silico* binding affinity and stability of the docked complex of Enceleamycin A and AKT2 (Zegzouti et al. 2009). The ADP generated during the reaction is measured by the ADP-GloTM Kinase. In the subsequent luciferase reaction, the newly produced ADP is transformed into ATP and generates light. The light generated correlates with the kinase activity. A concentration of less than 1 μg/mL of Enceleamycin A proved efficient in inhibiting the AKT2 enzyme. Enceleamycin A displayed an IC_{50} value of 0.736 μg/mL for AKT2 as displayed in Figure 10, consistent with a prior study showing that pyrano-naphthoquinones specifically inhibit the AKT kinase enzyme. However, the potential enzyme inhibition activity was comparatively less compared to pyrano-naphthoquinones (Salaski et al. 2009). With further in-depth research, Enceleamycin A can be used as a dual-action anticancer molecule with ROS formation and AKT2 inhibition to reduce the metastasis and invasiveness of cancer.
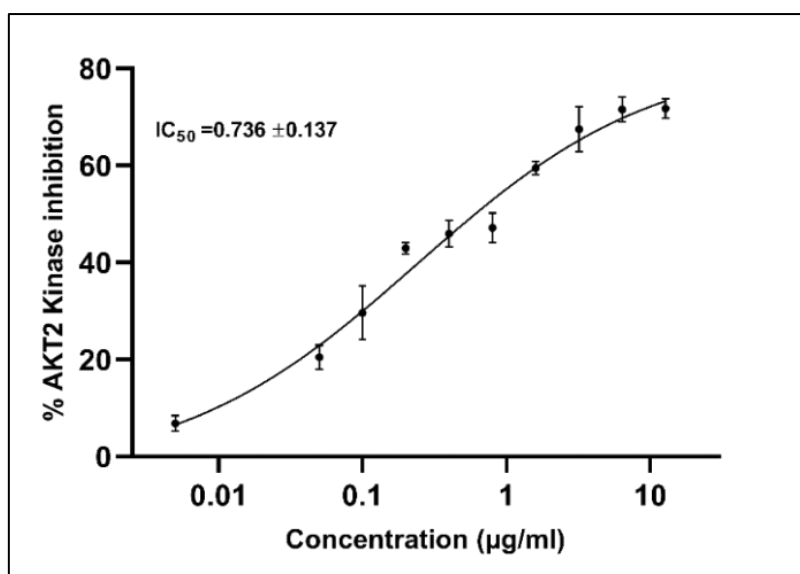
Figure 10. AKT2 kinase inhibition by Enceleamycin A with IC_{50} value of 0.736 μg/ml

3.8 Pharmacokinetics and Physiochemical Properties

The anticancer candidate molecule should have an approving biopharmaceutical property since it will interact with various cells and macromolecules inside the body. A molecule's acceptable ADMET (absorption, distribution, metabolism, excretion, and toxicity) characteristics are necessary for its consideration as a lead molecule for therapeutic application. The physicochemical and ADMET of Enceleamycin A was evaluated by the swissADME and pkCSM webtool (Daina and Zoete 2017; Pires et al. 2015). The bioavailability radar in Figure 11A, displays that the molecule falls under the optimum physicochemical properties (lipophilicity, size, polarity, insolubility, saturation, and flexibility). A molecule should follow Lipinski's and Veber's rules for drug-like properties (Lipinski et al. 2012; Veber et al. 2002). Enceleamycin A comes under all the designated Lipinski's rule of five (Mol. Wt. < 500 Daltons, No. of H-bond acceptors < 10, No. of H-bond donors < 5, octanol–water partition coefficients log P < 5 and molar refractivity < 140) and Veber's rule (topological polar surface area < 140 Å and No. of rotatable bonds < 10) which signifies its drug likeliness property. The pharmacokinetics displayed in the boiled-egg ADME profile in Figure 11B shows that gastro-intestinal tract effectively absorbs molecule and did not penetrate blood-brain barrier (BBB). The non-permeability of BBB signifies that molecule theoretically does not have side effects on the central nervous system (Ates-Alagoz et al. 2021).

Table 5. Physicochemical and pharmacokinetics property of Enceleamycin A using SwissADME and pkCSM webtool

Physicochemical properties		Pharmacokinetic properties	
Formula	$C_{17}H_{14}0_7$	Gastro-Intestinal absorption	Yes
Molecular weight	330.29 g/mol	BBB permeation	No
Rotatable bonds	0	P-Glycoprotein Inhibitor	No
Heavy atoms	24	P-Glycoprotein substrate	Yes
Aromatic heavy atoms	6	CYP-450 class enzyme inhibitor	No
H-bond donors	2	hERG I and II inhibitor	No
H-bond acceptors	7	Log Kp (skin permeation)	-7.79 cm/s
Log P	2.05	AMES toxicity	No
Molar refractivity	78.07	Hepatotoxicity	No
TPSA	102.29 Å	Skin sensitisation	No
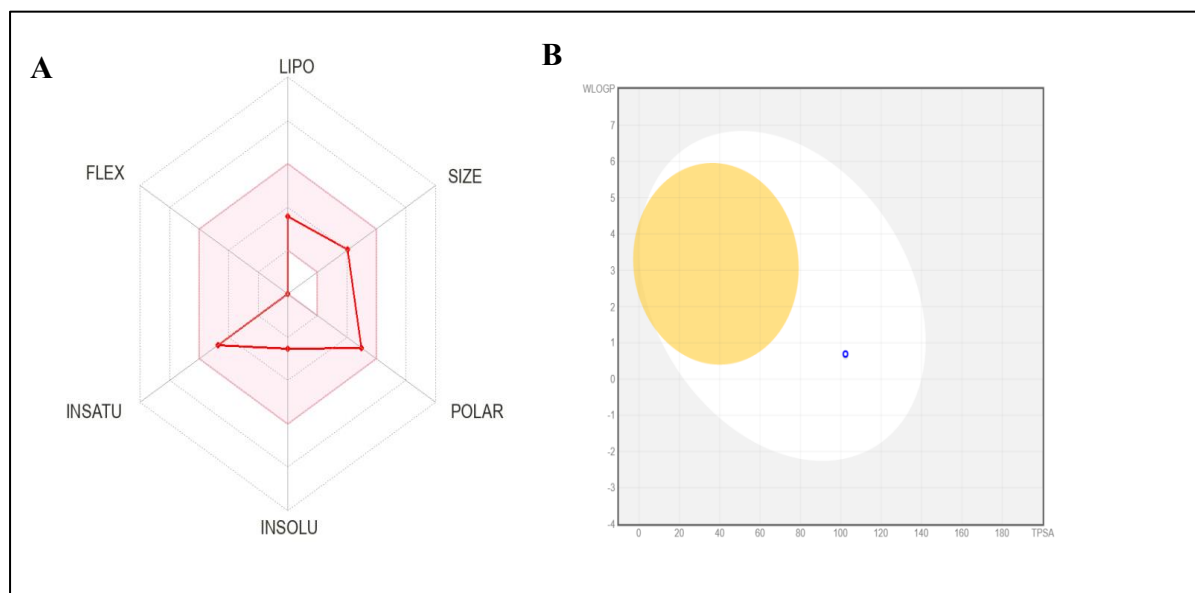
Figure 11. ADME property of Enceleamycin A. (**A**) Bioavailability radar of Enceleamycin A (**B**) Boiled-egg ADME profile where white egg part shows the gastro-intestinal absorption and yellow yolk part shows the Blood-brain barrier permeability, whereas the horizontal axis displays TPSA value and vertical axis shows the LogP value. The blue dot represents Enceleamycin A

Furthermore, the molecule did not inhibit the P-glycoprotein and CYP-450 class of enzymes, thus having a lower chance of corresponding drug interaction (Ates-Alagoz et al. 2021). The toxicity of molecules can damage organs and fail in late-stage drug development. So the toxicity of Enceleamycin A was evaluated by the pkCSM web tool, where the compound was negative to the Ames test, which assesses the carcinogenic effect. The molecule was non-hepatotoxic, not sensitive to skin, and a non-inhibitor of hERG I and II (Table 5). Based on these *in silico* findings, Enceleamycin A displayed desirable drug-likeness properties for a potential therapeutic candidate.
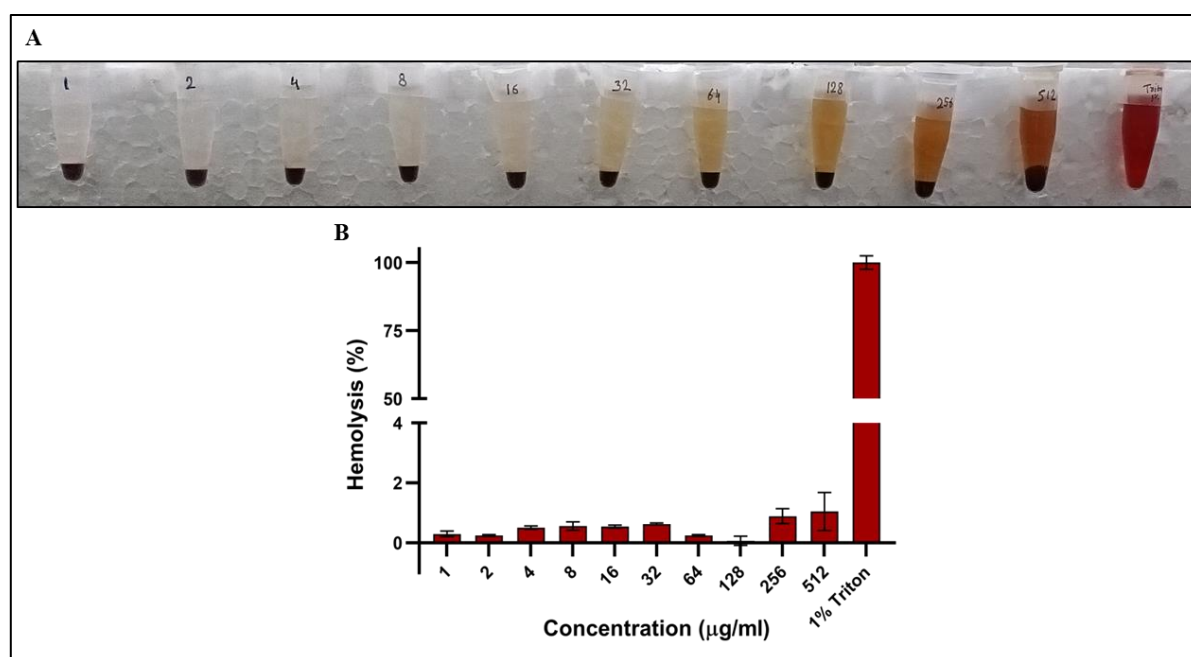
Figure 12. Hemolysis of Enceleamycin A (**A**) Hemolysis assay of Enceleamycin A demonstrating the intact pellet of red blood cells (**B**) Percentage of hemolysis of RBCs after treatment with Enceleamycin A

3.9 Hemolysis assay

The biocompatibility of Enceleamycin A was investigated by hemolysis assay for the in vivo applications. Hemolysis assay is one of the critical screening aspects for determining drug toxicity since these drugs interact with the blood components, mainly red blood cells (RBCs), during entry in humans (Ali et al. 2014). In vitro, hemolysis of Enceleamycin A was determined compared to 1% Triton X-100. The RBCs were found to be intact after treatment with Enceleamycin A. In contrast, they got dissolve in the presence of 1% of Triton X-100 as

shown in Figure 12A. As displayed in Figure 12B, Enceleamycin A showed negligible hemolytic effect on the human RBCs even at a concentration of 512 μg/mL, i.e., more than 400 times its IC_{50} against MDA-MB-231 cancer cells. Thus the reported anticancer compound is not toxic to human RBCs and can be further evaluated for *in vivo* animal studies.

Conclusion

The anticancer potential of Enceleamycins A, B, C and *N*-hydroxypyrazinone acid was investigated. Of the four compounds, Enceleamycin A showed prominent anticancer properties, particularly towards MDA-MB-231 (TNBC) cells with IC_{50} of 1.25 μg/mL. It also inhibits cell migration ability of TNBC cells at 1 μg/mL and above. The treatment of MDA-MB-231 cells by Enceleamycin A increases intracellular ROS formation, leading to apoptotic cell death, demonstrated by flow cytometry analysis. Molecular docking and MD simulation showed that Enceleamycin A can be a potential AKT2 inhibitor candidate. The *in silico* investigation was validated by the *in vitro* AKT2 enzyme assay, in which Enceleamycin A exhibited IC_{50} value of 0.73 μg/mL. According to *in silico* physicochemical and ADMET studies, Enceleamycin A showed good bioavailability and did not violate Lipinski's rule of five, making it a candidate drug-like molecule. The compound showed no prominent hemolytic effect on human RBCs. Altogether, this study presents essential insights about Enceleamycin A possessing therapeutic potential for cancer treatment, particularly triple-negative breast cancer cells by targeting AKT2 kinase signalling pathway.

References

Ali I, Wani WA, Saleem K, Hsieh MF (2014) Anticancer metallodrugs of glutamic acid sulphonamides: in silico, DNA binding, hemolysis and anticancer studies. *RSC adv* 4:29629-29641.

Ates-Alagoz Z, Kisla MM, Karadayi FZ, Baran S, Doğan TS, Mutlu P (2021) Design, synthesis, molecular docking and ADME studies of novel indole-thiazolidinedione derivatives and their antineoplastic activity as CDK6 inhibitors. *New J Chem* 45:18025-18038.

Azam SS, Abbasi SW (2013) Molecular docking studies for the identification of novel melatoninergic inhibitors for acetylserotonin-O-methyltransferase using different docking routines. *Theor Biol Med Model* 10:63.

Bell EW, Zhang Y (2019) DockRMSD: an open-source tool for atom mapping and RMSD calculation of symmetric molecules through graph isomorphism. *J Cheminform* 11:40.

Bellacosa A, de Feo D, Godwin AK, Bell DW, Cheng JQ, Altomare DA, Wan M, Dubeau L, Scambia G, Masciullo V, Ferrandina G, Benedetti Panici P, Mancuso S, Neri G, Testa JR (1995) Molecular alterations of the AKT2 oncogene in ovarian and breast carcinomas. *Int J Cancer* 64:280-285.

Chandan R, Chaithanya MS, Aditya M, Kiran KS (2023) Crystal structure determination, molecular docking and dynamics of arylidene cyanoacetates as potential JNK-3 inhibitors for Ischemia reperfusion injury. *J Biomol Struct Dyn* 41:8383-8391.

Clifford MN, Wight J (1976) The measurement of feruloylquinic acids and caffeoylquinic acids in coffee beans. Development of the technique and its preliminary application to green coffee beans. *J Sci Food Agric* 27:73-84.

Daina A, Michielin O, Zoete V (2017) SwissADME: a free web tool to evaluate pharmacokinetics, drug-likeness and medicinal chemistry friendliness of small molecules. *Sci Rep* 7:42717.

de Sena Pereira VS, da Silva Emery F, Lobo L, Nogueira F, Oliveira JIN, Fulco UL, Albuquerque EL, Katzin AM, de Andrade-Neto VF (2018) In vitro antiplasmodial

activity, pharmacokinetic profiles and interference in isoprenoid pathway of 2-aniline-3-hydroxy-1.4-naphthoquinone derivatives. *Malar J* 17:482.

De Vivo M, Masetti M, Bottegoni G, Cavalli A (2016) Role of Molecular Dynamics and Related Methods in Drug Discovery. *J Med Chem* 59:4035-4061.

Gangadharappa BS, Sharath R, Revanasiddappa PD, Chandramohan V, Balasubramaniam M, Vardhineni TP (2020) Structural insights of metallo-beta-lactamase revealed an effective way of inhibition of enzyme by natural inhibitors. *J Biomol Struct Dyn* 38:3757-3771.

Gao YD, Huang JF (2011) An extension strategy of Discovery Studio 2.0 for non-bonded interaction energy automatic calculation at the residue level. *Dongwuxue Yanjiu* 32:262–266.

Gener P, Rafael D, Seras-Franzoso J, Perez A, Pindado LA, Casas G, Arango D, Fernández Y, Díaz-Riascos ZV, Abasolo I, Schwartz S Jr (2019) Pivotal Role of AKT2 during Dynamic Phenotypic Change of Breast Cancer Stem Cells. *Cancers* 11:1058.

Hortobagyi GN (1997) Anthracyclines in the treatment of cancer: an overview. *Drugs* 54:1-7.

Hu J, Liu Z, Yu DJ, Zhang Y (2018) LS-align: an atom-level, flexible ligand structural alignment algorithm for high-throughput virtual screening. *Bioinformatics* 34:2209-2218.

Inagaki R, Ninomiya M, Tanaka K, Koketsu M (2015) Synthesis, Characterization, and Antileukemic Properties of Naphthoquinone Derivatives of Lawsone. *ChemMedChem* 10:1413-1423.

Justus CR, Leffler N, Ruiz-Echevarria M, Yang LV (2014) In vitro cell migration and invasion assays. *J Vis Exp* 88:51046.

Karakaş D, Akar RO, Gökmen Z, Deniz NG, Ulukaya E (2019) A novel 1,4-naphthoquinone-derived compound induces apoptotic cell death in breast cancer cells. *Turk J Biol* 43:256-263.

Khan A, Said MS, Borade BR, Gonnade R, Barvkar V, Kontham R, Dastager SG (2022) Enceleamycins A-C, Furo-Naphthoquinones from Amycolatopsis sp. MCC0218:

Isolation, Structure Elucidation, and Antimicrobial Activity. *J Nat Prod* 85:1267-1273.

Khraiwesh MH, Lee CM, Brandy Y, Akinboye ES, Berhe S, Gittens G, Abbas MM, Ampy FR, Ashraf M, Bakare O (2012) Antitrypanosomal activities and cytotoxicity of some novel imido-substituted 1,4-naphthoquinone derivatives. *Arch Pharm Res* 35:27-33.

Kumagai Y, Tsurutani Y, Shinyashiki M, Homma-Takeda S, Nakai Y, Yoshikawa T, Shimojo N (1997) Bioactivation of lapachol responsible for DNA scission by NADPH-cytochrome P450 reductase. *Environ Toxicol Pharmacol* 3:245-250.

Kumari R, Kumar R, Open Source Drug Discovery Consortium, Lynn A (2014) g_mmpbsa - A GROMACS tool for high-throughput MM-PBSA calculations. *J Chem Inf Model* 54:1951-1962.

Le XT, Lee J, Nguyen NT, Lee WT, Lee ES, Oh KT, Choi HG, Shin BS, Youn YS (2022) Combined phototherapy with metabolic reprogramming-targeted albumin nanoparticles for treating breast cancer. *Biomater Sci* 10:7117-7132.

Leyva E, López LI, de la Cruz RF, Espinosa-González CG (2017) Synthesis and studies of the antifungal activity of 2-anilino-/2, 3-dianilino-/2-phenoxy-and 2, 3-diphenoxy-1, 4-naphthoquinones. *Res Chem Intermed* 43:1813-27.

Lipinski CA, Lombardo F, Dominy BW, Feeney PJ (2012) Experimental and computational approaches to estimate solubility and permeability in drug discovery and development settings. *Adv Drug Deliv Rev* 46:3-26.

Liu T, Zhu J, Du W, Ning W, Zhang Y, Zeng Y, Liu Z, Huang JA (2020) AKT2 drives cancer progression and is negatively modulated by miR-124 in human lung adenocarcinoma. *Respir Res* 21:227.

Luo C, Wang Y, Wei C, Chen Y, Ji Z (2020) The anti-migration and anti-invasion effects of Bruceine D in human triple-negative breast cancer MDA-MB-231 cells. *Exp Ther Med* 19:273-279.

Malde AK, Zuo L, Breeze M, Stroet M, Poger D, Nair PC, Oostenbrink C, Mark AE (2011) An Automated Force Field Topology Builder (ATB) and Repository: Version 1.0. *J Chem Theory Comput* 7:4026-4037.

Milla P, Fiorito C, Soria F, Arpicco S, Cattel L, Gontero P (2014) Intravesical thermo-chemotherapy based on conductive heat: a first pharmacokinetic study with mitomycin C in superficial transitional cell carcinoma patients. *Cancer Chemother Pharmacol* 73:503-509.

Mock CD, Jordan BC, Selvam C (2015) Recent Advances of Curcumin and its Analogues in Breast Cancer Prevention and Treatment. *RSC Adv* 5:75575-75588.

Morris GM, Huey R, Lindstrom W, Sanner MF, Belew RK, Goodsell DS, Olson AJ (2009) AutoDock4 and AutoDockTools4: Automated docking with selective receptor flexibility. *J Comput Chem* 30:2785-2791.

Mosmann T (1983) Rapid colorimetric assay for cellular growth and survival: application to proliferation and cytotoxicity assays. *J Immunol Methods* 65:55-63.

Ng NS, Ooi L (2021) A Simple Microplate Assay for Reactive Oxygen Species Generation and Rapid Cellular Protein Normalization. *Bio Protoc* 11:e3877.

Pires DE, Blundell TL, Ascher DB (2015) pkCSM: Predicting Small-Molecule Pharmacokinetic and Toxicity Properties Using Graph-Based Signatures. *J Med Chem* 58:4066-4072.

Rahman MM, Islam MR, Akash S, Shohag S, Ahmed L, Supti FA, Rauf A, Aljohani ASM, Al Abdulmonem W, Khalil AA, Sharma R, Thiruvengadam M (2022) Naphthoquinones and derivatives as potential anticancer agents: An updated review. *Chem Biol Interact* 368:110198.

Rashid HU, Xu Y, Muhammad Y, Wang L, Jiang J (2019) Research advances on anticancer activities of matrine and its derivatives: An updated overview. *Eur J Med Chem* 161:205-238.

Redza-Dutordoir M, Averill-Bates DA (2016) Activation of apoptosis signalling pathways by reactive oxygen species. *Biochim Biophys Acta* 1863:2977-2992.

Riggio M, Perrone MC, Polo ML, Rodriguez MJ, May M, Abba M, Lanari C, Novaro V (2017) AKT1 and AKT2 isoforms play distinct roles during breast cancer progression through the regulation of specific downstream proteins. *Sci Rep* 7:44244.

Rychahou PG, Kang J, Gulhati P, Doan HQ, Chen LA, Xiao SY, Chung DH, Evers BM (2008) Akt2 overexpression plays a critical role in the establishment of colorectal cancer metastasis. *Proc Natl Acad Sci USA* 105:20315-20320.

Sæbø IP, Bjørås M, Franzyk H, Helgesen E, Booth JA (2023) Optimization of the Hemolysis Assay for the Assessment of Cytotoxicity. *Int J Mol Sci* 24:2914.

Salaski EJ, Krishnamurthy G, Ding WD, Yu K, Insaf SS, Eid C, Shim J, Levin JI, Tabei K, Toral-Barza L, Zhang WG, McDonald LA, Honores E, Hanna C, Yamashita A, Johnson B, Li Z, Laakso L, Powell D, Mansour TS (2009) Pyranonaphthoquinone lactones: a new class of AKT selective kinase inhibitors alkylate a regulatory loop cysteine. *J Med Chem* 52:2181-2184.

Sun L, Luo C, Liu J (2014) Hydroxytyrosol induces apoptosis in human colon cancer cells through ROS generation. *Food Funct* 5:1909-1914.

Sung H, Ferlay J, Siegel RL, Laversanne M, Soerjomataram I, Jemal A, Bray F (2021) Global Cancer Statistics 2020: GLOBOCAN Estimates of Incidence and Mortality Worldwide for 36 Cancers in 185 Countries. *CA Cancer J Clin* 71:209-249.

Testa JR, Bellacosa A (2001). AKT plays a central role in tumorigenesis. *Proc Natl Acad Sci USA* 98:10983.

Umar AK, Zothantluanga JH, Aswin K, Maulana S, Sulaiman Zubair M, Lalhlenmawia H, Rudrapal M, Chetia D (2022) Antiviral phytocompounds "ellagic acid" and "(+)-sesamin" of *Bridelia retusa* identified as potential inhibitors of SARS-CoV-2 3CL pro using extensive molecular docking, molecular dynamics simulation studies, binding free energy calculations, and bioactivity prediction. *Struct Chem* 33:1445-1465.

Veber DF, Johnson SR, Cheng HY, Smith BR, Ward KW, Kopple KD (2002) Molecular properties that influence the oral bioavailability of drug candidates. *J Med Chem* 45:2615-2623.

Vinayan A, Glynne-Jones R (2016) Anal cancer - What is the optimum chemoradiotherapy? *Best Pract Res Clin Gastroenterol* 30:641-653.

Webb B, Sali A (2016) Comparative Protein Structure Modeling Using MODELLER. *Curr Protoc Bioinformatics* 54:5-6

Wellington KW (2015) Understanding cancer and the anticancer activities of naphthoquinones–a review. *RSC Adv* 5:20309-20338.

Worsley CM, Veale RB, Mayne ES (2022) Inducing apoptosis using chemical treatment and acidic pH, and detecting it using the Annexin V flow cytometric assay. *PLoS One* 17:e0270599.

Yang J, Cron P, Good VM, Thompson V, Hemmings BA, Barford D (2002) Crystal structure of an activated Akt/protein kinase B ternary complex with GSK3-peptide and AMP-PNP. *Nat Struct Biol* 9:940-944.

Yao H, He G, Yan S, Chen C, Song L, Rosol TJ, Deng X (2017) Triple-negative breast cancer: is there a treatment on the horizon? *Oncotarget* 8:1913-1924.

Yin L, Duan JJ, Bian XW, Yu SC (2020) Triple-negative breast cancer molecular subtyping and treatment progress. *Breast Cancer Res* 22:61.

Zegzouti H, Zdanovskaia M, Hsiao K, Goueli SA (2009) ADP-Glo: A Bioluminescent and homogeneous ADP monitoring assay for kinases. *Assay Drug Dev Technol* 7:560-572.

Chapter 5

Summary and Future Perspectives

1. Overall summary

Historically, natural products have been essential to pharmacotherapy, especially for infectious diseases and cancer. Nonetheless, the need for novel bioactive compound is critical due to drug resistance, lack of new class of antibiotics, limitations of existing treatments, and evolving diseases. The Actinobacteria group is an excellent source of bioactive molecules because of their diversity and demonstrated capability to produce new metabolites. The *Streptomyces* genus of actinobacteria is a prominent producer of bioactive secondary metabolites and has been explored to a large extent. In recent years, due to rediscovery of existing compounds from *Streptomyces* genus, the screening for novel compounds has focused on the non-*Streptomyces* group, commonly known as rare actinobacteria. The *Amycolatopsis* genus belonging to rare actinobacteria has shown its potential to produce novel molecules with various structural and biological activities. The genome sequencing technology has revealed the unexplored biosynthetic potential of the *Amycolatopsis* genus. Approaches like one strain many compounds (OSMAC) can effectively elicit biosynthetic metabolic pathways to maximize the secondary metabolite diversity. The various studies have shown that the cultivation condition of microbes, including static or dynamic, can directly affect their chemical metabolic process and produce novel molecules.

In search of novel antimicrobial molecules, present study aimed to screen bioactive compound producing actinobacteria previously isolated from Western Ghats of India. The screening for antimicrobial activity was performed under shaking and static conditions using three fermentation media. From the 57 isolates screened, 21 displayed activity towards at least one of the test strains, i.e., *S. aureus, E. coli,* or *C. albicans*. The 16S rRNA gene sequences showed 20 isolates belong to *the Streptomyces* genus, whereas one isolate was a rare actinobacteria from *the Amycolatopsis* genus. *Amycolatopsis* sp. WGS_07 displayed potent activity against *S. aureus* only under static conditions with zone of inhibition of 34 mm. The strain was closely related to *A. silviterrae* of which no bioactivity was reported. The whole genome sequencing analysis of *Amycolatopsis* sp. WGS_07 yielded a genome size of 10,225,713 bp and showed 28 biosynthetic gene clusters associated with diverse secondary metabolites. The *Amycolatopsis* sp. WGS_07 was further investigated for large-scale production of bioactive molecules. The fermentation of 50L under static conditions yielded 52 g of crude extract and further purified based on bioactivity by silica-gel column chromatography followed by semi-preparative HPLC. The purification led to the isolating of four bioactive molecules, and their chemical structure was elucidated using NMR

spectroscopy, HR-MS and single crystal XRD. The purified compounds were characterized as three new furo-naphthoquinones, Enceleamycins A, B, C and one novel *N*-hydroxypyrazinone acid. Enceleamycin A possesses an unprecedented pentacyclic oxeto-furo-furo-naphthoquinone structure. Enceleamycin B contains a dihydroxylated naphthoquinone group, and Enceleamycin C has the furo-furo-naphthoquinone skeleton with hydroxy-aldehyde functionalities.

Naphthoquinones are naturally present in bacteria, fungi, and plants. They comprise a naphthalene ring system with two carbonyl groups and display various biological activities, like antibacterial, anticancer, antifungal, antimalarial, antitrypanosomal, and antiviral. The antibacterial studies of Enceleamycins A-C and *N*-hydroxypyrazinone acid showed that Enceleamycin A possesses potent antibacterial (MIC range of 2-8 μg/mL) activity towards various Gram-positive bacteria, including clinically isolated methicillin-resistant *S. aureus*. The MIC against Gram-positive bacteria of Enceleamycin C was 8-32 μg/mL, whereas MIC of Enceleamycin B and *N*-hydroxypyrazinone acid was 64 to >128 μg/mL. With maximum activity and yield, Enceleamycin A was further studied and found to have a bacteriostatic effect on the growth of MSSA and MRSA. Enceleamycin A displayed the synergistic effect with erythromycin against MRSA and additive effect in combination with ampicillin, vancomycin and ciprofloxacin. Enceleamycin A also showed significant biofilm inhibition and disruption at 1 and 2 μg/mL concentrations. The preliminary study indicates that MRSA treatment with Enceleamycin A results in the increase of intracellular ROS levels and results in the inhibition of bacterial growth. Altogether, the antibacterial study presents Enceleamycin A as a candidate therapeutic molecule for treating MRSA.

Cancer is among the most significant cause of mortality globally and there has been several cases of resistance towards the present anticancer drug. The Breast cancer, especially triple negative breast cancer (TNBC) is among most aggressive cancer type with low survival rate. The standard TNBC treatment is generally chemotherapy because absence of specific biomarkers. Since the FDA has approved several compounds with quinone moiety for various cancer chemotherapy, the present study investigated the anticancer potential of three novel furo-naphthoquinones, Enceleamycin A-C along with N-hydroxy pyrazinone acid. Enceleamycin A showed prominent anticancer properties, particularly against MDA-MB-231 (TNBC) cells with IC_{50} value of 1.25 μg/mL. It also demonstrated its ability to significantly inhibit MDA-MB-231 cell migration at 1 μg/mL and above. The primary mechanism of the naphthoquinones is forming reactive oxygen species (ROS) in cells. The intracellular ROS level increased in MDA-MB-231 cells after treatment with Enceleamycin A, leading to

apoptotic cell death, as demonstrated by flow cytometry analysis using Annexin V/PI staining. The early apoptosis percentage increased from 25% to 60.65%, and late apoptosis from 2.45% to 19.2% at 8 µg/mL.

The naphthoquinone molecules in previous studies have shown selective inhibition towards the serine-threonine kinase AKT, which plays essential role in chemo-resistance and invasiveness of breast cancer. The molecular docking of Enceleamycin A with AKT2 revealed a binding affinity of -7.14 Kcal/mol. Further, *in vitro* AKT2 enzyme assay was also performed to validate *in silico* investigation. Enceleamycin A inhibits the AKT2 enzyme *in vitro* with IC$_{50}$ value of 0.736 µg/ml. Molecular docking, MD simulation, and *in vitro* AKT2 enzyme assay showed that Enceleamycin A can be a potential AKT2 inhibitor candidate. According to *in silico* physicochemical and ADMET studies, Enceleamycin A showed good bioavailability and did not violate Lipinski's rule of five. The compound is non-hepatotoxic, not sensitive to skin, and a non-inhibitor of hERG I and II and was negative in the Ames test. Enceleamycin A showed a negligible hemolytic effect on the human RBCs even at a 512 µg/mL concentration, i.e., more than 400 times its IC$_{50}$ against MDA-MB-231 cancer cells. The anticancer study presents Enceleamycin A's therapeutic potential for cancer treatment, particularly TNBC cells, by targeting the AKT2 kinase signaling pathway.

2. Future Perspective

The species of the *Amycolatopsis* genus possess the potential to produce a high number of valuable pharmaceutical molecules. With the advances in genomics and metabolomics, it is found that the culture has potential to biosynthesize more secondary metabolites than reported. In the present study, the fermentation of *Amycolatopsis* sp. WGS_07 under static conditions has led to the isolation of four new molecules Enceleamycins A, B, C, and *N*-hydroxypyrazinone acid. The fermentation of *Amycolatopsis* sp. WGS_07 under different growth conditions and using various metabolite elicitors can help isolate even more new molecules. The whole genome of *Amycolatopsis* sp. WGS_07 showed the presence of various biosynthetic gene clusters, including the type II polyketide synthases (PKSs) gene clusters, which are generally responsible for synthesizing naphthoquinones. The biosynthetic gene cluster analysis and gene knockout study can help to predict and validate the pathway and genes responsible for the synthesis of Enceleamycins. It will help isolate other intermediates in Enceleamycin's biosynthetic pathways that might have more potent activity.

Enceleamycin A displayed significant antibacterial and anticancer activity; further, it can also be explored for other bioactivities like antiparasitic and antiviral. Enceleamycin A can also be

screened for treating theileriosis for cattle infected with *Theileria* since the resistance towards the marketed drug buparvaquone is increasing. For better solubility, stability, and efficacy, Enceleamycin A can be derivatized by incorporating other chemical groups, like hydroxyl, halogens, and amides. In addition to the *in silico* pharmacokinetics and toxicity, the *in vivo* study can further establish the pharmacokinetics, pharmacodynamics, and therapeutic potential of Enceleamycins A. Further, the study of expression of the marker genes for apoptotic pathway would be interesting and will give more clarity about the anticancer mechanism of enceleamycin A.

The discovery of Enceleamycin A and its antibacterial and anticancer properties, mechanism of action, and computational predictions opens further research and development avenues. This novel compound can be valuable in addressing critical medical needs in infectious disease treatment and cancer therapy.

ABSTRACT

The need for novel bioactive compounds is crucial due to the challenges posed by antimicrobial resistance and existing drug limitations. In this regard, actinobacteria cultures from the Western Ghats were screened for antimicrobial activity under shaking and static conditions. *Amycolatopsis* sp. WGS_07 showed potent activity against *S. aureus* only under static condition and was closely related to *A. silviterrae*. The genome sequencing analysis of *Amycolatopsis* sp. WGS_07 displayed the presence of biosynthetic gene clusters associated with diverse secondary metabolites. The large-scale fermentation of 50L and bioactivity-guided multiple chromatography purification resulted in isolating four bioactive molecules. The isolated compounds were identified as three novel furo-naphthoquinones, Enceleamycins A-C (**1-3**), and one new *N*-hydroxypyrazinone acid (**4**). Enceleamycin A displayed potent antibacterial activity against Gram-positive bacteria, followed by Enceleamycin C, whereas Enceleamycin B and *N*-hydroxypyrazinone acid were weakly active. Enceleamycin A revealed a bacteriostatic effect on the growth of MSSA and MRSA. It showed synergistic activity with erythromycin against MRSA. Enceleamycin A inhibits the growth of *S. aureus* by producing intracellular ROS. Overall, Enceleamycin A possesses therapeutic potential for bacterial treatment against MRSA. In addition, the anticancer activity of Enceleamycins A-C and *N*-hydroxypyrazinone demonstrated considerable inhibition of triple-negative breast cancer (TNBC) MDA-MB-231 cells by Enceleamycin A with an IC_{50} value of 1.25 μg/mL. Enceleamycin A raises intracellular ROS levels in TNBC cells, leading to apoptotic cell death, as demonstrated by Annexin V/PI staining. The molecular docking and simulation investigation revealed a better binding affinity of Enceleamycin A with AKT2. The *in silico* physicochemical and pharmacokinetics characteristics of Enceleamycin A demonstrated its drug-likeness. The hemolysis assay showed the non-hemolytic nature of Enceleamycin A. Altogether, the anticancer study presents essential insights about Enceleamycin A's therapeutic potential for cancer treatment, particularly against triple-negative breast cancer cells.

List of Publications:

From thesis:

1. **Khan, A**., Pradeep, S., & Dastager, S. G. (2023). In vitro anticancer evaluation of Enceleamycin A and its underlying mechanism. *RSC Advances*, *13*(48), 34183-34193.

2. **Khan, A**., Said, M. S., Borade, B. R., Gonnade, R., Barvkar, V., Kontham, R., & Dastager, S. G. (2022). Enceleamycins A–C, Furo-Naphthoquinones from Amycolatopsis sp. MCC0218: Isolation, Structure Elucidation, and Antimicrobial Activity. *Journal of Natural Products*, *85*(5), 1267-1273.

Other than thesis:

3. Sahu, A. K., Said, M. S., Hingamire, T., Gaur, M., **Khan, A**., Shanmugam, D., Barvkar, V. T., Dharne, M. S., Bharde, A. A., & Dastager, S. G. (2020). Approach to nigericin derivatives and their therapeutic potential. *RSC advances*, *10*(70), 43085-43091.

4. Said, M. S., Udavant, R., Sahu, A. K., **Khan, A.,** Nayak, R., Dastager, S. G., Kumar, P., & Gajbhiye, J. (2021). Total synthesis of (-)-2-methoxy-2-butenolide-3-cinnamate and its antimicrobial potentials. *Natural Product Research*, *35*(23), 5177-5182.

5. Naushin, S., Sardana, V., Ujjainiya, R., Bhatheja, N., Kutum, R., Bhaskar, A. K., …**Khan, A**., …. & Sengupta, S. (2021). Insights from a Pan India sero-epidemiological survey (phenome-India cohort) for SARS-CoV2. *Elife*, *10*, e66537.

List of patents:

From thesis:

1. Syed G Dastager; Abujunaid Khan; Madhukar Said : Novel furo-naphthoquinone and novel pyrazinone compound from Amycolatopsis and activities thereof. **(IN202211009245)** PCT/IN2023/050133

Other than thesis:

2. Syed G Dastager, Madhukar Shyam Said, **Abujunaid Khan**, Amul Kulkarni : Two step and faster synthesis of indolmycin. **(IN202111055049)** PCT/IN2022/051026

Conferences

1. Poster presentation

Conference: International Conference on BREEECH (Biotechnology for Resource Efficiency, Energy, Environment, Chemicals and Health) at CSIR-IIP, Dehradun, India.

Conference date: December 1-4, 2021

Title: Bioactive potentials of rare actinobacteria, *Amycolatopsis* sp.

Authors: Abujunaid Khan, Madhukar Said , Syed Dastager

Abstract:

The demand for new bioactive compounds are critical due to the rapid spread of antimicrobial resistance worldwide. The microbial natural products have played a pivotal role in the development of antimicrobial drugs over the past several decades. *Amycolatopsis* genus, so called rare Actinobacteria are known to produce novel secondary metabolites with various biological activities. The present study underscores the antimicrobial screening of actinobacteria using three different fermentation medium under static and shaking condition considering OSMAC (One Strain Many Compounds) strategy. *Amycolatopsis* sp. WGS_07 was found to be active against *S. aureus* under static condition only. Further, isolation of its major bioactive compound along with their derivatives was assessed using a large scale fermentation of 50 litres under static condition. Bioactivity guided purification using silica gel column chromatography coupled with semi-preparative HPLC led to the isolation of four compounds. After intensive characterization by 1D NMR, 2D NMR, XRD and Mass spectroscopy, three novel unprecedented Naphthoquinones along with one new pyrazinone acid derivative were probably identified. The compounds C-1 and C-3 were found to be active against Gram positive bacteria, against both susceptible and methicillin resistant *S. aureus* (MIC 2-32 µg/mL). Besides, these compounds were also screened for their antimalarial activity against *P. falciparum* (C-1 and C-3, $IC_{50} > 1 \mu M$), suggesting it as a potential antimalarial molecule. This study reveals that rare actinobacteria *Amycolatopsis* sp. can be a source of novel bioactive compounds under static condition and the isolated compounds can be used as a scaffold for antibacterial or antimalarial drug.

2. Poster presentation

Conference: International Workshop on "Biology and applications of Actinomycetes" at University of Mysore, Mysore, India

Conference date: 31st October- 1st November, 2019

Title: Rare Actinobacteria: A potential source for bioactive compounds

Authors: Abujunaid Khan, Syed Dastager

Abstract:

The demand for new antibiotics with broad-spectrum activity are increasing due to the rapid spread of antibiotic-resistant pathogens causing numerous infectious diseases. Considering the need of the society for a new antibiotic, the present work focuses on the screening of actinobacteria from the unexplored region of Western Ghats and North-East India for the antimicrobial compounds. Around 200 actinobacteria cultures were isolated from both the sites using different media and were identified by the 16S rRNA gene sequencing which reveals that majority of the isolates were of *Streptomyces* genera, the most common among the actinobacteria genera. The extraction of secondary metabolites from actinobacteria using different media and their antimicrobial study was carried out by agar well diffusion method against three test organisms i.e., *Escherichia coli* (NCIM 2065), *Staphylococcus aureus* (NCIM 2127) and yeast strain *Candida albicans* (NCIM 3102). 121 isolates were having activity against one of the test organism. *Streptomyces sp.* MS21 was targeted as it was showing broad-spectrum antimicrobial activity and there were no antimicrobial compounds reported from the closest strain of MS21. Fermentation of 30 litres was done and the broth was extracted thrice by an equal volume of ethyl acetate. The crude extract was partially purified by silica gel column chromatography. Further identification and characterization of the active compounds will be done with the help of preparative HPLC followed by NMR and LC-MS. The study reveals that the exploitation of actinobacteria from the unexplored region can still be a source for the novel antimicrobial compound.

Article

Enceleamycins A−C, Furo-Naphthoquinones from *Amycolatopsis* sp. MCC0218: Isolation, Structure Elucidation, and Antimicrobial Activity

Abujunaid Khan,[#] Madhukar S. Said,[#] Balasaheb R. Borade, Rajesh Gonnade, Vitthal Barvkar, Ravindar Kontham,[*] and Syed G. Dastager[*]

Cite This: https://doi.org/10.1021/acs.jnatprod.1c01160

Read Online

ACCESS | ⬛ Metrics & More | 📖 Article Recommendations | 🆂🅸 Supporting Information
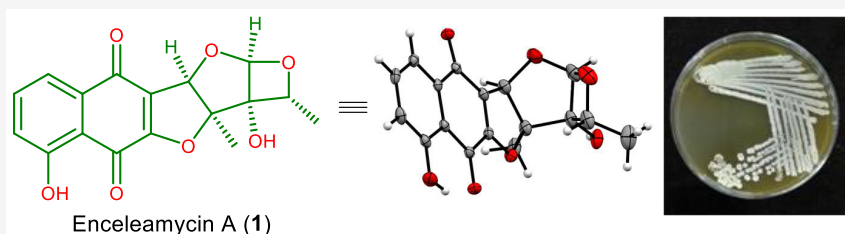
Enceleamycin A (1)

ABSTRACT: Three novel furo-naphthoquinones, enceleamycins A−C (**1**−**3**), and a new *N*-hydroxypyrazinone acid (**4**) were identified from the strain *Amycolatopsis* sp. MCC 0218, isolated from a soil sample collected from the Western Ghats of India. Their chemical structure and absolute and relative configurations were established by 1D and 2D NMR spectroscopy, single-crystal X-ray crystallography, and high-resolution mass spectrometry. Compounds **1** and **3** were active against methicillin-susceptible and -resistant *Staphylococcus aureus* with MIC values of 2−16 μg/mL.

The increase in antibiotic resistance is a big challenge to human health management. This crisis has been epitomized by the spread of multi-drug-resistant "ESKAPE" organisms (*Enterococcus* spp., *Staphylococcus aureus*, *Klebsiella* spp., *Acinetobacter baumannii*, *Pseudomonas aeruginosa*, and *Enterobacter* spp.).[1,2] Natural products from microbial sources have played a pivotal role in developing antimicrobial drugs over several decades.[3−5] The bacterial genus *Amycolatopsis*, rare actinobacteria, belongs to the Pseudonocardiaceae family and are producers of the important clinical antibiotics rifamycin and vancomycin.[6,7] The saalfelduracins,[8] thioamycolmides,[9] amycolasporins,[10] dibenzoyls,[10] thioalbamide A,[11] and pradimicin[12] have been isolated from different species of *Amycolatopsis*. Multiple growth conditions have been employed to maximize the secondary metabolite diversity by varying the parameters such as nutrients, time, temperature, pH, and aereation.[13−15]

Following a search for novel bioactive secondary metabolites from various bacteria and plants,[16−20] herein, we report the isolation, structure determination, and bioactivity evaluation of novel furo-naphthoquinone derivatives and the new *N*-hydroxypyrazinone acid from the *Amycolatopsis* sp. MCC 0218 strain, which was isolated from a soil sample collected from the Western Ghats of India (see the Supporting Information). The bacterial strain was cultured on a fermentation medium (50 L) in static conditions for 7 days at 28 °C, and the whole broth was extracted with EtOAc, which yielded about 52 g of extract. Bioactivity-guided purification by silica gel column chromatog-

raphy and semipreparative reversed-phase HPLC resulted in the isolation of three novel furo-naphthoquinones (**1**−**3**, enceleamycins A−C) along with *N*-hydroxypyrazinone acid **4**.
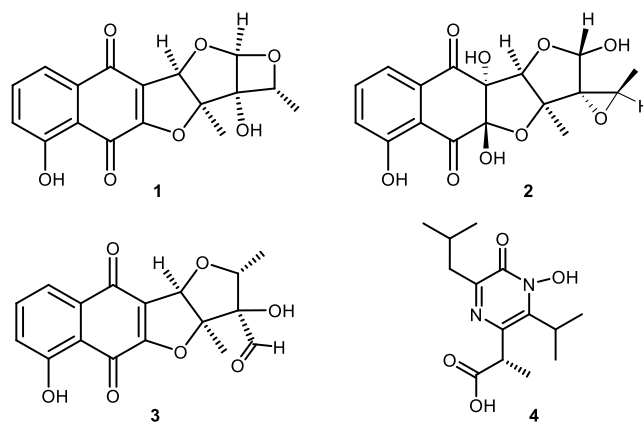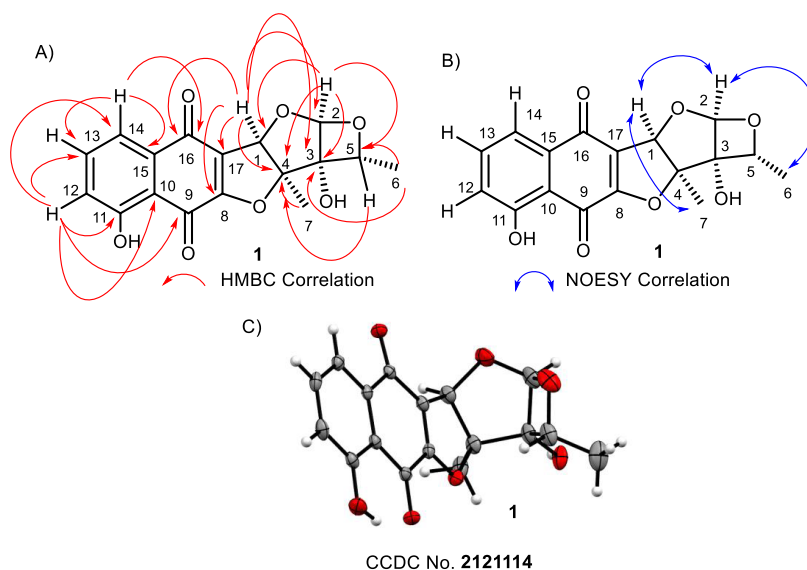
Figure 1. (A) Key HMBC correlations, (B) key NOESY correlations, and (C) ORTEP diagram of compound **1**.
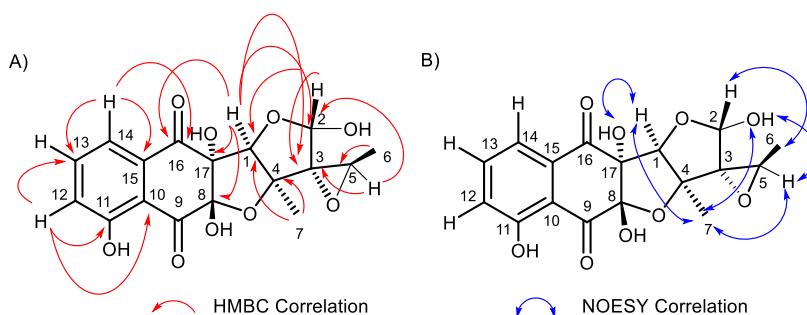
Figure 2. (A) Key HMBC correlations; (B) key NOESY correlations of compound **2**.

■ RESULTS AND DISCUSSION

Enceleamycin A (**1**) was obtained as a yellow solid. The molecular formula of **1** was determined to be $C_{17}H_{14}O_7$ by high-resolution mass spectrometry (HRMS), requiring 11 indices of hydrogen deficiency. The IR spectrum of **1** exhibits an absorption band at 3437 cm^{-1} for the hydroxy group and 1641 cm^{-1} for the conjugated enone. The electronic circular dichroism (ECD) spectrum showed a positive Cotton effect at 249 nm (CD, 0.06 mg/mL, CH_3CN), λ_{max} ($\Delta\varepsilon$) 249 (+23.51), 290 (−8.95) nm. The ^1H NMR spectrum of **1** in CD_3CN displayed proton signals for two sp^3 methyls [δ_H 1.34 (d, J = 6.1 Hz) and 1.59 (s)], three sp^3 methines [δ_H 5.74 (s), 5.72 (s), and 4.50 (q, J = 6.4 Hz)], three sp^2 methines [$\delta_H$ 7.25 (d, J = 8.4 Hz), 7.73−7.65 (m), and 7.64−7.56 (m)], and a phenolic proton [δ_H 11.51 (br s, 1 H)] (Table S1). The ^{13}C NMR spectrum of **1** in CD_3CN had 17 carbon signals. Based on DEPT and HSQC analyses, the presence of two methyls (δ_C 17.9 and 19.7), six methines [three olefinic (δ_C 119.9, 124.9, and 138.6); three oxygenated sp^3 (δ_C 75.9, 92.2, and 111.7)], and nine nonprotonated carbons [three olefinic (δ_C 116.3, 126.0, and 134.4), two olefinic oxygenated (δ_C 161.0 and 162.9), two oxygenated sp^3 (δ_C 87.4 and 100.2), and two carbonyl carbons (δ_C 184.0 and 181.6)] was established. The HMBC spectra showed correlations of H-12 (δ_H 7.25 and δ_C 124.9) with C-9 (C=O, δ_C 184.0) and C-10/C-11/C-13/C-14; H-13 (δ_H 7.73−7.65) with C-11/C-14/C-15; and H-14 (δ_H 7.64−7.56 and δ_C 119.9) with C-9 (C=O, δ_C 184.0)/C-10/C-11/C-12/C-13/C-15/C-16 (C=O, δ_C 181.6) and ^1H−^1H COSY cross-

correlations of H-12/H-13/H-14, suggesting the presence of a 5-hydroxy-1,4-naphthoquinone ring system (Figure 1, see the Supporting Information).

The HMBC correlations of H-1 [δ_H 5.74 (s), δ_C 92.2)] with C-2/C-3/C-4/C-7/C-8/C-16/C-17; H-7 [δ_H 1.59 (s), δ_C 19.7] with C-1/C-3/C-4; and H-2 [δ_H 5.72 (s)] with C-1/C-3/C-4/C-5 suggested the presence of two fused tetrahydrofuran moieties (head-to-tail) (Figure 1). ^1H−^1H COSY cross-peaks of H-5 [δ_H 4.50 (q, J = 6.4 Hz)] with H-6 [δ_H 1.34 (d, J = 6.1 Hz), δ_C 17.9] and HMBC correlations of H-5 with C-2/C-3/C-4, in combination with an unusual downfield shift of the C-2 signal (δ_H 5.72, δ_C 111.7, flanked by two oxygens), led us to assign the C-2 and C-3 fused oxetane and in turn provided the skeletal assignment of **1** possessing an unprecedented pentacyclic oxeto-furo-furo-naphthoquinone (Figure 1, Table S2, see the Supporting Information). Initially, the relative stereochemistry of **1** was assigned based on NOESY correlations between H-1/H-2/H-6/H-7, which revealed that these protons were cofacial (Figure 1B, Figure S9). A crystal of enceleamycin A (**1**) was prepared from cold DMSO and CH_3CN, which led to the establishment of the complete structure and absolute stereochemistry (1R, 2R, 3R, 4S, 5R) with the aid of signal-crystal X-ray diffraction analyses (Figure 1C).

Enceleamycins B and C (**2** and **3**) are congeners of enceleamycin A (**1**). Enceleamycin B (**2**) was isolated as a yellow powder. The ECD spectrum showed a negative Cotton effect at 273 nm (CD, 0.053 mg/mL, CH_3CN), λ_{max} ($\Delta\varepsilon$) 273 (−43.54), 243 (26.11) nm. The molecular formula of **2** was
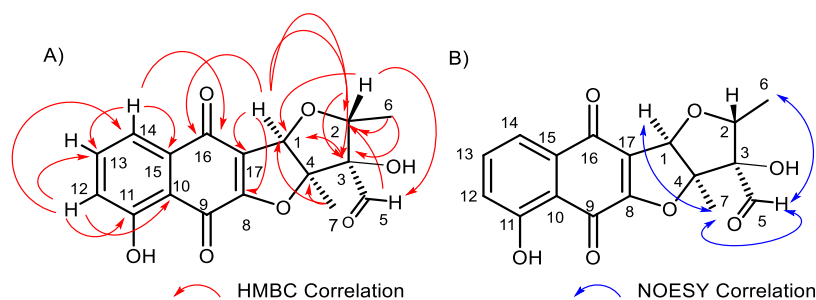
Figure 3. Key HMBC and NOESY correlations of compound **3**.

Scheme 1. Plausible Biosynthetic Conversion of Compound 1 into Compounds 2 and 3
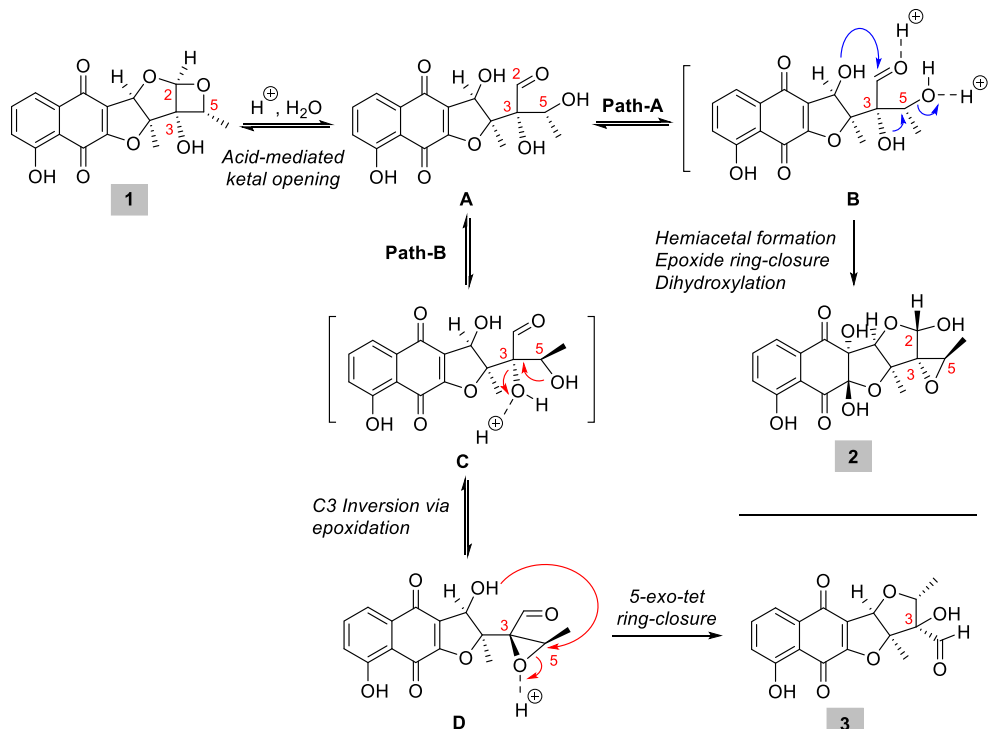
determined as $C_{17}H_{16}O_9$ based on HRMS (ESI) analysis, requiring 10 indices of hydrogen deficiency. The 1D and 2D NMR spectra of **2** are close overall to those of compound **1**, with a few exceptions in both the ^1H and ^{13}C NMR data. The ^1H NMR data for **2** (Table S1) in DMSO-d_6 show two methyls (δ_H 1.01 (d, J = 6.6 Hz) and 1.58 (s)), six methines [three oxygen-attached sp^3 (δ_H 3.94 (q, J = 6.6 Hz), 4.34 (s), and 5.01 (d, J = 4.3 Hz) and three sp^2 (δ_H 7.32 (dd, J = 0.83, 7.48 Hz), 7.56 (dd, J = 0.85, 7.48 Hz), and 7.75 (m)], one phenolic [δ_H 10.96 (br s, 1H)] proton, and three hydroxy protons [δ_H 6.93 (d, J = 4.3 Hz) for C2-OH, 5.04 (s) for C8-OH, and 7.09 (s) for C-17-OH]. The ^{13}C NMR spectrum (Table S1) of **2** in DMSO-d_6 had 17 carbon signals. Using DEPT and HSQC analyses established the presence of two methyls [δ_C 14.0 (C-6), 18.7 (C-7)], six methines [three oxygenated sp^3 δ_C 3.94 (C-5), 86.5 (C-1), and 96.3 (C-2) and three olefinic sp^2 δ_C 123.4, 136.9, and 119.3], and four carbons [with oxygenated δ_C 80.1 (C-3), 82.2 (C-17), 91.2 (C-4), and 102.9 (C-8)]. The presence of two new oxygenated carbon signals (δ_C 102.9 for C-8 and δ_C 82.2 for C-17) and a downfield resonance of carbonyl carbons C-9 (δ_C 188.5) and C-16 (δ_C 191.4) compared to compound **1** [C-9 (δ_C 184.0) and C-16 (δ_C 181.6)] led to the tentative assignment of the structure of **2** as the 8,17-dihydroxylated naphthoquinone

segment of **1** (Figure 2, Table S1, see the Supporting Information).

The HSQC data established all $^1J(^1H-^{13}C)$ connectivities; the remaining skeletal connectivities were confirmed by COSY and HMBC analyses in DMSO-d_6. Particularly, HMBC correlations of H-1 (δ_H 4.43) with C-2/C-3/C-4/C-7/C-8/C-16 and H-7 (δ_H 1.58) with C-1/C-3/C-4 confirmed the right-side furo-furan segment. In contrast to compound **1**, ^1H NMR data (in DMSO-d_6) of compound **2** showed a doublet for H-2 (δ_H 5.01, J = 4.3 Hz) via coupling with the C-2-OH proton (δ_H 6.93, J = 4.3 Hz), which led to the proposition of a cyclic hemiacetal right part instead of a furo-oxetane fused system. The formation of a cyclic hemiacetal could be attributed to the enzymatic (Brønsted acid-mediated) opening of the fused furo-oxetane bicyclic ring system of compound **1** followed by subsequent epoxide formation involving C-3 and C-5 hydroxy groups (*vide infra*).

This proposed structure was established through HMBC correlations of C-5−H with C-2/C-3/C-6 and of C-2−H with C-5/C-1/C-3 and subsequently by HSQC and NOESY analyses. NOESY correlations of H-1 with H-7 (methyl) and of H-7 (methyl) with H-1/H-5/C-2−OH indicated the cofacial nature of all these groups. NOESY correlation of H-2 with H-6
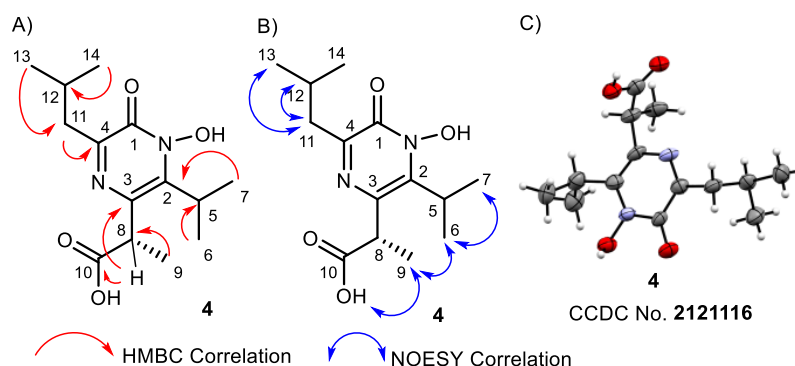
Figure 4. (A) Key HMBC correlations, (B) key NOESY correlations, and (C) ORTEP diagram of compound **4**.

(methyl) revealed the *trans* geometry of 1,2-substituents of the right-side tetrahydrofuran (THF) ring. Further, the NOESY correlation of H-1 with C-17−OH indicated the cofacial relation of these groups, which indirectly established the *trans* geometry of the C-8−C-17 vicinal diol. Based on the absolute stereochemistry of compound **1**, NOESY correlations observed, and anticipating the same biosynthetic origin for **1** and **2**, the stereochemistry of compound **2** was assigned as 1*R*, 2*S*, 3*R*, 4*S*, 5*R*, 8*S*, 17*S* (Figure 2).

Compound **3** (enceleamycin C) was isolated as a yellow powder. The molecular formula of **3** was identified as $C_{17}H_{14}O_7$ through HRMS (ESI) analysis, requiring 11 indices of hydrogen deficiency. The ECD spectrum showed a negative Cotton effect at 302 nm (CD, 0.026 mg/mL, CH_3CN), λ_{max} ($\Delta\varepsilon$) 302 (−34.63), 276 (18.24) nm. Similar to compound **1**, compound **3** contains a furo-naphthoquinone skeleton, with (Table S1) two methyl groups [δ_H 1.13 (d, J = 6.9 Hz) and 1.40 (s)], five methines [two oxygenated (δ_H 3.89 (q, J = 6.4 Hz) and 5.54 (s) and three olefinic hydrogens [δ_H 7.27 (dd, J = 1.1, 8.4 Hz), 7.72 (dd, J = 7.6, 8.4 Hz), and 7.61 (dd, J = 1.0, 7.4 Hz)], and one phenolic proton [δ_H 11.51 (br s, 1H)]. ^{13}C NMR (Table S1), DEPT, and HSQC analyses showed 17 carbon signals, including two methyls (δ_C 13.3, 17.7), six methines [three olefinic (δ_C 125.0, 119.9, and 138.7), two sp³ oxygenated (δ_C 77.7 and 84.5), one aldehyde (δ_C 202.3)], and nine carbons [three olefinic (δ_C 116.5, 123.3, and 134.5), two olefinic oxygenated (δ_C 162.3 and 162.9), two sp³ oxygenated (δ_C 88.6 and 98.7), and two carbonyl carbons (δ_C 184.0 and 181.8)]. A shielded H-2 signal (δ 3.89) and the presence of an aldehyde group (δ_H 9.74 and δ_C 202.2) led us to anticipate the reorganization (opening) of the strained oxetane ring system in compound **3** compared to **1** (Figure 3).

Next, systematic 2D NMR analyses were performed to elucidate the complete structure and relative stereochemistry of compound **3**. As observed for **1**, HMBC correlations of H-12 with C-10/C-11/C-13/C-14; H-13 with C-11/C-14/C-15; and H-14 with C-10/C-12/C-13/C-15/C-16/C-17 confirmed the presence of the naphthoquinone moiety. HMBC of H-1 with C-2/C-3/C-7/C-8/C-16/C-17; H-2 with C-3/C-5; H-6 with C-2/C-3; H-7 (methyl) with C-1/C-3/C-4; and H-5 with C-2/C-3/C-4 suggested the furo-furo-naphthoquinone skeleton possessing hydroxy-aldehyde functionalities at C-3. The presence of NOESY correlations of H-1/H-5/H-6/H-7 revealed the relative stereochemistry of **3** as presented in Figure 3 (entry B). Based on the absolute stereochemistry of C-1 and C-4 of enceleamycin A (**1**), the absolute stereochemistry for **3** was tentatively assigned as 1*R*, 2*R*, 3*R*, 4*S* (Figure 3).

A plausible biosynthetic conversion of enceleamycin A (**1**) into its structurally close congeners **2** and **3** is presented in

Scheme 1. The initial enzymatic (Brønsted acid-mediated) opening of the strained oxetane fused ketal moiety of **1** would deliver the trihydroxy aldehyde **A**, which subsequently undergoes ring-closure via two distinct pathways (paths A and B). Acid-mediated intramolecular 1,2-addition (5-*exo*-trig) of the C-1 hydroxy onto the aldehyde, followed by epoxide formation through C-5−OH activation (inversion at C-5), and dihydroxylation of the C-8−C-17 olefinic functionality of **A** would lead to the formation of enceleamycin B (**2**) (Scheme 1, path A). In an alternative route, intermediate **A** would undergo epoxide formation through C-3−OH activation (inversion at C-3) to give the corresponding epoxy aldehyde intermediate D, which could subsequently undergo 5-*exo*-tet ring-closure with C-1−OH (via epoxide opening) to furnish enceleamycin C (**3**) (Scheme 1, path B).

In addition to enceleamycins A−C (**1**−**3**), novel *N*-hydroxypyrazinone acid **4** was isolated from a common EtOAc extract as a white hairy crystalline solid. The ECD spectrum showed a positive Cotton effect at 241 nm (CD, 0.054 mg/mL, CH_3CN), λ_{max} ($\Delta\varepsilon$) 241 (55.67), 221 (−23.32) nm. The molecular formula of **4** was determined to be $C_{14}H_{22}N_2O_4$ by HRMS, requiring 5 indices of hydrogen deficiency. ^1H NMR analysis of **4** revealed the presence of five methyls [δ_H 0.91 (s, J = 6.8 Hz), 0.93 (s, J = 6.8 Hz), 1.44 (s, J = 7.2 Hz), 1.46 (d, J = 7.2 Hz), and 1.51 (d, J = 7.2 Hz)], three methines [δ_H 2.17 (m, 1H), 3.42−3.28 (m), and 3.98 (q, J = 6.8 Hz)], and a methylene [δ_H 2.69 (d, J = 6.8 Hz)]. The ^{13}C and DEPT NMR spectra showed 14 resonating signals, including five methyls (δ_C 17.6, 17.6, 18.9, 19.1, and 22.6), three sp³ methines (δ_C 28.8, 26.7, and 42.4), one methylene (δ_C 41.5), and five nonprotonated carbons [three olefinic (δ_C 132, 138.2, and 151.3), one amide (δ_C 151.1), and one for a carboxylic acid functionality (δ_C 177.9)]. Combined ^1H and ^{13}C NMR, DEPT, HSQC, and COSY analyses were used to establish all carbon and hydrogen connectivities (Figure 4, Table S1, see the Supporting Information).

COSY (^1H−^1H) correlations of H-5 [δ_H 3.42−3.28 (m, 1H)] with H-6 (methyl)/H-7 (methyl) and HMBC correlations of H-5 with C-2/C-6/C-7 revealed the presence of an isopropyl group. Similarly, COSY correlations of H-11 [δ_H 2.69 (d, J = 6.8 Hz, 2H)] with H-12 [δ_H 2.17 (m, 1H)] and of H-12 with H-13 and H-14 suggested the presence of an isobutyl chain. The H-8 [δ_H 3.89 (q, J = 6.8 Hz, 1H)] showed a COSY correlation with H-9 (methyl, δ_H 1.51 (d, J = 7.2 Hz, 3H)) and HMBC correlations with C-3/C-9/C-10, indicating the presence of a propionic acid moiety (Figure 4A). All these correlations led us to conclude that isopropyl, isobutyl, and propionic acid groups were attached to the pyrazinone ring. Further, key NOESY cross-correlations of −O<u>H</u>/H-6/H-7/H-9/−CO₂<u>H</u> and H-11/

H-12/H-13/H-14 have strongly supported our structural assignment. Moreover, the complete structure and absolute stereochemistry (*S* configurations at C-8) of **4** were rigorously established using single-crystal X-ray crystallography analyses (Figure 4).
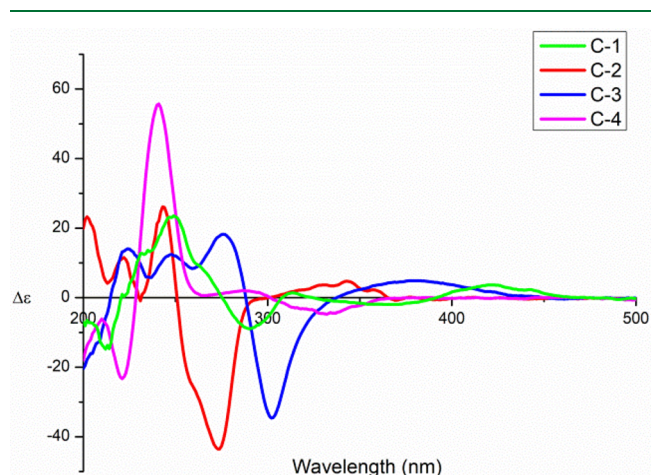

Figure 5. ECD spectra of compounds **1**−**4**. C-1 to C-4 refer to compounds **1**−**4**.

The presence of a furo-naphthoquinone substructure in several bioactive natural products isolated from terrestrial and marine organisms,[21−23] along with the potential biological activity of the secondary metabolites obtained from the *Amycolatopsis* genus, prompted us to screen the bioactive potentials of compounds **1**−**4**.

The isolated compounds showed selective inhibition toward the Gram-positive bacteria. Compounds **1** and **3** have antibacterial activity against tested Gram-positive bacteria (with MIC values ranging from 2 to 32 μg/mL), whereas

Table 1. Antibacterial Activity of Compounds 1−4

| bacterial strain | MIC (μg/mL) | | | | | |
	C-1	C-2	C-3	C-4	Ap[a]	Kn[b]
S. aureus ATCC 9144	2	128	8	128	0.03	8
S. epidermidis ATCC 12228	2	64	8	64	1	1
B. cereus ATCC 11778	8	>128	16	128	16	2
B. subtilis ATCC 6633	4	>128	16	128	0.03	0.5
M. luteus ATCC 9341	8	>128	32	64	0.03	8
L. monocytogenes ATCC19111	2	128	8	128	0.03	1
M. smegmatis ATCC 607	64	>128	64	>128	64	0.25
MRSA_3B	4	>128	16	128	8	>128
MRSA_6B	4	>128	8	128	8	>128
MRSA_9B	4	>128	16	128	16	128
MRSA_10B	4	128	8	128	4	>128
E. coli ATCC 8739	>128	>128	>128	>128	2	8
P. aeruginosa ATCC 9027	>128	>128	>128	>128	2	8

[a]Ampicillin (Ap) used as a reference standard. [b]Kanamycin (Kn) used as a reference standard. C refers to the compounds.

compounds **2** and **4** were less active (MIC values ranging from 64 to 128 μg/mL). These compounds also inhibited the growth of four different clinically isolated methicillin-resistant *S. aureus*.

■ EXPERIMENTAL SECTION

General Experimental Procedures. Optical rotations were measured on a JASCO P-2000 polarimeter. Ultraviolet−visible spectra were obtained on a Thermo Scientific Evolution 201 UV−visible spectrophotometer. CD spectra were obtained using a JASCO J-815 CD spectrometer. IR spectra were measured on a Bruker FTIR spectrometer. NMR spectra were recorded in CD_3CN or $CDCl_3$ using Bruker AV400 or 500 MHz spectrometers with tetramethylsilane (TMS) as an internal standard. HR-ESIMS analysis was carried out on an Agilent 6530 Q-TOF (Agilent, USA) mass spectrometer connected to an HPLC Prime Infinity II 1260 system (800 bar), and a dual electrospray ionization (ESI) source was used for ionization. For LC-based metabolite separation, a Hypersil GOLD C_{18} (2.1 × 150 mm, 1.9 μm particle size, Thermo Scientific, USA) column was used at 40 °C with a flow rate of 0.3 mL/min. Silica gel (60−100 mesh and 100−200 mesh, Hi-media, India) was used for the chromatography column (CC). Semipreparative HPLC was conducted on a Thermo Scientific Ultimate 3000 equipped with a DAD detector and a YMC column (250 × 10 m i.d., 10−20 μm), using a flow rate of 4.7 mL/min at a column temperature of 28 °C. The melting point was recorded on a Stuart SMP10 (BioCote). The single-crystal XRD was recorded on a Bruker d8 Advance, and crystal XRD data were collected using high-resolution (0.78 Å) Cu Kα radiation at low temperature (100 K).

Isolation and Identification of the Organism (*Amycolatopsis* sp. MCC 0218). *Amycolatopsis* sp. MCC 0218 was isolated from soil collected from the Western Ghats of Kerala, India. For the isolation of bacteria, a serial dilution method was followed and 100 μL dilutions were spread on ISP-2 (1% malt extract, 0.4% yeast extract, 0.4% dextrose, pH 7.0) agar plates and incubated for 10 days at 28 °C. The isolated culture was further subcultured on ISP-2 agar plates, 25% glycerol stocks were made for short-term storage, and lyophilized vials were made for long-term storage. The molecular identification of the strain was carried out by 16S rRNA gene sequence analysis and identified as *Amycolatopsis* sp. (GenBank No. MZ824481), showing 99.24% similarity to the strain *Amycolatopsis silviterrae* (GenBank No. KR818707) and 99.1% similarity to *Amycolatopsis vancoresmycina* (GenBank No. NR_025565). The top closest 15 cultures from the EZ-Biocloud database were used for the phylogeny tree construction by the neighbor joining method using Mega 6.0 software with 1000 bootstrap values. The *Amycolatopsis* sp. MCC 0218 was forming a clade with *Amycolatopsis silviterrae*. The strain *Amycolatopsis* sp. MCC 0218 was deposited at National Centre for Microbial Resource, Pune, India, under accession No. MCC 0218.

Culture and Antimicrobial Screening of *Amycolatopsis* sp. MCC 0218. Strain *Amycolatopsis* sp. MCC 0218 was subcultured on MGYP agar plates (0.3% malt extract, 1% dextrose, 0.3% yeast, 0.5% peptone, and 1.8% agar, pH 7.0) for 7 days at 28 °C. A loopful of culture was inoculated into a 250 mL Erlenmeyer flask containing 50 mL of seed medium, composed of 2% soy meal, 2% mannitol, and 0.4% dextrose, with the pH adjusted to 7 before sterilization. The seed culture was incubated at 28 °C on a rotary shaker at 150 rpm for 3 days. A 5 mL amount of the seed culture was used to inoculate into three different fermentation media in a 250 mL Erlenmeyer flask, each containing 50 mL of media. The seed culture was also streaked on plates contacting the medium used for fermentation with 2% agar. The fermentation media used were 5333 (composed of 1.5% starch, 0.4% yeast extract, 0.1% K_2HPO_4, and 0.05% $MgSO_4$), 5254 (composed of 2% soy meal, 2% glucose, 0.5% corn steep liquor, 0.1% NaCl, and 0.02% $CaCO_3$), and 5294 (composed of 1% starch, 1% glycerol, 1% dextrose, 0.2% yeast extract, 0.2% peptone, 0.25% corn steep liquor, 0.1% NaCl, and 0.3% $CaCO_3$). The pH of all three fermentation media was adjusted to 7.0 prior to sterilization (autoclaved at 121 °C for 20 min). The flasks were incubated in both static and shaking conditions (on a rotary shaker at 150 rpm) for 7 days at 28 °C. The whole broth and agar plate with cultures were extracted by 100 mL of ethyl acetate, and the

E

organic phase was separated and concentrated by a rotary evaporator. The crude extract was dissolved in 1.0 mL of HPLC grade ethyl acetate. For the bioactivity screening, 30 μL of crude extract was used against *S. aureus*, *E. coli*, and *C. albicans* by the disc diffusion method.

The crude extract of *Amycolatopsis* sp. MCC 0218 was found to be active in agar plate conditions with a zone of inhibition of 20 mm in 5254 medium and 22 mm in 5294 medium, whereas in static conditions the zone of inhibition was 22 mm in 5254 medium and 25 mm in 5294 medium against *S. aureus*. No activity was observed from cultures grown under any of the shaking conditions in the three fermentation media tested (Figure S3). Bioautography of the crude extract was done using *S. aureus* to check the major active compound zone from both the static and agar conditions, and it was found that the major active compound produced in both conditions appeared to be the same. No yellow pigment or antimicrobial activity was produced in shaking culture conditions (Figure S4). The time course of activity produced in the supernatant of the culture was performed by using 100 μL of cell-free supernatant using the fermentation media 5294 in a 500 mL flask containing 100 mL of media. Activity against *S. aureus* was observed from the third day of incubation, and maximum activity was observed on the eighth day of incubation (Figure S5).

Fermentation, Extraction, and Purification. The large-scale fermentation was carried out by using 500 mL Erlenmeyer flasks each containing 100 mL of 5294 fermentation medium. The cultures were incubated in static conditions for 7 days at 28 °C. The whole broth was extracted three times with an equal volume of ethyl acetate. The organic phase was separated and concentrated under reduced pressure to get a semisolid extract of about 52 g. The extract was subjected to silica gel column chromatography using petroleum (pet) ether with a gradient increase in ethyl acetate to give 20 fractions, AME-1 to AME-20 (*Amycolatopsis* ethyl acetate extract). Based on the bioactivity profile, AME-9, which was eluted with 70% ethyl acetate/pet ether, was further purified by semipreparative HPLC on a C_{18} column using gradient elution by water and acetonitrile to yield six fractions. Fraction AME-9-IV is confirmed as the major compound **1**, and fraction-AME-9-III was further fractionated by semipreparative HPLC to isolate compound **2**.

Based on the TLC profile and bioactivity, column fractions of AME-5 to AME-8 were combined and silica gel CC was performed using pet ether with a gradient increase in ethyl acetate to get fractions I to XII. Fraction VI from AME-5−8 eluted with 30% ethyl acetate/pet ether was further separated by semipreparative TLC in 20% ethyl acetate/pet ether followed by semipreparative HPLC with a chiral amylose column in normal phase with an isocratic mobile phase of 30% isopropanol/hexane to yield compound **3**. Fraction V from AME-5−8 eluted with 20% ethyl acetate/pet ether in silica gel CC was purified by semipreparative HPLC by a reversed-phase C_{18} column using a gradient mobile phase of acetonitrile and water to get compound **4**.

Enceleamycin A (1): yellow powder (5.25 g from 50 L, in 10.5% yield); $[\alpha]^{27}_D$ +51.60 (*c* 0.64, CH_3CN); UV (CH_3CN) λ_{max} (log ε) 202 (1.70), 222 (1.36), 289 (0.85), 416 (0.33) nm; IR (neat) (ν_{max}) 3437, 2891, 2821, 2103, 1641, 1443, 1212, 764 cm^{-1} (IR spectrum Figure S16); ^{1}H and ^{13}C NMR data (CD$_3$CN, 400.00 and 100.00 MHz, respectively), Table S1; melting point 171−173 °C; HR-ESI *m/z* [M + H]$^+$ (calcd for $C_{17}H_{15}O_7$ 331.0810; found 331.0812).

Enceleamycin B (2): yellow powder (0.186 g from 50 L, in 0.37% yield); $[\alpha]^{27}_D$ +93.35 (CH_3CN, *c* 0.53); UV (CH_3CN) λ_{max} (log ε) 232 (2.65), 345 (0.60) nm; IR (neat) (ν_{max}) 3435, 2879, 2103, 1640, 1445, 1338, 1200, 1056, 769 cm^{-1} (IR spectrum Figure S28); ^{1}H and ^{13}C NMR data (DMSO-d_6, 400.00 and 100.00 MHz, respectively), Table S1; melting point 187−189 °C; HR-ESI *m/z* [M+ Na]$^+$ (calcd for $C_{17}H_{16}O_9Na$ 387.0683; found 387.0687).

Enceleamycin C (3): yellow powder (0.032 g from 50 L, in 0.064% yield); $[\alpha]^{27}_D$ +84.26 (*c* 0.26, CH_3CN); UV (CH_3CN) λ_{max} (log ε) 202 (1.49), 216 (1.31), 288 (0.73), 418 (0.27) nm; IR (neat) (ν_{max}) 3416, 3013, 1522, 1441, 1336, 1214, 1151, 939, 765 cm^{-1} (IR spectrum Figure S39); ^{1}H and ^{13}C NMR data (CD$_3$CN, 400.00 and 100.00 MHz, respectively), Table S1; melting point 194−197 °C; HR-ESI *m/z* [M + Na]$^+$ (calcd for $C_{17}H_{14}O_7Na$, 353.0630; found 353.0632).

***N*-Hydroxypyrazinone acid (4):** white crystalline solid (0.146 g from 50 L, in 0.29% yield); $[\alpha]^{27}_D$ +97.84 (*c* 0.6, CH_3CN); UV

(CH_3CN) λ_{max} (log ε) 205 (1.26), 330 (0.97), 238 (0.97) nm; IR (neat) (ν_{max}) 3423, 2879, 2104, 1639, 1443, 1335, 1212, 1038, 941, 766 cm^{-1} (IR spectrum Figure S50); ^{1}H and ^{13}C NMR data (CDCl$_3$, 400.00 and 100.00 MHz, respectively), Table S1; melting point 108−110 °C; HR-ESI *m/z* [M + H]$^+$ (calcd for $C_{14}H_{23}N_2O_4$, 283.1651; found 283.1652).

Single-Crystal XRD Analysis. The recrystallization of enceleamycin A (**1**) was carried out in cold DMSO and CH_3CN solvent. The ORTEP view of compound **1** shows the atom-numbering scheme. The displacement ellipsoids, at the 50% probability level, and H atoms are shown as small spheres with arbitrary radii. The absolute configuration was established by anomalous dispersion effects (Flack parameter, 0.06(18)) in X-ray diffraction measurements carried out with Cu radiation. The single-crystal X-ray diffraction data analysis established that the compound has *R*, *R*, *R*, *S*, and *R* configurations at the C1, C2, C3, C4, and C5 positions, respectively (see the Supporting Information).

The recrystallization of *N*-hydroxypyrazinone acid (**4**) was carried out in methanol. The ORTEP view of compound **4** shows the atom-numbering scheme. The displacement ellipsoids are drawn at the 30% probability level, and H atoms are shown as small spheres with arbitrary radii. The single-crystal X-ray diffraction data analysis established the compound has *S* configurations at the C8A, C8B, C8C, and C8D positions in four different conformers of compound **4**.

Antibacterial Activity. The MICs of the purified compounds were carried out according to CLSI guidelines using Mueller Hinton broth (Hi-media, Mumbai) against a panel of six Gram-positive bacteria, *S. aureus*, *S. epidermidis*, *B. cereus*, *B. subtilis*, *M. luteus*, and *L. monocytogenes*, two Gram-negative bacteria, *E. coli* and *P. aeruginosa*, and four MRSA (methicillin-resistant *S. aureus*) clinical strains. The stock solution of compounds was made at 10 mg/mL in DMSO. The compounds (highest concentration 128 μg/mL) were serially diluted in 50 μL of Mueller Hinton broth, and 50 μL bacterial suspensions were added to reach the final desired cell density of 5 × 10^5 CFU mL^{-1} in each well of a 96-well microtiter plate except for the media control. The medium, untreated culture, DMSO, ampicillin, and kanamycin were used as controls. The plates were observed for MIC after an incubation of 18 h at 37 °C in shaking conditions. The MIC for *M. smegmatis* was determined following the above method in Middlebrook 7H9 medium, and the growth was observed after 48 h. The MICs were defined as the lowest concentration that inhibited the visible growth of bacteria.

■ ASSOCIATED CONTENT

ⓢ Supporting Information

The Supporting Information is available free of charge at https://pubs.acs.org/doi/10.1021/acs.jnatprod.1c01160.

Identification, bioactivity, UV, IR, CD, and 1D and 2D NMR spectra of enceleamycins A−C (**1**−**3**) and *N*-hydroxypyrazinone acid (**4**) (PDF)

X-ray crystallographic data for **1** (CIF)

X-ray crystallographic data for **4** (CIF)

■ AUTHOR INFORMATION

Corresponding Authors

Syed G. Dastager − *NCIM-Resource Center, CSIR-National Chemical Laboratory, Pune 411008, India; Academy of Scientific and Innovative Research (AcSIR), Ghaziabad 201002, India;* ⓞ orcid.org/0000-0002-8316-1242; Phone: +91-20-25902505; Email: sg.dastager@ncl.res.in

Ravindar Kontham − *Organic Chemistry Division, CSIR-National Chemical Laboratory, Pune 411008, India; Academy of Scientific and Innovative Research (AcSIR), Ghaziabad 201002, India;* ⓞ orcid.org/0000-0002-5837-2777; Phone: +91-20-25902301; Email: k.ravindar@ncl.res.in

Authors

Abujunaid Khan − *NCIM-Resource Center, CSIR-National Chemical Laboratory, Pune 411008, India; Academy of Scientific and Innovative Research (AcSIR), Ghaziabad 201002, India*

Madhukar S. Said − *Organic Chemistry Division, CSIR-National Chemical Laboratory, Pune 411008, India; Academy of Scientific and Innovative Research (AcSIR), Ghaziabad 201002, India*

Balasaheb R. Borade − *Organic Chemistry Division, CSIR-National Chemical Laboratory, Pune 411008, India; Academy of Scientific and Innovative Research (AcSIR), Ghaziabad 201002, India*

Rajesh Gonnade − *Center for Material Characterization, CSIR-National Chemical Laboratory, Pune 411008, India; Academy of Scientific and Innovative Research (AcSIR), Ghaziabad 201002, India;* ⊙ orcid.org/0000-0002-2841-0197

Vitthal Barvkar − *Department of Botany, Savitribai Phule Pune University (University of Pune), Pune 411007, India;* ⊙ orcid.org/0000-0003-4009-5924

Complete contact information is available at:
https://pubs.acs.org/10.1021/acs.jnatprod.1c01160

Author Contributions

[#]A.K. and M.S.S. contributed equally.

Notes

The authors declare no competing financial interest.

■ REFERENCES

(1) Ventola, C. L. *Pharm. Ther.* **2015**, *40*, 277−283.

(2) Levy, S. B.; Marshall, B. *Nat. Med.* **2004**, *10*, 122−129.

(3) Devi, S. *Advances in Pharmaceutical Biotechnology*; Springer: Singapore, 2020; pp 317−331.

(4) Moloney, M. G. *Trends Pharmacol. Sci.* **2016**, *37*, 689−701.

(5) De Simeis, D.; Serra, S. *Antibiotics* **2021**, *10*, 483−515.

(6) Lechevalier, M. P.; Prauser, H.; Labeda, D. P.; Ruan, J. S. *Int. J. Syst. Evol* **1986**, *36*, 29−37.

(7) Chen, S.; Wu, Q.; Shen, Q.; Wang, H. *Chem. Bio. Chem.* **2016**, *17*, 119−128.

(8) Um, S.; Seibel, E.; Schalk, F.; Balluff, S.; Beemelmanns, C. *J. Nat. Prod* **2021**, *84*, 1002−1011.

(9) Pan, C.; Kuranaga, T.; Liu, C.; Lu, S.; Shinzato, N.; Kakeya, H. *Org. Lett.* **2020**, *22*, 3014−3017.

(10) Jin, Y.; Aobulikasimu, N.; Zhang, Z.; Liu, C.; Cao, B.; Lin, B.; Guan, P.; Mu, Y.; Jiang, Y.; Han, L.; Huang, X. *J. Nat. Prod* **2020**, *83*, 3545−3553.

(11) Frattaruolo, L.; Fiorillo, M.; Brindisi, M.; Curcio, R.; Dolce, V.; Lacret, R.; Truman, A. W.; Sotiga, F.; Lisanti, M. P.; Cappello, A. R. *Cells* **2019**, *8*, 1408−1427.

(12) Almeida, L. C.; Bauermeister, A.; Rezende-Teixeira, P.; Santos, E. A. D.; Machado-Neto, J. A.; Costa-Lotufo, L. V. *Biochem. Pharmacol.* **2019**, *168*, 38−47.

(13) Bode, H.; Bethe, B.; Hofs, R.; Zeeck, A. *Chem. Bio. Chem.* **2002**, *3*, 619−627.

(14) Pan, R.; Bai, X.; Chen, J.; Zhang, H.; Wang, H. *Front. Microbiol* **2019**, *10*, 294−314.

(15) Yao, F. H.; Liang, X.; Qi, S. H. *Nat. Prod. Res.* **2020**, *35*, 1−10.

(16) Sahu, A. K.; Said, M. S.; Hingamire, T.; Gaur, M.; Khan, A.; Shanmugam, D.; Barvkar, V. T.; Dharne, M. S.; Bharde, A. A.; Dastager, S. G. *RSC Adv.* **2020**, *10*, 43085−43091.

(17) Ram, H.; Sahu, A. K.; Said, M. S.; Banpurkar, A. G.; Gajbhiye, J. M.; Dastager, S. G. *J. Hazard. Mater.* **2019**, *380*, 120868−120877.

(18) Dan, V. M.; Vinodh, J. S.; Sandesh, C. J.; Sanawar, R.; Lekshmi, A.; Kumar, R. A.; Santhosh Kumar, T. R.; Marelli, U. K.; Dastager, S. G.; Pillai, M. R. *ACS Chem. Bio* **2020**, *15*, 780−788.

(19) Said, M. S.; Chinchansure, A. A.; Nawale, L.; Durge, A.; Wadhwani, A.; Kulkarni, S. S.; Sarkar, D.; Joshi, S. P. *Nat. Prod. Res.* **2015**, *29*, 2080−2086.

(20) Durge, A.; Jadaun, P.; Wadhwani, A.; Chinchansure, A. A.; Said, M.; Thulasiram, H. V.; Joshi, S. P.; Kulkarni, S. S. *Nat. Prod. Res.* **2014**, *31*, 1468−1471.

(21) Bringmann, G.; Haagen, Y.; Gulder, T. A.; Gulder, T.; Heide, L. *J. Org. Chem.* **2007**, *72*, 4198−4204.

(22) Katsuyama, Y.; Sone, K.; Satou, R.; Izumikawa, M.; Takagi, M.; Fujie, M.; Satoh, N.; Shin-ya, K.; Ohnishi, Y. *Chem. Bio. Chem.* **2016**, *17*, 1021−1028.

(23) Guo, Z.; Pan, G.; Xu, Z.; Yang, D.; Zhu, X.; Huang, Y.; Zhao, X.; Jiang, Y.; Duan, Y.; Shen, B. *J. Antibiot. Res.* **2017**, *70*, 414−422.

Check for updates

In vitro anticancer evaluation of Enceleamycin A and its underlying mechanism†

Abujunaid Khan,[ab] S. Pradeep[ab] and Syed G. Dastager ⓘ *[ab]

It has become more crucial than ever to find novel anticancer compounds due to the rise in cancer mortality and resistance to the present chemotherapeutic drugs. Naphthoquinones are regarded as privileged structures for their ability to inhibit various cancers. The current study examined three novel furo-naphthoquinones (Enceleamycins A–C) previously isolated from *Amycolatopsis* sp. MCC 0218 for their anticancer potential. Enceleamycin A demonstrated considerable cytotoxicity for triple-negative breast cancer (TNBC) MDA-MB-231 cells with an IC_{50} value of 1.25 μg mL^{-1} (3.78 μM). It also showed the ability to inhibit MDA-MB-231 cell migration. Enceleamycin A raises intracellular ROS levels in TNBC cells, ultimately leading to apoptotic cell death, as demonstrated by Annexin V/PI staining. The molecular docking and simulation investigation revealed better binding affinity of Enceleamycin A with AKT2, which plays a vital role in breast cancer's invasiveness and chemo-resistance. Enceleamycin A inhibits the AKT2 enzyme *in vitro* with an IC_{50} value of 0.736 μg mL^{-1} (2.22 μM), further validating the docking study. The *in silico* physicochemical and pharmacokinetics characteristics of Enceleamycin A demonstrated its drug-likeness. Intriguingly, Enceleamycin A is non-hemolytic in nature. Taken together, Enceleamycin A could be a candidate molecule for treating TNBC cells by targeting the AKT2 signaling pathway.

1. Introduction

Cancer is a non-communicable disease and is associated with rapid and uncontrolled cell growth.[1] With approximately twenty million new cases and ten million fatalities in the year 2020, it's the second largest cause of mortality globally. With an estimated 2.3 million new cases, breast cancer has surpassed lung cancer as the most frequently detected cancer.[2,3] Among breast cancer, 10–15% of all cases are from triple-negative breast cancer (TNBC), which is considered more aggressive with a low survival rate. It does not express the three receptors, namely, progesterone (PR), estrogen (ER), and human epidermal growth factor receptor-2 (HER2).[4,5] There are limited options for specific and effective therapy against TNBC due to the absence of validated biomarkers. So chemotherapy is generally used as the standard TNBC treatment, but the prognosis remains poor.[6–8] Considering this, developing new anticancer agents with increased potency and high specificity is essential.

In several kinds of human cancer, an aberration in the PI3K-AKT-mTOR signaling pathway contributes to tumor development.[9] AKT, also known as protein kinase B (PKB), belongs to

a serine–threonine kinase family and is essential for the smooth functioning of this pathway.

In several kinds of human cancer, an aberration in the PI3K-AKT-mTOR signaling pathway contributes to tumor development.[9] AKT, also known as protein kinase B (PKB), belongs to a serine–threonine kinase family and is essential for the smooth functioning of this pathway. Among the three AKT isomers, AKT2 is closely associated with cancer cell metabolism, angiogenesis, proliferation, metastasis, and drug resistance.[10,11]

The elevated AKT2 expression is frequently detected in various human tumors, including breast, lung, prostate, pancreatic, colorectal, and ovarian. Overexpression of AKT2 is correlated with cancer aggressiveness and poor survival rates.[10,12,13] The AKT2 inhibition in breast cancer effectively reduces the colony formation abilities and invasion of non-cancer stem cells (non-CSC) and CSCs.[14] All these functions of AKT2 make this signaling molecule a promising target for cancer therapy.

Naphthoquinones comprise a naphthalene ring system bearing two carbonyl groups, naturally distributed in bacteria, fungi, and plants. They display various biological activities, like anticancer, antibacterial, antifungal, antimalarial, antiviral, antitrypanosomal, and antiinflammatory.[15–20] Naphthoquinone like structures as in Fig. 1 have been approved by FDA and are used in various cancer chemotherapy. Mitomycin (a benzoquinone) is used to treat bladder and anal cancer.[21,22] Anthraquinones, such as doxorubicin, daunorubicin, idarubicin, mitoxantrone, and epirubicin, are commonly used to treat

aNCIM-Resource Center, Biochemical Sciences Division, CSIR-National Chemical Laboratory, Pune – 411008, India. E-mail: sg.dastager@ncl.res.in

bAcademy of Scientific and Innovative Research (AcSIR), Ghaziabad – 201002, India
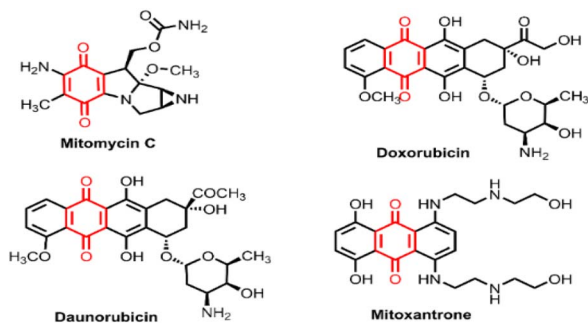
‌

Fig. 1 Structure of anticancer drugs with quinone moiety.[21–23]

various solid and hematologic cancers.[23] Thus, these molecules continue to attract in developing new drugs for cancer therapy.

The primary mechanism of the naphthoquinones is suggested to be reactive oxygen species (ROS) formation in the cell. Cancer cells often have a higher concentration of ROS than normal cells because of the higher metabolic demands; producing even higher amounts of ROS by naphthoquinones in the cell can lead to cell death.[1,24] Also, the pyrano-naphthoquinone molecules like lactoquinomycin, frenolicin B, and kalafungin were found to have selective inhibition towards the serine–threonine kinase AKT.[25] Therefore, the dual-action molecule with the ability to produce ROS and inhibit the AKT2 signaling pathway would result in potent anticancer drug with higher specificity and low resistance.

In our previous study, three novel furo-naphthoquinones, Enceleamycin A–C, were isolated and characterized from rare actinobacteria, *Amycolatopsis* sp. MCC0218 produced under static incubation.[26] As depicted in Fig. 2, Enceleamycin A and B possess an unprecedented pentacyclic oxeto-furo-furo-naphthoquinone structure, with the latter containing a dihydroxylated group, whereas Enceleamycin C has the furo-furo-naphthoquinone skeleton with hydroxy-aldehyde functionalities. The isolated Enceleamycins displayed selective inhibition towards the Gram-positive bacteria.[26]

Based on the anticancer potential of naphthoquinones and the need for novel antineoplastic drug, we have demonstrated the anticancer activity of Enceleamycins against MDA-MB-231, A549, and HeLA cell lines. With the maximum activity, Enceleamycin A was further considered for the ROS formation ability and apoptosis assay in the MDA-MB-231 cells. Moreover, Enceleamycin A displayed binding affinity to the serine–threonine kinase AKT2, determined by the molecular docking and

molecular dynamic (MD) simulation, which was further validated *in vitro*. The molecule's physicochemical and pharmacokinetic characteristics were examined *in silico*, and its hemolytic effect was also established. The findings from our research can stimulate interest in exploring the microbial naphthoquinones as potential anticancer medication by targeting AKT2 kinase signalling pathway.

2. Results and discussion

2.1 Cell viability assay

Previous studies have shown that naphthoquinones exhibit anticancer effects on different types of cancer.[15–17] In order to investigate and compare the anticancer activity of novel furo-naphthoquinones, Enceleamycins A–C, the cytotoxicity was evaluated against triple-negative breast cancer cells (MDA-MB-231), lung cancer cells (A549), cervical cancer cells (HeLa) and HFF cells (non-cancer human foreskin fibroblasts) and Vero (non-cancer monkey kidney epithelial cells) by the MTT assay.[27] Tables 1 and S2† lists the half maximum inhibitory concentration values whereas, the Fig. 3 and S8† shows the dose–response viability in presence of Enceleamycins and doxorubicin at concentrations varying from 0.1 to 100 μg mL^{-1}.

The Enceleamycins displayed strong to moderate inhibitory activity towards these cell lines. The results indicated that Enceleamycin A has potential activity towards the MDA-MB-231 (TNBC cells) with an EC$_{50}$ value of 1.25 μg mL^{-1} (3.78 μM), followed by HeLa and A549 cells with an EC$_{50}$ value of 1.51 (4.57 μM), and 1.98 μg mL^{-1} (5.99 μM), respectively. The EC$_{50}$ value of Enceleamycin A was better than the standard anticancer drug doxorubicin in all the cell lines tested. Furthermore,

Table 1 The IC$_{50}$ (μg mL^{-1}) of Enceleamycin A, B, C and doxorubicin against cancer cells and normal cells by MTT method[d]

	HFF	MDA-MB-231		A549		HeLa	
	CC$_{50}$[a]	EC$_{50}$[b]	SI[c]	EC$_{50}$[b]	SI[c]	EC$_{50}$[b]	SI
A	3.97	1.25	3.17	1.98	2.0	1.51	2.62
B	70.95	23.49	3.02	46.68	1.51	30.53	2.32
C	7.60	2.59	2.93	3.51	2.16	7.27	1.04
Std	8.96	3.28	2.73	2.68	2.83	1.69	4.49

^{a} CC$_{50}$ is the concentration that achieved 50% cytotoxicity. ^{b} EC$_{50}$ is effective concentration that achieved 50% inhibition. ^{c} SI is the selectivity index for the cancer cells with respect to the non-cancer human foreskin fibroblasts (HFF) cells. ^{d} A, B, C: Enceleamycin A, B, C, Std: doxorubicin.
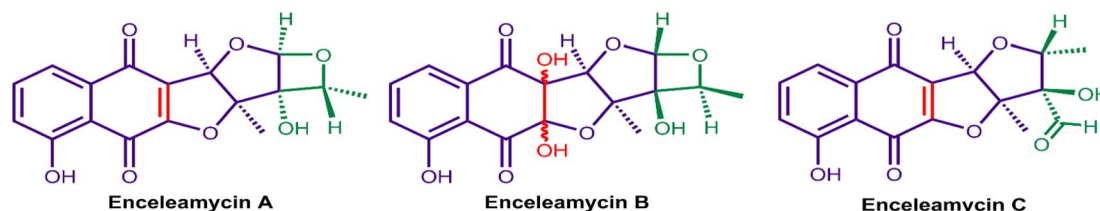

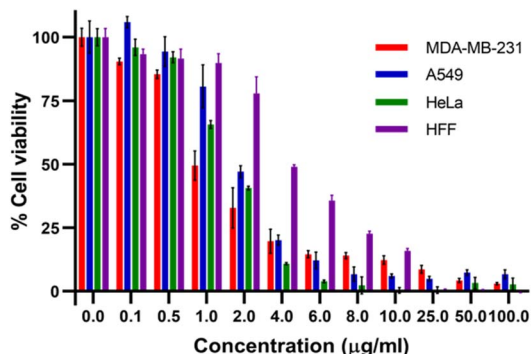**Fig. 2** Structure of Enceleamycin A, B and C isolated from *Amycolatopsis* sp. MCC0218.[26]

Fig. 3 Viability of MDA-MB-231, A549, HeLa and Vero cells after treatment with Enceleamycin A at different concentration from 0.1 to 100 μg mL^{-1}. Data are presented as mean of ±SEM (standard error of the mean), $n = 3$.

Enceleamycin A displayed better inhibitory activity towards the cancer cells compared to the non-cancer HFF cells with selectivity index (SI) in the range of 2.0 to 3.17. The selectivity index of Enceleamycin A against cancer cells with respect to non-cancer Vero cells was in the range of 2.35 to 3.73 (Table S2†). Enceleamycin A exhibited strong anticancer activity, followed by Enceleamycin C, whereas Enceleamycin B showed moderate activity. The potential bioactivity of Enceleamycin A and C may be due to the presence of double bond in the second naphthalene ring, which acts as an electron acceptor and results in formation of semiquinone or hydroquinone. The subsequent reduction of Enceleamycin A and C may result in ROS formation and thereby leading to cell death.[1,24]

With the maximum activity of Enceleamycin A against the MDA-MB-231 cells, the dose–response viability at 4 h, 24 h, and 48 h was determined as shown in Fig. 4. Interestingly, the MDA-MB-231 cell growth was inhibited within 4 hours of treatment by Enceleamycin A with an IC$_{50}$ value of 7.7 μg mL^{-1} (23.3 μM). The difference in inhibition after 24 and 48 h of treatment was not much at lower concentrations up to 2 μg mL^{-1}; however, at 4 μg mL^{-1} and above, maximum inhibition was observed at 48 hours

of treatment. The sulforhodamine B (SRB) assay of Enceleamycin A in Table S1 and Fig. S7† demonstrated lethal activity against nine human cancer cells lines originating from breast, liver, colon, oral, cervical, lung, prostate, ovarian, and leukemia. Similar to the results of MTT assay, Enceleamycin A showed better lethal activity than the anticancer drug adriamycin against most cancer cell lines tested. Furthermore, we selected Enceleamycin A for the evaluation of the probable mode of action against MDA-MB-231 cells and its drug-likeness because of its specific potent activity towards the MDA-MB-231 cells, high yield compared to Enceleamycin B and C,[26] and lack of treatment options for TNBC cells.[5,6]

2.2 Anti-migration assay

Cell migration is crucial during the whole process of cancer development. Cancer cells have the ability to migrate, which is essential to invade surrounding tissues and cause tumor metastasis. The study of cell migration inhibition is appealing as metastatic progression is considered the leading cause of death in cancer patients.[28]

To examine the inhibitory impact of Enceleamycin A on the MDA-MB-231 cell migration, an *in vitro* anti-migration assay was conducted by a scratch/wound healing assay.[29] The images of cell migration in Fig. 5A were recorded in Olympus CKX53 inverted microscope at 0 and 24 hours of treatment and the migration of cells was measured in micrometers using MagVision software. The rate of relative migration for MDA-MB-231 cells treated with Enceleamycin A was 45.25%, 43.01%, 25.55%, and 6.99% at 0 μg mL^{-1}, 0.5 μg mL^{-1}, 1.0 μg mL^{-1} and 2.0 μg mL^{-1} respectively. The migration ability of MDA-MB-231 cells was significantly inhibited with 1.0 and 2.0 μg mL^{-1} concentrations of Enceleamycin A as shown in Fig. 5B. These results demonstrated that Enceleamycin A suppresses the MDA-MB-231 cell's ability to migrate in a concentration-dependent manner.

2.3 Measurements of intracellular reactive oxygen species (ROS)

Since naphthoquinones are known for producing intracellular ROS, we quantified the ROS production after treatment with Enceleamycin A by 2′,7′-dichlorofluorescein diacetate (H2-DCFDA). Cellular esterases deacetylate the cell-permeable dye to a non-fluorescent molecule, which upon oxidation by ROS, transforms into highly fluorescent 2′,7′-dichlorofluorescein (DCF).[30] These ROS at lower concentration plays a vital role in the homeostasis of cells; however, when in excess, it leads to the death of cells through apoptosis.[31,32] In the ROS assay, the MDA-MB-231 cells in the presence of Enceleamycin A demonstrated a relative increase in fluorescence intensity at 24 and 48 hours as the concentration was raised from 2 to 50 μg mL^{-1} compared to the untreated control. The graph in Fig. 5C displayed MDA-MB-231 cells after treatment with Enceleamycin A resulted in concentration and time-dependent increase in intracellular levels of ROS. It is known that excessive ROS formation within the cell can induce apoptosis and results in cell death.
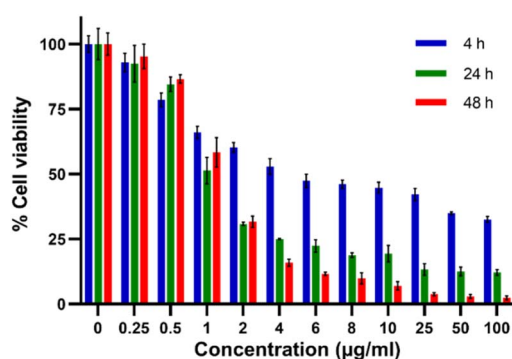

Fig. 4 Dose dependent cell viability of MDA–MB-231 cells at 4, 24 and 48 h treatment with Enceleamycin A. Cell growth inhibition was observed within 4 h treatment with IC50 value of 7.7 μg mL^{-1} (23.3 μM). Data are presented as mean of ±SEM (standard error of the mean), $n = 3$.
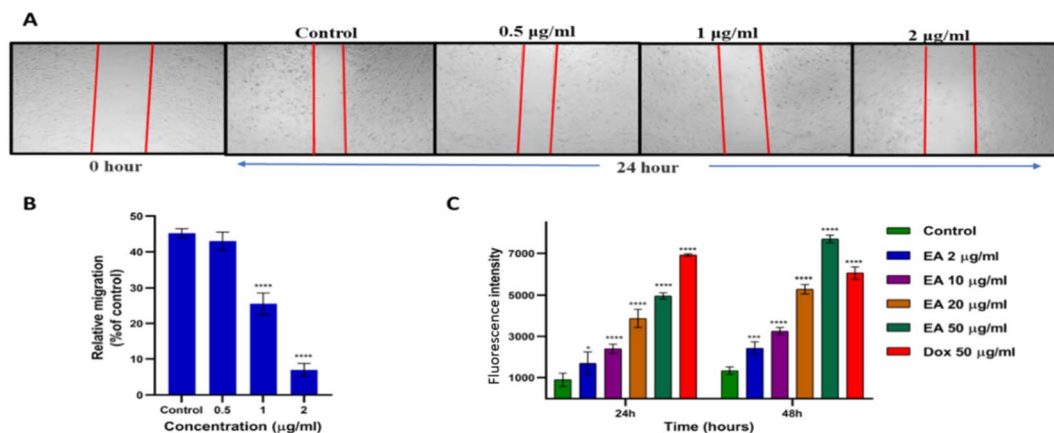
Fig. 5 Enceleamycin A effect on the migration and ROS formation ability in MDA-MB-231 cells. (A) Migration of MDA-MB-231 cells in presence of Enceleamycin A at 0, 0.5, 1 and 2 μg mL^{-1} after 24 hours. (B) Statistical data analyses for MDA-MB-231 cells mobility in presence of Enceleamycin A at 0 (control), 0.5, 1 and 2 μg mL^{-1} after 24 hours. One-way ANOVA Dunnett test was used to determine statistical significance; ****$p < 0.0001$. Data are presented as mean of ±SEM (standard error of the mean), $n = 3$. (C) Statistical data analyses of ROS formation by MDA-MB-231 cells after treatment with Enceleamycin A (EA) at 24 and 48 hours. Two-way ANOVA Dunnett test was used to determine statistical significance; *$p < 0.05$, **$p < 0.01$, ***$p < 0.001$, ****$p < 0.0001$. Data are presented as mean of ±SEM (standard error of the mean), $n = 3$.

2.4 Apoptosis detection in MDA-MB-231 cells

To determine whether the ROS production by Enceleamycin A in MDA-MB-231 cells results in apoptotic cell death, we perform the apoptosis assay using flow cytometry. The apoptotic analysis in cancer cells is based on the movement of phosphatidylserine from the inner membrane to the outer membrane, which eventually recognizes by Annexin V. In Fig. 6A, the scatter plot for control and treated cells was demonstrated with four distinct populations of unstained for viable cells, Annexin V-Alexa flour for early apoptotic cells, and Annexin V/propidium iodide dual stained for late apoptotic cells.[33] The early/late apoptosis ratio shown in Fig. 6B was 25.8%/2.45%, 49.7%/ 10.7%, 58.4%/14.85, and 60.65%/19.2% at the concentration 0, 2, 4, and 8 μg mL^{-1} respectively, after 48 hours of treatment with Enceleamycin A. These observations demonstrated the concentration-dependent apoptosis in the MDA-MB-231 cells by Enceleamycin A.

2.5 Molecular docking

The inhibitory activity of the novel ligand Enceleamycin A against the intended protein target of the PI3K-AKT-mTOR pathway was examined using molecular docking. The protein target considered for molecular docking were PI3Kα (4TV3), AKT1 (3O96), AKT2 (1O6L), mTOR (1E7U), and S6K1 (3A62). The top rank from the cluster of a receptor with the lowest binding energy and 0 RMSD was considered appropriate for visualizing the interactions between the protein and ligand complex. The details of the best molecular fit conformations were displayed by Autodock 4.2.6 (ref. 34 and 35) and the best molecular fit pose was visualized by Biovia discovery studio v20.1.0.19295.[36,37] Enceleamycin A displayed better binding affinity with AKT2 compared to the other proteins of PI3K-AKT pathway shown in Tables S3, S4 and Fig. S10.† The binding energy calculated was −7.14 kcal mol^{-1} for the

docked complex. The non-bond interactions gave us information about active sites, the nature of bonding, the distance between the native ligand and the protein, and the donor and acceptor atoms. The active sites of the interacting Enceleamycin A and AKT2 displayed in Fig. 7C and Table S5,† were Lys 181, Glu 200, Gly 295, Asp 293, Glu 193, Phe 163, Leu 183, Lys 191, which signifies that the novel ligand is interacting with the A polypeptide chain of AKT2 protein. The interaction distance of active site Lys 181 and Glu 200 was of 2.2 and 2.0 Å, respectively in Fig. 7D by conventional hydrogen bonding. The other interactions include the carbon hydrogen bond for Gly 295 and Asp 293, electrostatic pi–anion for Glu 193, hydrophobic pi–pi stacked for Phe 163, hydrophobic alkyl for Leu 183 and hydrophobic pi–alkyl for Lys 191. Fig. 7E and Table S5† displays the hydrogen bond donor and acceptor details of the interacting complex of Enceleamycin A and AKT2 in which Lys 181 acts as a H-bond donor and Glu 200 as an H-bond acceptor.

To further validate the docking method, the AKT2 (1O6L) protein was re-docked with the native ligand AMP-PNP (phosphoaminophosphonic acid-adenylate ester). Both re-docked, and native ligands interacted with the protein AKT2 with significant overlap and resemblance as shown in Fig. 7F. The RMSD (root mean square deviation) value of the interactions was computed by the DockRMSD and found to be 1.262 Å, considered a reliable docking procedure since the value was <2.0 Å.[38] The RMSD value calculated for the superimposed ligand conformation using LS-align was 0.684 Å, which is <1 Å denotes strongly aligned atom pairs.[39]

2.6 MD simulation analysis

Molecular dynamics (MD) simulation is a computational tool for drug development. It is extensively used to investigate how the molecules shift their form and interact with other molecular species in a variety of environments.[40] To confirm
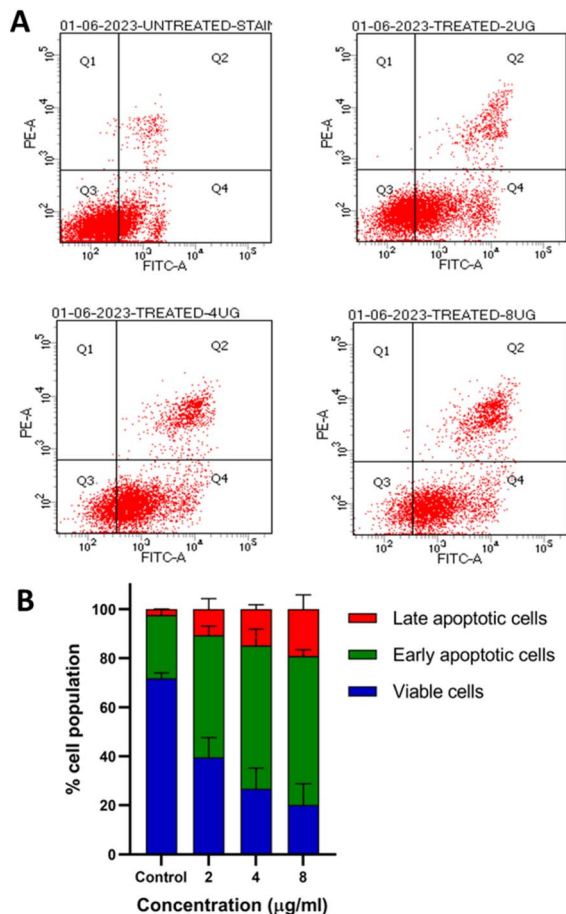
Fig. 6 Apoptosis detection in MDA-MB-231 cells after treatment with Enceleamycin A. (A) Enceleamycin A effect on apoptosis of MDA-MB-231 cells based on Annexin V-Alexa flour-488 and PI staining. The cell stages were given as viable-Q3, early apoptotic-Q4 and late apoptotic-Q2. (B) Percentage of viable, early and late apoptotic cells in the population based on flow cytometry data analysis. Data are presented as mean of $\pm$SEM (standard error of the mean), $n = 3$.

the structural stability of the docked complex of Enceleamycin A and AKT2, MD simulations were run for 100 ns using GROMACS package. Molecular mechanics Poisson–Boltzmann surface area (MM-PBSA), a technique for determining binding free energy of protein–ligand complexes, has become more popular. The MM-PBSA technique was implemented via the g_mmpbsa tool[41] by which the binding energy of -10.481 ± 3.398 kcal mol^{-1} was observed as shown in Table S6† during the run of 100 ns demonstrating the potential affinity between the Enceleamycin A and AKT2. For the evaluation of stability of the simulated systems, the trajectories produced after the simulations were analyzed to determine RMSD for backbone atom, Root mean square fluctuation (RMSF) for C-alpha, radius of gyration (R_g) and interacting hydrogen bonds.

RMSD calculates the variation between the protein's starting location and final structure. The RMSD values displayed low fluctuation throughout the 100 ns period, and were almost constant from around 70 to 100 ns demonstrating the structural stability of the protein–ligand complex

in Fig. 8A. The protein–ligand interactions appear energetically advantageous and contribute to the complexes' stability based on the low RMSD values. RMSF, which evaluates the flexibility of each residue over time, may be used to determine the variations in the protein residues. The RMSF score estimates the stability of protein–ligand complexes, with larger values suggesting less stability and greater flexibility. The major fluctuation was observed only in the designated A (150–170) and B (305–325) region of protein loop which is conserved structurally and functionally for the serine and threonine kinase family[42] shown in Fig. 8B. This major fluctuation might be due to the inhibition of AKT2 by Enceleamycin A affecting the phosphorylation responsible for protein functionality.

The understanding of protein's radius of gyration (R_g) is essential to comprehend the effect of inhibitors on the compactness of protein. In our simulation, the radius of gyration was found to be 2.17 and displayed lesser deviation throughout the 100 ns run as depicted in Fig. 8C. The intermolecular H-bonds between interacting atom pairs impacts the stability and molecular recognition process of protein–ligand complex's. To ascertain the dynamic stability of complex, the number of H-bonds interacting with the ligand and receptor protein was measured over the 100 ns run. In Fig. 8D, the hydrogen bond interaction was observed throughout the 100 ns run and the interaction was increased from 70 ns onwards. Hydrogen bond occupancy was similar to the results inferred from molecular docking, with Lys 181 occupying 16.08%, followed by Glu 200 occupying 10.79% during the MD run. Thus, it appears that the predicted system is stable.

2.7 ADP-Glo kinase assay

An *in vitro* assay using the AKT2 kinase enzyme system was conducted to confirm further the *in silico* binding affinity and stability of the docked complex of Enceleamycin A and AKT2.[43] The ADP generated during the reaction is measured by the ADP-GloTM Kinase. In the subsequent luciferase reaction, the newly produced ADP is transformed into ATP and generates light. The light generated correlates with the kinase activity. A concentration of less than 1 µg mL^{-1} of Enceleamycin A proved efficient in inhibiting the AKT2 enzyme. Enceleamycin A displayed an IC$_{50}$ value of 0.736 µg mL^{-1} (2.22 µM) for AKT2 as shown in Fig. 9, consistent with a prior study showing that pyrano-naphthoquinones specifically inhibit the AKT kinase enzyme. However, the potential enzyme inhibition activity was comparatively less compared to pyrano-naphthoquinones.[25] With further in-depth research, Enceleamycin A can be used as a dual-action anticancer molecule with ROS formation and AKT2 inhibition to reduce the metastasis and invasiveness of cancer.

2.8 Pharmacokinetics and physicochemical properties

The anticancer candidate molecule should have an approving biopharmaceutical property since it will interact with various cells and macromolecules inside the body. A molecule's
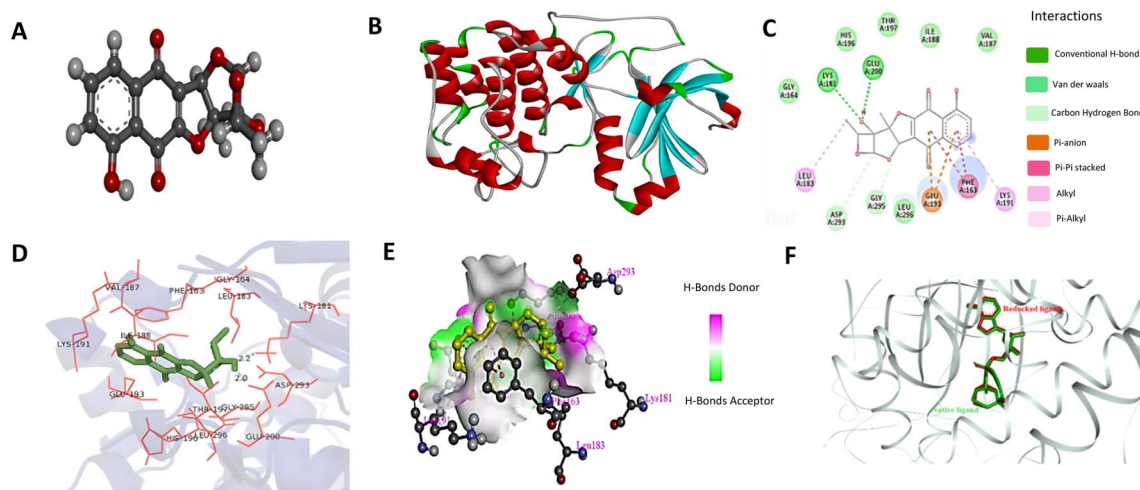
Fig. 7 Molecular docking of Enceleamycin A with AKT2 protein and docking validation. (A) Enceleamycin A in protein databank (pdb) format where red indicates oxygen atom, light grey represents hydrogen atom and dark grey represents carbon atom, (B) AKT2 (1O6L) receptor, where α-helices are denoted in red, β-sheets in yellow, and turns & loops in green. (C) Two-dimensional diagram of the docked complex (AKT2 and Enceleamycin A) showing the active sites and the type of interactions. (D) Three-dimensional diagram displaying the interaction of active site Lys 181 and Glu 200 with distance of 2.2 and 2.0 Å, respectively. (E) Three-dimensional diagram with hydrogen bond display of the interacting complex, where the pink shade represents the H-bond donor and green shade represents the H-bond acceptor. (F) Docking validation of native ligand AMP-PNP to AKT2 (1O6L) and displaying the super-imposition of the redocked native ligand protein complex.

acceptable ADMET (absorption, distribution, metabolism, excretion, and toxicity) characteristics are necessary for its consideration as a lead molecule for therapeutic application. The physicochemical and ADMET of Enceleamycin A was evaluated by the SwissADME[44] and pkCSM[45] webtool. The bioavailability radar in Fig. 10A, displays that the molecule falls under the optimum physicochemical properties

(lipophilicity, size, polarity, insolubility, saturation, and flexibility). A molecule should follow Lipinski's[46] and Veber's[47] rules for drug-like properties. Enceleamycin A comes under all the designated Lipinski's rule of five (mol. wt < 500 Daltons, no. of hydrogen H-bond acceptors < 10, no. of H-bond donors < 5, octanol–water partition coefficients log P < 5 and molar refractivity < 140) and Veber's rule (topological
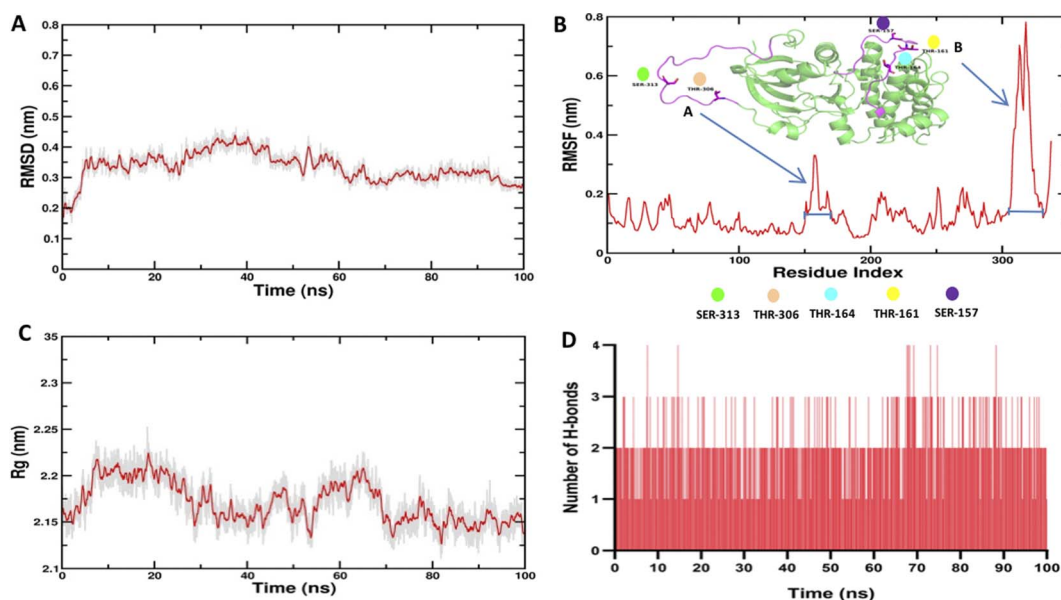
Fig. 8 Plots displaying the MD simulation data of simulated complex (Enceleamycin A with AKT2 protein) for the 100 ns simulation. (A) Plot displaying the RMSD values of simulated complex for 100 ns. (B) Plot displaying the RMSF value of simulated complex for 100 ns where labeling in the residue index region ranging from 150 to 170 and 305 to 325 correlates with the designated A and B loop in pink colour. These loops contain serine and threonine residues responsible for phosphorylation that shows the higher fluctuation. (C) Plot displaying the radius of gyration (R_g) of simulated complex for 100 ns. (D) Plot displaying the number of hydrogen bonds interacting within the simulated complex for 100 ns.

Fig. 9 AKT2 kinase inhibition by Enceleamycin A with IC_{50} value of 0.736 μg mL^{-1} (2.22 μM). Data are presented as mean of $\pm$SEM (standard error of the mean), $n = 3$.

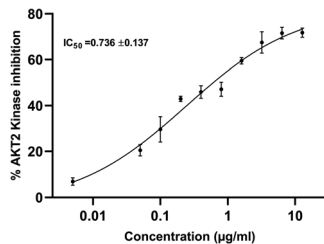**Table 2** Physicochemical property of Enceleamycin A using SwissADME

Physicochemical properties	
Formula	$C_{17}H_{14}O_7$
Molecular weight	330.29 g mol^{-1}
Number of heavy atoms	24
Number of aromatic heavy atoms	6
Number of rotatable bonds	0
Number H-bond acceptors	7
Number of H-bond donors	2
log P	2.05
Molar refractivity	78.07
TPSA	102.29 Å

polar surface area < 140 Å and no. of rotatable bonds < 10) as displayed in Table 2, which signifies its drug likeliness property. The pharmacokinetics displayed in the boiled-egg ADME profile in Fig. 10B and Table 3 shows that the gastro-intestinal tract effectively absorbed the molecule and did not penetrate the blood–brain barrier (BBB). The non-permeability of BBB signifies the molecule theoretically does not have side effects on the central nervous system.[48]

Furthermore, the molecule did not inhibit the P-glycoprotein and CYP-450 class of enzymes, thus having a lower chance of corresponding drug interaction.[48] The toxicity of molecules can damage organs and fail in late-stage drug development. So the toxicity of Enceleamycin A was evaluated by the pkCSM web tool, where the compound was negative to the Ames test, which assesses the carcinogenic effect. The molecule was non-hepatotoxic, not sensitive to skin, and a non-inhibitor of hERG I and II.

In addition to Enceleamycin A, the physicochemical and pharmacokinetics of Enceleamycin B and C was also evaluated as shown in Fig. S11, S12 and Tables S7–S14.† The Enceleamycin A displayed most acceptable physicochemical properties

Table 3 Pharmacokinetics property of Enceleamycin A using SwissADME and pkCSM webtool

Pharmacokinetic properties	
GI absorption	Yes
BBB permeation	No
P-Glycoprotein substrate	Yes
P-Glycoprotein inhibitor	No
CYP-450 class enzyme inhibitor	No
hERG I and II inhibitor	No
log K_p (skin permeation)	-7.79 cm s^{-1}
AMES toxicity	No
Hepatotoxicity	No
Skin sensitisation	No

and lowest toxicity followed by Enceleamycin C and B. Based on these *in silico* findings, Enceleamycin A displayed desirable drug-likeness properties for a potential therapeutic candidate.
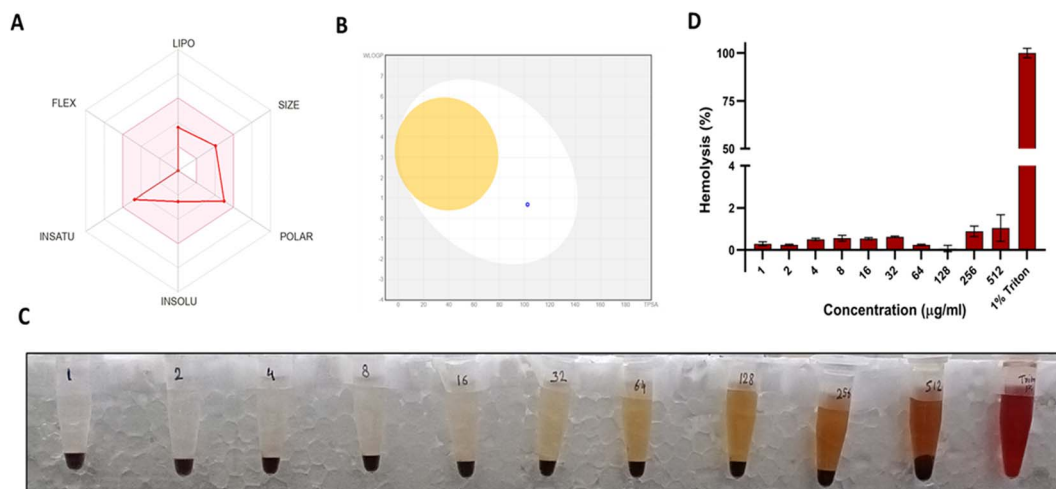
Fig. 10 ADME property and hemolysis of Enceleamycin A. (A) Bioavailability radar of Enceleamycin A. (B) Boiled-egg ADME profile where white egg part shows the gastro-intestinal absorption and yellow yolk part shows the blood–brain barrier permeability, whereas the horizontal axis displays TPSA value and vertical axis shows the log P value. The blue dot represents Enceleamycin A. (C) Hemolysis assay of Enceleamycin A demonstrating the intact pellet of red blood cells. (D) Percentage of hemolysis of RBCs by Enceleamycin A displaying less than 2% hemolysis at highest tested concentration of 512 μg mL^{-1} (1550.15 μM). Data are presented as mean of $\pm$SEM (standard error of the mean), $n = 3$.

3. Conclusions

The present study investigated the anticancer potential of three novel furo-naphthoquinones, Enceleamycin A, B and C previously isolated by our group from *Amycolatopsis* sp. Of the three, Enceleamycin A showed prominent anticancer properties, particularly against the MDA-MB-231 (TNBC) cells with an IC_{50} value of 1.25 μg mL^{-1} (3.78 μM). It also inhibits the cell migration ability of TNBC cells. The treatment of MDA-MB-231 cells by Enceleamycin A increases intracellular ROS formation, leading to apoptotic cell death, demonstrated by flow cytometry analysis. Molecular docking and MD simulation showed that Enceleamycin A can be a potential AKT2 inhibitor candidate. The *in silico* investigation was validated by the *in vitro* AKT2 enzyme assay, in which Enceleamycin A exhibited IC_{50} value of 0.73 μg mL^{-1} (2.22 μM). According to *in silico* physicochemical and ADMET studies, Enceleamycin A showed good bioavailability and did not violate Lipinski's rule of five, making it a candidate drug-like molecule. The compound showed no prominent hemolytic effect on human RBCs. Altogether, this study presents essential insights about Enceleamycin A possessing therapeutic potential for cancer treatment, particularly triple-negative breast cancer cells.

4. Experimental

4.1 Materials

Enceleamycin A ($C_{17}H_{14}O_7$), B ($C_{17}H_{16}O_9$) and C ($C_{17}H_{14}O_7$), used in the experiments were isolated in our previous study from *Amycolatopsis* sp. MCC 0218.[26] Heat-inactivated FBS (Fetal bovine serum) and DMEM (Dulbecco's modified eagle's medium) were obtained from GIBCO. Trypsin EDTA and 3-(4,5-dimethylthiazol-2-yl)-2,5-diphenyl tetrazolium bromide (MTT) were purchased from Himedia. Standard doxorubicin and H2-DCFDA dye was purchased from Sigma. MDA-MB-231, A549, HeLa, HFF and Vero cells were obtained from NCCS (National Center for Cell Science), Pune.

4.2 Cell viability assay

The MTT assay, which measures cellular metabolic activity, was used to examine cell viability.[27] The cell lines used for the study were MDA-MB-231, A549, HeLa, HFF and Vero. DMEM with 10% FBS was the media used for the growth and assay of all the cells. The seeding of 10 000 cells per well was done of these cells in 96-well plate and incubated at 37 °C with 5% CO_2 for 20 hours. The stock solution of 20 mg mL^{-1} was made of compounds Enceleamycin A, B and C in dimethyl sulfoxide (Hi-Media, Mumbai). The stock solution of the compounds were diluted to 1 mg mL^{-1} in complete medium (DMEM + 10% FBS) and was further diluted to 100 μg mL^{-1} and 10 μg mL^{-1} working solution in DMEM media. The final DMSO concentration at the highest concentration tested at 100 μg mL^{-1} was 0.5% *i.e.* below toxicity level and was used as a negative control. The stock solution of 20 mg mL^{-1} of the standard drug doxorubicin was made in MQ water, filter sterilized and further diluted to working solution in complete media similar to the Enceleamycins. The cells were treated with different concentrations of compound in the range of 0.1 to 100 μg mL^{-1} for 48 hours. 100 μL of MTT solution (0.5 mg mL^{-1}) was added after the media was removed, and the solution was incubated for 4 h at 37 °C in the dark. Subsequently, the MTT solution was decanted, and the solubilization of formazan crystals was done by adding 100 μl DMSO. Biotek synergy H1 microplate reader was used to capture the reading at 570 nm. In addition, inhibition of MDA-MB-231 cells was determined for Enceleamycin A at 4, 24, and 48 h for the time point study.

4.3 Anti-migration assay

To estimate the anti-migration impact of Enceleamycin A on MDA-MB-231 cells, a scratch/wound healing assay was conducted.[28,29] In a 24-well plate, 1.5×10^5 cells per well were seeded in DMEM (10% FBS). After the confluency, linear gaps were scratched at the bottom of the plate by a sterile micropipette tip (200 μL), and the detached cells were subsequently eliminated with 1× phosphate buffer saline (PBS). The adherent cells on the plate were incubated with Enceleamycin A (0.5, 1, and 2 μg mL^{-1}) in serum-free DMEM media for 24 hours at 37 °C with 5% CO_2 to eliminate the interference of cell proliferation. The wound images were obtained using an inverted microscope at 0 and 24 h, respectively, and the % of cell migration was calculated with reference to scratch width (SW) at 0 h and 24 h: (SW at 0 h − SW at 24 h/SW at 0 h) × 100.

4.4 Measurement of intracellular ROS

The intracellular ROS production level was assessed by the 2′,7′-dichlorofluorescein diacetate (H2-DCFDA) dye.[30] In brief, seeding 1×10^4 cells per well of MDA-MB-231 cells was done in 96-well plate and kept for 24 hours. After being washed with DPBS, the cells were incubated at 37 °C in the dark for 30 minutes with H2-DCFDA (20 μM) in DMEM complete media. The culture was treated with a varying concentration of Enceleamycin A (2, 10, 20, and 50 μg mL^{-1}) in DMEM complete media for 24 and 48 h. After incubation, RFU was measured at 485/535 (excitation/emission) in a micro-plate reader.

4.5 Apoptosis detection in MDA-MB-231 cell line

The apoptotic-like features in MDA-MB-231 cells after treatment with Enceleamycin A were estimated by Alexa Fluor® 488 Annexin V/Dead Cell Apoptosis Kit (ThermoFisher Scientific).[33] In brief, seeding of 3.5×10^5 cells per well of MDA-MB-231 cells was done in a 6-well plate and enable to grow overnight. The culture was treated with Enceleamycin A (2, 4, and 8 μg mL^{-1}) for 48 h. After being washed with binding buffer (1×), the cells were stained for 30 min by Alexa Flour Annexin V and propidium iodide at 37 °C in the dark. Stained cells were assessed for the percentage of apoptotic cells relative to untreated and unstained cells by flow cytometry.

4.6 Docking analysis

Canonical SMILES of the novel ligand, Enceleamycin A, were converted to protein data bank format using Open Babel

software. The 3-dimensional structure of the PI3K-AKT-mTOR pathway receptors was retrieved from the Protein Data Bank. Water molecules, native ligands, and other heteroatoms from the protein were removed using PyMOL (v.1.74) before docking. Molecular docking was performed using Autodock 4.2.6.[34,35] The final DLG file contained important details, *viz.*, top ten conformations for every run consisting of rank, free binding energy (kcal mol^{-1}), mean RMSD, and inhibitory constant (μM). The docking parameter was analyzed based on the lowest binding energy of the ligand–protein complex. Autodock tools 4.2.6, Discover Studio v20.1.0.19295 from Biovia, and PyMOL v.1.74 were used in molecular docking to visualize and study the two-dimensional, three-dimensional and surface annotation of Enceleamycin A interaction with the protein.[36,37] The docked complex was validated by redocking of AKT2 with native ligand, and the RMSD value was calculated from the DockRMSD[38] and LS-align web tool.[39]

4.7 Molecular dynamics simulations

MD simulation of the docking complex was carried out with reading biomolecular coordinates, solvation of desired protein, setting periodic boundary conditions, and generating the input files for equilibration and production using the Gromacs v 2020.6 and visualization and analysis using VMD v 1.9.3 and PyMOL v 1.7.4.5 software. The ligand Protein interaction, having the lowest binding energy, from molecular docking is considered for MD simulation. The novel ligand bound to the AKT2 receptor was analyzed using the GROMOS 54A7 force field of the GROMACS simulation software. With the help of MOD-ELLER9 v 14,[51] the missing residues from the crystal structure's 1O6L (Ile450, Thr451, Pro452, Pro453, Asp454, Arg455, Tyr456, Asp457, Ser458, Leu459, Gly460, Leu461, Leu462, Glu463, Leu464, Asp464, Gln464, Arg464, Glu465, Glu466) were put back together. By using the Automated Topology Builder (ATB) repository, the force fields of the ligand was created.[52] Hydrogen was added to the heavy atoms using the GROMACS module pdb2gmx. The structures were then solvated within cubic periodic box with water stretching 2 Å on all sides outside the protein by applying the simple point charge (SPCE) water model.[53] After that, systems were maintained with an appropriate salt concentration of 0.15 M by introducing suitable amount of Na$^+$ and Cl$^-$ ions to neutralize the system. The steepest descent method was subsequently employed to minimize the energy of all systems in the solvated state over a time frame of 2000 steps. To perform equilibration in the NVT (no. of atoms, volume, and temperature) ensemble, the systems were then gradually heated to a temperature of 310 K by a V-rescale thermostat with a 0.1 ps coupling constant.[54] Further to achieve equilibration in the NPT (no. of atoms, pressure, and temperature) ensemble, the Parrinello–Rahman barostat was implemented to keep solvent density at 1 bar and 310 K with 0.1 ps coupling constant. To check the stability of protein and ligand complex, the resultant each structure generated from NPT equilibration phase was utilized for final NPT ensemble production run for 100 ns simulation.[55]

4.8 ADP-Glo kinase assay

The AKT2 kinase activity was measured in the presence of Enceleamycin A by employing ADP-Glo kinase assay and the AKT2 Kinase enzyme system (Promega). The assay is based on quantifying ADP produced during the kinase reaction. The reaction was done in 96-well plates in which 10 μL of AKT2 (10 ng), 5 μL of modified AKT substrate (1 μg), 5 μL of ATP (50 μM), and 5 μL of inhibitor was added followed by an hour-long incubation at ambient temperature. To terminate the kinase reaction, 5 μL of the ADP-Glo reagent was applied for 40 min. At last, 10 μL of kinase detection reagent was added and left for 30 min. Biotek synergy H1 microplate reader detected the luminescence. The relative activity (%) of kinase was calculated compared to the control without an inhibitor.[43]

4.9 Physicochemical and pharmacokinetics analysis

In silico physicochemical and pharmacokinetic properties were detected for Enceleamycins using the SwissADME online program.[44] The SMILES notations generated from ChemDraw 20.0 was submitted as an input file to the SwissADME web tool, which provides a reliable prediction of physicochemical (TPSA, number of hydrogen bond acceptor and donor, and solubility), pharmacokinetics (GI absorption, BBB permeability, and CYP inhibitor) and drug-likeness (Lipinski's rule of five and Veber's rule) properties. In addition, the toxicity profile, like the Ames test, skin sensitivity, and hepatotoxicity, was generated by the pkCSM web tool.[45]

4.10 Hemolysis assay

Hemolytic activity of Enceleamycin A was performed on the RBCs of human blood sample. The blood sample of 5 mL was decanted after being centrifuged at 5000 rpm for 10 min. The RBCs were suspended in Phosphate buffer saline (PBS) and washed three times by centrifugation for 10 min at 5000 rpm, and the pelleted RBCs were resuspended in 25 mL of PBS. The compound was twofold diluted in PBS and added to RBCs suspension to achieve concentrations varying from 1 to 512 μg mL^{-1}. Triton X-100 (1% v/v) and DMSO (0.5%) in PBS were considered positive and negative controls, respectively. The treated suspensions were kept for 60 min at 37 °C and centrifuged at 5000 rpm for 10 minutes. The resultant supernatant was added to the 96-well plate with a flat bottom. At 570 nm, the absorbance was measured, and the relative percentage of hemolysis was estimated compared to the suspension treated with 1% Triton X-100. The following equation calculates the percent of hemolysis: % hemolysis = [absorbance of the sample (treated with Enceleamycin A)] ÷ [absorbance of the positive control (treated with 1% Triton X-100)] × 100.[49,50]

Author contributions

AK: conceptualization, investigation, methodology, and writing – original draft. SP: investigation and methodology. SGD: supervision, resources, writing – review & editing.

Conflicts of interest

There are no conflicts to declare.

Acknowledgements

Notes and references

1 K. W. Wellington, *RSC Adv.*, 2015, **5**, 20309–20338.
2 H. ur Rashid, Y. Xu, Y. Muhammad, L. Wang and J. Jiang, *Eur. J. Med. Chem.*, 2019, **161**, 205–238.
3 H. Sung, J. Ferlay, R. L. Siegel, M. Laversanne, I. Soerjomataram, A. Jemal and F. Bray, *Ca-Cancer J. Clin.*, 2021, **71**, 209–249.
4 D. Karakaş, R. O. Akar, Z. Gökmen, N. G. Deniz and E. Ulukaya, *Turk. J. Biol.*, 2019, **43**, 256–263.
5 L. Yin, J. J. Duan, X. W. Bian and S. C. Yu, *Breast Cancer Res.*, 2020, **22**, 1–13.
6 H. Yao, G. He, S. Yan, C. Chen, L. Song, T. J. Rosol and X. Deng, *Oncotarget*, 2017, **8**, 1913.
7 X. T. Le, J. Lee, N. T. Nguyen, W. T. Lee, E. S. Lee, K. T. Oh, H. G. Choi, B. S. Shin and Y. S. Youn, *Biomater. Sci.*, 2022, **10**, 7117–7132.
8 C. D. Mock, B. C. Jordan and C. Selvam, *RSC Adv.*, 2015, **92**, 75575–75588.
9 J. R. Testa and A. Bellacosa, *Proc. Natl. Acad. Sci. U. S. A.*, 2001, **98**, 10983–10985.
10 P. G. Rychahou, J. Kang, P. Gulhati, H. Q. Doan, L. A. Chen, S. Y. Xiao, D. H. Chung and B. M. Evers, *Proc. Natl. Acad. Sci. U. S. A.*, 2008, **105**, 20315–20320.
11 T. Liu, J. Zhu, W. Du, W. Ning, Y. Zhang, Y. Zeng, Z. Liu and J. A. Huang, *Respir. Res.*, 2020, **21**, 1–15.
12 M. Riggio, M. C. Perrone, M. L. Polo, M. J. Rodriguez, M. May, M. Abba, C. Lanari and V. Novaro, *Sci. Rep.*, 2017, **7**, 44244.
13 A. Bellacosa, D. De Feo, A. K. Godwin, D. W. Bell, J. Q. Cheng, D. A. Altomare, M. Wan, L. Dubeau, G. Scambia, V. Masciullo and G. Ferrandina, *Int. J. Cancer*, 1995, **64**, 280–285.
14 P. Gener, D. Rafael, J. Seras-Franzoso, A. Perez, L. Alamo Pindado, G. Casas, D. Arango, Y. Fernández, Z. V. Díaz-Riascos, I. Abasolo and S. Schwartz Jr, *Cancers*, 2019, **11**, 1058.
15 R. Inagaki, M. Ninomiya, K. Tanaka and M. Koketsu, *ChemMedChem*, 2015, **10**, 1413–1423.
16 M. M. Rahman, M. R. Islam, S. Akash, S. Shohag, L. Ahmed, F. A. Supti, A. Rauf, A. M. Aljohani, W. Al Abdulmonem, A. A. Khalil and R. Sharma, *Chem.-Biol. Interact.*, 2022, **368**, 110198.
17 E. Leyva, L. I. López, R. F. G. de la Cruz and C. G. Espinosa-González, *Res. Chem. Intermed.*, 2017, **43**, 1813–1827.
18 V. S. de Sena Pereira, F. da Silva Emery, L. Lobo, F. Nogueira, J. I. Oliveira, U. L. Fulco, E. L. Albuquerque, A. M. Katzin and V. F. de Andrade-Neto, *Malar. J.*, 2018, **17**, 1–11.
19 X. Li and Y. Song, *Eur. J. Med. Chem.*, 2023, **260**, 115772.
20 M. H. Khraiwesh, C. M. Lee, Y. Brandy, E. S. Akinboye, S. Berhe, G. Gittens, M. M. Abbas, F. R. Ampy, M. Ashraf and O. Bakare, *Arch. Pharm. Res.*, 2012, **35**, 27–33.
21 P. Milla, C. Fiorito, F. Soria, S. Arpicco, L. Cattel and P. Gontero, *Cancer Chemother. Pharmacol.*, 2014, **73**, 503–509.
22 A. Vinayan and R. Glynne-Jones, *Best Pract. Res. Clin. Gastroenterol.*, 2016, **30**, 641–653.
23 G. N. Hortobagyi, *Drugs*, 1997, **54**, 1–7.
24 Y. Kumagai, Y. Tsurutani, M. Shinyashiki, S. Homma-Takeda, Y. Nakai, T. Yoshikawa and N. Shimojo, *Environ. Toxicol. Pharmacol.*, 1997, **3**, 245–250.
25 E. J. Salaski, G. Krishnamurthy, W. D. Ding, K. Yu, S. S. Insaf, C. Eid, J. Shim, J. I. Levin, K. Tabei, L. Toral-Barza and W. G. Zhang, *J. Med. Chem.*, 2009, **52**, 2181–2184.
26 A. Khan, M. S. Said, B. R. Borade, R. Gonnade, V. Barvkar, R. Kontham and S. G. Dastager, *J. Nat. Prod.*, 2022, **85**, 1267–1273.
27 T. Mosmann, *J. Immunol. Methods*, 1983, **65**, 55–63.
28 C. R. Justus, N. Leffler, M. Ruiz-Echevarria and L. V. Yang, *J. Vis. Exp.*, 2014, **88**, e51046.
29 C. Luo, Y. Wang, C. Wei, Y. Chen and Z. Ji, *Exp. Ther. Med.*, 2020, **19**, 273–279.
30 N. S. Ng and L. Ooi, *Bio-Protoc.*, 2021, **11**, e3877.
31 L. Sun, C. Luo and J. Liu, *Food Funct.*, 2014, **5**, 1909–1914.
32 M. Redza-Dutordoir and D. A. Averill-Bates, *Biochim. Biophys. Acta, Mol. Cell Res.*, 2016, **1863**, 2977–2992.
33 C. M. Worsley, R. B. Veale and E. S. Mayne, *PLoS One*, 2022, **17**, e0270599.
34 S. S. Azam and S. W. Abbasi, *Theor. Biol. Med. Model.*, 2013, **10**, 1–16.
35 G. M. Morris, R. Huey, W. Lindstrom, M. F. Sanner, R. K. Belew, D. S. Goodsell and A. J. Olson, *J. Comput. Chem.*, 2009, **30**, 2785–2791.
36 A. K. Umar, J. H. Zothantluanga, K. Aswin, S. Maulana, M. S. Zubair, H. Lalhlenmawia, M. Rudrapal and D. Chetia, *Struct. Chem.*, 2022, **33**, 1445–1465.
37 Y. D. Gao and J. F. Huang, *Dongwuxue Yanjiu*, 2011, **32**, 262–266.
38 E. W. Bell and Y. Zhang, *J. Cheminf.*, 2019, **11**, 40.
39 J. Hu, Z. Liu, D. J. Yu and Y. Zhang, *Bioinformatics*, 2018, **34**, 2209–2218.
40 H. M. De Vivo, M. Masetti, G. Bottegoni and A. Cavalli, *J. Med. Chem.*, 2016, **59**, 4035–4061.
41 R. Kumari, R. Kumar, Open Source Drug Discovery Consortium and A. Lynn, *J. Chem. Inf. Model.*, 2014, **54**, 1951–1962.
42 J. Yang, P. Cron, V. M. Good, V. Thompson, B. A. Hemmings and D. Barford, *Nat. Struct. Mol. Biol.*, 2002, **9**, 940–944.
43 H. Zegzouti, M. Zdanovskaia, K. Hsiao and S. A. Goueli, *Assay Drug Dev. Technol.*, 2009, **7**, 560–572.
44 A. Daina and V. Zoete, *Nat. Sci. Rep.*, 2017, **7**, 42717.

45 D. E. Pires, T. L. Blundell and D. B. Ascher, *J. Med. Chem.*, 2015, **58**, 4066–4072.

46 C. A. Lipinski, F. Lombardo, B. W. Dominy and P. J. Feeney, *Adv. Drug Deliv. Rev.*, 2012, **64**, 4–17.

47 D. F. Veber, S. R. Johnson, H. Cheng, B. R. Smith, K. W. Ward and K. D. Kopple, *J. Med. Chem.*, 2002, **45**, 2615–2623.

48 Z. Ates-Alagoz, M. M. Kisla, F. Z. Karadayi, S. Baran, T. S. Doğan and P. Mutlu, *New J. Chem.*, 2021, **45**, 18025–18038.

49 I. Ali, W. A. Wani, K. Saleem and M. F. Hsieh, *RSC Adv.*, 2014, **4**, 29629–29641.

50 I. P. Sæbø, M. Bjørås, H. Franzyk, E. Helgesen and J. A. Booth, *Int. J. Mol. Sci.*, 2023, **24**, 2914.

51 B. Webb and A. Sali, *Curr. Protoc. Bioinf.*, 2016, **54**, 5–6.

52 A. K. Malde, L. Zuo, M. Breeze, M. Stroet, D. Poger, P. C. Nair, C. Oostenbrink and A. E. Mark, *J. Chem. Theory Comput.*, 2011, **7**, 4026–4037.

53 M. N. Clifford and J. Wight, *J. Sci. Food Agric.*, 1976, **27**, 73–84.

54 B. S. Gangadharappa, R. Sharath, P. D. Revanasiddappa, V. Chandramohan, M. Balasubramaniam and T. P. Vardhineni, *J. Biomol. Struct. Dyn.*, 2020, **38**, 3757–3771.

55 R. Chandan, M. S. Chaithanya, M. Aditya and K. S. Kiran, *J. Biomol. Struct. Dyn.*, 2022, 1–9.